

this document downloaded from

**vulcanhammer.net**

Since 1997, your complete online resource for information geotechnical engineering and deep foundations:

The Wave Equation Page for Piling

*Online books on all aspects of soil mechanics, foundations and marine construction*

Free general engineering and geotechnical software

*And much more...*

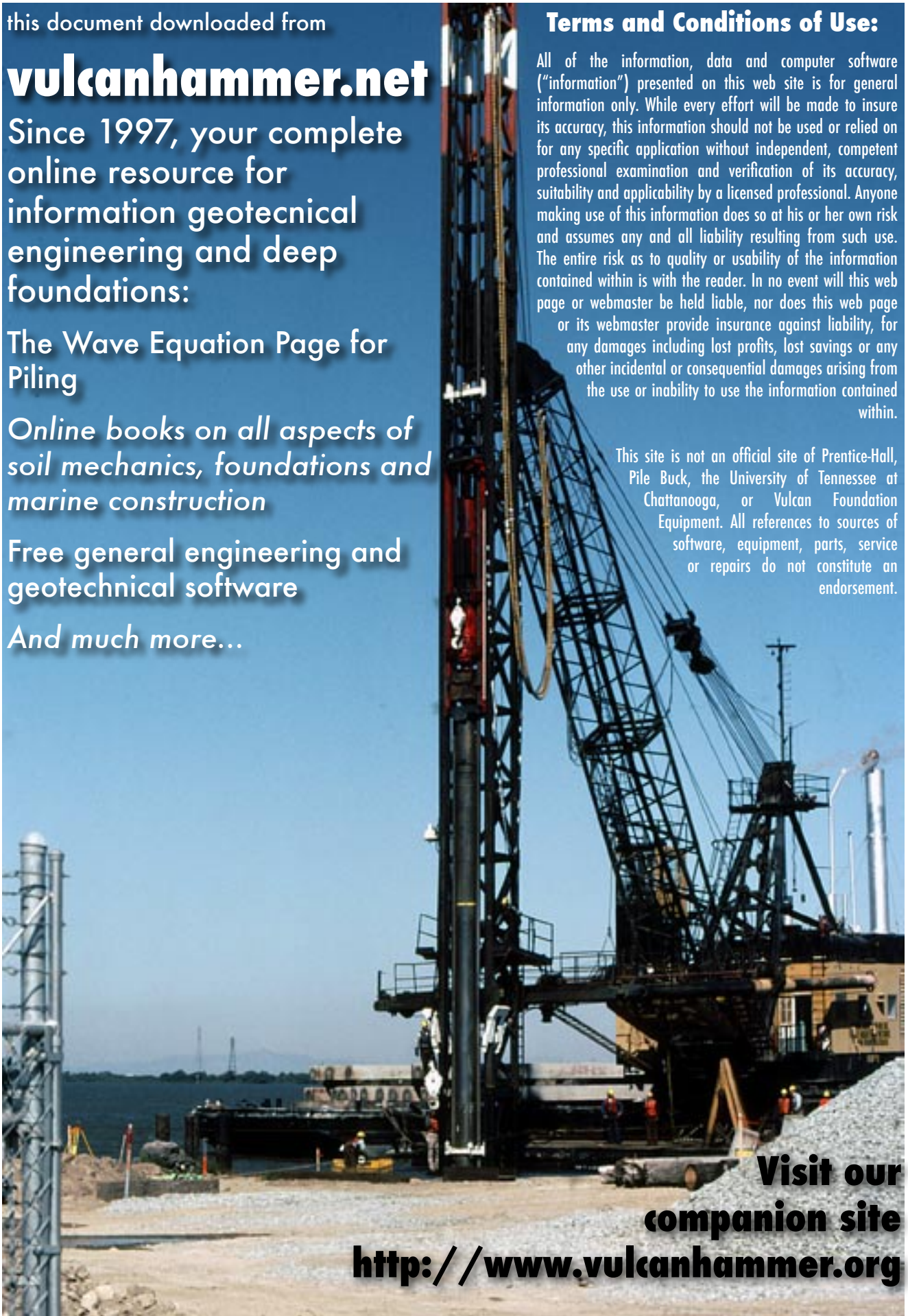
## Terms and Conditions of Use:

All of the information, data and computer software ("information") presented on this web site is for general information only. While every effort will be made to insure its accuracy, this information should not be used or relied on for any specific application without independent, competent professional examination and verification of its accuracy, suitability and applicability by a licensed professional. Anyone making use of this information does so at his or her own risk and assumes any and all liability resulting from such use. The entire risk as to quality or usability of the information contained within is with the reader. In no event will this web page or webmaster be held liable, nor does this web page or its webmaster provide insurance against liability, for any damages including lost profits, lost savings or any other incidental or consequential damages arising from the use or inability to use the information contained within.

This site is not an official site of Prentice-Hall, Pile Buck, the University of Tennessee at Chattanooga, or Vulcan Foundation Equipment. All references to sources of software, equipment, parts, service or repairs do not constitute an endorsement.

**Visit our  
companion site**

**<http://www.vulcanhammer.org>**



# **Investigation of the Resistance of Pile Caps to Lateral Loading**

Robert L. Mokwa

Dissertation submitted to the Faculty of the  
Virginia Polytechnic Institute and State University  
in partial fulfillment of the requirements for the degree of

Doctor of Philosophy

in

Civil Engineering

## Committee

Dr. J. Michael Duncan, Chairman

Dr. Richard M. Barker

Dr. Thomas L. Brandon

Dr. George M. Filz

Dr. Rakesh K. Kapania

September 28, 1999  
Blacksburg, Virginia

# **INVESTIGATION OF THE RESISTANCE OF PILE CAPS TO LATERAL LOADING**

by Robert L. Mokwa

Dr. J. Michael Duncan, Chairman  
Charles E. Via, Jr. Department of Civil and Environmental Engineering

## **ABSTRACT**

Bridges and buildings are often supported on deep foundations. These foundations consist of groups of piles coupled together by concrete pile caps. These pile caps, which are often massive and deeply buried, would be expected to provide significant resistance to lateral loads. However, practical procedures for computing the resistance of pile caps to lateral loads have not been developed, and, for this reason, cap resistance is usually ignored.

Neglecting cap resistance results in estimates of pile group deflections and bending moments under load that may exceed the actual deflections and bending moments by 100 % or more. Advances could be realized in the design of economical pile-supported foundations, and their behavior more accurately predicted, if the cap resistance can be accurately assessed.

This research provides a means of assessing and quantifying many important aspects of pile group and pile cap behavior under lateral loads. The program of work performed in this study includes developing a full-scale field test facility, conducting approximately 30 lateral load tests on pile groups and pile caps, performing laboratory geotechnical tests on natural soils obtained from the site and on imported backfill

materials, and performing analytical studies. A detailed literature review was also conducted to assess the current state of practice in the area of laterally loaded pile groups.

A method called the “group-equivalent pile” approach (abbreviated GEP) was developed for creating analytical models of pile groups and pile caps that are compatible with established approaches for analyzing single laterally loaded piles. A method for calculating pile cap resistance-deflection curves (p-y curves) was developed during this study, and has been programmed in the spreadsheet called *PYCAP*.

A practical, rational, and systematic procedure was developed for assessing and quantifying the lateral resistance that pile caps provide to pile groups. Comparisons between measured and calculated load-deflection responses indicate that the analytical approach developed in this study is conservative, reasonably accurate, and suitable for use in design. The results of this research are expected to improve the current state of knowledge and practice regarding pile group and pile cap behavior.

## ACKNOWLEDGEMENTS

The author wishes to express his deepest gratitude to his advisor, Dr. Michael Duncan, for his guidance and friendship during this study. The opportunity to work with Professor Duncan has been the highlight of my professional career, and has also been an enriching personal experience that has made my studies at Virginia Tech not only academically and technically fulfilling, but an exciting and rewarding experience as well.

The author would also like to recognize the contributions and helpful suggestions provided by his dissertation advisory committee members: Dr. Richard Barker, Dr. Tom Brandon, Dr. George Filz, Dr. Rakesh Kapania, and Dr. Jim Mitchell. Dr. Brandon's contributions during the initial site investigation and his assistance in setting up the data acquisition system are gratefully acknowledged.

A special note of recognition and appreciation goes to Virginia Tech graduate students Sami Arsoy, Craig Benedict, Jeff McGregor, and Brain Metcalfe for their valuable assistance during the construction and testing phases of the project.

Dr. Tom Murray reviewed the design drawings of the loading apparatus and steel connections. Dr. Richard Barker and Dr. Tom Cousins reviewed the pile cap structural design details. Dennis Huffman and Brett Farmer fabricated several parts of the field load test apparatus. Jim Coffey provided valuable assistance in transporting heavy equipment and trouble-shooting mechanical problems. Clark Brown provided patient answers to numerous questions regarding electronics and instrumentation. Dwight Paulette was very helpful in providing equipment and in locating a site at Kentland Farms for conducting the load tests. Thanks also to fellow students and friends who provided assistance in erecting and moving the large tent shelter at the site. Without the able assistance of these many people, this study would not have been possible

The author would also like to thank his colleagues, especially Chris Baxter, Diane Baxter, Harry Cooke, Yaco Esterhuizen, Jim Kuenzli, Vinnie Perrone, Carmine Polito, and C.J. Smith, for their friendships and enjoyable, stimulating discussions.

The Virginia Transportation Research Council and the Virginia Department of Transportation provided funding for this project. In addition, the author was funded by a Charles E. Via, Jr. Fellowship through the Virginia Tech Civil and Environmental Engineering Department, and by an academic Instructorship position.

A special note of gratitude goes to Mr. Scott Aker of Coalfield Services, Inc., Wytheville, Virginia, for his generous donation of approximately \$5,000 in piles and pile driving equipment and services.

The author wishes to thank his family for their understanding and support. My parents, Leonard and Kathy, my brother and sisters, Sue, Tim, Judi, and Jean, and their spouses and children have all been a source of guidance, patience, encouragement, and friendship.

Finally, and perhaps most importantly, the author wishes to express his sincere appreciation to his wife Nicki for her companionship, continuous encouragement, and great understanding in this challenging endeavor. I am forever grateful and thankful for her support and love, and for the many beautiful bike rides that we enjoyed together through Ellett Valley.

## TABLE OF CONTENTS

### CHAPTER 1 – INTRODUCTION

1.1 Background .....	1
1.2 Objectives and Scope of Research .....	2

### CHAPTER 2 - MECHANICS OF PILE CAP AND PILE GROUP BEHAVIOR

2.1 Introduction .....	6
2.2 Pile Cap Resistance – State of Practice .....	7
2.3 Behavior of Laterally Loaded Single Piles .....	9
2.3.1 Winkler Approach .....	10
2.3.2 p-y Method of Analysis .....	13
2.3.3 Elasticity Theory .....	16
2.3.4 Finite Element Method .....	17
2.4 Pile Group Behavior – Experimental Research .....	18
2.4.1 Background .....	18
2.4.2 Full-Scale Field Tests .....	19
2.4.3 1g Model Tests .....	22
2.4.4 Centrifuge Tests .....	24
2.5 Pile Group Efficiency .....	26
2.5.1 Background .....	26
2.5.2 Group Efficiency Factors .....	27
2.6 P-Multipliers .....	33
2.6.1 Background .....	33
2.6.2 Experimental Studies .....	35
2.6.3 Relationship Between $f_m$ and $G_e$ .....	37
2.7 Pile Group Behavior – Analytical Studies .....	39
2.7.1 Background .....	39
2.7.2 Closed-Form Analytical Approaches .....	39
2.7.3 Elasticity Methods .....	39
2.7.4 Hybrid Methods .....	41
2.7.5 Finite Element Methods .....	42
2.8 Summary .....	44

### CHAPTER 3 - FIELD LOAD TEST FACILITY

3.1 Introduction .....	75
3.2 In-Ground Facility .....	75
3.2.1 Piles .....	75
3.2.2 Concrete for Pile Caps and Bulkhead .....	76
3.2.3 Reinforcing Steel for Pile Caps and Bulkhead .....	77
3.2.4 Roads, Drainage, Weatherproofing .....	80
3.3 Loading Equipment .....	80

3.4 Instrumentation.....	82
3.5 Data Acquisition Hardware.....	84
3.6 Data Acquisition Software.....	87
3.7 Construction Schedule and Cost.....	88

**CHAPTER 4 - SUBSURFACE CONDITIONS AT THE FIELD LOAD TEST SITE**

4.1 Site Description.....	98
4.2 Geology.....	98
4.3 Subsurface Conditions.....	98
4.4 Subsurface Investigation.....	99
4.4.1 Soil Borings.....	99
4.4.2 Observation Well.....	100
4.4.3 Dilatometer Tests.....	100
4.4.4 Block Samples.....	101

**CHAPTER 5 - SOIL PARAMETERS**

5.1 Introduction.....	107
5.2 Natural Soils.....	107
5.2.1 Soil Description.....	107
5.2.2 Index Properties and Unit Weights.....	108
5.2.3 Consolidation Tests.....	109
5.2.4 Strength Tests.....	109
5.3 Backfill Soils.....	111
5.3.1 Soil Description and Index Properties.....	111
5.3.2 Standard Density Relationships.....	112
5.3.3 In-Place Densities.....	113
5.3.4 Strength Tests.....	115
5.4 Summary.....	117

**CHAPTER 6 - LATERAL LOAD TESTS**

6.1 Introduction.....	137
6.2 Load Tests.....	137
6.2.1 Deformations.....	138
6.2.2 Rotations.....	139
6.3 Single Pile Resistance.....	140
6.3.1 Effect of Pile-Head Load Connection.....	140
6.3.2 Effect of Soil Type and Density.....	142
6.3.3 Effect of Pile Head Rotational Restraint.....	143
6.3.4 Effect of Cyclic Loading.....	145
6.4 Pile Cap Resistance.....	146
6.4.1 Resistance With and Without Cap Embedment.....	146
6.4.2 Resistance From Sides and Front of Caps.....	148



6.4.3	Effect of Repetitive Load Applications.....	150
6.4.4	Effect of Pile Depth.....	150
6.4.5	Effect of Pile Length.....	151
6.4.6	Effect of Backfill Type and Density.....	152
6.4.7	Effect of Cyclic Loading.....	153
6.4.8	Ground Surface Movements.....	154
6.4.9	Effect of Sustained Loading.....	155
6.5	Passive Load Resistance Without Piles.....	155
6.5.1	Effect of Backfill Type on Passive Load Resistance.....	155
6.5.2	Effect of Cyclic Loading.....	156
6.6	Summary.....	157

**CHAPTER 7 - ANALYSIS OF LATERALLY LOADED PILE GROUPS**

7.1	Introduction.....	196
7.2	Single Pile Model.....	197
7.2.1	Background.....	197
7.2.2	Single Pile p-y Curve.....	197
7.2.3	Calculations for p-y Curves.....	199
7.2.4	Comparisons of Measured and Calculated Deflections.....	200
7.2.5	Single Pile Rotational Restraint.....	202
7.3	Pile Group Model.....	205
7.3.1	Background.....	205
7.3.2	Group Pile p-y Curves.....	206
7.3.3	Pile-Head Rotations.....	206
7.3.4	Pile-Head Rotational Stiffness Calculations.....	207
7.3.5	Comparisons of Measured and Calculated Pile Group Deflections with No Cap Resistance.....	212
7.4	Pile Cap Model.....	214
7.4.1	Background.....	214
7.4.2	Passive Earth Pressure Resistance.....	214
7.4.3	Three-Dimensional Effects.....	218
7.4.4	Pile Cap Stiffness.....	222
7.4.5	Pile Cap p-y Curves.....	224
7.5	Comparison of Measured and Calculated Load-Deflection Results.....	226
7.5.1	Background.....	226
7.5.2	Pile Caps Embedded in Natural Soil.....	228
7.5.3	Pile Caps Backfilled with Granular Backfill.....	229
7.6	Comparisons with Results of Load Tests Performed by Others.....	230
7.6.1	Background.....	230
7.6.2	Zafir and Vanderpool (1998) Case Study.....	230
7.7	Summary of Design Method.....	231
7.8	Summary.....	236

**CHAPTER 8 – SUMMARY AND CONCLUSIONS**

8.1 Literature Review .....	280
8.2 Field Load Tests .....	284
8.3 Soil Parameters.....	286
8.4 Analytical Approach .....	287
8.5 Recommendations for Future Research .....	289
<b>REFERENCES .....</b>	<b>291</b>
<b>APPENDIX A - LITERATURE REVIEW TABLES .....</b>	<b>303</b>
<b>APPENDIX B - DETAILS OF LOAD TEST FACILITY.....</b>	<b>325</b>
<b>APPENDIX C - SOIL BORING LOGS .....</b>	<b>331</b>
<b>APPENDIX D - LABORATORY TEST RESULTS.....</b>	<b>343</b>
<b>APPENDIX E - EQUATIONS FOR <math>K_Q</math> AND <math>K_C</math> FACTORS FOR THE BRINCH HANSEN (1961) THEORY .....</b>	<b>357</b>
<b>APPENDIX F - LOG SPIRAL EARTH PRESSURE THEORY .....</b>	<b>359</b>
<b>APPENDIX G - PASSIVE WEDGE MODEL FOR <math>\phi = 0</math>.....</b>	<b>374</b>
<b>APPENDIX H - EQUATIONS FOR COMPUTING THE INITIAL ELASTIC STIFFNESS, <math>K_{MAX}</math> .....</b>	<b>379</b>
<b>VITA.....</b>	<b>383</b>

**LIST OF TABLES**

Table 2.1	Summary of previous load tests performed to evaluate the lateral resistance of pile caps .....	49
Table 2.2	Summary of full-scale field test details .....	50
Table 2.3	Geotechnical centrifuge facility details .....	50
Table 2.4	Summary of pile group efficiency test data .....	51
Table 2.5	Summary of p-multiplier ( $f_m$ ) test data .....	56
Table 5.1	Summary of index test results on samples of natural soil.....	119
Table 5.2	Summary of consolidation test results on samples of natural soil .....	121
Table 5.3	Summary of UU results on samples of natural soil .....	122
Table 5.4	Summary of CU results on samples of natural soil.....	123
Table 5.5	Summary of CD test results on samples of natural soil.....	124
Table 5.6	Average results from field moisture-density tests .....	125
Table 5.7	Summary of CD test results on compacted New Castle sand samples.....	126
Table 5.8	Summary of CD test results on compacted crusher run gravel samples.....	127
Table 5.9	Friction angles for New Castle sand and crusher run gravel .....	128
Table 6.1	Summary of lateral load tests conducted at setup location A – NE pile cap versus NW pile cap.....	160
Table 6.2	Summary of lateral load tests conducted at setup location B – SE pile cap versus bulkhead .....	162
Table 6.3	Summary of lateral load tests conducted on the individual north pile.....	163
Table 6.4	Summary of lateral load tests conducted on the individual south pile.....	164

Table 6.5	Measured angular rotations.....	165
Table 6.6	Distribution of pile cap lateral resistance in natural soil.....	166
Table 7.1	Friction angles, $\delta$ , between various soils and foundation materials ....	238
Table 7.2	Typical values of the soil adhesion factor.....	239
Table 7.3	Typical range of values for Poisson's ratio.....	240
Table 7.4	Typical range of $E_i$ values for various soil types .....	241
Table 7.5	Equations for $E_i$ by several test methods .....	242
Table 7.6	Summary of results from <i>PYCAP</i> analyses.....	243
Table 7.7	Parameters used to calculate pile cap p-y curves.....	244
Table 7.8	Soil parameters used in the Zafir and Vanderpool case study .....	245
Table A.1	Summary of pile group lateral load tests .....	304
Table A.2	Summary of pile group analytical studies.....	318
Table B.1	Pile driving system specifications.....	326
Table B.2	Summary of pile driving data .....	327
Table B.3	Potentiometer standard specifications.....	328
Table B.4	Instrument calibration data .....	329
Table B.5	Cost of equipment and materials.....	330

## LIST OF FIGURES

Figure 2.1	Comparison of published load versus deflection curves.....	59
Figure 2.2	p-y models for laterally loaded piles.....	60
Figure 2.3	Description of terms used to describe pile group arrangements.....	61
Figure 2.4	Group efficiency versus pile spacing for all reported pile arrangements (square, in-line, and side-by-side). .....	62
Figure 2.5	Group efficiency versus pile spacing for piles in a box arrangement....	63
Figure 2.6	Influence of group size on group efficiency for piles in a box arrangement.....	64
Figure 2.7	Group efficiency versus pile spacing for a single row of piles oriented in the direction of load (in-line arrangement).....	65
Figure 2.8	Influence of group size on group efficiency for a single row of piles oriented in the direction of load (in-line arrangement) .....	66
Figure 2.9	Group efficiency versus pile spacing for a single row of piles oriented perpendicular to the direction of load (side-by-side arrangement) .....	67
Figure 2.10	Influence of soil type on group efficiency for piles in a box arrangement.....	68
Figure 2.11	Pile group efficiency versus normalized displacement.....	69
Figure 2.12	Variation of p-multiplier with depth.....	70
Figure 2.13	p-multiplier as a function of pile spacing for leading row and first trailing row .....	71
Figure 2.14	p-multiplier as a function of pile spacing for the second and third trailing rows .....	72
Figure 2.15	Proposed p-multiplier design curves.....	73
Figure 2.16	Proposed group efficiency design curve for piles in a square (box) arrangement.....	74

Figure 3.1	Plan view of field test site.....	89
Figure 3.2	Foundation construction photos.....	90
Figure 3.3	Plan view of anchor rod layout.....	91
Figure 3.4	Tent shelter photos.....	92
Figure 3.5	Hydraulic ram and steel struts positioned in loading trench.....	93
Figure 3.6	NE pile cap instrumentation plan.....	94
Figure 3.7	Instrumentation in place for measuring deflections during lateral load test.....	95
Figure 3.8	Instrumentation layout for individual piles.....	96
Figure 3.9	Photos of data collection system.....	97
Figure 4.1	Site location map.....	102
Figure 4.2	Subsurface profile at Kentland Farms field test facility.....	103
Figure 4.3	Site plan and subsurface investigation drawing.....	104
Figure 4.4	Standard penetration test results.....	105
Figure 4.5	Excavating soil block samples.....	106
Figure 5.1	Summary of index parameters for natural soils at the test facility.....	129
Figure 5.2	Natural soil strength parameters based on UU triaxial tests.....	130
Figure 5.3	Initial tangent modulus ( $E_i$ ) for natural soil, New Castle sand, and crusher run gravel.....	131
Figure 5.4	Maximum values of $p'$ versus $q$ for CU and CD triaxial tests on natural soil.....	132
Figure 5.5	Relative density ( $D_r$ ) comparison of scalped and unscalped crusher run gravel.....	133
Figure 5.6	Effect of density on strength of New castle sand and crusher run gravel.....	134

Figure 5.7	Distribution of $\phi_o$ and $\Delta\phi$ for New Castle sand and crusher run gravel.....	135
Figure 5.8	Soil parameter distributions for analytical models .....	136
Figure 6.1	Typical load-deflection curve for SE pile cap backfilled with compacted gravel .....	167
Figure 6.2	Typical results from lateral load tests performed at the field test facility .....	168
Figure 6.3	Description of pile cap rotation angles .....	169
Figure 6.4	Single pile load testing arrangement.....	170
Figure 6.5	Pinned connection – clevis yoke and tongue .....	171
Figure 6.6	Rigid strut connection.....	172
Figure 6.7	Comparison of load connectors used at the north pile.....	173
Figure 6.8	Effect of soil type and density on load deflection response of single piles.....	174
Figure 6.9	Effect of pile-head rotational restraint .....	175
Figure 6.10	Response curve based on back calculated $k_{m\theta}$ value for pile in natural soil.....	176
Figure 6.11	Effect of cyclic loading on single piles embedded in natural soil .....	177
Figure 6.12	Effect of cyclic loading on south pile backfilled with 5.7 feet of compacted sand.....	178
Figure 6.13	Load deflection response with and without pile cap embedment in natural soil.....	179
Figure 6.14	NE pile cap with soil excavated from the sides and front.....	180
Figure 6.15	Effect of pile cap side resistance.....	181
Figure 6.16	Effect of repetitive loading on pile cap deflections .....	182

Figure 6.17	Effect of pile cap depth on load-deflection response.....	183
Figure 6.18	Effect of pile length on load-deflection response .....	184
Figure 6.19	Comparison between natural soil and compacted gravel backfill .....	185
Figure 6.20	Effect of backfill type and density on load-deflection response of SE pile group.....	186
Figure 6.21	Cyclic response of NE and NW caps backfilled with compacted gravel.....	187
Figure 6.22	Cyclic response of SE cap backfilled with compacted crusher run gravel.....	188
Figure 6.23	Vertical deflection of gravel backfill surface in front of NE 36-in-deep pile cap .....	189
Figure 6.24	Effect of sustained load on NE and NW pile caps backfilled with compacted gravel .....	190
Figure 6.25	Effect of sustained load on SE cap embedded in natural soil .....	191
Figure 6.26	Passive resistance of embedded bulkhead in undisturbed soil and compacted gravel .....	192
Figure 6.27	Effect of sustained load on bulkhead embedded in natural soil.....	193
Figure 6.28	Cyclic response of bulkhead backfilled with dense crusher run gravel.....	194
Figure 6.29	Vertical deflection of gravel backfill surface in front of embedded bulkhead.....	195
Figure 7.1	Soil parameters for calculating p-y curves.....	246
Figure 7.2	Example of p-y calculations using spreadsheet <i>PYPILE</i> .....	247
Figure 7.3	p-y curves for <i>LPILE Plus 3.0</i> analyses.....	249
Figure 7.4	Single pile load testing arrangement.....	250
Figure 7.5	Measured response of south pile in natural soil.....	251



Figure 7.6	Calculated load-deflection curves for the south pile in natural soil, using p-y curves from <i>PYSHEET</i> .....	252
Figure 7.7	Calculated load-deflection curves for the south pile in natural soil, using <i>LPILE Plus 3.0</i> default curves.....	253
Figure 7.8	Pile-head loading connection.....	254
Figure 7.9	Calculated slope versus deflection curves for the south pile using best match $k_{m\theta}$ values.....	255
Figure 7.10	Comparison of calculated load versus deflection curves using best fit $k_{m\theta}$ ratios.....	256
Figure 7.11	Conceptual model for estimating pile group rotational restraint .....	257
Figure 7.12	Details for rotational restraint calculations .....	258
Figure 7.13	$k_{m\theta}$ approximation.....	259
Figure 7.14	Calculated response for the NE pile group with no cap resistance.....	260
Figure 7.15	Calculated response for the NW pile group with no cap resistance ....	261
Figure 7.16	Calculated response for the SE pile group with no cap resistance .....	262
Figure 7.17	Log spiral approximation.....	263
Figure 7.18	Graphical representation of the log spiral earth pressure method.....	264
Figure 7.19	$\phi = 0$ passive wedge model.....	265
Figure 7.20	Comparison of measured and calculated passive resistance for bulkhead in natural soil and gravel .....	266
Figure 7.21	<i>PYCAP Summary</i> worksheet for bulkhead in natural soil .....	267
Figure 7.22	<i>PYCAP Summary</i> worksheet for bulkhead backfilled with compacted gravel .....	268
Figure 7.23	<i>Elasticity</i> worksheet for the bulkhead in natural soil.....	269
Figure 7.24	<i>Hyperbola</i> worksheet for the bulkhead in natural soil.....	270

Figure 7.25	Comparison of calculated versus observed load-deflection behavior of bulkhead in natural soil and gravel.....	271
Figure 7.26	p-y curves for 36-in-deep pile cap in four different soils .....	272
Figure 7.27	Comparison between calculated and measured responses for pile caps in natural soil .....	273
Figure 7.28	Comparison between calculated and measured responses for pile caps backfilled with crusher run gravel .....	274
Figure 7.29	Comparison between calculated and measured responses of SE cap backfilled with New Castle sand.....	275
Figure 7.30	“Group equivalent pile” p-y curves for the Zafir and Vanderpool (1998) case study .....	276
Figure 7.31	<i>Summary</i> worksheet from <i>PYCAP</i> for the Zafir and Vanderpool case study .....	277
Figure 7.32	Calculated responses for the Zafir and Vanderpool (1998) case study.....	278
Figure 7.33	Approximate relationship between the friction angle and dry unit weight of granular soils.....	279
Figure B.1	Building a 200 kip load cell using ¼-inch strain gauges connected in a Wheatstone full-bridge circuit .....	331
Figure B.2	Load cell strain gauge circuit for measuring load.....	332
Figure B.3	Single pile test setup .....	333
Figure B.4	Calibration curves for load cells .....	334
Figure B.5	Calibration curve for deflection transducer No. 11 .....	335
Figure C.1	Soil Boring Log BH-1.....	336
Figure C.2	Soil Boring Log BH-2.....	337
Figure C.3	Soil Boring Log BH-3.....	338
Figure C.4	Soil Boring Log BH-4.....	339

Figure C.5	Soil Boring Log BH-5.....	340
Figure C.6	Soil Boring Log BH-6.....	341
Figure D.1	Consolidation curves for natural soil, strain vs. $\log p$ .....	342
Figure D.2	UU triaxial stress versus strain curves for natural soil (1 of 3) .....	344
Figure D.3	UU triaxial stress versus strain curves for natural soil (2 of 3) .....	346
Figure D.4	UU triaxial stress versus strain curves for natural soil (3 of 3) .....	347
Figure D.5	Grain size distribution curves for New Castle sand.....	348
Figure D.6	Grain size distribution curves for crusher run gravel.....	349
Figure D.7	Distribution of relative density values based on nuclear gage field test results.....	350
Figure D.8	CD triaxial stress versus strain curves for New Castle sand, $D_r = 20$ % (1 of 3) .....	351
Figure D.9	CD triaxial stress versus strain curves for New Castle sand, $D_r = 60$ % (2 of 3) .....	352
Figure D.10	CD triaxial stress versus strain curves for New Castle sand, $D_r = 80$ % (3 of 3) .....	353
Figure D.11	CD triaxial stress versus strain curves for crusher run gravel, $D_r = 50$ % (1 of 3) .....	354
Figure D.12	CD triaxial stress versus strain curves for crusher run gravel, $D_r = 70$ % (2 of 3) .....	355
Figure D.13	CD triaxial stress versus strain curves for crusher run gravel, $D_r = 90$ % (3 of 3) .....	365
Figure F.1	Log spiral approximation.....	367
Figure F.2	Dimensions for log spiral method.....	368
Figure F.3	Free body diagrams of the log spiral failure zone.....	369

Figure F.4	Example of <i>Log Spiral</i> worksheet.....	370
Figure F.5	<i>PYCAP Summary</i> worksheet for bulkhead in natural soil .....	373
Figure G.1	$\phi = 0$ passive wedge model .....	378

## **CHAPTER 1**

### **INTRODUCTION**

#### **1.1 BACKGROUND**

Bridges and buildings are often supported on deep foundations. These foundations consist of groups of piles coupled together by concrete pile caps. These pile caps, which are often massive and deeply buried, would be expected to provide significant resistance to lateral loads. However, practical procedures for computing the resistance of pile caps to lateral loads have not been developed, and, for this reason, cap resistance is usually ignored.

Neglecting cap resistance results in estimates of pile group deflections and bending moments under load that may exceed the actual deflections and bending moments by 100 % or more. Advances could be realized in the design of economical pile-supported foundations, and their behavior more accurately predicted, if the cap resistance can be accurately assessed. An understanding of soil-pile-cap interactions and the mechanics of load transfer is necessary to develop a method that can be used to compute displacements, shears, and moments in pile groups.

The results of an extensive literature search conducted as part of this study indicates that over the past three decades only limited testing and research has been conducted in the area of pile cap resistance to lateral loads. These earlier studies provide evidence that the lateral resistance provided by pile caps is often significant, and that in many cases the cap resistance is as large as the lateral resistance provided by the piles themselves.

## **1.2 OBJECTIVES AND SCOPE OF RESEARCH**

There is clearly a need for improved understanding of the factors that control the magnitude of cap resistance, and for rational analytical procedures to include cap resistance in the design of pile groups to resist lateral loads. An in-depth study was undertaken to address this need by accomplishing the following objectives:

1. Evaluate the state of knowledge with respect to the lateral load resistance of piles, pile groups, and pile caps.
2. Design and construct a field test facility to perform lateral load tests on pile groups with and without caps, and on individual piles.
3. Perform field load tests to evaluate the accuracy of theoretical and analytical methods for estimating the performance of pile groups, with caps embedded in natural soils, and with caps backfilled with commonly used backfill materials.
4. Perform laboratory and in situ tests to evaluate the properties of the natural soils encountered at the field test facility and on soils imported for use as backfill.
5. Develop an analytical method or procedure that can be used by practicing engineers for including the lateral resistance of pile caps in the design of deep foundation systems.

Chapter 2 provides a review of past experimental and analytical studies pertaining to lateral resistance, testing, and analysis of piles, pile groups, and pile caps. Included in

the review is a discussion of the current state of knowledge with regard to pile cap resistance, an overview of methods available for analyzing the lateral response of single piles, and a synopsis of full-scale and model tests that have been performed over the last 50 years to evaluate the lateral load resistance of piles in closely spaced groups.

Piles in closely spaced groups behave differently than single isolated piles because of pile-soil-pile interactions that take place in the group. It is generally recognized that deflections of a pile in a closely spaced group are greater than the deflections of an individual pile at the same load per pile because of these interaction effects. The maximum bending moments in pile within a group will also be larger than for a single similarly loaded pile, because the soil behaves as if it has less resistance, allowing the group to deflect more for the same load per pile. The experimental and analytical studies that have been conducted to evaluate group interaction effects have been summarized in a series of tables, and selected studies relevant to this research have been reviewed in more detail. Results from these studies have been assimilated into design charts for evaluating group efficiencies and  $p$ -multipliers. These design charts are used in the analytical procedure that was developed as part of this study.

A field test facility was designed and constructed specifically for use in this project to perform lateral load tests on deep foundations and to investigate the lateral load resistance of pile caps. Developing this facility and conducting the load tests performed in it represent a major effort of this study. The facility is located at Virginia Tech's Kentland Farms, approximately 10 miles west of Blacksburg, Virginia. The test foundations consist of three pile groups, each with four piles. One group has a pile cap 18 inches thick and two have 36-inch-thick pile caps. The facility also includes two individual test piles, and a buried concrete wall (or bulkhead) with no piles. The piles are all HP10x42 steel sections ranging from 10 to 19 feet in length. Chapter 3 describes details of the in-ground facilities, the equipment that was used to apply horizontal loads to the foundations, the instrumentation that was used to measure deflections and loads, and the data acquisition system.

The site where the load test facility is located lies within the floodplain of the New River and is underlain by fine-grained alluvial soils. Chapter 4 describes the subsurface investigation and in situ tests that were conducted at the site to characterize the soil stratigraphy and to obtain soil samples for laboratory testing.

Chapter 5 describes the laboratory testing program conducted to develop soil parameters that were subsequently used in analyses of the lateral load tests. The laboratory tests included soil classification, unit weight, strength (UU, CU, and CD triaxial tests), and consolidation. Tests were performed on samples of the natural soil from the field test facility and on samples of imported materials that were used as backfill around the piles, pile caps, and bulkhead.

Lateral load tests were conducted at the field test facility from early June through October, 1998. Thirty-one tests were performed on three groups of piles with embedded caps, on two single piles, and on a buried concrete bulkhead. The results of the load tests are discussed in Chapter 6. Compressive loads were applied to the piles, pile caps and bulkhead using a 200-ton-capacity hydraulic ram. Displacements and rotations of the foundations were measured using electronic transducers, which provided sufficient data to evaluate displacements and rotations along three mutually perpendicular axes (parallel to the direction of loading, perpendicular to the direction of loading, and vertical).

Tests on the single piles were reviewed to examine the effects of the pile-head load connection, the effects of soil type and density, the effects of pile head rotational restraint, and the effects of cyclic loading. Tests performed on the pile groups and pile caps were used to compare the response of the pile foundation with cap resistance (cap fully embedded) and without cap resistance (soil removed from around the cap). In addition, the effects of cap side resistance, the effects of cap depth, the effects of pile length, the effects of cap backfill type and density, the effects of cyclic loading, and the effects of sustained loading were also evaluated using the test results.



Chapter 7 describes the procedure that was developed for analyzing the response of pile groups to lateral loads. The accuracy of the procedure was evaluated by comparing the computed response of the pile groups at the Kentland Farms load test facility to the results of the load tests discussed in Chapter 6. The method developed is called the “group-equivalent pile” (GEP) method. The GEP method makes it possible to analyze a pile group using computer programs developed for analyzing single piles, such as *LPILE Plus 3.0* (1997). Each component of the method is described including the development of p-y curves for single piles, the modifications that are made to the single pile model to account for group effects, the development of a group-equivalent pile, and the method that was developed for calculating pile cap p-y curves.

Pile cap p-y curves are calculated using an *EXCEL* spreadsheet, called *PYCAP*, that was developed during this study. *PYCAP* contains a macro that is used to calculate passive pressures based on the log spiral earth pressure theory. The ultimate load resistance of the pile cap is determined by modifying the log spiral earth pressure force using three-dimensional correction factors from Ovesen’s (1964) tests on embedded anchor blocks. The pile cap p-y curves are developed using a hyperbolic formulation, which is defined by the ultimate cap load resistance and the initial elastic stiffness of the cap. The cap’s initial elastic stiffness is determined using elasticity equations developed by Douglas and Davis (1964) for estimating the horizontal displacement of a vertical rectangle in a semi-infinite homogenous elastic mass.

Chapter 8 contains a summary of the results, and the conclusion drawn from them. Recommendations are also given for future studies and research.

## **CHAPTER 2**

# **MECHANICS OF PILE CAP AND PILE GROUP BEHAVIOR**

### **2.1 INTRODUCTION**

The response of a laterally loaded pile within a group of closely spaced piles is often substantially different than a single isolated pile. This difference is attributed to the following three items:

1. The rotational restraint at the pile cap connection. The greater the rotational restraint, the smaller the deflection caused by a given lateral load.
2. The additional lateral resistance provided by the pile cap. As discussed in Chapter 1, verifying and quantifying the cap resistance is the primary focus of this research.
3. The interference that occurs between adjacent piles through the supporting soil. Interference between zones of influence causes a pile within a group to deflect more than a single isolated pile, as a result of pile-soil-pile interaction.

A comprehensive literature review was conducted as part of this research to examine the current state of knowledge regarding pile cap resistance and pile group behavior. Over 350 journal articles and other publications pertaining to lateral resistance, testing, and analysis of pile caps, piles, and pile groups were collected and reviewed.

Pertinent details from these studies were evaluated and, whenever possible, assimilated into tables and charts so that useful trends and similarities can readily be observed. Some of the data, such as graphs that present  $p$ -multipliers as functions of pile spacing, are utilized as design aids in subsequent chapters.

This chapter addresses three topics. The first is a review of the current state of practice regarding the lateral resistance of pile caps. The second is a brief review of the most recognized analytical techniques for analysis of single piles. This discussion of single piles is necessary to set the stage for the third topic, which is a review of published field and analytical research conducted to study the behavior of laterally loaded pile groups.

## **2.2 PILE CAP RESISTANCE – STATE OF PRACTICE**

A literature search was performed to establish the state of knowledge with regard to pile cap resistance to lateral loads. The focus of the literature review was directed towards experimental and analytical studies pertaining to the lateral resistance of pile caps, and the interaction of the pile cap with the pile group.

There is a scarcity of published information available in the subject area of pile cap lateral resistance. Of the publications reviewed, only four papers were found that describe load tests performed to investigate the lateral resistance of pile caps. The results from these four studies, summarized in Table 2.1 and Figure 2.1, show that the lateral load resistance provided by pile caps can be very significant, and that in some cases the cap resistance is as large as the resistance provided by the piles themselves.

Beatty (1970) tested two 6-pile groups of step-tapered piles and determined that approximately 50 percent of the applied lateral load was resisted by passive pressure on the pile cap.

Kim and Singh (1974) tested three 6-pile groups of 10BP42 piles and found that removal of soil beneath the pile caps significantly increased the measured deflections, rotations, and bending moments. This effect increased as the load increased.

Rollins et al. (1997) performed static lateral testing on a group of 9 piles and determined the lateral load resistance of the pile cap was greater than the lateral resistance provided by the piles themselves.

Zafir and Vanderpool (1998) tested a group of four drilled shafts, two feet in diameter, embedded in an 11-foot-diameter, 10-foot-thick cap, and determined that the lateral load resistance of the cap was approximately equal to the lateral resistance provided by the drilled shafts. Their measurements showed that the lateral resistance at loads less than 450 tons was provided entirely by passive pressure on the cap.

No systematic method has been reported in the literature for unlinking the cap resistance from the lateral resistance provided by the piles. For the most part, the studies described above addressed only a portion of the cap resistance. For example, the static tests performed by Rollins et al. (1997) considered only the passive resistance at the front of the cap, and only dynamic loads. Kim and Singh (1974) considered only the soil in contact with the bottom of the pile cap. The pile caps in Kim and Singh's study were constructed on the ground surface, and thus the results do not include any passive resistance at the front of the cap or frictional resistance of soil along the sides of the cap. The tests by Beatty (1970) only involved the passive resistance at the front of the cap. The tests by Zafir and Vanderpool (1998) were performed on an atypical pile cap, which consisted of a large, deep circular embedded cap.

These studies indicate that the lateral resistance of pile caps can be quite significant, especially when the pile cap is embedded beneath the ground surface. There is clearly a need for a rational method to evaluate the magnitude of pile cap resistance, and for including this resistance in the design of pile groups to resist lateral loads.

## 2.3 BEHAVIOR OF LATERALLY LOADED SINGLE PILES

Three criteria must be satisfied in the design of pile foundations subjected to lateral forces and moments: 1) the soil should not be stressed beyond its ultimate capacity, 2) deflections should be within acceptable limits, and 3) the structural integrity of the foundation system must be assured.

The first criteria can be addressed during design using ultimate resistance theories such as those by Broms (1964a, 1964b) or Brinch Hansen (1961). The second and third criteria apply to deflections and stresses that occur at working loads. The behavior of piles under working load conditions has been the focus of numerous studies over the past 40 to 50 years. A brief review of the most widely recognized analytical techniques is provided in this section. Many of these techniques can be modified to predict the behavior of closely spaced piles, or pile groups. Modifications for group response are often in the form of empirically or theoretically derived factors that are applied, in various ways, to account for group interaction effects.

Analytical methods for predicting lateral deflections, rotations and stresses in single piles can be grouped under the following four headings:

- Winkler approach,
- p-y method,
- elasticity theory, and
- finite element methods.

These techniques provide a framework for the development of analytical techniques that can be used to evaluate the response of piles in closely spaced groups, which is the subject of Section 2.7.

### 2.3.1 Winkler Approach

The Winkler approach, also called the subgrade reaction theory, is the oldest method for predicting pile deflections and bending moments. The approach uses Winkler's modulus of subgrade reaction concept to model the soil as a series of unconnected linear springs with a stiffness,  $E_s$ , expressed in units of force per length squared ( $FL^{-2}$ ).  $E_s$  is the modulus of soil reaction (or soil modulus) defined as:

$$E_s = \frac{-P}{y} \quad \text{Equation 2.1}$$

where  $p$  is the lateral soil reaction per unit length of the pile, and  $y$  is the lateral deflection of the pile (Matlock and Reese, 1960). The negative sign indicates the direction of soil reaction is opposite to the direction of the pile deflection. Another term that is sometimes used in place of  $E_s$  is the coefficient (or modulus) of horizontal subgrade reaction,  $k_h$ , expressed in units of force per unit volume (Terzaghi 1955). The relationship between  $E_s$  and  $k_h$  can be expressed as:

$$E_s = k_h D \quad \text{Equation 2.2}$$

where  $D$  is the diameter or width of the pile.  $E_s$  is a more fundamental soil property because it is not dependent on the pile size. The behavior of a single pile can be analyzed using the equation of an elastic beam supported on an elastic foundation (Hetenyi 1946), which is represented by the 4<sup>th</sup> order differential beam bending equation:

$$E_p I_p \frac{d^4 y}{dx^4} + Q \frac{d^2 y}{dx^2} + E_s y = 0 \quad \text{Equation 2.3}$$

where  $E_p$  is the modulus of elasticity of the pile,  $I_p$  is the moment of inertia of the pile section,  $Q$  is the axial load on the pile,  $x$  is the vertical depth, and  $y$  is the lateral deflection of the pile at point  $x$  along the length of the pile.

The governing equation for the deflection of a laterally loaded pile, obtained by applying variational techniques (minimization of potential energy) to the beam bending equation (Reddy 1993), and ignoring the axial component, is:

$$\frac{d^4 y}{dx^4} + \frac{E_s}{E_p I_p} y = 0 \quad \text{Equation 2.4}$$

Solutions to Equation 2.4 have been obtained by making simplifying assumptions regarding the variation of  $E_s$  (or  $k_h$ ) with depth. The most common assumption is that  $E_s$  is constant with depth for clays and  $E_s$  varies linearly with depth for sands. Poulos and Davis (1980) and Prakash and Sharma (1990) provide tables and charts that can be used to determine pile deflections, slopes, and moments as a function of depth and non-dimensional coefficients for a constant value of  $E_s$  with depth.

The soil modulus for sand and normally consolidated clay is often assumed to vary linearly with depth, as follows:

$$E_s = kx \quad \text{Equation 2.5}$$

where  $k$  (defined using the symbol  $n_h$  by Terzaghi, 1955) is the constant of horizontal subgrade reaction, in units force per volume. For this linear variation of  $E_s$  with depth, Matlock and Reese (1960) and Poulos and Davis (1980) present nondimensional coefficients that can be used to calculate pile deflections, rotations, and bending moments for various pile-head boundary conditions. Gill and Demars (1970) present other formulations for the variation of  $E_s$  with depth, such as step functions, hyperbolic functions, and exponential functions.

The subgrade reaction method is widely employed in practice because it has a long history of use, and because it is relatively straight forward to apply using available chart and tabulated solutions, particularly for a constant or linear variation of  $E_s$  with depth. Despite its frequent use, the method is often criticized because of its theoretical shortcomings and limitations. The primary shortcomings are:

1. the modulus of subgrade reaction is not a unique property of the soil, but depends intrinsically on pile characteristics and the magnitude of deflection,
2. the method is semi-empirical in nature,
3. axial load effects are ignored, and
4. the soil model used in the technique is discontinuous. That is, the linearly elastic Winkler springs behave independently and thus displacements at a point are not influenced by displacements or stresses at other points along the pile (Jamiolkowski and Garassino 1977).

Modifications to the original subgrade reaction approach have been proposed to account for some of these shortcomings. One of these modifications attempts to convert the Winkler model to a continuous model by coupling the springs using an inter-spring shear layer component (Georgiadis and Butterfield 1982). This model also accounts for the contribution of edge shear along the pile boundaries. The model has not gained widespread acceptance because of difficulties associated with obtaining soil parameters necessary to develop coefficients for use in the model (Horvath 1984).

McClelland and Focht (1956) augmented the subgrade reaction approach using finite difference techniques to solve the beam bending equation with nonlinear load versus deflection curves to model the soil. Their approach is known as the  $p$ - $y$  method of analysis. This method has gained popularity in recent years with the availability of powerful personal computers and commercial software such as COM624 (1993) and LPILE Plus3.0 (1997). A brief summary of the  $p$ - $y$  method of analysis is presented in the following section.



### 2.3.2 $p$ - $y$ Method of Analysis

The  $p$ - $y$  approach for analyzing the response of laterally loaded piles is essentially a modification or “evolutionary refinement” (Horvath 1984) of the basic Winkler model, where  $p$  is the soil pressure per unit length of pile and  $y$  is the pile deflection. The soil is represented by a series of nonlinear  $p$ - $y$  curves that vary with depth and soil type. An example of a hypothetical  $p$ - $y$  model is shown in Figure 2.2 (a).

The method is semi-empirical in nature because the shape of the  $p$ - $y$  curves is determined from field load tests. Reese (1977) has developed a number of empirical or “default” curves for typical soil types based on the results of field measurements on fully instrumented piles. The most widely used analytical expression for  $p$ - $y$  curves is the cubic parabola, represented by the following equation:

$$\frac{p}{p_{ult}} = 0.5 \left( \frac{y}{y_{50}} \right)^{\frac{1}{3}} \quad \text{Equation 2.6}$$

where  $p_{ult}$  is the ultimate soil resistance per unit length of pile and  $y_{50}$  is the deflection at one-half the ultimate soil resistance. To convert from strains measured in laboratory triaxial tests to pile deflections, the following relationship is used for  $y_{50}$ :

$$y_{50} = A e_{50} D \quad \text{Equation 2.7}$$

where  $e_{50}$  is the strain at  $\frac{1}{2}$  the maximum principal stress difference, determined in a laboratory triaxial test,  $D$  is the pile width or diameter, and  $A$  is a constant that varies from 0.35 to 3.0 (Reese 1980).

The deflections, rotations, and bending moments in the pile are calculated by solving the beam bending equation using finite difference or finite element numerical techniques. The pile is divided into a number of small increments and analyzed using  $p$ - $y$  curves to represent the soil resistance.

In this representation, the axial load in the pile,  $Q$ , is implicitly assumed constant with depth, to simplify computations. This assumption does not adversely effect the analysis because  $Q$  has very little effect on the deflection and bending moment. Furthermore, the maximum bending moment is generally only a relatively short distance below the groundline, or pile cap, where the value of  $Q$  is undiminished (Reese, 1977).

Four additional equations are necessary to balance the number of equations and the number of unknowns in the finite difference formulation. These four equations are represented by boundary conditions, two at the pile top and two at the bottom of the pile. At the bottom of the pile, one boundary condition is obtained by assuming a value of zero moment, or:

$$EI \left( \frac{d^2 y}{dx^2} \right) = 0 \quad \text{Equation 2.8}$$

The second boundary condition at the pile bottom involves specifying the shear of the pile using the following expression at  $x = L$ :

$$EI \left( \frac{d^3 y}{dx^3} \right) + Q \left( \frac{dy}{dx} \right) = V \quad \text{Equation 2.9}$$

where  $V$  is the shear force, which is usually set equal to zero for long piles.

The two boundary conditions at the top of the pile depend on the shear, moment, rotation, and displacement circumstances at the pile top. These are generalized into the following four categories:

1. Pile not restrained against rotation. This is divided into two subcategories: (a) “flagpole” and (b) free-head conditions.

2. Vertical load applied eccentrically at the ground surface (moment loading condition).
3. Pile head extends into a superstructure or is partially restrained against rotation (partially restrained condition).
4. Pile head rotation is known, usually assumed = 0 (fixed-head condition).

Category	Shear V	Moment M	Rotation $\theta$	Displacement y
1(a). free-head - “flagpole”	known ( $> 0$ )	known ( $> 0$ at groundline)	unknown ( $> 0$ )	unknown ( $> 0$ )
1(b). free-head - pinned	known ( $> 0$ )	known ( $= 0$ )	unknown ( $> 0$ )	unknown ( $> 0$ )
2. moment loading	known ( $= 0$ )	known ( $> 0$ )	unknown ( $> 0$ )	unknown ( $> 0$ )
3. partially restrained	known ( $> 0$ )	M/ $\theta$ known	M/ $\theta$ known	unknown ( $> 0$ )
4. fixed-head	known ( $> 0$ )	unknown ( $< 0$ )	known ( $= 0$ )	unknown ( $> 0$ )

The  $p$ - $y$  method is readily adapted to computer implementation and is available commercially in the computer programs LPILEPlus 3.0 (1997) and COM624 (1993). The method is an improvement over the subgrade reaction approach because it accounts for the nonlinear behavior of most soils without the numerical limitations inherent in the subgrade reaction approach. However, the method has some limitations, as described below:

1. The  $p$ - $y$  curves are independent of one another.  
Therefore, the continuous nature of soil along the length of the pile is not explicitly modeled.

2. Suitable  $p$ - $y$  curves are required. Obtaining the appropriate  $p$ - $y$  curve is analogous to obtaining the appropriate value of  $E_s$ ; one must either perform full-scale instrumented lateral load tests or adapt the existing available standard curves (default curves) for use in untested conditions. These default curves are limited to the soil types in which they were developed; they are not universal.
3. A computer is required to perform the analysis.

Other representations of  $p$ - $y$  curves have been proposed such as the hyperbolic shape by (Kondner 1963). Evans (1982) and Mokwa et al. (1997) present a means of adjusting the shape of the  $p$ - $y$  curve to model the behavior of soils that have both cohesion and friction using Brinch Hansen's (1961)  $f$ - $c$  ultimate theory. In situ tests such as the dilatometer (Gabr 1994), cone penetrometer (Robertson et al. 1985), and pressuremeter (Ruesta and Townsend 1997) have also been used to develop  $p$ - $y$  curves.

### 2.3.3 Elasticity Theory

Poulos (1971a, 1971b) presented the first systematic approach for analyzing the behavior of laterally loaded piles and pile groups using the theory of elasticity. Because the soil is represented as an elastic continuum, the approach is applicable for analyzing battered piles, pile groups of any shape and dimension, layered systems, and systems in which the soil modulus varies with depth. The method can be adapted to account for the nonlinear behavior of soil and provides a means of determining both immediate and final total movements of the pile (Poulos 1980).

Poulos's (1971a, 1971b) method assumes the soil is an ideal, elastic, homogeneous, isotropic semi-infinite mass, having elastic parameters  $E_s$  and  $\nu_s$ . The pile is idealized as a thin beam, with horizontal pile deflections evaluated from integration of

the classic Mindlin equation for horizontal subsurface loading. The Mindlin equation is used to solve for horizontal displacements caused by a horizontal point load within the interior of a semi-infinite elastic-isotropic homogeneous mass. Solutions are obtained by integrating the equation over a rectangular area within the mass. The principle of superposition is used to obtain displacement of any points within the rectangular area. Details of the Mindlin equation can be found in Appendix B of *Pile Foundation Analysis and Design* by Poulos and Davis (1980).

The pile is assumed to be a vertical strip of length  $L$ , width  $D$  (or diameter,  $D$ , for a circular pile), and flexural stiffness  $E_p I_p$ . It is divided into  $n+1$  elements and each element is acted upon by a uniform horizontal stress  $p$ . The horizontal displacements of the pile are equal to the horizontal displacements of the soil. The soil displacements are expressed as:

$$\{y_s\} = \frac{d}{E_s} [I_s] \{p\} \quad \text{Equation 2.10}$$

where  $\{y_s\}$  is the column vector of soil displacements,  $\{p\}$  is the column vector of horizontal loading between soil and pile, and  $[I_s]$  is the  $n+1$  by  $n+1$  matrix of soil-displacement influence factors determined by integrating Mindlin's equation, using boundary element analyses (Poulos 1971a). The finite difference form of the beam bending equation is used to determine the pile displacements. The form of the equation varies depending on the pile-head boundary conditions. Poulos and Davis (1980) present expressions for free-head and fixed-head piles for a number of different soil and loading conditions. One of the biggest limitations of the method (in addition to computational complexities) is the difficulty in determining an appropriate soil modulus,  $E_s$ .

### 2.3.4 Finite Element Method

The finite element method is a numerical approach based on elastic continuum theory that can be used to model pile-soil-pile interaction by considering the soil as a three-dimensional, quasi-elastic continuum. Finite element techniques have been used to

analyze complicated loading conditions on important projects and for research purposes. Salient features of this powerful method include the ability to apply any combination of axial, torsion, and lateral loads; the capability of considering the nonlinear behavior of structure and soil; and the potential to model pile-soil-pile-structure interactions. Time-dependent results can be obtained and more intricate conditions such as battered piles, slopes, excavations, tie-backs, and construction sequencing can be modeled. The method can be used with a variety of soil stress-strain relationships, and is suitable for analyzing pile group behavior, as described in Section 2.7.5. Performing three-dimensional finite element analyses requires considerable engineering time for generating input and interpreting results. For this reason, the finite element method has predominately been used for research on pile group behavior, rarely for design.

## **2.4 PILE GROUP BEHAVIOR – EXPERIMENTAL RESEARCH**

### **2.4.1 Background**

The literature review also encompassed the current state of practice in the area of pile group behavior and pile group efficiencies. This section describes relevant aspects of experimental studies reported in the literature. Analytical studies of pile group behavior are described in Section 2.7.

Table A.1 (located in Appendix A) contains a summary of 37 experimental studies in which the effects of pile group behavior were observed and measured. The table includes many relevant load tests that have been performed on pile groups during the past 60 years. The references are organized chronologically. Multiple references indicate that a particular test was addressed in more than one published paper.

The conventions and terms used to describe pile groups in this dissertation are shown in Figure 2.3. Most pile groups used in practice fall into one of the following three categories, based on the geometric arrangement of the piles:

1. Figure 2.3 (a) – **in-line arrangement**. The piles are aligned in the direction of load.
2. Figure 2.3 (b) – **side-by-side arrangement**. The piles are aligned normal to the direction of load.
3. Figure 2.3 (c)– **box arrangement**. Consists of multiple in-line or side-by-side arrangements.

Pile rows are labeled as shown in Figure 2.3(c). The leading row is the first row on the right, where the lateral load acts from left to right. The rows following the leading row are labeled as 1<sup>st</sup> trailing row, 2<sup>nd</sup> trailing row, and so on. The spacing between two adjacent piles in a group is commonly described by the center to center spacing, measured either parallel or perpendicular to the direction of applied load. Pile spacings are often normalized by the pile diameter,  $D$ . Thus, a spacing identified as  $3D$  indicates the center to center spacing in a group is three times the pile diameter. This convention is used throughout this document.

The experimental studies described in Table A1 are categorized under three headings:

1. full-scale field tests (15 studies)
2. 1g model tests (16 studies)
3. geotechnical centrifuge tests (6 studies)

Pertinent details and relevant test results are discussed in the following sections.

#### **2.4.2 Full-Scale Field Tests**

Full-scale tests identified during the literature review include a wide variety of pile types, installation methods, soil conditions, and pile-head boundary conditions, as shown in Table 2.2.

The earliest reported studies (those by Feagin and Gleser) describe the results of full-scale field tests conducted in conjunction with the design and construction of large pile-supported locks and dams along the Mississippi River. O'Halloran (1953) reported tests that were conducted in 1928 for a large paper mill located in Quebec City, Canada, along the banks of the St. Charles River. Load tests performed in conjunction with the Arkansas River Navigation Project provided significant amounts of noteworthy design and research data, which contributed to advancements in the state of practice in the early 1970's. Alizadeh and Davisson (1970) reported the results of numerous full-scale lateral load tests conducted for navigation locks and dams that were associated with this massive project, located in the Arkansas River Valley.

Ingenious methods were devised in these tests for applying loads and monitoring deflections of piles and pile groups. The load tests were usually conducted during design and, very often, additional tests were conducted during construction to verify design assumptions. In many instances, the tests were performed on production piles, which were eventually integrated into the final foundation system.

The most notable difference between the tests conducted prior to the 1960's and those conducted more recently is the sophistication of the monitoring instruments. Applied loads and pile-head deflection were usually the only variables measured in the earlier tests. Loads were typically measured manually by recording the pressure gauge reading of the hydraulic jack.

A variety of methods were employed to measure deflections. In most cases, more than one system was used to provide redundancy. For example, Feagin (1953) used two completely independent systems. One system used transit and level survey instruments, and the other system consisted of micrometers, which were embedded in concrete and connected to piano wires under 50 pound of tension. Electronic contact signals were used to make the measurements with a galvanometer connected in series with a battery. O'Halloran (1953) manually measured horizontal deflections using piano wire as a point of reference. The piano wires, which were mounted outside the zone of influence of the



test, were stretched across the centerline of each pile, at right angles to the direction of applied load. Deflection measurements were made after each load application by measuring the horizontal relative displacement between the pile center and the piano wire.

Over the last 30 to 40 years, the level of sophistication and overall capabilities of field monitoring systems have increased with the advent of personal computers and portable multi-channel data acquisition systems. Hydraulic rams or jacks are still commonly used for applying lateral loads for static testing. However, more advanced systems are now used for cyclic and dynamic testing. Computer-driven servo-controllers are often used for applying large numbers of cyclic loads. For example, Brown and Reese (1985) applied 100 to 200 cycles of push-pull loading at 0.067 Hz using an MTS servo valve operated by an electro-hydraulic servo controller.

A variety of methods have been used to apply dynamic loads. Blaney and O'Neill (1989) used a linear inertial mass vibrator to apply dynamic loads to a 9-pile group at frequencies as high as 50 Hz. Rollins et al. (1997) used a statnamic loading device to apply large loads of short duration (100 to 250 msec) to their test pile group. The statnamic device produces force by igniting solid fuel propellant inside a cylinder (piston), which causes a rapid expansion of high-pressure gas that propels the piston and forces the silencer and reaction mass away.

Powerful electronic systems are now available to facilitate data collection. These systems usually have multiple channels for reading responses from a variety of instruments at the same time. It is now possible to collect vast amounts of information during a test at virtually any frequency and at resolutions considerably smaller than is possible using optical or mechanical devices.

Pile deflections and rotations are often measured using displacement transducers, linear potentiometers, and linear variable differential transformers (LVDT's). In addition to measuring deflections, piles are often instrumented with strain gauges and slope

inclinometers. Information obtained from these devices can be used to calculate stresses, bending moments, and deflections along the length of a pile.

Whenever possible, strain gauges are installed after the piles are driven to minimize damage. A technique commonly used with closed-end pipe piles is to attach strain gauges to a smaller diameter steel pipe or sister bar, which is then inserted into the previously driven pile and grouted in place. This method was used in the tests performed on pipe piles by Brown (1985), Ruesta and Townsend (1997), and Rollins et al. (1998).

In some cases, strain gauges are attached prior to installing piles. For instance, gauges are often attached to steel H-piles prior to driving; or gauges may be attached to the reinforcing steel cage prior to pouring concrete for bored piles (drilled shafts). Meimon et al. (1986) mounted strain gauges on the inside face of the pile flange and mounted a slope inclinometer tube on the web face. They protected the instruments by welding steel plates across the ends of the flanges creating a boxed-in cross-section, and drove the piles close-ended.

Applied loads are usually measured using load cells. Ruesta and Townsend (1997) used ten load cells for tests on a 9-pile group. One load cell was used to measure the total applied load, and additional load cells were attached to the strut connections at each pile. Additional instruments such as accelerometers, geophones, and earth pressure cells are sometimes used for specialized applications.

### **2.4.3 1g Model Tests**

The majority of experiments performed on pile groups fall under the category of 1g model tests. Model tests are relatively inexpensive and can be conducted under controlled laboratory conditions. This provides an efficient means of investigation. For instance, Cox et al. (1984) reported on a study in which tests on 58 single piles and 41 pile groups were performed. They varied the geometric arrangement of piles within groups, the number of piles per group, and the spacing between piles. Liu (1991) performed 28 sets of tests on pile groups in which the pile spacing, group configuration,

and pile lengths were varied. Franke (1988) performed a number of parametric studies by varying the arrangement, size, and spacing of piles within groups; the length and stiffness of the piles; the pile head boundary conditions; and the relative density of the backfill soil.

Aluminum is the most frequently used material for fabricating model piles. Small diameter aluminum pipes, bars, or tubes were used in 8 of the 16 model tests reported in Table A.1. Other materials such as mild steel and chloridized-vinyl (Shibata et al. 1989) have also been used. Tschebotarioff (1953) and Wen (1955) used small wood dowels to represent timber piles in their model tests

Sand was by far the most commonly used soil (12 out of 16 tests); however, silt and clay soils were used as well. A variety of techniques were used to place soil and install piles. In some studies, soil was placed first and the piles were subsequently driven, pushed or bored into place. In other cases, the piles were held in place as soil was placed around them. Techniques for installing soil included tamping, pluviation, raining, dropping, flooding, and “boiling”. Shibata et al. (1989) applied the term boiling to the technique of pumping water with a strong upward gradient through the bottom of a sand-filled tank.

The primary shortcomings of 1g model testing are related to scaling and edge effects. Scaling effects limit the applicability of model tests in simulating the performance of prototypes. Models are useful in performing parametric studies to examine relative effects, but it is appropriate to exercise caution in extrapolating results obtained from model tests to full-scale dimensions. Items such as at-rest stress levels, soil pressure distributions, and soil particle movements are all factors influenced by scaling (Zhang and Hu 1991).

Edge effects become significant if the size of the test tank is too small relative to the size of the model pile. Prakash (1962) reported the results of tests in a large test tank in which the zone of influence (or zone of interference) extended a distance of 8 to 12

times the pile width in the direction of loading and 3 to 4 times the pile width normal to the direction of loading. Experimental apparatus that do not meet these guidelines would involve edge effects, which are not easily quantified.

As discussed in the following paragraphs, centrifuge tests have become increasingly popular in the last decade as a means of overcoming scaling effects inherent in 1g model testing.

#### **2.4.4 Centrifuge Tests**

Similar to 1g model testing, a geotechnical centrifuge provides a relatively rapid method for performing parametric studies. The advantage of centrifuge modeling lies in the ability of the centrifuge to reproduce prototype stress-strain conditions in a reduced scale model (McVay et al. 1995).

For additional information pertaining to centrifuge mechanics, the reader is referred to the 20<sup>th</sup> Rankine Lecture by Schofield (1980), which provides a detailed discussion of centrifuge testing principles. Schofield explains the mechanics behind centrifuge modeling in terms of Newtonian physics and the theory of relativity. In essence, the gravitational force of a prototype body is indistinguishable from, and identical to, an inertial force created in the centrifuge. Thus, if the product of depth times acceleration is the same in model and prototype, the stresses at every point within the model will theoretically be the same as the stresses at every corresponding point in the prototype (Schofield 1980).

Four studies that investigated the lateral resistance of pile groups using geotechnical centrifuges were found during the literature study, and these are summarized in Table A.1. Some details about the facilities are provided in Table 2.3. Significant aspects of the studies are discussed in the following paragraphs.

The first centrifuge tests on model pile groups were performed by Barton (1984) on groups consisting of 2, 3, and 6 piles at various spacings and orientations with respect

to the direction of load. Zhang and Hu (1991) examined the effect of residual stresses on the behavior of laterally loaded piles and pile groups. Adachi et al. (1994b) examined pile-soil-pile interaction effects by testing two piles at various spacings and orientations. In these three studies, the soil was placed and the piles were installed prior to starting the centrifuge (i.e., pile installation occurred at 1g).

McVay et al. (1994) was the first to install pile groups in flight, laterally load them, and measure their response without stopping the centrifuge. The results from McVay's study indicates that piles have greater resistance to lateral and axial loads when driven at prototype stress levels (centrifuge in motion during pile installation), as opposed to 1g installation. The difference in behavior is attributed to the significantly greater dilation of the test sand at 1g and resulting decrease in density and strength (McVay et al. 1995).

McVay et al. (1994, 1995, and 1998) measured group efficiencies and back-calculated p-multipliers for pile groups ranging in size from 3 by 3 to 3 by 7 (3 rows oriented parallel to the direction of loading and 7 rows oriented normal to the direction of load). Spacings of 3 and 5 times the pile diameter were tested using both loose- and medium-dense sand backfill.

Centrifuge testing appears to provide a relatively efficient means of systematically investigating several variables at prototype stress conditions. Factors that impact centrifuge test results include boundary conditions or edge effects between the model foundation and the centrifuge bucket (model container), and soil behavior incongruities caused by installing piles at 1g, rather than in flight. Additional inconsistencies between model and prototype behavior may arise when testing clayey soils. Schofield (1980) describes these limitations and attributes them to changes in water contents, pore pressures, and equivalent liquidities, which are difficult to model in the centrifuge.

## 2.5 PILE GROUP EFFICIENCY

### 2.5.1 Background

Piles are usually constructed in groups and tied together by a concrete cap at the ground surface. Piles in closely spaced groups behave differently than single isolated piles because of pile-soil-pile interactions that take place in the group. It is generally recognized that deflections of a pile in a closely spaced group are greater than the deflections of an individual pile at the same load because of these interaction effects. The maximum bending moment in a group will also be larger than that for a single pile, because the soil behaves as if it has less resistance, allowing the group to deflect more for the same load per pile.

The most widely recognized standard for quantifying group interaction effects is the group efficiency factor,  $G_e$ , which is defined in Equation 2.11 as the average lateral capacity per pile in a group divided by the lateral capacity of a single pile (Prakash 1990).

$$G_e = \frac{(Q_u)_g}{n(Q_u)_s} \quad \text{Equation 2.11}$$

Where  $(Q_u)_g$  is the ultimate lateral load capacity of the group,  $n$  is the number of piles in the group, and  $(Q_u)_s$  is the ultimate lateral load capacity of a single pile. A somewhat different definition for the group efficiency factor, one that is based on p-multipliers, is described in Section 2.6.

The analysis of pile group behavior can be divided into widely-spaced closely-spaced piles. Model tests and a limited number of full-scale tests indicate that piles are not influenced by group effects if they are spaced far apart.

Piles installed in groups at close spacings will deflect more than a single pile subjected to the same lateral load per pile because of group effects (Bogard and Matlock, 1983). There is general agreement in the literature that group effects are small when

center-to-center pile spacings exceed 6 pile diameters (6D) in a direction parallel to the load and when they exceed 3D measured in a direction perpendicular to the load. This approximation has been validated through experimental tests by Prakash (1967), Franke (1988), Lieng (1989), and Rao et al. (1996).

Group efficiency factors can be evaluated experimentally by performing load tests on pile groups and on comparable single piles. The next section summarizes over 60 years of experimental research in the area of pile group efficiencies.

### 2.5.2 Group Efficiency Factors

Fourteen of the studies included in Table A.1 involve experimental evaluations of the group efficiency factor,  $G_e$ , or provide enough information to calculate  $G_e$  using Equation 2.11. The references for these 14 studies are tabulated chronologically in Table 2.4. Pertinent data from these papers are presented in Table 2.4 for three geometric arrangements, defined in Figure 2.3 as: box, in-line, and side-by-side. Some of the references, such as Cox et al. (1984) and Shibata et al. (1989), include multiple tests conducted using different geometric arrangements and pile spacings. For clarity, these tests were arranged into separate rows of the table. Of the 85 separate tests described in Table 2.4, only five percent (4 tests) were full-scale. The remaining tests were performed on reduced scale models, either 1g model or centrifuge. The large percentage of model tests is due to the relative ease and lower cost of these tests, as opposed to full-scale field tests.

The studies summarized in Table 2.4 were examined in detail to determine the factors that most significantly effect overall group efficiency. Because most of these factors are interrelated, those with greatest significance are identified first. In order of importance, these factors are:

- pile spacing
- group arrangement

- group size
- pile-head fixity
- soil type and density
- pile displacement

### ***Pile Spacing***

Center to center pile spacing is the dominant factor affecting pile group efficiency. Cox et al. (1984) measured group efficiencies ranging from 0.59 at 1.5D spacing to 0.95 at 3D spacing for a 3-pile in-line arrangement in very soft clay. For the same arrangement of piles in medium dense sand, Sarsby (1985) reported nearly the same values of group efficiencies ranging from 0.66 at 2D spacing to 0.80 at 8D spacing.

The results for all of the tests summarized in Table 2.4, are plotted in Figure 2.4 as a function of center to center pile spacing. The most significant trend in this figure is the increase of  $G_e$  with pile spacing. However, there is a large amount of scatter in the data indicating that other factors also influence the value of  $G_e$ . To estimate accurate values of group efficiency, it is necessary to consider factors in addition to pile spacing.

### ***Group Arrangement and Group Size***

After pile spacing, the next most significant factor appears to be the geometric arrangement of piles within the group. Observable trends are evident in Figure 2.4, where the group arrangements (square, in-line, and side-by-side) are delineated using different symbols. Piles in square arrangements are represented by solid squares, in-line arrangements are identified by solid circles, and side-by-side arrangements are identified by open circles. The three outlying data points (shown as solid circles) at 8D spacing represent results from Sarsby's (1985) 1g model tests. These tests were performed on small (less than 1/4-inch-diameter) steel bars. The bars were repeatedly pushed laterally to deflections greater than 20 times the pile diameter, and  $G_e$  values were determined by extrapolating the resistance curves back to zero deflection. Because the test procedure is



questionable, and the results are not consistent with those from other more reasonable test procedures, no weight is placed on these tests in the development of recommendations for design.

For clarity, the test results are plotted and described separately based on the arrangement of piles within a group, as follows:

- box arrangement - Figures 2.5 and 2.6
- in-line arrangement – Figures 2.7 and 2.8
- side-by-side arrangement - Figure 2.9

Design curves were visually fitted through the data points for the three types of pile arrangements, using engineering judgement, as described below.

**Box arrangement.** Test results from Table 2.4 for multiple rows of piles oriented in box arrangements are plotted in Figure 2.5, along with the proposed design curve. The design curve is linear between  $G_e = 1.0$  at a spacing of  $6D$ , and  $G_e = 0.25$  at a spacing of  $1D$ .

There is no clear effect of group size, as can be seen in Figure 2.6. This may be a result of scatter in the data. One could logically infer that shadowing effects would increase with group size. If this were the case, group efficiency would be expected to decrease as group size increased. As additional data becomes available, it may be possible to quantify the effect of group size.

**In-line arrangement.** Test results from Table 2.4 for single rows of piles oriented in the direction of load (in-line arrangement) are plotted in Figure 2.7, along with proposed design lines. Based on this plot, it can be noted that group efficiency is influenced by the number of piles in the line. This can be seen more clearly in Figure 2.8, where the data points are plotted using symbols that indicate the number of piles per line, either 2, 3, or 4. The following conclusions can be drawn from this plot:

1. At the same pile spacing, a single row of in-line piles will have a greater group efficiency than piles in a box arrangement.
2. At a given spacing, the group efficiency decreases as the number of piles in a line increase.

As additional data become available, it may be possible to refine the design lines shown in Figures 2.7 and 2.8.

**Side-by-side arrangement.** Test results from Table 2.4 for single rows of piles oriented normal to the direction of load (side-by-side arrangement) are plotted in Figure 2.9, along with the proposed design line. From this plot, it is concluded that:

1. Piles oriented in side-by-side arrangements are effected by pile spacing to a lesser degree than in-line or box arrangements of piles.
2. For practical purposes, side-by-side piles spaced at 3D or greater experience no group effects. In other words, side-by-side piles spaced at 3D or greater will behave the same as single isolated piles.

#### ***Pile Head Fixity***

Approximately 80 % of the tests described in Table 2.4 were reportedly performed on free-headed piles, with either pinned or “flag pole” boundary conditions. The remaining 20 % of the tests were performed on piles with fixed-head boundary conditions. It is postulated, that the boundary conditions for some of the tests reported in Table 2.4 were partially restrained, rather than fixed or free headed. Significant conclusions regarding the impact of pile head restraint on group efficiency are not possible because of inconsistencies regarding the classification of boundary conditions and the small number of fixed-headed tests. The unequal distribution of boundary

conditions among the tests becomes even more significant when the data is divided into subgroups based on geometric characteristics (i.e., box, in-line, and side-by-side).

Determining the actual degree of fixity under which test piles are loaded is probably a more significant issue than ascertaining the effect that pile-head fixity has on the value of  $G_e$ . To determine  $G_e$  by direct comparison, the boundary condition for the piles in the group should be the same as the single pile boundary condition. If this is not the case, than  $G_e$  may be evaluated inaccurately. For free-headed piles, this determination is not difficult. However, it is very difficult to achieve completely fixed-head conditions for single piles and pile groups. As discussed subsequently in the section on p-multipliers, there are other approaches available for determining  $G_e$  that can be used if the boundary conditions of the group do not match those of the single pile. However, for these methods to yield accurate results, the boundary conditions must be known.

#### *Soil Type and Density*

Sixty-six percent of the tests described in Table 2.4 were performed in sand, 27 % in clay, and 7 % in silt. The results are plotted in Figure 2.10 as a function of soil type, for piles in box arrangements. There does not appear to be any significant trends in this data, except possibly for the tests performed in silty soil. These tests were performed by Prakash and Saran (1967) and appear to yield slightly lower  $G_e$  values than tests performed in clay or sand, at comparable spacings. However, because these were the only tests performed using silty soil and the points are not far below the design line, it seems reasonable to use the same design lines for piles in silt.

The following three studies provide useful information pertaining to the sensitivity of  $G_e$  to soil type or soil density.

- 1.) McVay et al. (1995) performed centrifuge tests on pile groups embedded in loose and medium dense sand at 3D and 5D spacings. From these studies, they

concluded that group efficiency is independent of soil density.

- 2.) Two separate studies were performed on the same 3 by 3 pile group at a site in Texas. The first series of tests were performed with the piles embedded in native clayey soils, and a  $G_e$  of 0.75 was determined (Brown and Reese 1985). The second series of tests were performed after the native soils were replaced with compacted sand. The  $G_e$  determined in this case was 0.77, almost exactly the same as for piles in clay. Thus, changing the soil type from a stiff clay to a medium dense sand had essentially no effect on the measured  $G_e$ .
- 3.) Brown and Shie (1991) investigated group efficiencies using detailed three-dimensional finite element analyses with two different soil models, Von Mises for saturated clay and extended Drucker-Prager for sand. They concluded that the variation in group efficiencies between the two models was too small to warrant consideration in design.

In general, it appears that soil type and soil density do not significantly affect pile group efficiencies.

### ***Pile Displacement***

Group efficiency as defined in Equation 2.11 is independent of pile displacement. It remains to be determined, however, whether  $G_e$  varies with pile displacement, all other things being equal. To gain insight into this question, results from six of the studies described in Table 2.4 were used to calculate values of group efficiency for a range of

pile displacements. The results of these calculations are plotted in Figure 2.11. Based on these plots, it appears that  $G_e$  first decreases as displacement increases, and then becomes constant at deflections in excess of 0.05D (5 % of the pile diameter). The small variations in  $G_e$  at deflections greater than 0.05D fall within the typical range of experimental data scatter, and are insignificant with respect to practical design considerations.

The proposed design curves presented in Figures 2.5 through 2.10 were computed using data for deflections greater than 0.05D. Based on the review of available literature, this appears reasonable, and will yield conservative results for deflections less than 0.05D.

The writer believes that the design curves presented in this section, which are based on the compilation of experimental evidence in Table 2.4, represent the best and most complete values of  $G_e$  that can be currently established. They are recommended as state-of-the-art values for use in analysis and design of laterally loaded pile groups.

## **2.6 P-MULTIPLIERS**

### **2.6.1 Background**

Measurements of displacements and stresses in full-scale and model pile groups indicate that piles in a group carry unequal lateral loads, depending on their location within the group and the spacing between piles. This unequal distribution of load among piles is caused by “shadowing”, which is a term used to describe the overlap of shear zones and consequent reduction of soil resistance. A popular method to account for shadowing is to incorporate p-multipliers into the p-y method of analysis. The p-multiplier values depend on pile position within the group and pile spacing. This section summarizes the current state of knowledge pertaining to p-multipliers, and presents recommendations based on a compilation of available research data.

The concept of  $p$ -multipliers (also called  $f_m$ ) were described by Brown et al. (1988) as a way of accounting for pile group effects by making adjustments to  $p$ - $y$  curves. The multipliers are empirical reduction factors that are experimentally derived from load tests on pile groups. Because they are determined experimentally, the multipliers include both elasticity and shadowing effects. This eliminates the need for a separate  $y$ -multiplier, which is found in many elasticity-based methods. The procedure follows the same approach used in the  $p$ - $y$  method of analysis, except that a multiplier, with a value less than one, is applied to the  $p$ -values of the single pile  $p$ - $y$  curve. This reduces the ultimate soil resistance and softens the shape of the  $p$ - $y$  curve, as shown in Figure 2.2 (b).

Table 2.5 summarizes the results from 11 experimental studies, which present  $p$ -multipliers for pile groups of different sizes and spacings. In these studies, which include 29 separate tests,  $p$ -multipliers were determined through a series of back-calculations using results from instrumented pile-group and single pile load tests. The general procedure for calculating multipliers from load tests results is summarized below.

**Step 1 – Assemble load test data.** Data is required from lateral load tests performed on groups of closely spaced piles and a comparable single pile. At a minimum, the instrumentation program should provide enough data to develop load versus deflection curves for each pile in the group and the single pile. Ideally, the piles will be fully instrumented so that deflections are measured at the top of each pile and strains caused by bending and deformation are measured throughout the length of the piles.

**Step 2 – Develop and adjust single pile  $p$ - $y$  curves.** The goal of this step is to develop a set of  $p$ - $y$  curves that accurately model the soil conditions at the test site based on the measured load response of the single pile. Trial  $p$ - $y$  curves, determined by any suitable method, are adjusted until a good match is obtained between the calculated and the measured response of the single pile.

**Step 3 – Determine  $f_m$  values.** The multipliers are determined in this step through a trial and error process using the  $p$ - $y$  curves developed for the single pile and the measured load versus deflection responses for piles in the group. Trial values of  $f_m$  are adjusted until a good match is obtained between the measured and calculated load versus deflection response curves for each pile.

### 2.6.2 Experimental Studies

Brown and Reese (1985), Morrison and Reese (1986), and McVay et al. (1995) did not detect any significant variation in the response of individual piles within a given row; therefore, they used average response curves for each row of piles rather than attempting to match the response curves for every pile in the group. A similar approach was used by Ruesta and Townsend (1997) and Rollins et al. (1998). In all of these cases, loads were essentially the same for piles in a given row. The current state of practice is thus to use individual row multipliers, rather than separate multipliers for each pile. This approach was followed in all of the studies reported in Table 2.5.

The similarity in behavior between piles in a row is attributed to the pile spacing, which ranged from 3D to 5D in the studies described herein. As discussed in the group efficiency section (see Figure 2.9), side-by-side piles at spacings greater than or equal to 3D are not affected by adjacent piles in the same row. However, at spacings less than 3D, the outer corner piles will take a greater share of load than the interior piles, as demonstrated in Franke's (1988) model tests, and as supported by elasticity-based methods (Poulos 1971b). This implies that corner piles will experience greater bending moments and stresses than interior piles at spacings less than 3D. Ignoring this behavior is unconservative, and could result in overstressed corner piles (in the leading row) for piles spaced at less than 3D.

Franke (1988) performed model tests on 3 side-by-side piles and measured the load that was taken up by each pile. At 3D spacing, the load distribution between the corner piles and center pile was the same. At 2D spacing the corner piles resisted 20 %

more load than the center pile, and at 1D spacing the corner piles resisted 60 % more load.

The generally accepted approach is to assumed that  $p$ -multipliers are constant with depth. That is, a constant  $p$ -multiplier is applied to the set of  $p$ - $y$  curves for all depths in a given pile row. Thus, individual  $p$ - $y$  curves for a pile are adjusted by the same amount, regardless of variations in the soil profile or depth below the ground surface.

The suitability of this assumption was investigated by Brown et al. (1988) during large-scale tests performed on fully instrumented piles. They reported back-calculated  $f_m$  values along the length of three piles, one from each row of the group. As shown in Figure 2.12, variation of  $f_m$  was small and had no affect on the calculated response curve. In reality, the  $p$ - $y$  modifier approach uses an average multiplier that is determined by back-calculating an overall response curve. The modifier is adjusted until the calculated response curve matches the measured response curve. Thus, assuming a constant value of  $f_m$  with depth is reasonable, because the variation of  $f_m$  is implicitly accounted for during the back-calculation procedure.

The test results summarized in Table 2.5 clearly show that the lateral capacity of a pile in a group is most significantly affected by its row position (leading row, first trailing row, etc.) and the center to center pile spacing. The leading row carries more load than subsequent rows; consequently, it has the highest multiplier. Multipliers experimentally measured in these studies are plotted in Figures 2.13 and 2.14 as a function of pile spacing. Figure 2.13 (a) contains data for the leading row, Figure 2.13 (b) the first trailing row, Figure 2.14 (a) the second trailing row, and Figure 2.14 (b) the third and subsequent trailing rows.

Conservative design curves were fitted to the data points using engineering judgement. The four  $f_m$  curves are plotted together in Figure 2.15, which is presented as a proposed design aid. Tests by McVay et al, (1997) indicate that  $f_m$  is essentially the



same for the third, fourth, and subsequent trailing rows. Thus, it appears reasonable to use the 3<sup>rd</sup> trailing row multiplier for the 4<sup>th</sup> pile row and all subsequent rows.

The bending moments computed for the corner piles should be increased if the spacing normal to the direction of load (side-by-side spacing) is less than 3D. Based on the load distributions that were measured by Franke (1988), the bending moments computed using the p-multipliers presented in Figure 2.15 should be adjusted as follows for the corner piles:

<u>side-by-side spacing</u>	<u>corner pile moment modification factor</u>
3D	1.0
2D	1.2
1D	1.6

### 2.6.3 Relationship Between $f_m$ and $G_e$

The overall pile group efficiency,  $G_e$ , can be calculated if the p-multipliers for each row are known, as shown by Equation 2.12.

$$G_e = \frac{\sum_{i=1}^N f_{mi}}{N} \quad \text{Equation 2.12}$$

Where  $N$  is the number of rows in the direction of load and  $f_{mi}$  is the p-multiplier for row  $i$ . Equation 2.12 was used to calculate group efficiencies for seven of the studies reported in Table 2.5. For the purpose of this discussion, the approach used in Equation 2.11 is designated Method A and the approach represented by Equation 2.12 is designated Method B. Group efficiencies calculated using Method A and Method B are plotted together in Figure 2.16, along with the proposed design curve. Method A data points are shown as open squares and Method B points are shown as solid squares.

Group efficiencies calculated using the two different equations should theoretically be the same, and it can be seen that the two approaches yield similar results. However, there can be some discrepancy when results obtained from the two equations are compared. Discrepancies can arise as a result of inconsistencies in matching the single pile and the pile group boundary conditions.

When Method A (Equation 2.11) is used, a direct comparison is made between the resistance of a single pile and the resistance of a pile within the group at a given deflection. However, a direct comparison is not valid unless the pile-head fixity conditions of the single pile are identical to those of the group pile. This is practically impossible. Thus, either analytical adjustments are incorporated into the evaluation, or the difference is simply ignored. If analytical adjustments are used, an estimate of the degree of fixity of both the single pile and group pile is required.

A similar type of judgement regarding pile-head fixity is required for Method B, where  $G_e$  is determined from Equation 2.12. The pile-head boundary condition of the single pile must be estimated when the initial single pile p-y curve is developed. Likewise, pile-head boundary conditions for the group pile must be assumed when  $f_m$  is evaluated during the back-calculation procedure. One way to reduce the uncertainties of these assumptions is to develop the initial set of p-y curves by testing a free-headed single pile, because the free-headed single pile boundary condition is not difficult to obtain in the field. Values of  $f_m$  can then be determined for either a pinned- or fixed-headed group by applying the appropriate boundary conditions during the back-calculation step of the procedure.

The design curves (or design lines, since a linear approximation was assumed) in Figures 2.5, 2.6, 2.7, 2.8, 2.9, 2.10, 2.13, and 2.14 are considered suitable for all except the largest projects, where lateral load behavior of pile groups is an extremely critical issue. For projects where the expense can be justified, these curves can be verified or improved by performing on-site full-scale load tests on groups of instrumented piles.

## 2.7 PILE GROUP BEHAVIOR – ANALYTICAL STUDIES

### 2.7.1 Background

Single pile analytical techniques are not sufficient in themselves to analyze piles within a closely spaced group because of pile-soil-pile interactions and shadowing effects. Numerous methods have been proposed over the last 30 years for evaluating the lateral resistance of piles within a closely spaced group. Table A.2 (Appendix A) summarizes many of these methods, which are classified under four categories, as:

1. closed-form analytical approaches,
2. elasticity methods,
3. hybrid methods, and
4. finite element methods.

Pertinent features of these approaches are described in the following paragraphs.

### 2.7.2 Closed-Form Analytical Approaches

Many of the methods in this category combine empirical modifying factors with single-pile analytical techniques. The oldest techniques simply involve applying a group efficiency factor to the coefficient of subgrade reaction. Kim (1969) used this approach to model the soil and replaced the pile with an equivalent cantilever beam. Bogard and Matlock (1983) used a group efficiency factor to soften the soil response and modeled the pile group as an equivalent large pile. This method is similar to the  $p$ -multiplier approach, which was described in the Section 2.6.

### 2.7.3 Elasticity Methods

Methods that fall into this category model the soil around the piles as a three-dimensional, linearly elastic continuum. Mindlin's equations for a homogenous,

isotropic, semi-infinite solid are used to calculate deformations. This is similar to the single pile approach except elastic interaction factors are incorporated into the analyses. These factors are used to address the added displacements and rotations of a pile within a group caused by movements of adjacent piles.

In the original approach used by Poulos (1971b), the expression for single pile deflection, Equation 2.10, was modified for pile-soil-pile interaction effects by including the influence factors,  $\mathbf{a}_r$  and  $\mathbf{a}_q$ , to account for the additional horizontal displacements and rotations of pile  $i$  caused by displacement of pile  $j$ . These factors were defined as follows:

$$\mathbf{a}_r = \frac{\text{additional displacement caused by adjacent pile}}{\text{displacement of pile caused by its own loading}}$$

$$\mathbf{a}_q = \frac{\text{additional rotation caused by adjacent pile}}{\text{rotation of pile caused by its own loading}}$$

Poulos and Davis (1980) present the interaction factors in chart form for various conditions. The displacement and rotations of any pile in the group is obtained using the principle of superposition. This implies that the increase in displacement of a pile due to all the surrounding piles can be calculated by summing the increases in displacement due to each pile in turn using interaction factors (Poulos 1971b).

Using the principle of superposition, the displacement of a pile within a group,  $y_k$ , is determined by modifying the single pile equation (Equation 2.10) using the interaction factors and the principle of superposition. The deflection of pile  $k$ , within a group is given by:

$$y_k = y_s \left[ \sum_{j=1}^n (p_j \mathbf{a}_{kj}) + p_k \right] \quad \text{Equation 2.13}$$

where  $y_s$  is the displacement of a single pile,  $p_j$  is the load on pile  $j$ ,  $a_{kj}$  is the interaction factor corresponding to the spacing and angle between piles  $k$  and  $j$ ,  $n$  is the number of piles in the group, and  $p_k$  is the load on pile  $k$ .

The total load on the group,  $p_g$ , is determined by superposition as:

$$p_g = \sum_{j=1}^n p_j \quad \text{Equation 2.14}$$

In addition to Poulos's chart solutions, there are a number of computer programs available including: PIGLET, DEFPIG, and PILGPI (Poulos 1989).

Other elastic continuum methods are available that use numerical techniques in place of Mindlin's equations. These include the boundary element method (Banerjee and Davies, 1978 and 1979), algebraic equations fitted to finite element results (Randolph 1981), numerical procedures (Iyer and Sam 1991), semi-empirical methods using radial strain components (Clemente and Sayed 1991), and finite element methods (discussed under a separate heading).

#### 2.7.4 Hybrid Methods

These methods are called hybrid because they combine the nonlinear  $p$ - $y$  method with the elastic continuum approach.  $p$ - $y$  curves are used to model the component of soil deflection that occurs close to individual piles (shadow effect) and elastic continuum methods are used to approximate the effects of pile-soil interaction in the less highly stressed soil further from the piles. Focht and Koch (1973) developed the original hybrid procedure in which elasticity-based  $\alpha$ -factors are used in conjunction with  $y$ -multipliers. Reese et al. (1984) modified the Focht-Koch approach by using solutions from  $p$ - $y$  analyses to estimate elastic deflections where load-deflection behavior is linear. O'Neill et al. (1977) modified the Focht-Koch approach by adjusting unit-load transfer curves individually to account for stresses induced by adjacent piles. Additional hybrid

approaches include Garassino's (1994) iterative elasticity method and Ooi and Duncan's (1994) group amplification procedure.

### 2.7.5 Finite Element Methods

Finite element approaches typically model the soil as a continuum. Pile displacements and stresses are evaluated by solving the classic beam bending equation (Equation 2.3) using one of the standard numerical methods such as Galerkin (Iyer and Sam 1991), collocation, or Rayleigh-Ritz (Kishida and Nakai 1977). Various types of elements are used to represent the different structural components. For instance, the computer program Florida Pier (McVay et al. 1996) uses three-dimensional two-node beam elements to model the piles, pier columns, and pier cap, and three-dimensional 9-node flat shell elements for the pile cap. Interface elements are often used to model the soil-pile interface. These elements provide for frictional behavior when there is contact between pile and soil, and do not allow transmittal of forces across the interface when the pile is separated from the soil (Brown and Shie 1991).

Another finite element computer program that has been used to analyze pile groups is the computer program GPILE-3D by Kimura et al. (1995). Kimura and his co-workers initially used column elements in the computer program to represent the piles. They later discovered that column elements alone were not sufficient to adequately model the response of pile groups; thus, subsequent modifications were made to their computer code to model the piles with both beam and column elements. They found that using this combination of elements with the Cholesky resolution method allowed them to better simulate the load-displacement relationship of a nonlinear pile in a 3-D analysis.

The soil stress-strain relationship incorporated into the finite element model is one of the primary items that delineate the various finite element approaches. This relationship may consist of a relatively straightforward approach using the subgrade reaction concept with constant or linearly varying moduli, or a complex variation of the elastic continuum method. For instance, Sogge's (1984) one-dimensional approach

models the soil as a discrete series of springs with a stiffness equivalent to the modulus of subgrade reaction. Sogge used the modulus of subgrade reaction, as defined in Equation 2.5, to develop  $p$ - $y$  curves for input into the computer model.

Desai et al. (1980) used a much more rigorous approach to calculate the soil modulus in their two-dimensional approach. They calculated nonlinear  $p$ - $y$  curves using the tangent modulus,  $E_{st}$ , obtained from a modified form of the Ramberg-Osgood model. Brown and Shie (1991) performed a three-dimensional study using a simple elastic-plastic constant yield strength envelope (Von Mises surface) to model a saturated clay soil and a modified Drucker-Prager model with a nonassociated flow rule for sands.

Adachi et al. (1994) performed a 3-D elasto-plastic analysis using a Drucker-Prager yield surface for the soil and a nonlinear model (trilinear curve) for the concrete piles, which accounted for the decrease in bending rigidity and cracking at higher loads. The pile response was modeled using a bending moment versus pile curvature relationship with three points of deflection, defined as: (1) the initial cracking point of the concrete, (2) the yield point of the reinforcing steel, and (3) the ultimate concrete capacity. A hyperbolic equation was fit to the three points to obtain a smooth curve for the computer analysis.

The current trend in finite element analyses is the development of more user-friendly programs such as Florida Pier (Hoit et al. 1997). The developers of these programs have attempted to overcome some of the difficulties that practicing engineers have with the finite element method by incorporating interactive graphical pre- and post-processors. For instance, in Florida Pier the finite element mesh is internally created in the pre-processor based on the problem geometry. Florida Pier's post-processor displays the undeflected and deflected shape of the structure, along with internal forces, stresses, and moments in the piles and pier columns.

## **2.8 SUMMARY**

A comprehensive literature review was conducted to examine the current state of knowledge regarding pile cap resistance and pile group behavior. Over 350 journal articles and other publications pertaining to lateral resistance, testing, and analysis of pile caps, piles, and pile groups were collected and reviewed. Pertinent details from these studies were evaluated and, whenever possible, assimilated into tables and charts so that useful trends and similarities can readily be observed.

Of the publications reviewed, only four papers were found that described load tests performed to investigate the lateral resistance of pile caps. These studies indicate that the lateral resistance of pile caps can be quite significant, especially when the cap is embedded beneath the ground surface.

A review of the most widely recognized techniques for analyzing laterally loaded single piles was provided. These techniques provide a framework for methods that are used to evaluate the response of closely spaced piles, or pile groups. Modifications of single pile techniques are often in the form of empirically or theoretically derived factors that are applied, in various ways, to account for group interaction effects.

Piles in closely spaced groups behave differently than single isolated piles because of pile-soil-pile interactions that take place in the group. Deflections and bending moments of piles in closely spaced groups are greater than deflections and bending moments of single piles, at the same load per pile, because of these interaction effects.

The current state of practice regarding pile group behavior was reviewed from an experimental and analytical basis. Thirty-seven experimental studies were reviewed in which the effects of pile group behavior were observed and measured. These included 15 full-scale field tests, 16 1g model tests, and 6 geotechnical centrifuge tests. Approximately 30 analytical studies were reviewed that addressed pile group lateral



behavior. These studies included closed-form analytical approaches, elasticity methods, hybrid methods, and finite element methods.

Based on these studies, the following factors were evaluated to determine their influence on pile group behavior, and more specifically, pile group efficiency ( $G_e$ ).

1. **Pile spacing.** Pile spacing is the most dominant factor affecting pile group behavior. Group effects are negligible when center to center pile spacing exceeds 6 pile diameters (6D) in the direction of load and when they exceed 3D measured in a direction normal to load. The efficiency of a pile group decreases as pile spacings drop below these values.
2. **Group arrangement.** After pile spacing, the next most significant factor appears to be the geometric arrangement of piles within the group. Group efficiencies were evaluated for the three most common geometric arrangements used in practice, which are defined in Figure 2.3 as: box arrangement, in-line arrangement, and side-by-side arrangement.
3. **Group Size.** The effect of group size on piles in box arrangements or side-by-side arrangements could not be discerned from the data available. Sufficient data was available to evaluate the influence of group size on in-line arrangements of piles, as shown in Figure 2.7. At a given spacing, the group efficiency decreases as the number of piles in a line increase.
4. **Pile head fixity.** Significant conclusions regarding the impact of pile head restraint on group efficiency were not possible because of limited experimental data. However, quantifying the actual degree of fixity under which test piles are loaded is probably a more significant issue than ascertaining the effect that pile-head fixity has on the value of group efficiency.

5. **Soil type and density.** Based on the evaluation of 37 experimental studies in different soils, there is no significant relationship between soil type or density and group efficiency.
6. **Pile displacement.** The influence of pile displacement on group efficiency ( $G_e$ ) was evaluated using the results from six experimental studies. As shown in Figure 2.11,  $G_e$  first decreases as displacement increases, and then becomes constant at deflections in excess of 0.05D (5 % of the pile diameter). The small variations in  $G_e$  at deflections greater than 0.05D fall within the typical range of experimental data scatter, and are insignificant with respect to practical design considerations.

Measurements of displacements and stresses in full-scale and model pile groups indicate that piles in a group carry unequal lateral loads, depending on their location within the group and the spacing between piles. This unequal distribution of load among piles is caused by “shadowing”, which is a term used to describe the overlap of shear zones and consequent reduction of soil resistance. A popular method to account for shadowing is to incorporate p-multipliers ( $f_m$ ) into the p-y method of analysis. The p-multiplier values depend on pile position within the group and pile spacing. The multipliers are empirical reduction factors that are experimentally derived from load tests on pile groups. Because they are determined experimentally, the multipliers include both elasticity and shadowing effects.

The results from 11 experimental studies were reviewed in which p-multipliers for pile groups of different sizes and spacings were developed. In these studies, which include 29 separate tests, p-multipliers were determined through a series of back-calculations using results from instrumented pile-groups and single pile load tests.

Multipliers applied to p-y curves and group efficiency factors represent two approaches for quantifying group interaction effects. Because these approaches theoretically represent the same phenomenon, the factors summarized above for

empirically derived  $G_e$  values apply equally as well to the empirically derived  $f_m$  values. Three additional factors that are more specific to p-multipliers are summarized below:

1. **Depth.** The p-y modifier approach uses an average multiplier that is determined by back-calculating an overall response curve. The modifier is adjusted until the calculated response curve matches the measured response curve. Thus, assuming a constant value of  $f_m$  with depth is reasonable, because the variation of  $f_m$  is implicitly accounted for during the back-calculation procedure.
2. **Row position.** The lateral capacity of a pile in a group is significantly affected by its row position (leading row, first trailing row, etc.) and the center to center pile spacing. The leading row carries more load than subsequent rows; consequently, it has the highest multiplier. Multipliers decrease going from the leading to the trailing row, which has the lowest multiplier.
3. **Corner pile effects.** At spacings less than  $3D$ , the outer corner piles will take a greater share of load than interior piles, and consequently, will experience greater bending moments and stresses. Ignoring this behavior is unconservative, and could result in overstressed corner piles. Recommendations were presented for modifying bending moments computed for the corner piles if the spacing normal to the direction of load (side-by-side spacing) is less than  $3D$ .

Design lines were developed for estimating pile group efficiency values and p-multipliers as functions of pile arrangement and pile spacing. To the extent possible, the lines account for the factors described above. The design lines are presented in chart form, as follows:

- Group efficiency versus pile spacing for piles in a box arrangement – Figure 2.5.

- Group efficiency versus pile spacing for piles oriented in-line – Figure 2.7.
- Group efficiency versus pile spacing for piles oriented side-by-side – Figure 2.9.
- p-multipliers for the leading row, 1<sup>st</sup> trailing row, 2<sup>nd</sup> trailing row, and 3<sup>rd</sup> and subsequent trailing rows – Figure 2.15.

These design lines represent state-of-the-art values for use in analysis and design of laterally loaded pile groups. The writer believes that these lines are suitable for all except the largest projects, where lateral load behavior of pile groups is an extremely critical issue. For projects where the expense can be justified, these lines can be verified or improved by performing full-scale load tests on groups of instrumented piles.

Table 2.1. Summary of previous load tests performed to evaluate the lateral resistance of pile caps.

Reference	Pile Type	Cap Size	Foundation Soils	Cap Contribution*
Beatty 1970	2 x 3 group of step-tapered mandrel driven concrete piles	not reported	miscellaneous fill over soft silty clay and clay	more than 50%
Kim and Singh 1974	2 x 3 group of 10BP42 steel piles	12' long x 8' wide x 4' thick	silty and sandy clay, with $S_{uavg} \approx 1$ tsf in top 15'	about 50%
Rollins et al. 1997	3 x 3 group of 12" dia. steel pipe piles	9' long x 9' wide x 4' thick	compacted sandy gravel fill over silt and clay	about 50%
Zafir and Vanderpool 1998	2 x 2 group of 2' dia. drilled shafts	11' diameter by 10' thick	silty sand, clayey sand, and sandy clay with caliche layers	more than 50%

\* "Cap Contribution" reflects the approximate contribution of the pile cap to the lateral load resistance of the pile group at a given lateral deflection.

Table 2.2 Summary of full-scale field test details.

<b>Pile Type</b>	<b>Installation Method</b>	<b>Soil Type</b>	<b>Pile Head Boundary Condition</b>
steel – 9	driven – 13	sand – 8	fixed-head – 6
concrete – 4	bored - 3	clay - 6	free-head – 5
timber - 4	–	not reported - 1	pinned-head - 5

Table 2.3 Geotechnical centrifuge facility details.

<b>Reference</b>	<b>Facility Location</b>	<b>Approx. Arm Radius (ft)</b>	<b>Test Acceleration (gravity)</b>	<b>Container Capacity (ft<sup>3</sup>)</b>
Barton (1984)	Cambridge, England	13	30g to 120g	8
Zhang and Hu (1991)	S.W. Institute of Mechanics, China	35	50g	not reported
Adachi et al. (1994)	Kyoto University, Japan	8	40g	2
McVay et al. (1994, 1995, 1998)	University of Florida, USA	5	45g	1.25

Table 2.4. Summary of pile group efficiency test data.

Reference	Group arrangement	Group size	c/c pile spacing	$G_e$	Type of test	Pile type	Soil	Deflection (dia.)
Prakash and Saran (1967)	box	2x2	3D	0.48	1g model fixed-head	0.355 in dia. aluminum tube	silt (ML) strength not reported	0.11D
		2x2	4D	0.66				
		2x2	5D	0.78				
		3x3	3D	0.49				
		3x3	4D	0.59				
		3x3	5D	0.63				
Cox et al. (1984)	in-line	1x3	1.5D	0.59	1g model free-head	1.0 in dia. steel tube	v. soft clay $S_u = .042$ ksf	0.2D
		1x3	2D	0.70				
		1x3	3D	0.81				
		1x3	4D	0.86				
		1x3	6D	0.95				
		1x5	1.5D	0.54				
		1x5	2D	0.59				
		1x5	3D	0.78				
Cox et al. (1984)	side-by-side	3x1	1.5D	0.76	1g model free-head	2.0 in dia. steel tube	v. soft clay $S_u = .042$ ksf	0.2D
		3x1	2D	0.85				
		3x1	4D	0.99				
		5x1	1.5D	0.80				
		5x1	2D	0.85				
		5x1	3D	0.98				
Brown and Reese (1985)	box	3x3	3D	0.75	full scale field free-head	10.75 in dia pipe piles.	stiff OC clay $S_u = 1.2$ to 1.7 ksf	0.05D

Table 2.4. Continued.

Reference	Group arrangement	Group size	c/c pile spacing	$G_e$	Type of test	Pile type	Soil	Deflection (dia.)
Sarsby (1985)	in-line	1x2	2D	0.70	1g model free-head	0.24 in dia. mild steel bars	sand (SP) $\phi = 38^\circ$	extrapo- lated to zero
		1x2	4D	0.78				
		1x2	8D	0.84				
		1x2	12D	0.90				
		1x3	2D	0.66				
		1x3	4D	0.74				
		1x3	8D	0.82				
		1x3	12D	0.84				
		1x4	2D	0.64				
		1x4	4D	0.74				
1x4	8D	0.80						
Morrison and Reese (1986)	box	3x3	3D	0.77	full scale field free-head	10.75 in dia pipe piles.	med. dense sand $D_r = 50\%$ $\phi = 38.5^\circ$	0.05D
Franke (1988)	in-line	1x3	2D	0.60	1g model free-head	0.16 in dia. type not reported	fine sand $D_r$ not reported	not reported
		1x3	3D	0.65				
		1x3	4D	0.80				
		1x3	6D	1.0				
Franke (1988)	side-by-side	3x1	1D	0.74	1g model free-head	0.16 in dia. type not reported	fine sand $D_r$ not reported	not reported
		3x1	2D	0.85				
		3x1	3D	1.0				
		3x1	4D	1.0				



Table 2.4. Continued.

Reference	Group arrangement	Group size	c/c pile spacing	$G_e$	Type of test	Pile type	Soil	Deflection (dia.)
Lieng (1989)	in-line	1x2	2D	0.77	1g model free-head	5.9 in dia. aluminum pipes	dry loose sand $D_r$ not reported	0.03D to 0.05D
		1x2	3D	0.93				
		1x2	4D	0.94				
		1x2	5D	0.99				
Lieng (1989)	side-by-side	2x1	2D	0.92	1g model free-head	5.9 in dia. aluminum pipes	dry loose sand $D_r$ not reported	0.07D to 0.13D
		2x1	3D	1.0				
		2x1	4D	1.0				
Shibata et al. (1989)	in-line	1x2	2D	0.75	1g model free-head	0.87 in dia. aluminum tubes	uniform sand $D_r = 20\%$	0.1D to 0.3D
		1x2	2.5D	0.76				
		1x2	5D	1.0				
Shibata et al. (1989)	side-by-side	4x1	2D	0.62	1g model free-head	0.87 in dia. aluminum tubes	uniform sand $D_r = 20\%$	0.1D to 0.3D
		4x1	2.5D	0.75				
		4x1	5D	1.0				
Shibata et al. (1989)	box	3x3	2D	0.40	1g model free-head	0.87 in dia. aluminum tubes	uniform sand $D_r = 20\%$	0.1D to 0.3D
		3x3	2.5D	0.45				
		3x3	5D	0.70				
		4x4	2D	0.34				
		4x4	2.5D	0.40				
		4x4	5D	0.70				

Table 2.4. Continued.

Reference	Group arrangement	Group size	c/c pile spacing	$G_e$	Type of test	Pile type	Soil	Deflection (dia.)
Shibata et al. (1989)	box	3x3	2D	0.58	1g model free-head	0.87 in dia. chloridized-vinyl tubes	uniform sand $D_r = 20\%$	0.1D to 0.3D
		3x3	2.5D	0.78				
		3x3	5D	1.0				
		4x4	2D	0.43				
		4x4	2.5D	0.60				
		4x4	5D	0.98				
Adachi et al. (1994)	in-line	1x2	2D	0.81	40g centrifuge pinned-head	63 in dia. prototype	v. dense sand $D_r = 90\%$	0.07D to 0.10D
			4D	0.92				
Adachi et al. (1994)	side-by-side	2x1	2D	0.92	40g centrifuge pinned-head	63 in dia. prototype	v. dense sand $D_r = 90\%$	0.07D to 0.10D
			4D	1.0				
Kotthaus et al. (1994)	in-line	1x3	3D	0.70	50g centrifuge fixed-head	59 in dia. prototype	v. dense sand $D_r = 98\%$ $\phi = 38^\circ$	0.10D
		1x3	4D	0.83				
McVay et al. (1994, 1995)	box	3x3	3D	0.73	45g centrifuge free-head	17 in dia. prototype	loose sand $D_r = 33\%$	0.15D
		3x3	5D	0.92				
McVay et al. (1994, 1995)	box	3x3	3D	0.74	45g centrifuge free-head	17 in dia. prototype	med. dense sand $D_r = 55\%$	0.15D
		3x3	5D	0.95				

Table 2.4. Concluded.

Reference	Group arrangement	Group size	c/c pile spacing	$G_e$	Type of test	Pile type	Soil	Deflection (dia.)
Rao et al. (1996)	in-line	1x2	3D	0.78	1g model fixed head	0.85 in dia. mild steel pipes	marine clay (CH) $S_u=1.8$ ksf	0.47D
		1x2	4D	0.96				
		1x2	5D	0.99				
		1x2	6D	1.05				
Rao et al. (1996)	in-line	2x1	3D	0.97	1g model fixed head	0.85 in dia. mild steel pipes	marine clay (CH) $S_u=1.8$ ksf	0.47D
		2x1	4D	0.99				
		2x1	5D	1.0				
Ruesta and Townsend (1997)	box	4x4	3D	0.80	full-scale free-head	30 in square prestressed concrete	loose fine sand $D_r = 30\%$ $\phi = 32^\circ$	0.05D to 0.1D
Rollins et al. (1998)	box	3x3	3D	0.67	full-scale pinned-head	12 in dia. steel pipe	CL-ML and CL $S_u = .5$ to 1.0 ksf	0.065D

Table 2.5. Summary of p-multiplier ( $f_m$ ) test data.

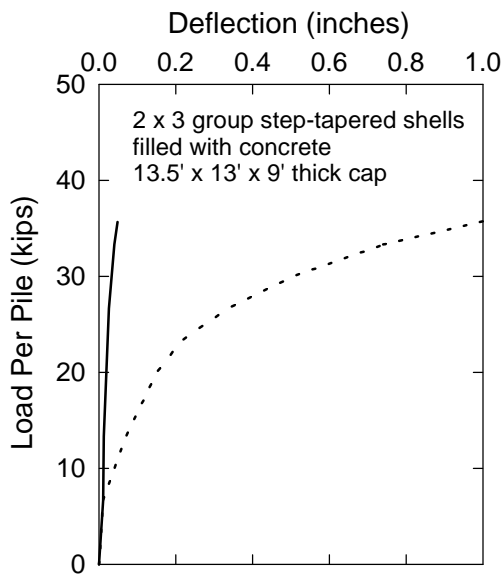
Reference and soil type	Pile size and arrangement	c/c pile spacing (dia.)	Deflection range (diameter)	$G_e$	p-multiplier ( $f_m$ )				
					Leading row	1 <sup>st</sup> trailing row	2 <sup>nd</sup> trailing row	3 <sup>rd</sup> trailing row	4 <sup>th</sup> trailing row
Cox et al. (1984), very soft clay	1 in dia., in-line 1x4 and 1x3	1.5D 2D 3D 4D 6D	0 to 0.25D	0.53	0.77	0.50	0.40	0.47	
				0.59	0.80	0.53	0.55	0.49	
				0.81	0.96	0.77	0.77	0.74	
				0.89	0.97	0.87	0.84	--	
				0.95	1.00	0.92	0.92	--	
Brown and Reese (1985), stiff clay	10.75 in dia., box 3x3	3D	0 to 0.23D	0.60	0.70	0.60	0.50		
Meimon et al. (1986), stiff silty clay	11 in square, 2 piles in-line	3D	0 to 0.1D	0.70	0.90	0.50			
Morrison and Reese (1986), med. dense sand	10.75 in dia., box 3x3	3D	0 to 0.23D	0.50	0.80	0.40	0.30		

Table 2.5. Continued.

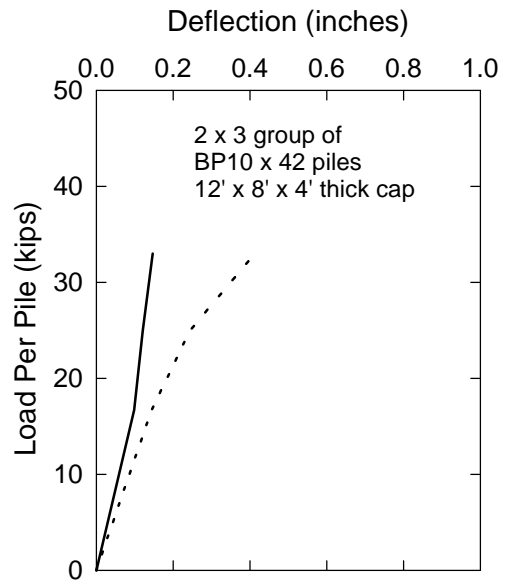
Reference and soil type	Pile size and arrangement	c/c pile spacing (dia.)	Deflection range (diameter)	$G_e$	p-multiplier ( $f_m$ )				
					Leading row	1 <sup>st</sup> trailing row	2 <sup>nd</sup> trailing row	3 <sup>rd</sup> trailing row	4 <sup>th</sup> trailing row
Lieng (1989), loose sand	5.9 in dia., 2 piles in-line	2D 3D 4D 5D 6D	0 to 0.13D	--	not measured	0.33 0.60 0.80 0.93 1.0			
Brown and Shie (1991), computed-FEM, avg. soil	10.75 in dia., 2 piles in-line	2D 3D 5D	0 to 0.14D	-- 0.70 0.90	0.80 0.90 1.0	-- 0.50 0.80			
McVay et al. (1994, 1995), loose sand	16.88 in dia, box. 3x3	3D 5D	0 to 0.14D 0 to 0.20D	0.48 0.85	0.65 1.0	0.45 0.85	0.35 0.70		
McVay et al. (1994, 1995), med. dense sand	16.88 in dia, box. 3x3	3D 5D	0 to 0.16D 0 to 0.19D	0.50 0.85	0.80 1.0	0.40 0.85	0.30 0.70		

Table 2.5. Concluded

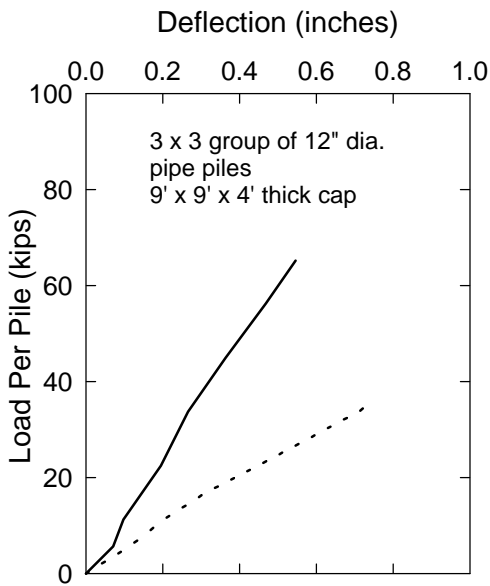
Reference and soil type	Pile size and arrangement	c/c pile spacing (dia.)	Deflection range (diameter)	$G_e$	p-multiplier ( $f_m$ )				
					Leading row	1 <sup>st</sup> trailing row	2 <sup>nd</sup> trailing row	3 <sup>rd</sup> trailing row	4 <sup>th</sup> trailing row
Ruesta and Townsend (1997), loose sand	30 in square, box 4x4	3D	0 to 0.10D	0.53	0.80	0.70	0.30	0.30	
McVay et al. (1998), med. dense sand	16.88 in dia., box 3x3 to 3x7	3D	0 to 0.20D	0.50	0.80	0.40	0.30	--	--
		3D	0 to 0.26D	.045	0.80	0.40	0.30	0.30	--
		3D	0 to 0.27D	0.40	0.80	0.40	0.30	0.20	0.30
		3D	0 to 0.26D	0.38	0.80	0.40	0.30	0.20	0.20
		3D	0 to 0.20D	0.34	0.80	0.40	0.30	0.20	0.20
McVay et al. (1998), continued		3x3	<i>continued from previous row</i>				--	<b>5<sup>th</sup> trailing row</b>	<b>6<sup>th</sup> trailing row</b>
		3x4					--		
		3x5					--		
		3x6					3x6	0.30	--
		3x7					3x7	0.20	0.30
Rollins et al. (1998), clayey silt	12 in dia. box 3x3	3D	0 to 0.19D	0.47	0.60	0.40	0.40		



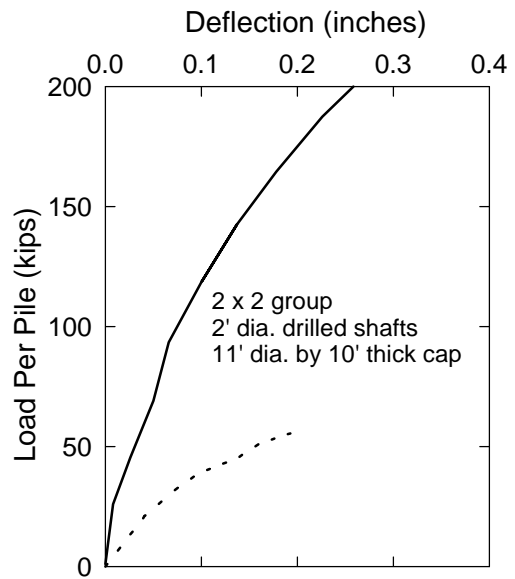
(a) Beatty, 1970.



(b) Kim and Singh, 1974.



(c) Rollins et al., 1997.



(d) Zafir and Vanderpool, 1998.

Legend for all 4 plots

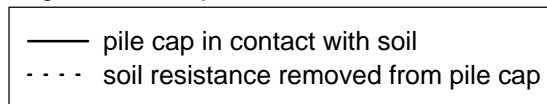
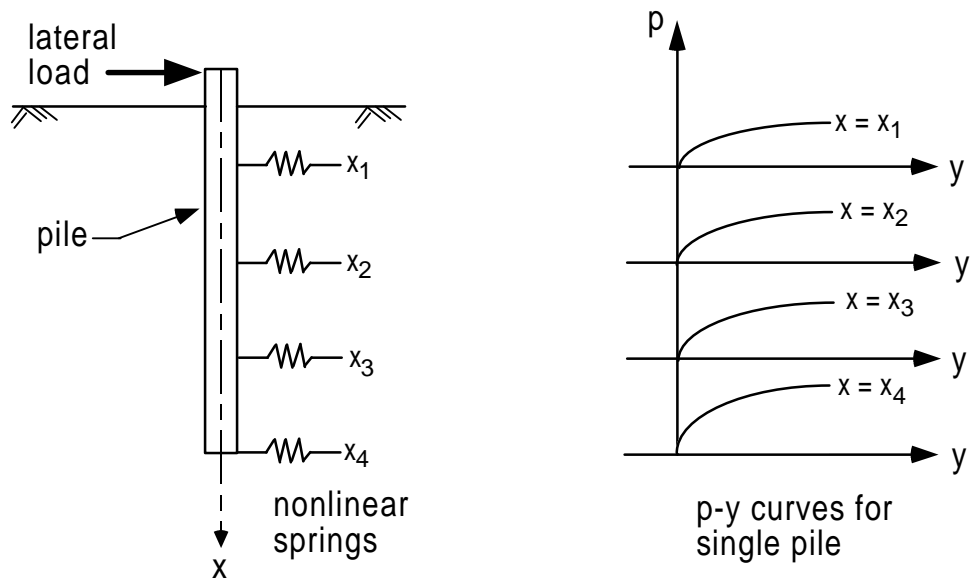
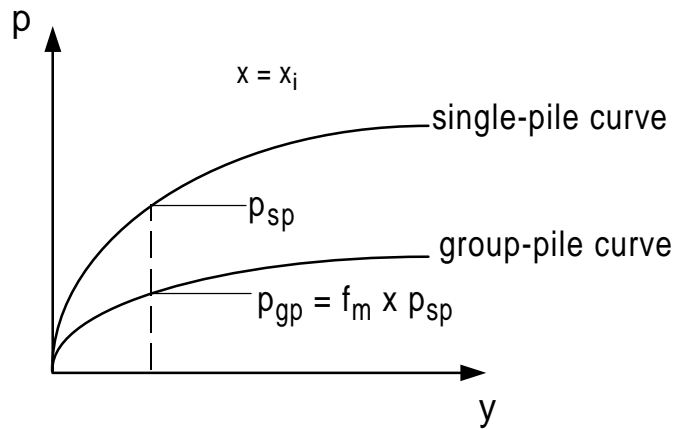


Figure 2.1. Comparison of published load versus deflection curves.



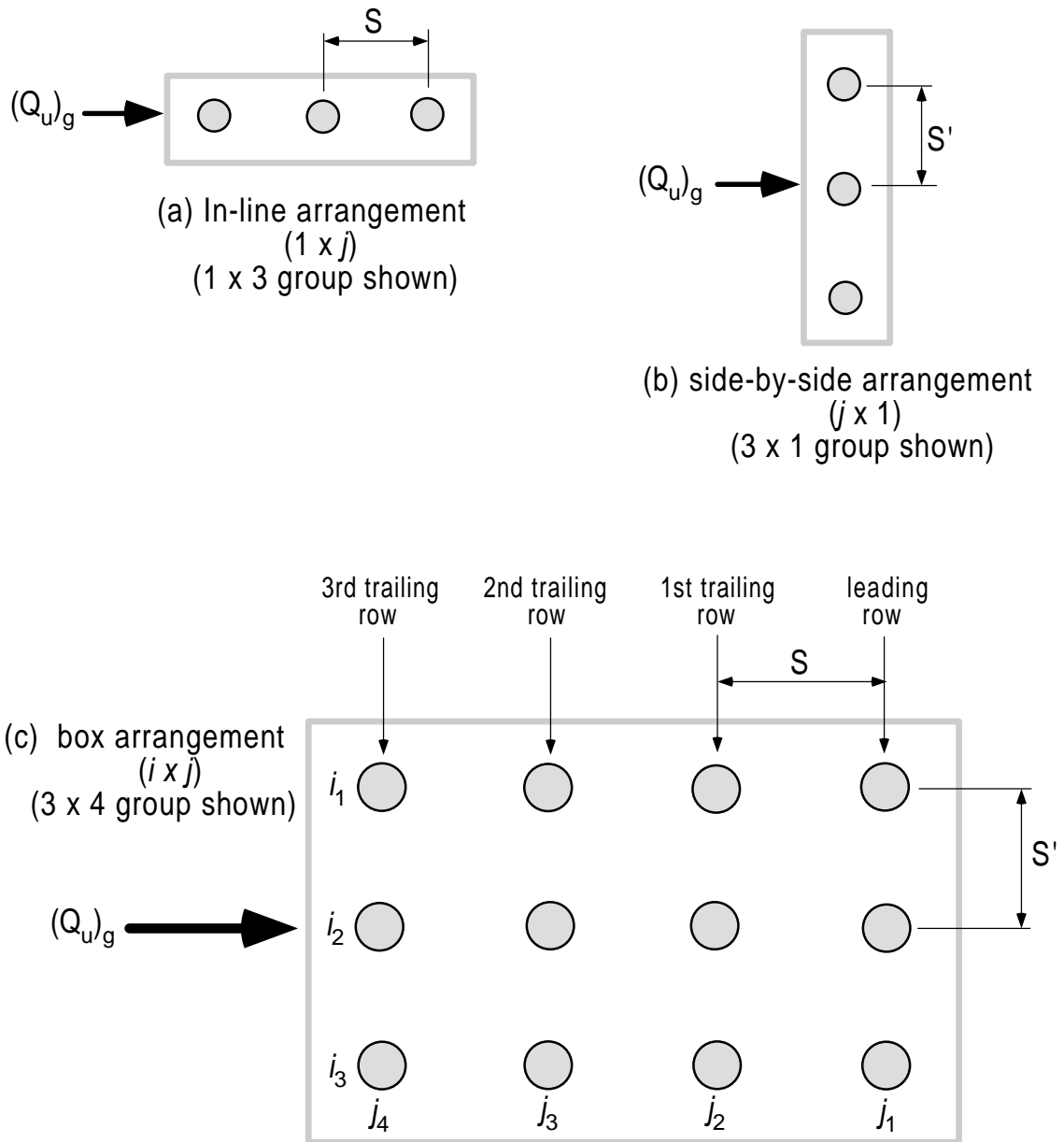
(a) Single pile model.



(b) P-multiplier concept for lateral group analysis.

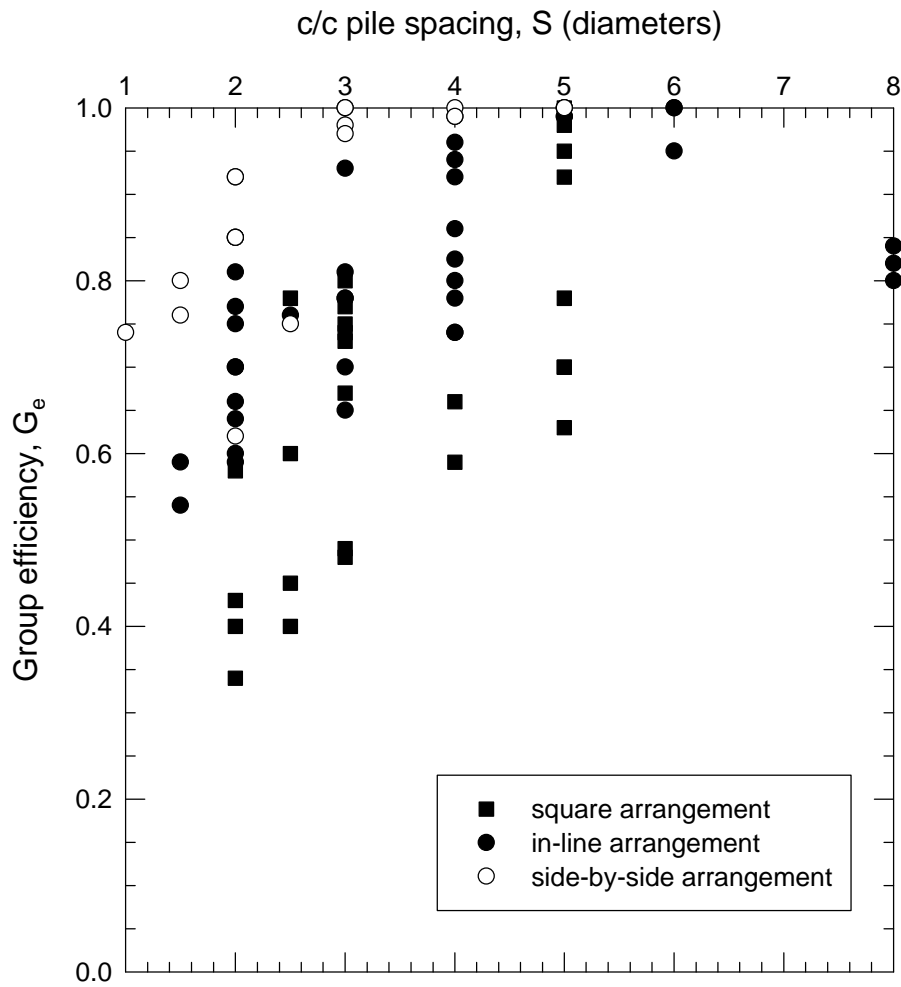
Figure 2.2. p-y Models for laterally loaded piles.





$S$  = c/c spacing in direction of load  
 $S'$  = c/c spacing perpendicular to direction of load  
 $i$  = number of in-line rows  
 $j$  = number of side-by-side rows  
 $(Q_u)_g$  = horizontal load applied to pile group

Figure 2.3. Description of terms used to describe pile group arrangements.



where,  $G_e = \frac{(Q_u)_g}{n(Q_u)_s}$

Figure 2.4. Group efficiency versus pile spacing for all reported pile arrangements (square, in-line, and side-by-side).

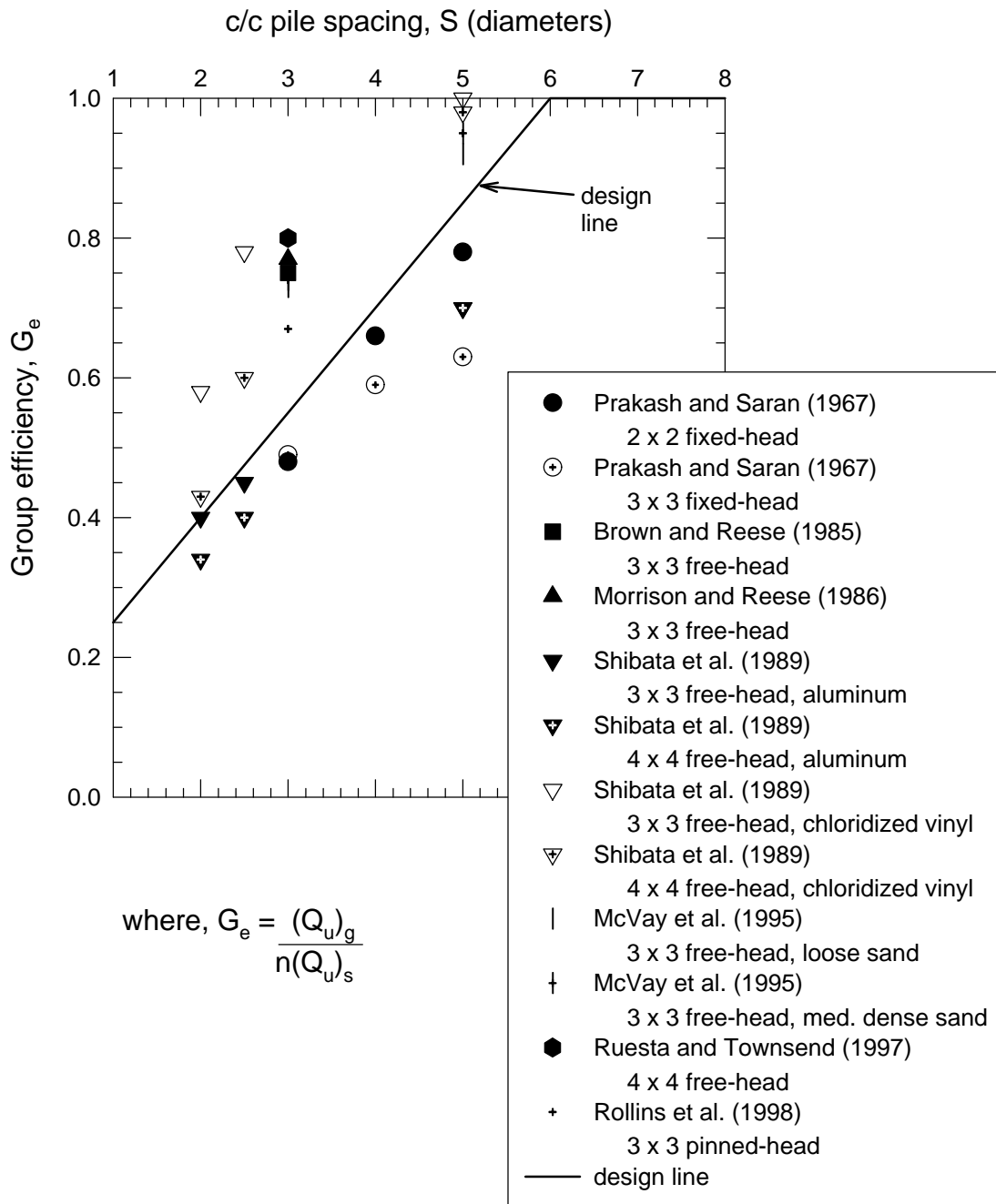
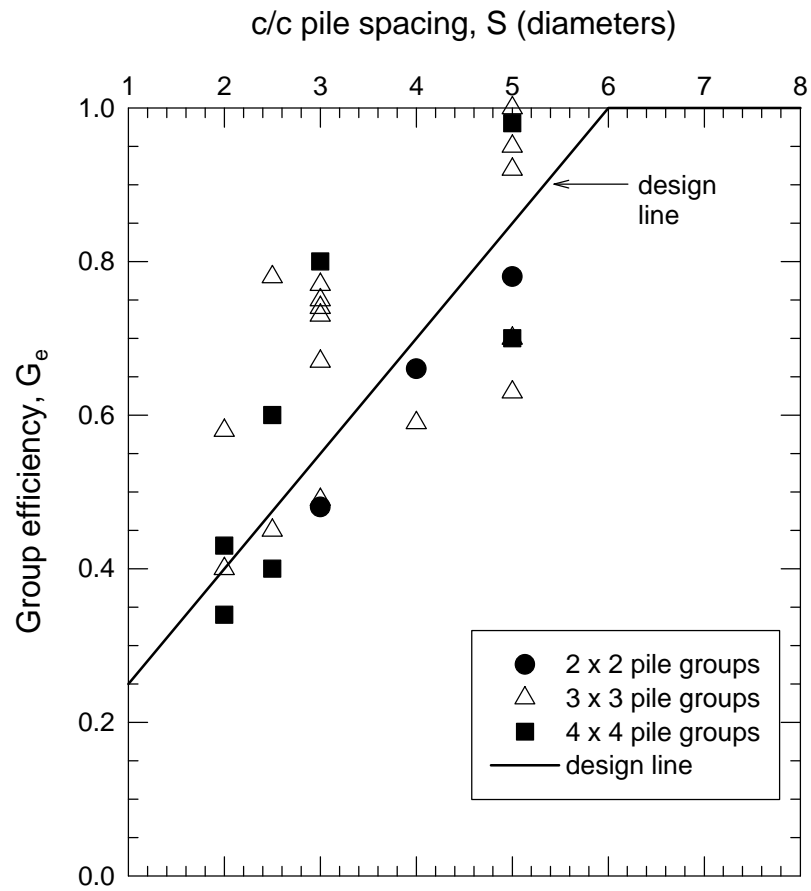
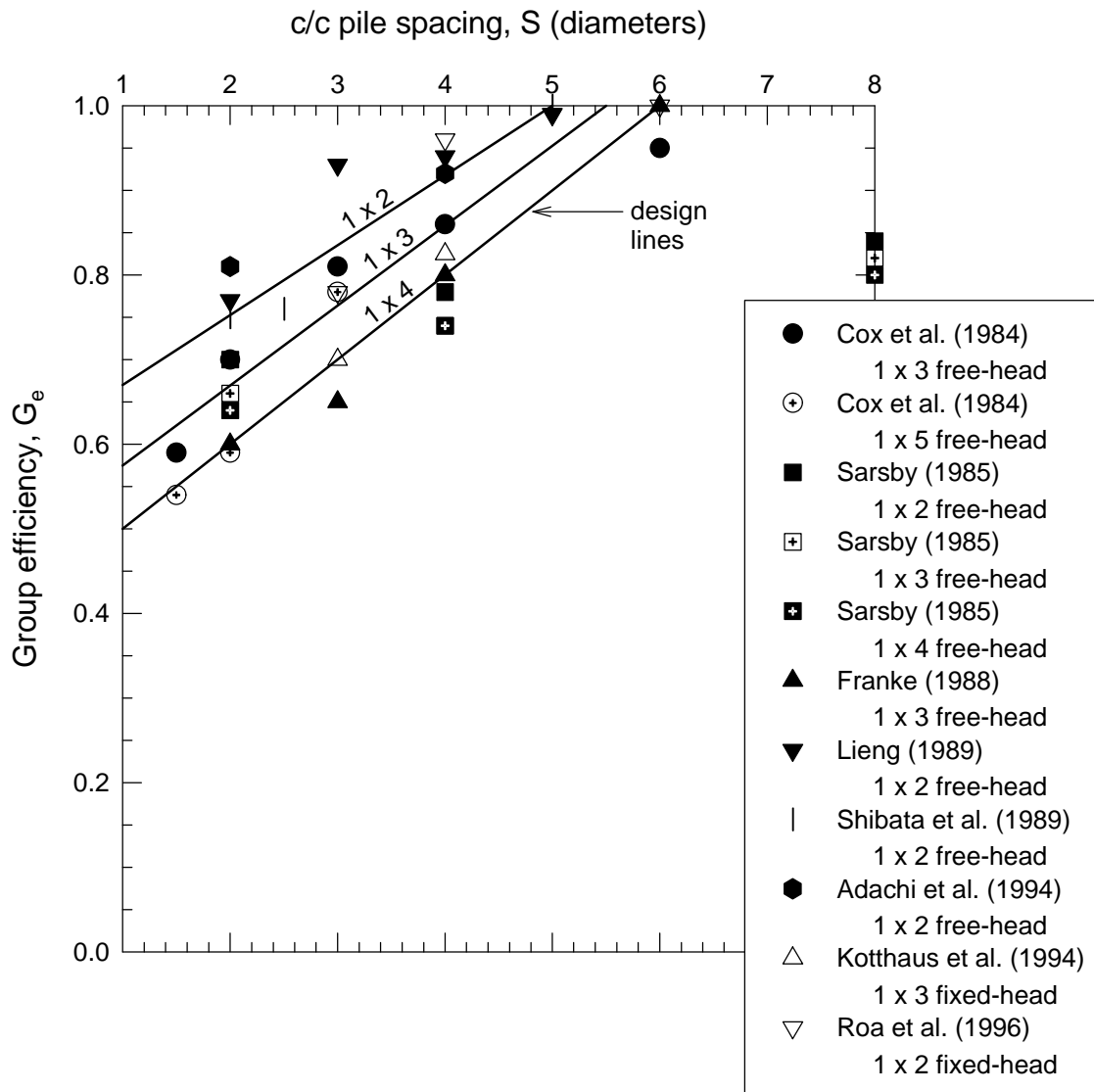


Figure 2.5. Group efficiency versus pile spacing for piles in a box arrangement.



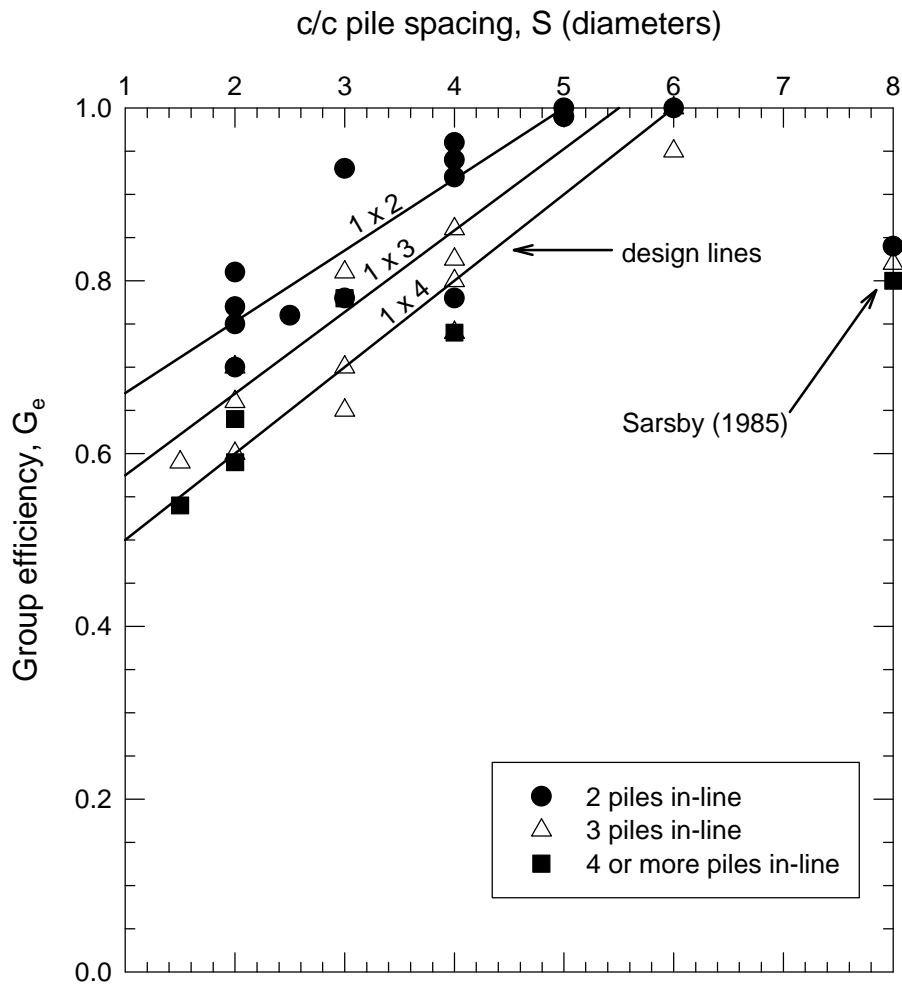
where,  $G_e = \frac{(Q_u)_g}{n(Q_u)_s}$

Figure 2.6. Influence of group size on group efficiency for piles in a box arrangement.



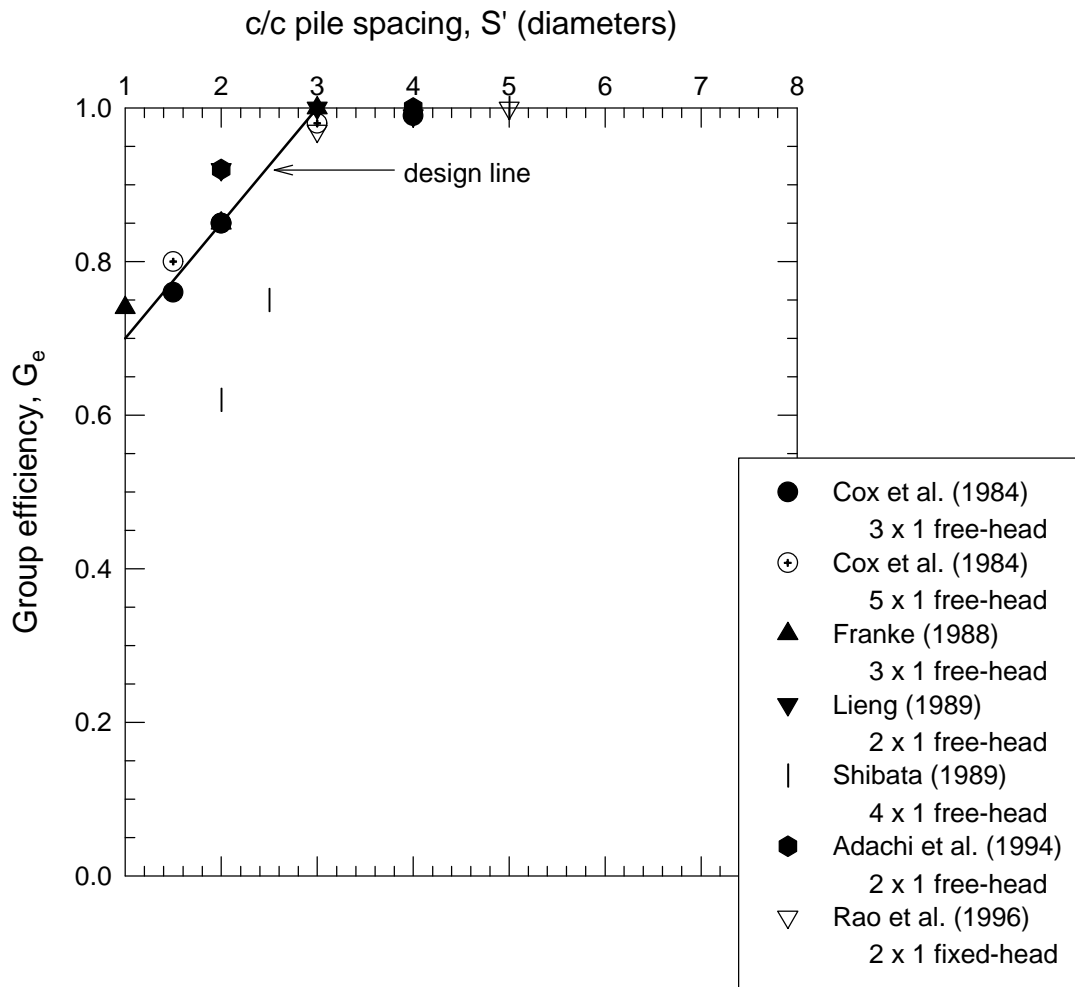
$$\text{where, } G_e = \frac{(Q_u)_g}{n(Q_u)_s}$$

Figure 2.7. Group efficiency versus pile spacing for a single row of piles oriented in the direction of load (in-line arrangement).



where,  $G_e = \frac{(Q_u)_g}{n(Q_u)_s}$

Figure 2.8. Influence of group size on group efficiency for a single row of piles oriented in the direction of load (in-line arrangement).



$$\text{where, } G_e = \frac{(Q_u)_g}{n(Q_u)_s}$$

Figure 2.9. Group efficiency versus pile spacing for a single row of piles oriented perpendicular to the direction of load (side-by-side arrangement).

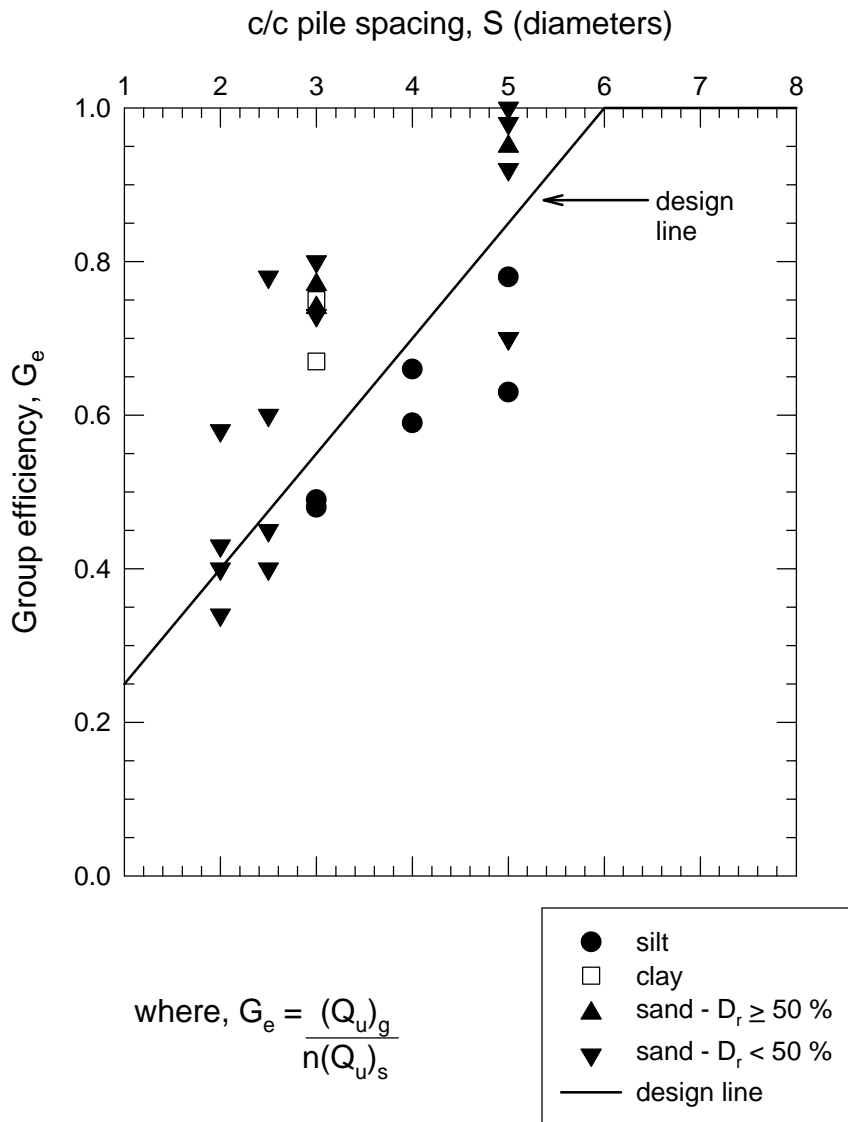


Figure 2.10. Influence of soil type on group efficiency for piles in a box arrangement.



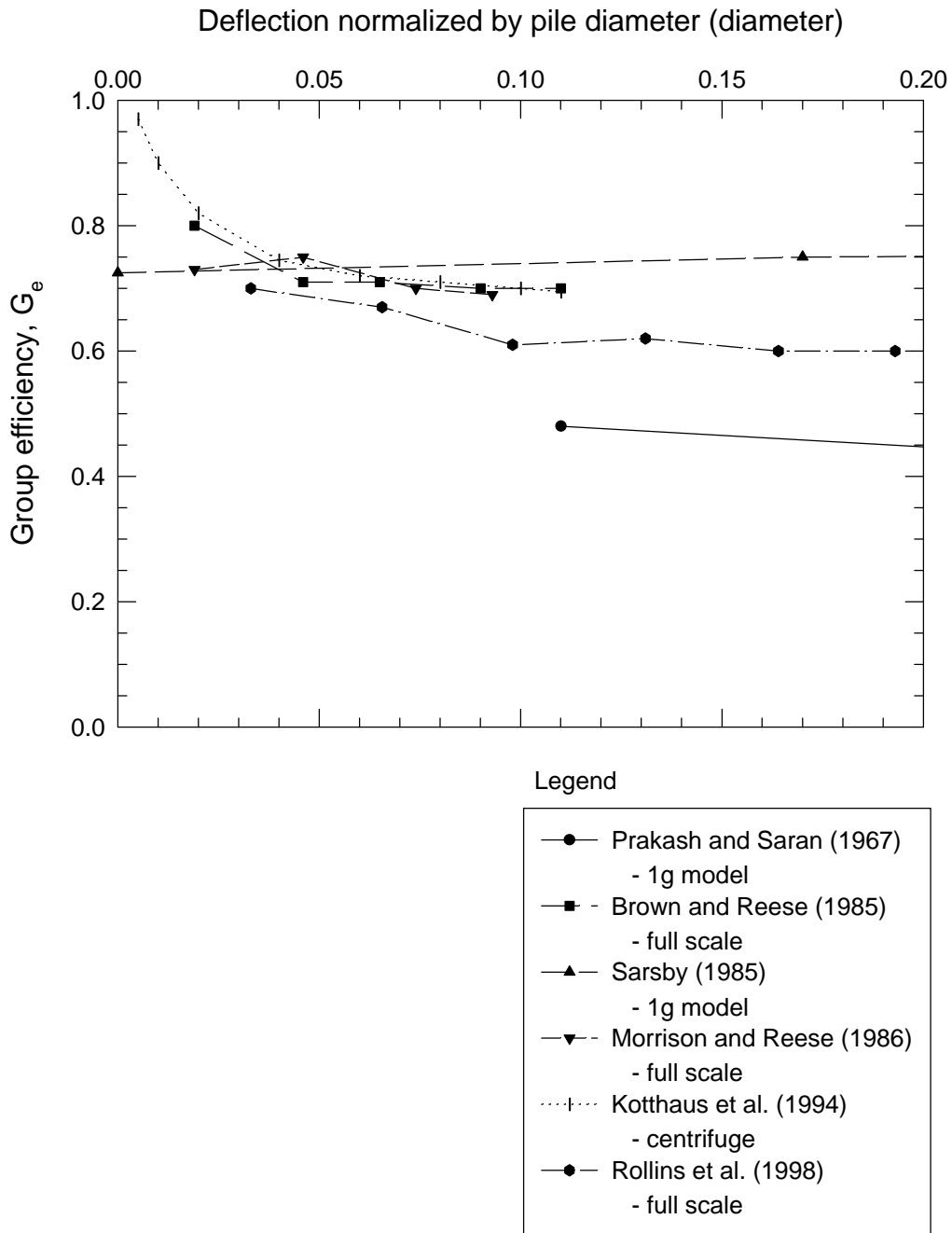


Figure 2.11. Pile group efficiency versus normalized displacement.

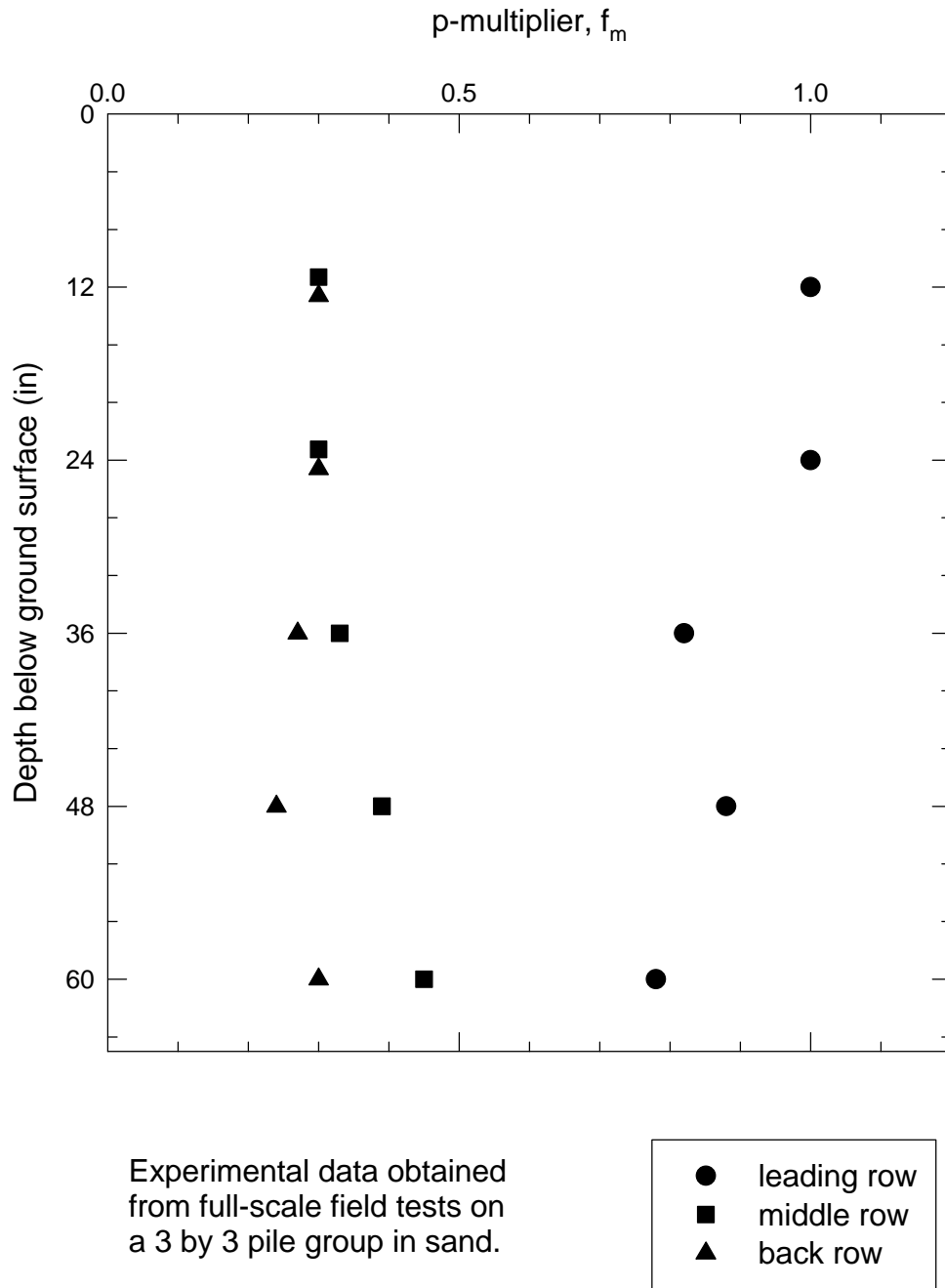


Figure 2.12. Variation of p-multiplier with depth.

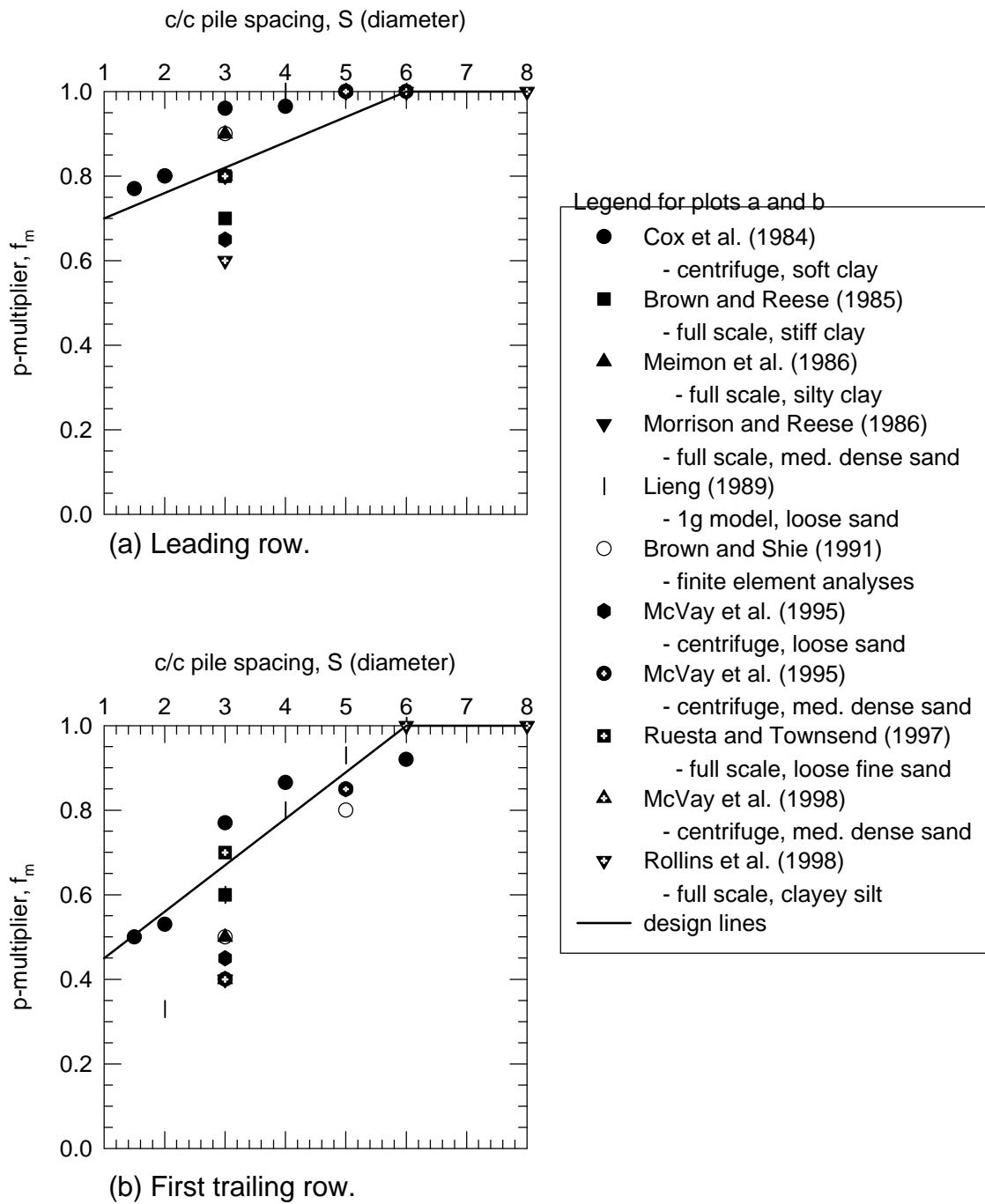


Figure 2.13. p-multiplier as a function of pile spacing for leading row and first trailing row.

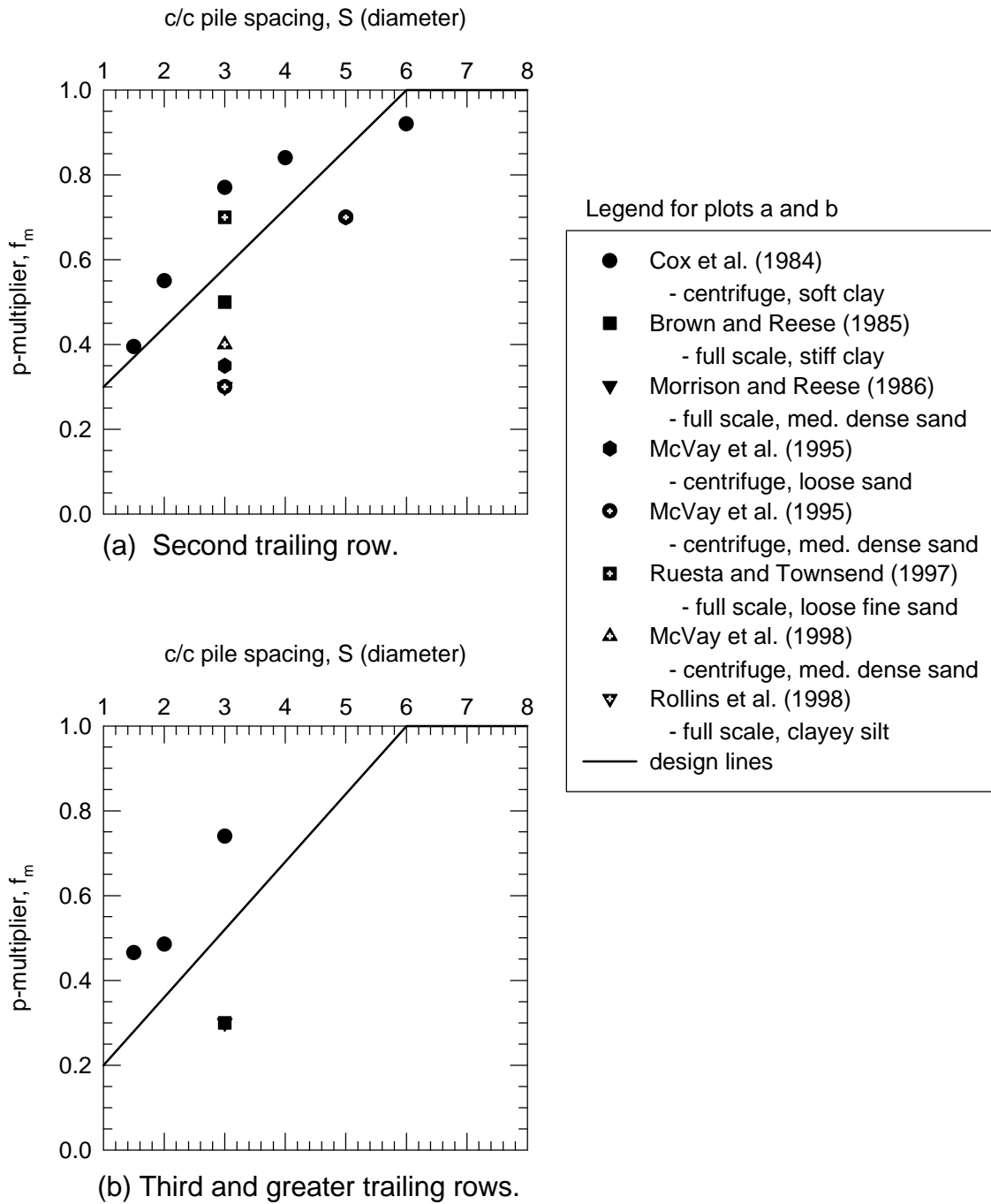
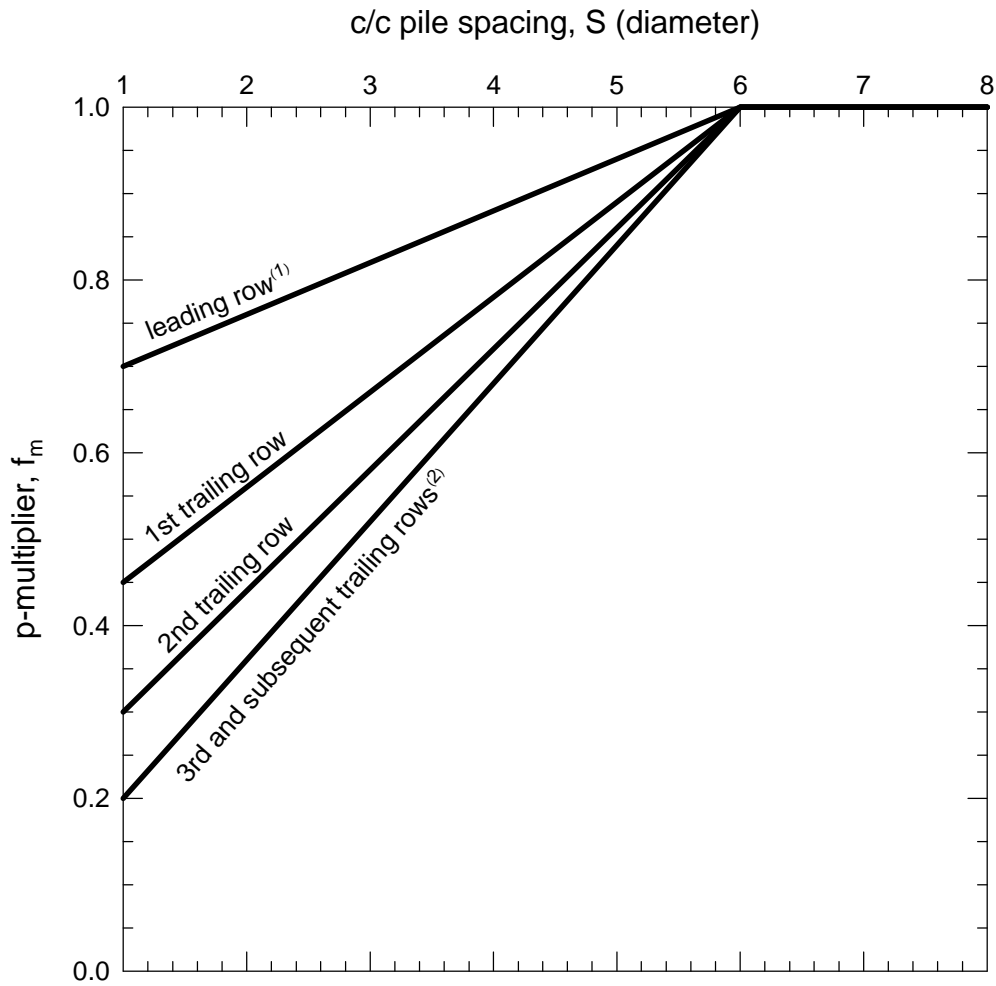


Figure 2.14. p-multiplier as a function of pile spacing for the second and third trailing rows.

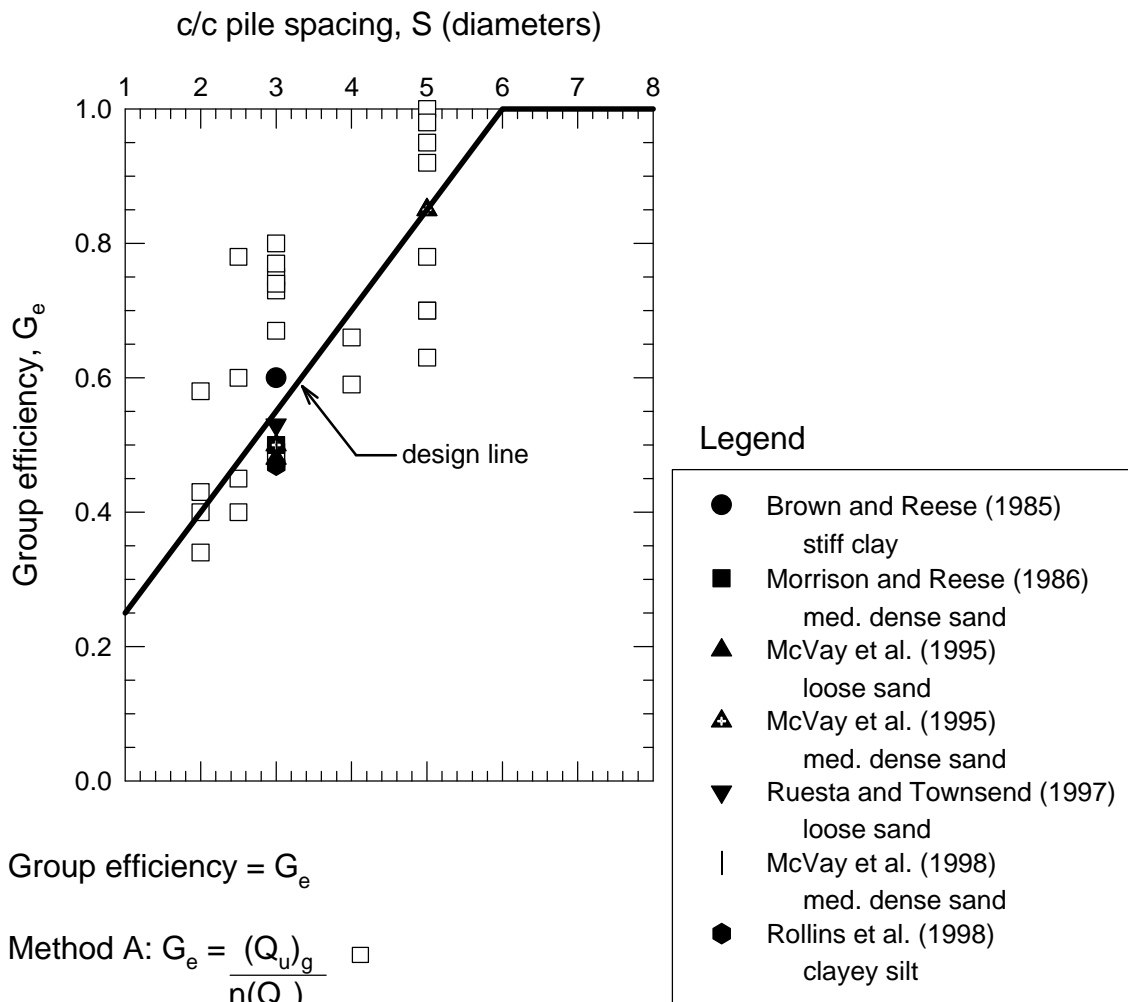


Notes:

- (1) The term row used in this chart refers to a line of piles oriented perpendicular to the direction of applied load.
- (2) Use the  $f_m$  values recommended for the 3rd trailing row for all rows beyond the third trailing row.
- (3) Bending moments and shear forces computed for the corner piles should be adjusted as follows:

<u>side by side spacing</u>	<u>corner pile factor</u>
3D	1.0
2D	1.2
1D	1.6

Figure 2.15 Proposed p-multiplier design curves.



Group efficiency =  $G_e$

Method A:  $G_e = \frac{(Q_u)_g}{n(Q_u)_s}$  □

Method B:  $G_e = \frac{\sum f_m}{N}$  ■

where,  $(Q_u)_g$  = lateral capacity of pile group at a given deflection

$(Q_u)_s$  = lateral capacity of single pile at a given deflection

$\sum f_m$  = sum of row p-multipliers

N = No. of rows in the direction of load

Figure 2.16. Proposed group efficiency design curve for piles in a square (box) arrangement.

## CHAPTER 3

### FIELD LOAD TEST FACILITY

#### 3.1 INTRODUCTION

During the period from July 1997 through June 1998, a field test facility was developed at Virginia Tech for performing lateral load tests on deep foundations. The test site is located at Virginia Tech's Kentland Farms, approximately 10 miles west of Blacksburg, Virginia. The facility is designed to investigate the factors that control the lateral load resistance of pile caps and integral bridge abutments. This chapter describes details of the in-ground facilities, the equipment that was used to apply horizontal loads to the foundations, the instrumentation that was used to measure deflections and loads, and the data acquisition system.

#### 3.2 IN-GROUND FACILITY

The test foundations consist of three groups of four piles each, one with a cap 18 inches deep and two with 36 inch deep caps, two individual test piles, and an embedded bulkhead with no piles, as shown in Figure 3.1. The features of the facility are described in the following paragraphs. Figure 3.2 contains photographs taken during construction of the facility.

##### 3.2.1 Piles

The piles, all HP10x42, were installed on August 28, 1997, by Coalfield Services, Inc. of Wytheville, Virginia. The piles were driven using an International Construction Equipment (ICE) model 30S diesel pile hammer, with a rated energy of 22,500 foot-pounds at a stroke of 7.5 feet. Table B.1, in Appendix B, contains detailed information about the pile hammer and pile driving system components.

The piles in all of the groups were installed at a center-to-center spacing of 4D (40 inches). The piles beneath the southeast cap were driven 10 feet and the others were driven to a maximum depth of 19.3 feet, or to refusal, whichever occurred first. Refusal was defined as 15 blows per inch. The two northern piles in the northeast cap met with refusal at depths between 17 and 18 feet, and the two individual piles reached refusal at 19 feet. Detailed pile driving data is summarized in Table B.2.

### **3.2.2 Concrete for Pile Caps and Bulkhead**

The three pile caps and the bulkhead were constructed of reinforced concrete, with their tops at or below ground. The caps are 5 ft by 5 ft in plan dimensions and are located at three corners of a quadrant, such that each cap can be loaded against its neighbor, as shown in Figure 3.1. The fourth corner of the quadrant contained the bulkhead, which had no piles, and consisted of a monolithic block of reinforced concrete approximately 6.3 feet in length, 3 feet in width, and 3.5 feet in depth.

The caps and the bulkhead were positioned so that the loading axis passed through their centroids. Excavations were trimmed to neat lines and grades using a small backhoe and hand shovels. Concrete was poured against undisturbed ground wherever possible, so that the first series of load tests could measure the resistance of the pile caps in contact with the natural ground at the site.

It was necessary to use wood forms at some locations to provide access for the threaded anchor rods used for attaching loading equipment. The anchor rods were cast in the concrete and extend horizontally approximately 4 inches outside the caps. Each of the pile caps and the bulkhead had 4 anchor rods extending outwards in each direction of loading, as shown in Figure 3.3. The anchor rods provided a means for attaching the loading equipment directly to the caps and the bulkhead.

Three separate concrete pours were involved in constructing the pile caps and the bulkhead:



- the NE and NW pile caps were poured on October 24, 1997,
- the SE pile cap was poured on November 19, 1997, and
- the bulkhead was poured on February 17, 1998.

Concrete was delivered to the site in ready-mix trucks and was placed in one continuous pour at each pile cap or integral abutment; no construction joints were necessary. Concrete slump tests were performed on each truckload in conformance with ASTM C-143. The concrete slump ranged from 4 in to 4.5 in. High early strength concrete with a design strength of 4,000 psi was used, and was vibrated in place using hand-operated concrete vibrators. To minimize curing cracks, the concrete surfaces were kept moist using wet burlap covered with plastic for 28 days. No loads were applied to the concrete structures until after the 28 day concrete curing period was complete. The strength of the concrete was checked by performing compression tests, in general accordance with the ASTM C-39 test procedure. The 28 day compressive strengths ranged from 4,200 psi to 5,200 psi, with an average value of 4,770 psi.

### **3.2.3 Reinforcing Steel for Pile Caps and Bulkhead**

The pile caps and bulkhead were reinforced as follows:

- The 36 in deep caps were reinforced in the transverse and longitudinal directions with No. 8 bars at 6 in spacing in the bottom face and No.6 bars at 5 in spacing in the top face.
- The 18 in deep cap was reinforced in the transverse and longitudinal directions with No. 6 bars at 7 in spacing in the bottom face and No.4 bars at 14 in spacing in the top face.

- The bulkhead was reinforced with No. 4 bars spaced at 5 inches on both faces.

Pile cap design standards vary widely in regards to reinforcement and pile embedment requirements. AASHTO specifications for Highway Bridges (AASHTO 1994) recommends at least 12 in of pile embedment; however, for special cases, it may be reduced to 6 in. According to Kim (1984), standards for minimum pile embedment vary between state agencies over a range of 6 to 24 inches. Some states require reinforcement only near the top of the cap, while others call for reinforcement at both the bottom and top of the cap. The Virginia Department of Transportation typically requires that steel piles be embedded a minimum of 12 in, and that steel reinforcement be placed at the top of the piles (personal communication with Ashton Lawler, 1998).

Based on the results of full-scale lateral load tests, Kim (1984) determined the optimum location for steel reinforcement was near the base of the cap. Kim's results indicate that lateral deflections and rotations of pile caps with reinforcement in the top are approximately twice as large as for pile caps with reinforcement located at the base. These differences are attributed to the fixity of the pile to the pile cap. Paduana (1971) performed lateral load tests on full-scale embankment piles with fixed-head and free-head conditions, and found that fixed-head piles resist approximately twice as high lateral load as free-head piles at the same lateral deflection. Thus, to minimize lateral deflections, a fixed condition (no rotation or zero slope) at the pile to pile cap connection is desirable, although 100% restraint between the pile and cap cannot be achieved in the field.

To achieve as much pile restraint as possible, and because of ambiguities regarding the optimum placement of the reinforcing steel, the pile caps in this study were heavily reinforced in both the top and bottom faces. In accordance with ACI 7.7, a minimum of 3 inches of cover was used on reinforcing bars, and at least 5 inches of cover was used on the piles.

The piles extended to within 0.3 ft of the top surface of the caps. Reinforcing bars were welded between the flanges of the piles and the bottom grid of reinforcement to securely connect the rebar cage to the piles. As noted by Kim (1984), the research and development division of the Cement and Concrete Association of England recommends welding reinforcing bars to embedded piles to achieve optimum anchorage. Because of the unknown effects that welding may have on the properties of standard carbon grade reinforcing steel, the welded bars were not considered to be part of the bending or shear reinforcement. Attaching the rebar cage to the piles minimized movement of the reinforcing bars and the threaded anchor bars during concrete placement.

Provisions in the ACI code for steel reinforcement were exceeded for bending (ACI 10.5), shear (ACI 11.5), shrinkage and temperature cracking (ACI 7.12.2). As recommended by Clarke (1973), for added shear reinforcement, ACI standard stirrup hooks were used to form an enclosed cubical rebar cage.

High strength (60 ksi yield strength) one-inch-diameter steel anchor rods were embedded in the caps and abutment at the locations shown in Figure 3.3. The anchor rods were threaded at both ends and were spaced to match the holes in the clevis base plates. A steel frame made of 2 in x 2 in x 1/8-thick welded angles was fabricated and inserted inside of the bulkhead rebar cage. The steel frame was used to support the anchor rods and 1/2-inch-thick anchor plate. Additional No. 4 and No. 5 bars were used as needed to support the threaded 1-inch-diameter anchor rods and to prevent them from moving during concrete placement.

Except for the east-west aligned rods in the NE cap, the embedded ends of the anchor rods were secured inside of the cap by bolting a 1/2-inch-thick steel plate to the rods. This helps distribute the applied load evenly between the rods and prevents the rods from pulling out or pushing through the cap when loaded. The east-west aligned rods in the NE cap pass completely through the cap and are threaded at both ends. At the end of the 28-day concrete curing period, the rods were secured within the caps by bolting 1/2-

inch-thick steel plates onto both ends. The anchor bars used in the bulkhead were threaded throughout their length.

#### **3.2.4 Roads, Drainage and Weatherproofing**

The entrance road leading to the site was covered with a layer of geotextile reinforcing fabric and gravel to facilitate wet-weather access. Additional site grading was performed for diversion of surface runoff, and 160 feet of 4-inch-diameter slotted ADS drain pipe was installed to help keep the site dry.

A large tent shelter, manufactured by Cover-It, Inc. of West Haven Connecticut, was erected to protect the test area during inclement weather, and to provide a degree of environmental control during load testing. The tent was 18 ft by 28 ft in plan dimensions and had approximately 8 ft of vertical clearance. The frame was made from 15 gauge galvanized steel tubing and the cover consisted of a reinforced waterproof nylon fabric. The tent was large enough to shelter a test setup, including reference beams and monitoring equipment, as shown in Figure 3.4. After testing at one location, the tent ground anchors were moved and positioned at the next test location.

### **3.3 LOADING EQUIPMENT**

Lateral loads were applied to the pile caps and the bulkhead using an Enerpac 200-ton double-acting hydraulic ram (model RR-20013) which was purchased for the project. The struts and connections in the load path were designed to apply maximum compressive loads of 150 kips and maximum tensile loads of 100 kips. The configuration of the loading apparatus is shown in Figure 3.5. Loads were applied through the pipe struts and clevis connections by pressurizing the ram cylinder using an Enerpac hydraulic pump (model PEM 3405BR). As can be seen in Figure 3.5, the ram and struts were located below the ground surface in a 2-foot-wide trench that was excavated between the caps.

The pipe struts were fabricated by welding one-inch-thick steel plates to the ends of 6-inch-diameter schedule 80 steel pipe (6.625 in outside diameter and 0.432 in wall thickness). The clevis pin connector consisted of two pieces fabricated from 1-inch-thick ASTM A-36 steel plate stock. The eye bracket or tongue piece was attached to the anchor rods that extend from the sides of the cap and bulkhead. The other piece of the connection, called a female clevis bracket, was attached to the end of the pipe strut. The two clevis pieces were joined together using a 1.5-inch-diameter solid steel pin, which allowed the pipe strut to rotate upwards or downwards around an axis aligned perpendicular to the direction of loading.

The ram plunger attached to a load cell connected to the shorter (15.5-inch-long) pipe strut. The base of the ram was bolted to the ram base adapter, which was bolted to the longer (27.8-inch-long) pipe strut. When the individual piles were tested, the long pipe strut was removed from the lineup, and the ram base adapter was connected directly to the female clevis bracket. The clevis connectors, pipe struts, and ram base adapter were fabricated in the Structural and Materials Laboratory at Virginia Tech.

The 9-inch-diameter hydraulic ram was held in place by a steel cradle fabricated from ½-inch steel plates. Only the bottom half of the steel cradle was in position at the time of the photograph shown in Figure 3.5. The cradle was anchored to a 12 cubic foot block of reinforced concrete embedded in the bottom of the loading trench. The ram could move freely in either direction parallel to the axis of the trench, but was restrained from buckling by the steel cradle and the weight of the concrete block.

The hydraulic pump was powered by a 5000 watt Northstar generator purchased for the project. The ram force was controlled by a remote pendant switch, which operated a 24-volt solenoid valve that advanced or retracted the ram.

After testing was completed at a setup, the loading system was disassembled and moved to the next test location. The system was used to test the individual piles by

removing the large pipe strut and connecting the ram base adapter directly to the clevis connection.

### 3.4 INSTRUMENTATION

The magnitude of the applied force was monitored using load cells and a data acquisition system that were built for the project. Two different load cells, identified as the 200 kip and the 150 kip load cells, were used during the tests.

The 200 kip load cell was capable of measuring either compressive or tensile forces. It was fabricated from a 16-inch-long, 2.5-inch-diameter, high strength bar of cold-rolled steel with a full bridge of strain gauges attached to the outside, and waterproofed, as shown in Figure B.1. Prior to attaching the strain gauges, one end of the bar was welded to a 1.5-inch-thick steel plate, and the other end was cut with threads to match those of the ram plunger. Eight  $\frac{1}{4}$ -inch strain gauges were installed on the exterior of the round bar using M-Bond 200 polyurethane strain gauge cement. The strain gauges used were type CEA-06-125UN-120, gage factor 2.065, made by Micro-Measurements Division of Measurements Group, Inc. Each gauge level consisted of a pair of gauges on either side of the round bar. The 4 pairs allowed completion of a full Wheatstone bridge circuit, as shown in Figure B.2, which canceled out the bending effects.

Prior to testing the SE cap and bulkhead (location B in Figure 3.1), the 200 kip load cell was damaged as a result of flooding in load trench B. Because of difficulties in repairing the load cell in the narrow loading trench, a second load cell was calibrated and substituted for the 200 kip load cell. This load cell had a capacity of 150 kips, and was used for the remainder of the tests.

The 150 kip load cell was constructed of high strength cold-rolled steel and had an hourglass shape, as can be seen in the photographs in Figure B.3. The ends of the load cell were 5 inches in diameter and about one inch thick. The ends had a slightly convex surface for centering the load. The central portion of the load cell was 6 inches long and 3 inches in diameter, and contained the strain gauges, which were mounted and wired

using the same techniques that were used to construct the 200 kip load cell. The load cell was temporarily held in place during testing by sandwiching it between two steel plates held together with four  $\frac{3}{4}$ -inch-diameter threaded rods, as shown in Figure B.3(a). The 150 kip load cell could be removed between tests and stored inside to protect it from environmental damage.

The load cells were calibrated in the lab under controlled conditions using a Satek universal testing machine. The data acquisition equipment used during calibration, including excitation voltage, power and signal lead lengths, shielding, data acquisition hardware, data channel assignment, and cable connectors, was identical to those used during the field tests. Prior to calibration, the load cells were subjected to approximately 50 load/unload cycles. As indicated by the calibration curves shown in Figure B.4, the load cells exhibited linear responses with no measurable hysteresis. The resolution of the load cells were determined during calibration to be approximately 1 kip.

Displacements and rotations of the caps were measured using 12 linear deflection transducers (6 per cap). These provided sufficient data to evaluate displacements of the caps along three mutually perpendicular directions (parallel to the direction of loading, perpendicular to the direction of loading, and vertical). The instruments were mounted on temperature-stable wood reference beams, which were mounted on posts located outside the zone of influence of the foundations. The instruments were positioned at the locations shown in Figure 3.6, which made it possible to determine rotations as well as deflections of the pile caps.

Two types of electronic displacement transducers were used during the tests: 1) Longfellow linear transducers manufactured by Waters Manufacturing of Wayland, Massachusetts and 2) Celesco cable-extension position transducers, manufactured by Celesco Transducer Products, Inc. of Canoga Park, California. Photographs of the transducers are shown in Figure 3.7. Standard specifications are provided in Table B.3.

Six Celesco cable-extension position transducers were used to measure deflections and slopes of the individual piles. The Celesco transducers were clamped onto the pile flanges and onto the vertical telltale, at the locations shown in Figure 3.8. The instrument cables were attached to wood reference beams, which were mounted on posts driven into the ground, outside of the zone of influence caused by loading.

Data from the instruments were electronically recorded with the Keithley 500 data acquisition system using the Lab Tech Notebook Pro software package running on a personal computer, as described in the following sections. Dial gauges were used for mechanical verification of the electronic data collection system. The dial gauges used were model A1-921 manufactured by Teclock Corporation.

The transducers were calibrated in the laboratory under controlled conditions using a Mitutoyo height gauge (model number 192-116). The data acquisition equipment used for calibration, including: excitation voltage, excitation and signal lead lengths, shielding, data acquisition hardware, data channel assignment, and cable connectors were identical to those used during the field tests. Scale factors or calibration curves were developed for the instruments, and in all cases, the voltage versus displacement curves exhibited linear response with no measurable hysteresis. An example calibration curve for one of the displacement transducer is shown in Figure B.5. The calibration factors for all of the displacement transducers are provided in Table B.4. The zero intercept of the calibration curves was not needed because zero readings were obtained at the beginning of each test. The resolution of the instruments were determined during calibration to be approximately 0.002 in.

### **3.5 DATA ACQUISITION HARDWARE**

The electronic deflection measuring devices and the load cell strain gauges produce a voltage signal that was monitored through an analog-to-digital data acquisition system. The hardware for the analog-to-digital system included a Keithley model 500A data acquisition system and a personal computer.



The Keithley 500A is a general purpose data acquisition and control unit that served as an interface between the computer and electronic measurement devices. All incoming commands from the computer were decoded and directed through the Keithley internal motherboard circuitry. The motherboard controlled the 0.8 amp, +15 volt, excitation power supply and served as a link between the computer and the input modules. The Keithley motherboard contained slots for up to 10 input modules. A variety of input modules are available, depending on the system requirements. This study incorporated one AMM2 module and three AIM3A modules, as described below.

The AMM2 module was connected to the first slot of the Keithley motherboard. The AMM2 is a global conditioning master measurement module that consists of a high-speed software-controlled gain amplifier that controls the signal conditioning and switching circuitry for all the other modules. During load testing, the local amplifier gain was set at x1 for the electronic transducers and x10 for the load cell strain gauges. A 2 kHz low-pass filter was used to minimize analog/digital noise. After analog conditioning, signals were routed to the 16-bit analog/digital (A/D) converter section of the module for analog-to-digital conversion using a 16-bit successive approximation converter, with controllable sampling rates of up to 50 kHz. The AMM2 converter range was set at 10 V for the transducers and the load cell strain gauges.

The load cell strain gauges and the deflection transducers were connected to individual terminal channels of AIM3A modules, which were installed in slots 2 through 4 of the Keithley system. The AIM3A is an analog input module that accepts input signals of 100 mV full scale through 10 V full scale, and outputs a signal of 10 V full scale to the AMM2 A/D converter module. The AIM3A module produces full 16-bit precision results at a rated linearity of 0.005 percent. Input signals from the measuring devices were connected to individual channels of the module using screw terminal strips, which were accessed through the back of the Keithley control box. A maximum of 32 single-ended or 16 differential (floating) inputs can be connected to a single AIM3A module. Shielded cables were used for all the instruments, which were connected as

differential inputs to the AIM3A modules. This type of wiring scheme is often used when there are multiple inputs with different ground points. The voltage input is limited to 10 V per channel when differential inputs are used, but the possibility of ground loop errors and common mode noise is reduced.

Cables from the electronic instruments were routed to plastic terminal strips mounted on a plywood board as shown in Figure 3.9(a). The board functioned as an electronic junction between the instruments and the Keithley control system. The instrument cables contained leads for positive and negative signals, positive voltage, ground, and shield lines. Electromotive force was routed from the Keithley system to a positive voltage regulator on the terminal board. The regulator reduced the voltage from +15 V to +10 V. The voltage was jumped to each terminal on the board using 20 gauge lead wires.

A Gateway 2000 4DX-33V personal computer with 640 kilobytes of system memory and a floppy disk drive was used for data acquisition. The computer controlled the operation of the system through an interface card that contained data and address bus buffers, address decoding circuits, and programmable interval timers. The computer and Keithley 500A were powered by a 120 volt AC dedicated power source produced by a 1600-watt Honda generator. The generator was used solely for powering the data acquisition hardware during load testing. A separate generator was used for powering the hydraulic pump.

The complete data collection system including the Keithley 500, personal computer, and terminal board were attached to a steel frame mounted inside a minivan, as shown in Figure 3.9(b). This protected the sensitive electronic instruments from the elements and vandalism, and provided a means for transporting the system to and around the site.

### 3.6 DATA ACQUISITION SOFTWARE

The computer program Labtech Notebook Pro (LNP), by Laboratory Technologies Corporation, was used to control the data acquisition hardware. LNP was written using BASIC Version 3.0 programming language and was configured to interface directly with the Keithley data acquisition system. The data acquisition and process control functions were established in LNP using block functions. The block functions established characteristics such as type of input signal, block name, sampling rate, channel number, interface device, scale factor, and offset constant.

Individual block functions were established for each type of electronic instrument. Various sampling rates, ranging from 0.2 Hz to 1 Hz were used during the initial load tests. For static testing, a sampling rate of 0.2 Hz was found optimal. A summary of the instrument channel numbers and interface devices is provided in Table B.4. The block scale factor corresponds to the calibration slope shown in the table.

The block offset constant is a value that is added to the input value, and was set equal to zero for all of the transducers. Separate blocks were established for elapsed time and for the load cell.

During data acquisition, LNP places raw data from the analog-to-digital converter in a buffer, and subsequently copies it to a file on the computer's hard disk. When LNP writes the data from a block's buffer to a file, it is converted from voltage units to engineering units in ASCII real number format using the block offset constant and scale factor. The buffer was transferred to a file on the computer's hard disk continually during the tests. (LNP offers a number of formats for downloading data; the format described above was used in this study) After a test, the data file was copied to a diskette and stored for later processing. Items in the output file such as field width, number of significant digits, column headings, time, date, and comments can be controlled during the initial software configuration. The data file created in this manner can be readily copied into a spreadsheet for manipulation and plotting.

The software was configured to display 5 different screens on the computer monitor during testing. The screens showed real time plots of deflection versus time and load versus time, and digital displays of deflection and load. The display was monitored during testing, and deflection readings of selected instruments were manually recorded at various load intervals to serve as a backup to the electronic data.

### **3.7 CONSTRUCTION SCHEDULE AND COST**

Design of the field test facility began in June 1997. The field investigation was initiated about the same time and continued intermittently throughout the fall and winter months. Construction activities started in September 1997 and were essentially complete in April 1998. Work on the instrumentation was conducted in May 1998. Load testing began in June 1998 and ended in October 1998.

Approximate costs of materials and supplies for building the field test facility are listed in Table B.5. The total was about \$34,000. The majority of design and construction work was performed by Virginia Tech graduate research assistants. Salary costs are not reflected in the table, but are estimated to be about \$20,000. In addition, because the test site was developed at Virginia Tech, where there are well-equipped geotechnical and structural laboratory facilities, it was possible to utilize other equipment and supplies at no cost to the project. The total estimated purchase or rental value of this other equipment is about \$16,000. Thus, in total, it has been possible to develop a test site with an estimated value of \$70,000 under a research project with a total budget of \$36,000.

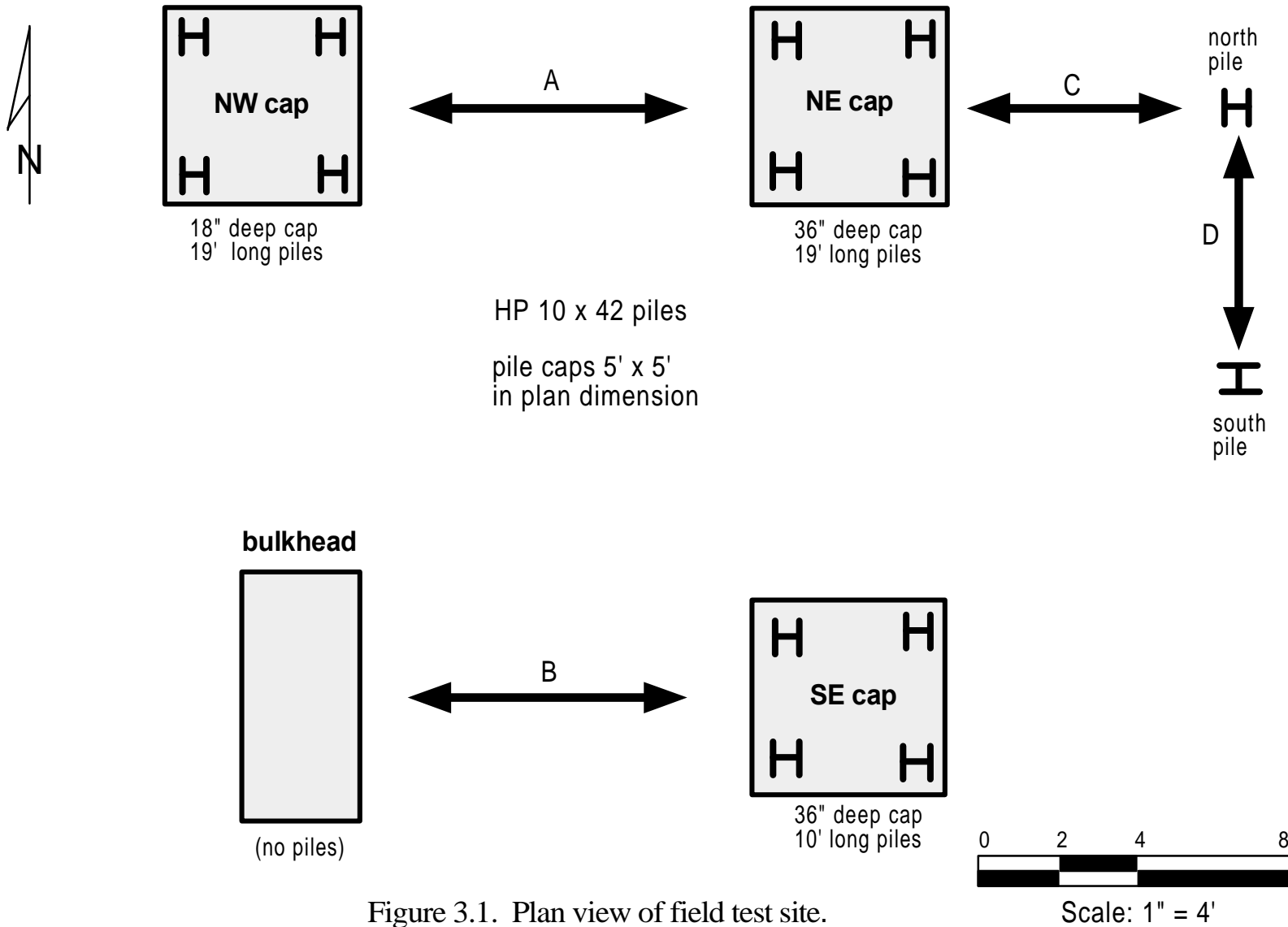


Figure 3.1. Plan view of field test site.



(a) Rebar in place for 18" deep cap.



(b) Finishing concrete surface of 36" deep cap.



(c) Trench at setup A, ready for loading equipment.



(d) Installing hydraulic ram in loading trench.

Figure 3.2. Foundation construction photos.

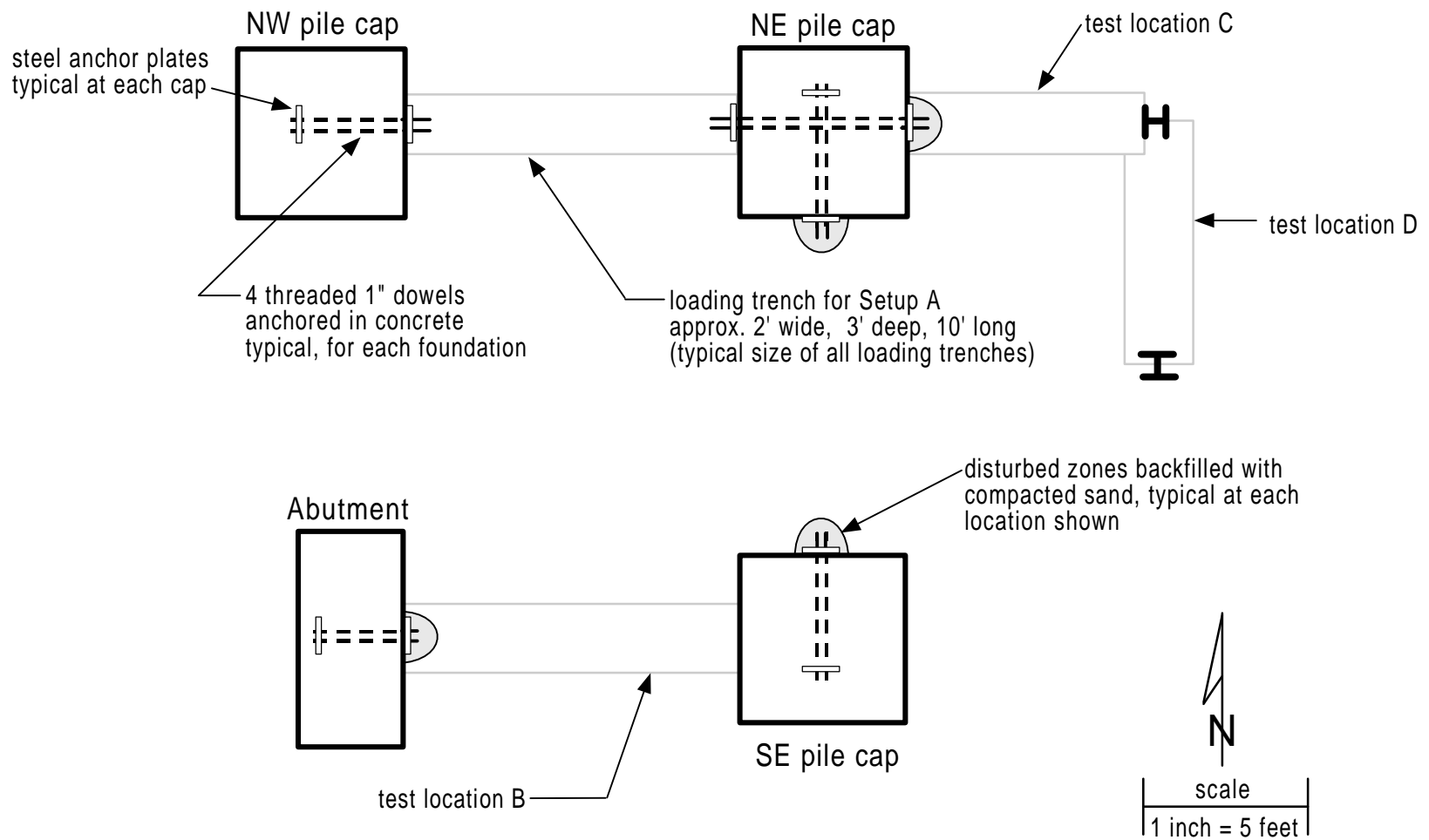


Figure 3.3. Plan view of anchor rod layout.



(a) Erecting tent frame.



(b) Tent frame under construction.



(c) View of tent from the east.



(d) View of tent from the west.

Figure 3.4. Tent shelter photos.



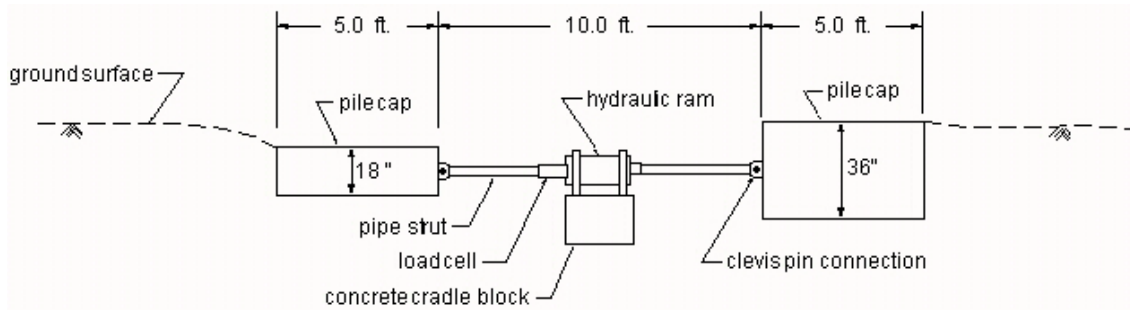
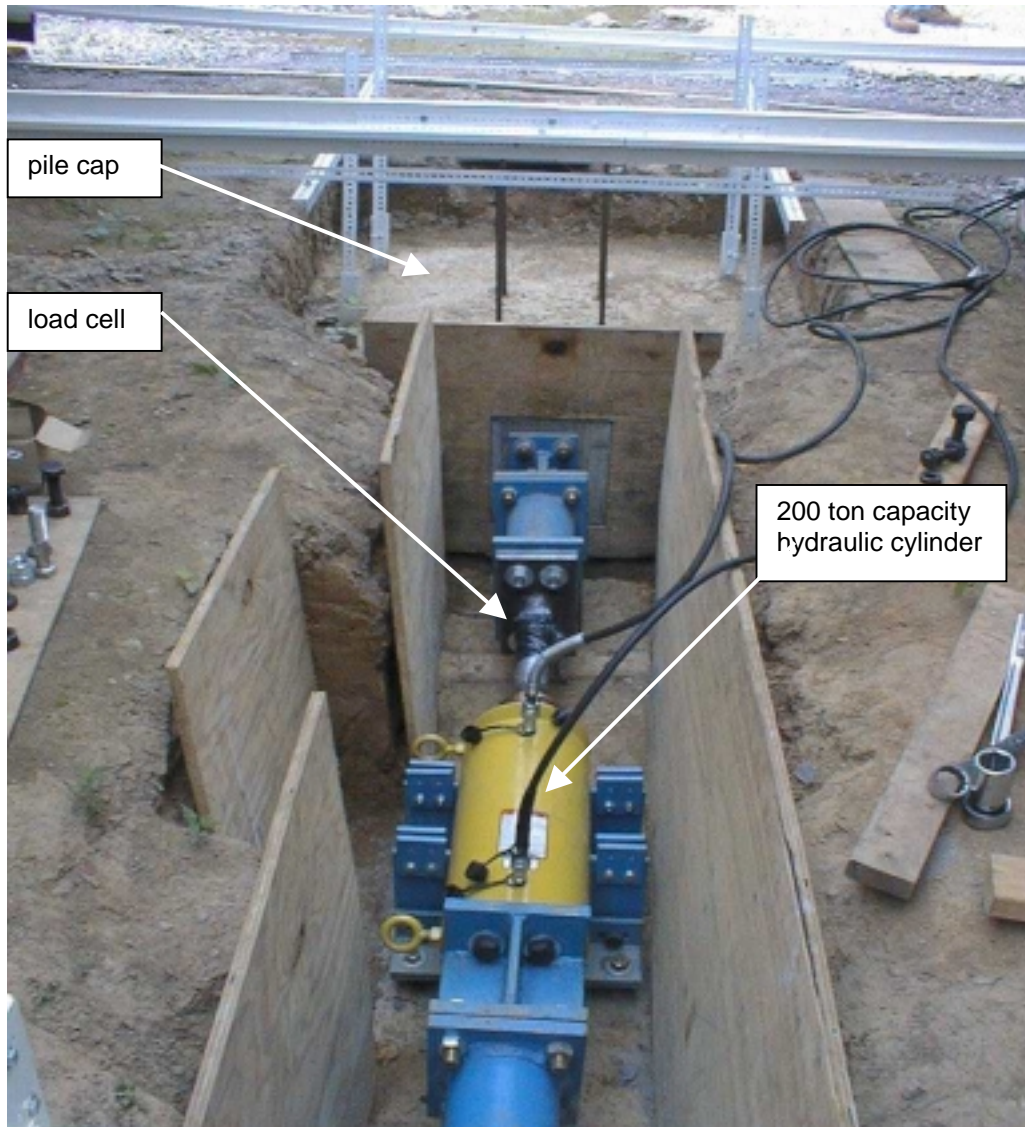
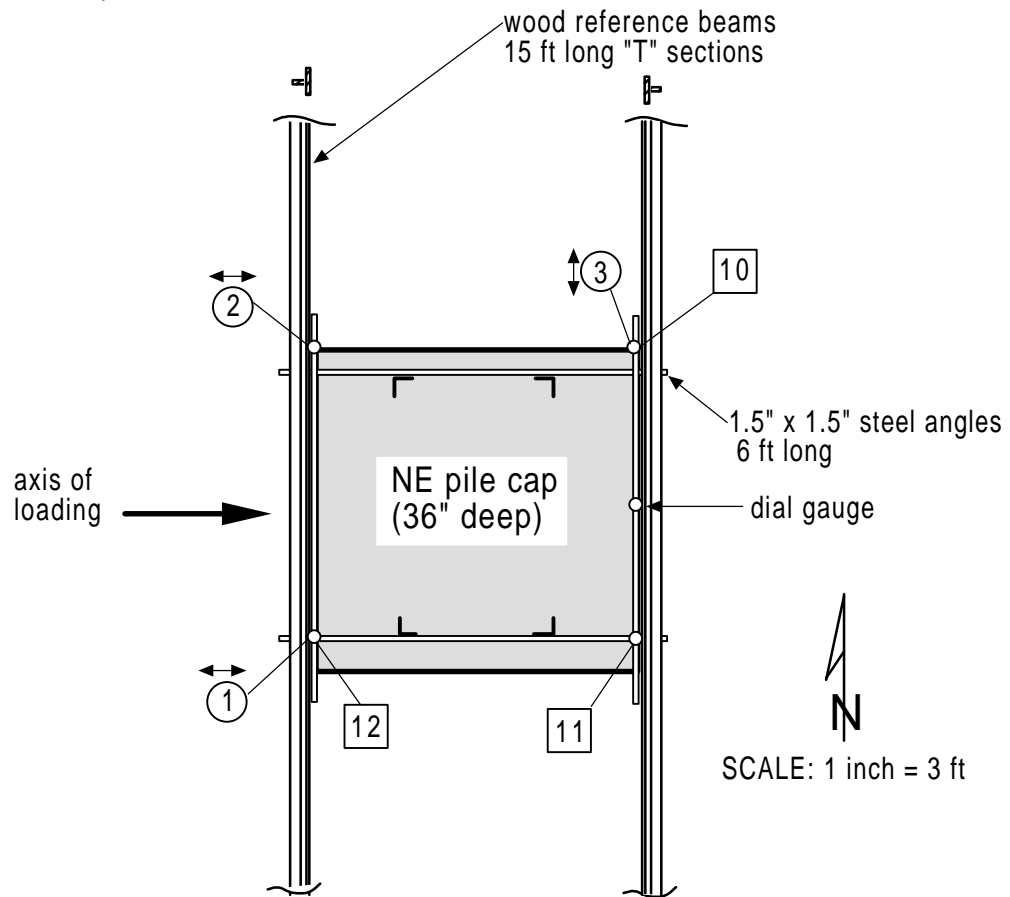


Figure 3.5. Hydraulic ram and steel struts positioned in loading trench.



**LEGEND**

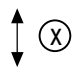
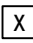
- 
 Linear potentiometer positioned in the horizontal plane, arrows designate direction of measurement, "x" indicates instrument number.
- 
 Linear potentiometer positioned for vertical deflection measurement, "x" indicates instrument number.

Figure 3.6. NE pile cap instrumentation plan.

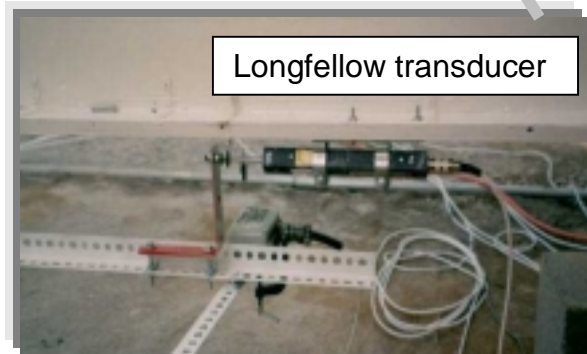
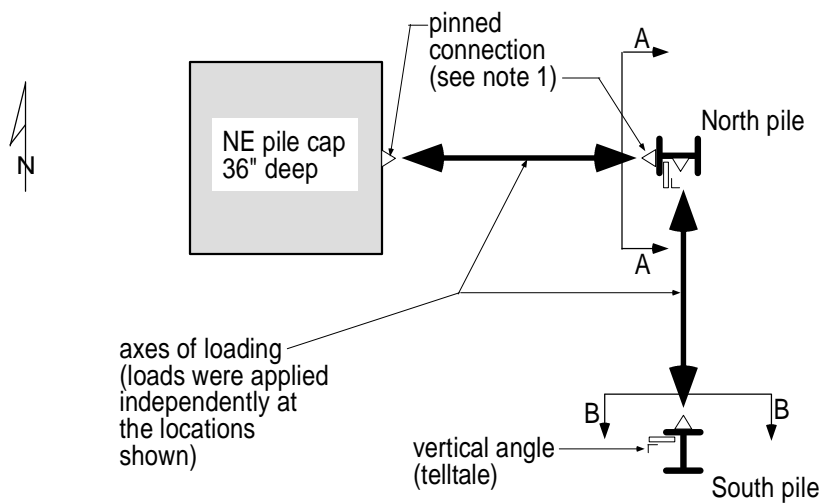
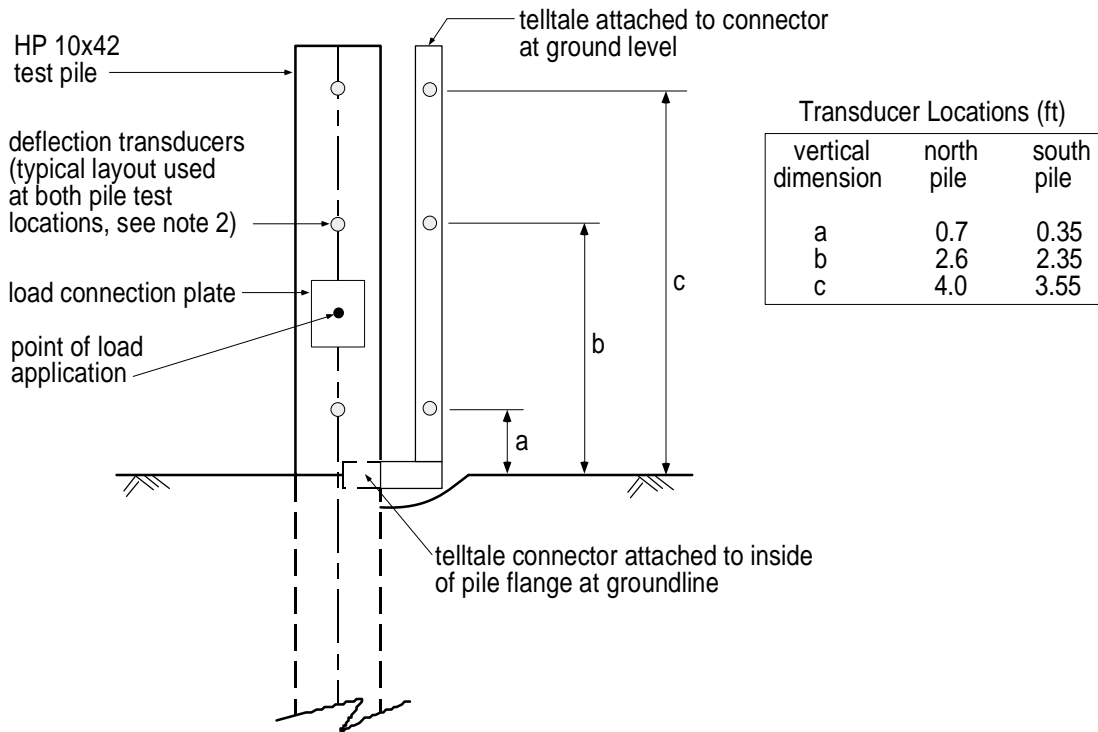


Figure 3.7. Instrumentation in place for measuring deflections during lateral load test.



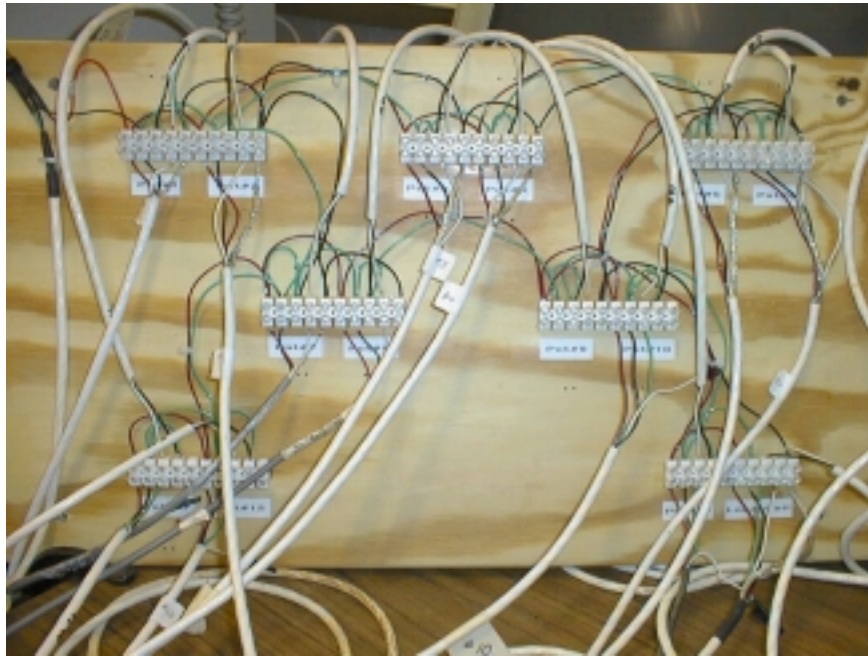
(a.) Plan view - scale: 1 in = 5 ft.



(b.) Sections A-A (north pile) and B-B (south pile) - scale: 1 in = 2 ft.

Figure 3.8. Instrumentation layout for individual piles.





(a) Instrument terminal board.



(b) Data collection system mounted inside of minivan.

Figure 3.9. Photos of data collection system.

## **CHAPTER 4**

# **SUBSURFACE CONDITIONS AT THE FIELD LOAD TEST SITE**

### **4.1 SITE DESCRIPTION**

As shown in Figure 4.1, the test site is located at Virginia Tech's Kentland Farms facility, approximately ten miles west of Blacksburg, VA. The site where the load test facility is located lies within the flood plain of the New River, in an area of the farm that has not been cultivated in recent years. The surface topography is relatively flat, and the New River is approximately  $\frac{1}{4}$  mile south of the site.

Prior to construction of the test facility, the topsoil layer and herbaceous vegetation were removed with a bulldozer. The subgrade was free of tree roots.

### **4.2 GEOLOGY**

The site is underlain by alluvial soils deposited by the New River. The alluvial soils range in composition from silt to sand, and are about 20 to 30 ft thick at the site. The alluvial soils are underlain by the Elbrook Formation, which consists of dark gray fine-grained limestone and dolomite, with red shale interbeds, and is of Cambrian age. The Elbrook Formation has been associated with karst features such as sinkhole development, subsurface cavities, solution features, and pinnacled bedrock in the region (Stose, 1913; Johnson, 1993). No karst features have been found at the test site.

### **4.3 SUBSURFACE CONDITIONS**

The soil stratigraphy at the test site is shown in Figure 4.2. The near surface soils consist of hard, partially saturated lean sandy clay and sandy silt, which is overconsolidated due to desiccation. Thin gravel and cobble seams within the fine-

grained soils at depths of 4.5 feet, 5 feet, and 17 feet below original ground surface. Standard penetration test blow counts (SPT N-values) ranged from 30 in the desiccated crust to about 10 at a depth of 15 feet. Blow counts in the gravel and cobble seams were greater than 50. Drilling to depths deeper than 20 feet was difficult. At these depths, auger cuttings and gravel fragments in split spoon samples indicated the presence of gray to white fine-grained weathered limestone or brecciated limestone and shale.

From August 1997 to October 1998, the water table depth varied from a high of about 10 feet in March, to a low of about 18 feet in December, based on periodic readings of a ground water monitoring well.

#### **4.4 SUBSURFACE INVESTIGATION**

Various in situ techniques were used to determine soil stratification, shear strength, soil modulus, state of stress in the ground, and groundwater levels, and to obtain samples for laboratory testing. The subsurface investigation included:

- Solid-stem auger borings with Standard Penetration Tests (SPTs),
- Dilatometer soundings (DMTs), and
- Large block samples to obtain high-quality samples for laboratory tests.

The locations of the borings, DMT soundings, and block sample excavations are shown in Figure 4.3.

##### **4.4.1 Soil Borings**

Six solid-stem auger borings were drilled at the site using a Mobile B80 drill rig. The subsurface materials encountered were identified, described, and classified in general accordance with ASTM D2488. Copies of the soil boring logs are included in Appendix

C. Standard penetration tests were performed during the drilling operation in general accordance with ASTM D1586. N-values obtained during the SPT tests are shown in Figure 4.4. Relatively undisturbed tube samples were obtained by pushing 3-inch-diameter Shelby tubes in general accordance with ASTM D1587. The split spoon and Shelby tube samples were transported to Virginia Tech's soil mechanics laboratory for subsequent testing.

#### **4.4.2 Observation Well**

A 2-inch-diameter slotted pvc standpipe piezometer (MW-1) was installed at the site using the drill rig and 4-inch-diameter solid stem augers. The bottom 10-foot-long slotted section of the pipe was set at a depth interval from 11 to 21 feet below ground surface. The annulus was backfilled with sand from the bottom of the drill hole to about 4 feet above the top of the slotted section of pipe. The remainder of the annulus was filled with bentonite hole plug. The water level in the piezometer has been measured and recorded periodically during construction of the site, and is measured each time a load test is performed.

#### **4.4.3 Dilatometer Tests**

Seven DMT soundings were performed at the site in August 1997. DMT measurements were taken at 8-inch intervals to a maximum depth of about 16 feet. This depth was limited by the durability of the membrane on the DMT blade as well as by the penetration ability of the blade, which was advanced using the hydraulic system on a Mobile B80 drill rig.

To the extent possible, the DMT tests were performed in accordance with the information and recommendations given in Schertmann (1988). Other soundings were attempted in addition to the seven successful soundings, but these were only advanced to shallow depths before difficulties in obtaining pressure readings necessitated abortion of the tests. Most of these problems can be attributed to membrane damage inflicted by advancing the DMT blade through the upper two gravel and cobble seams. The deepest



soundings were limited by the depth at which the lower gravel and cobble seam was encountered. The DMT test is best-suited to more easily-penetrated, homogenous soil layers (Schmertmann, 1988). As the experience at this site confirms, obstructions such as gravels, cobbles, boulders, and cemented layers have the potential to thwart advancement of the blade, or to damage the membrane of the blade during advancement. The DMT soundings were primarily used qualitatively as a means of identifying changes in the soil stratigraphy.

#### **4.4.4 Block Samples**

Three block samples were excavated at the location shown in Figure 4.3 for the purpose of obtaining high quality undisturbed samples for triaxial testing. On the average, the soil blocks were 9 x 10 x 11 inches, and were excavated at depths ranging from 1 to 2.5 feet below the ground surface. Photographs taken at various stages of the block sampling operation are shown in Figure 4.5. The blocks of soil were excavated over a four-hour period on June 23, 1998, using small hand tools and razor wire. The work was performed from two parallel trenches that were excavated the previous evening with a small backhoe. The soil blocks were obtained by carefully carving a block from the undisturbed soil between the trenches. The blocks were set on plywood sheets, wrapped numerous times with plastic wrap, and sealed in plastic bags immediately after removing them from the ground. They were then transported to the laboratory on the plywood sheets, with great care to minimize shock and vibration.

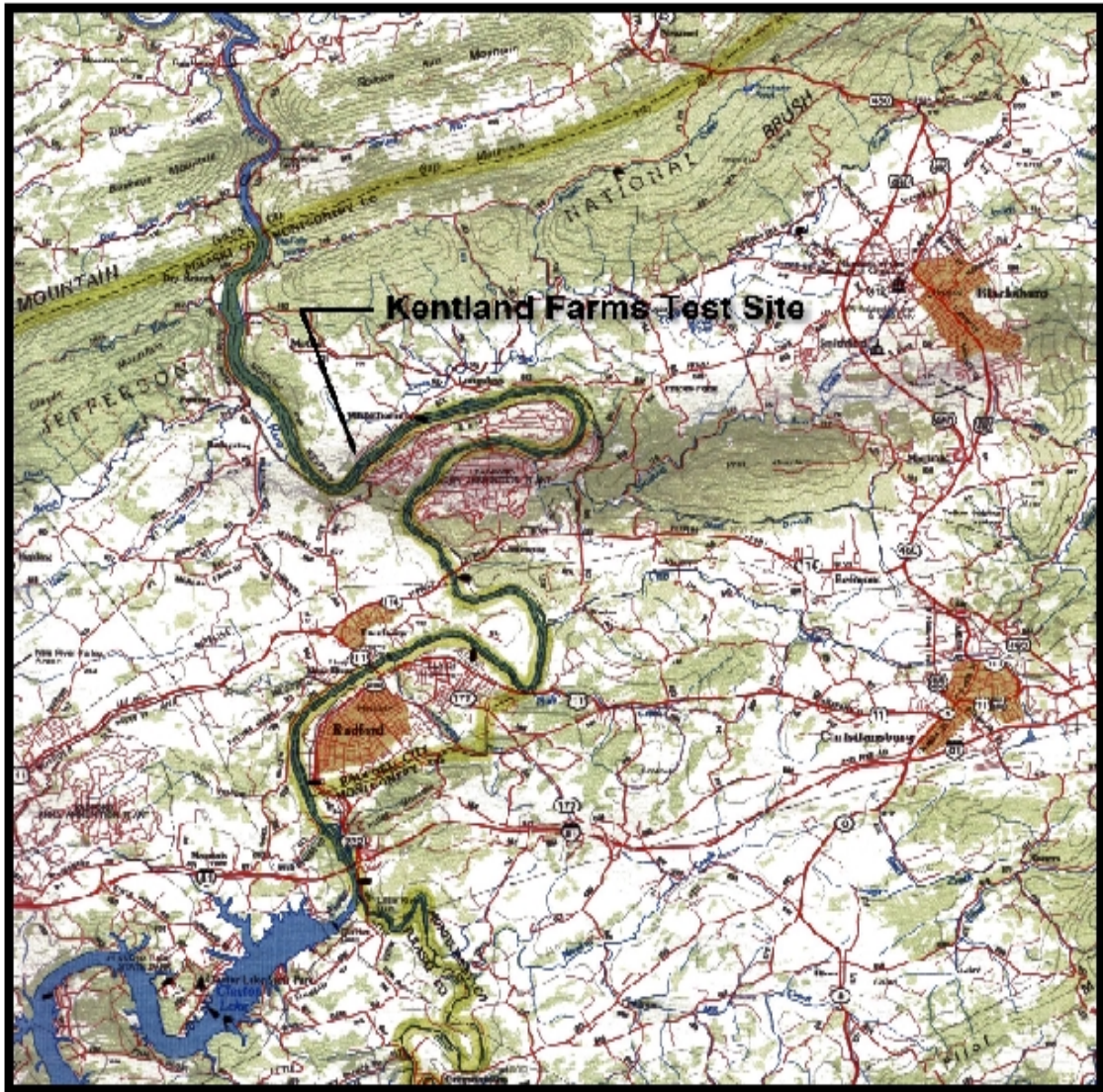


Figure 4.1. Site location map.

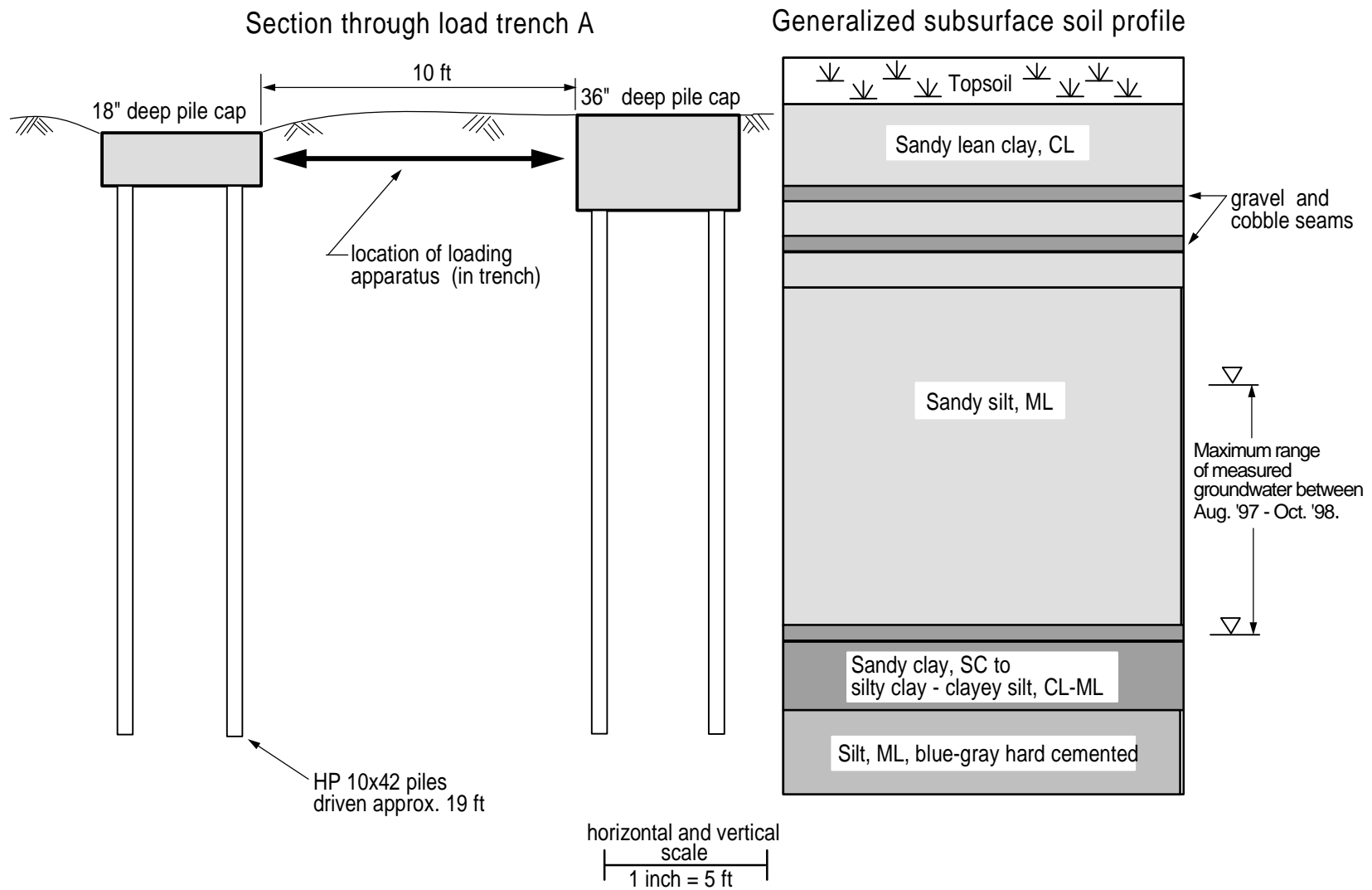


Figure 4.2. Subsurface profile at Kentland Farms field test facility.

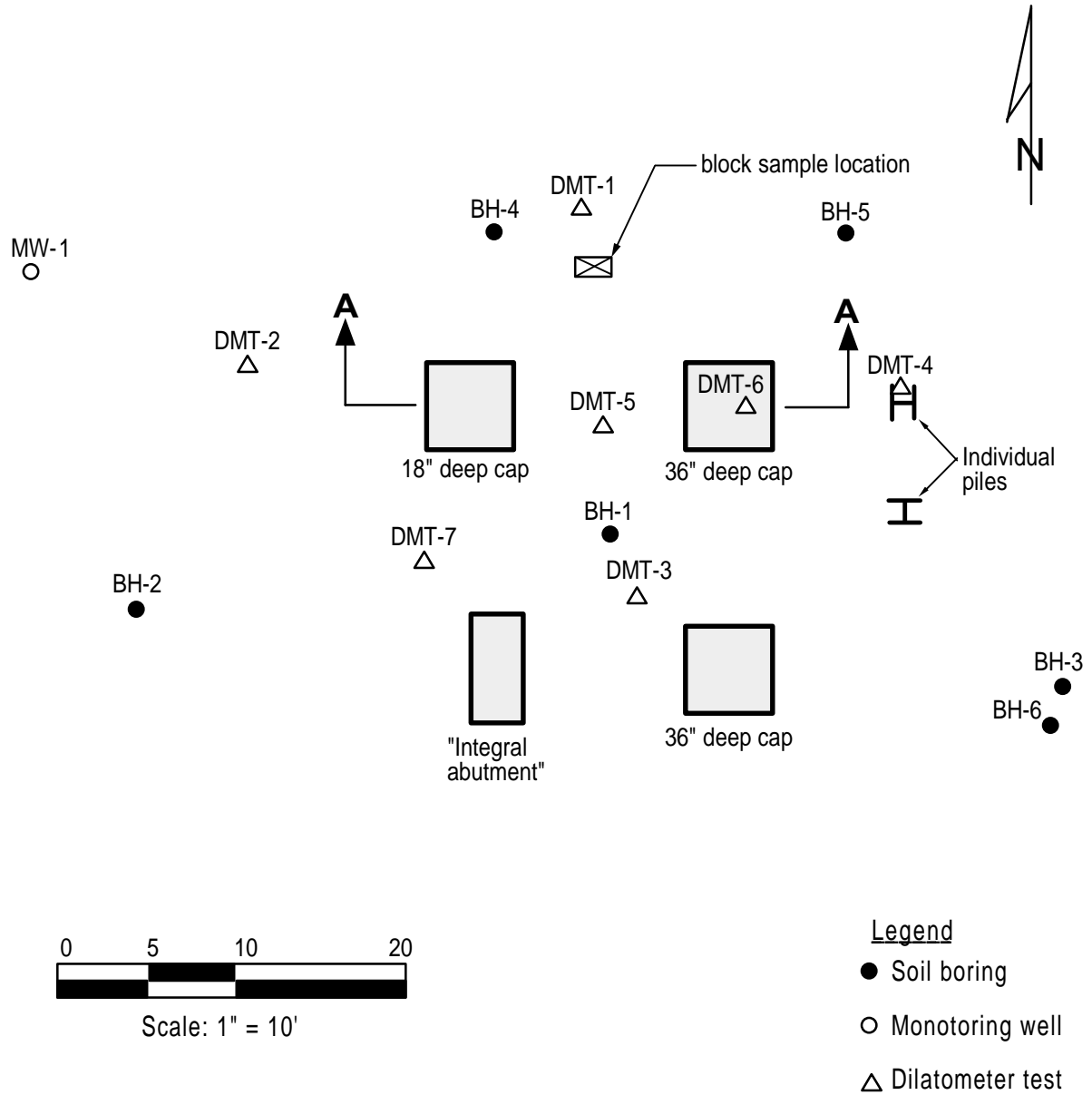


Figure 4.3. Site plan and subsurface investigation drawing.

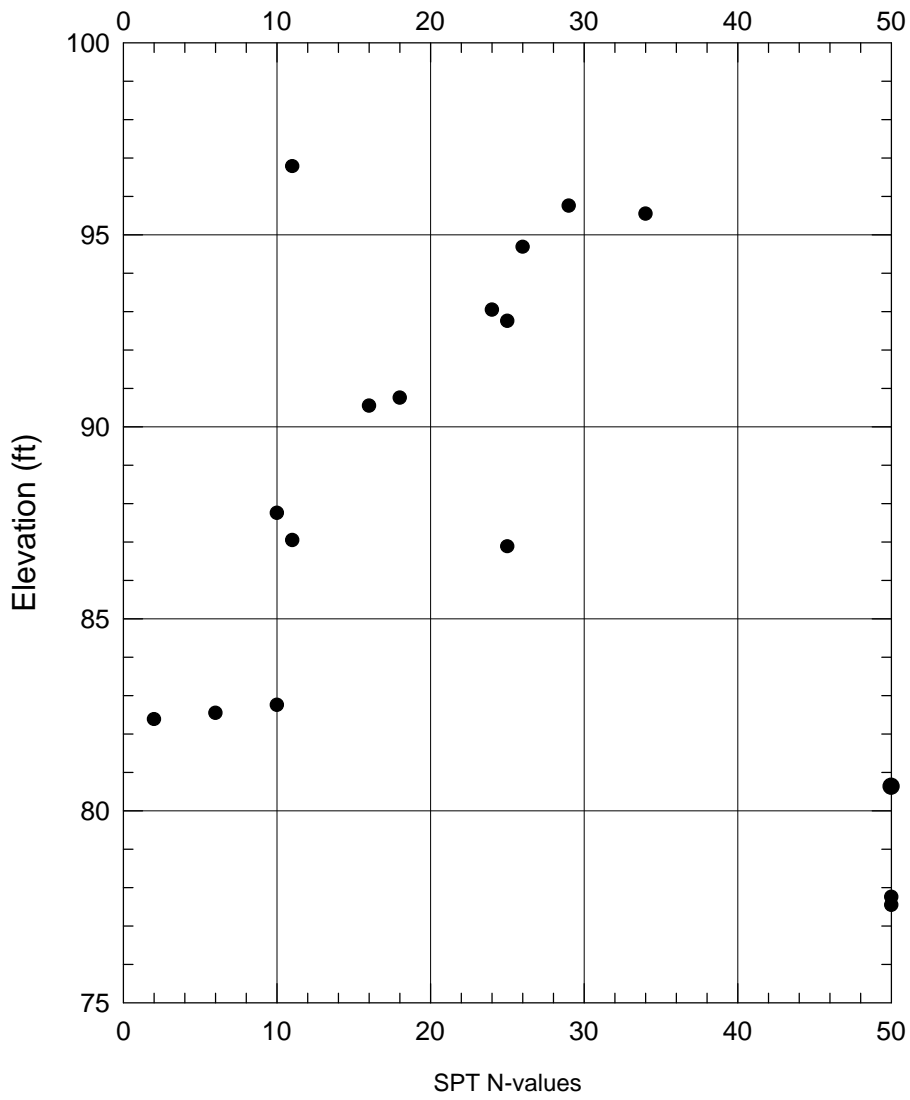


Figure 4.4. Standard penetration test results.



(a) Parallel trenches for digging block samples.



(b) Carving block samples.



(c) Block sample excavation almost complete.



(d) Block sample wrapped in cellophane.

Figure 4.5. Excavating soil block samples.



## **CHAPTER 5**

### **SOIL PARAMETERS**

#### **5.1 INTRODUCTION**

The focus of the laboratory testing program was to develop soil parameters that will be used to perform analyses of the full-scale lateral load tests. The laboratory tests included soil classification, unit weight, strength (UU, CU, and CD triaxial tests), and consolidation.

Tests were performed on soil samples obtained from the field test facility (natural soils) and on samples of imported materials that were used as backfill around the piles, pile caps, and bulkhead. Section 5.2 describes the results of tests on the natural soils, which consist of clayey and silty sands. Test results for the two backfill soils, crusher run gravel and New castle sand, are described in Section 5.3.

#### **5.2 NATURAL SOILS**

##### **5.2.1 Soil Description**

Test results for samples obtained at different depths are described according to the project benchmark, which was established at an arbitrary elevation of 100.00 feet. The actual elevation of the benchmark is unknown, but judging from the USGS Radford North quadrangle map, it is approximately 1700 feet above mean sea level. The ground surface in the area of the test foundations was relatively flat. The average surface elevation, after stripping the topsoil, was 97.5 ft.

The soil conditions at the site, which covers an area about 100 feet by 50 feet, are quite uniform. The soil profile revealed by six borings and two test pits was as follows:

<u>Elevation (ft)</u>	<u>Soil Description</u>
97.5 to 94.0	Brown silty sand and sandy lean clay with fine sands and frequent small roots.
94.0 to 88.5	Dark brown, moist sandy lean clay with occasional gravel.
88.5 to 84.5	Brown moist sandy silt with lenses of silty sand.
84.5 to 80.5	Brown, moist sandy silt and silty sand.
80.5 to 77.5	Light brown sandy lean clay and sandy silt with trace of gravel.

In general, the soils at the site consist of sandy clay, sandy silt, and silty sand with thin layers of gravel. In accordance with the Unified Soil Classification System (ASTM D2487), the soils are classified as ML, CL, SC, and CL-ML. Chapter 4 contains a description of the subsurface conditions encountered during the in situ investigation.

### **5.2.2 Index Properties and Unit Weights**

Index tests were performed to provide data necessary for classifying the soil and for developing correlations with various soil parameters. The percentage of soil passing the number 200 sieve, Atterberg limits, and natural moisture contents were determined in general accordance with ASTM D1140, D4318, and D2216. Summaries of results from these tests are shown in Table 5.1 and Figure 5.1.

Moist unit weights of the natural soil were estimated from triaxial and consolidation samples, and sand cone tests that were performed in the near-surface soils in accordance with (ASTM D 1556). Most of the values of unit weight fall between 115 and 125 pcf as shown in Figure 5.1 (d).



### 5.2.3 Consolidation Tests

Three one-dimensional consolidation tests were performed in general accordance with ASTM D2435, on specimens trimmed from undisturbed samples. Samples BH-4, ST-4, and BH-4 ST-5 were trimmed conventionally from undisturbed soil samples to represent vertical consolidation properties of the soil. Sample BH-4, SST-3 was trimmed such that it represented horizontal consolidation properties of the soil. The test specimens were loaded at twenty-four hour intervals using a load-increment ratio of one, and they were unloaded at twenty-four hour intervals using a load-increment ratio of four. Stress-strain curves from these tests are included in the Appendix D (Figure D.1), and the test results are summarized in Table 5.2.

### 5.2.4 Strength Tests

A total of 31 triaxial tests were performed on specimens trimmed from undisturbed Shelby tube samples and block samples. Of the 31 triaxial tests, 22 were UU (Unconsolidated-Undrained), 3 were CD (Consolidated-Drained), 3 were CU (Consolidated-Undrained), and 3 were staged CU tests. The UU specimens were tested at their natural moisture content. The CD and CU specimens were saturated by applying back pressure. The CD, CU and 21 of the UU specimens were carved from Shelby tube samples. These specimens were all trimmed to a nominal diameter of 1.4 inches and a nominal height of 3 inches.

Ten of the UU specimens were carved from block samples. Four of these were trimmed vertically and the remaining 6 were trimmed horizontally. Seven of the specimens were trimmed to a nominal diameter of 1.4 inches and a nominal height of 3 inches. The other 3 specimens were trimmed vertically to a nominal diameter of 2.8 inches and a nominal height of 5.6 inches.

**Total stress shear strength parameters.** A summary of the UU triaxial results is presented in Table 5.3. Plots of  $p$  versus  $q$  at failure are shown in Figure 5.2(a) for tests performed on samples obtained at 4 different elevations. The same results are re-plotted

in Figure 5.2(b) as a function of  $q$  at failure and cell pressure. The undrained strength parameters were estimated using the curves and transformation equations shown in Figure 5.2(b), with emphasis on values measured at cell pressures less than 7 psi. The total stress parameters for the natural soils, determined in this manner, are as follows:

<u>Elevation (ft)</u>	<u><math>\phi</math> (deg)</u>	<u><math>c</math> (psi)</u>
96.0	38	7.0
92.8	35	6.0
90.5	23	4.7
88.2	28	4.4

There was no discernable difference in undrained behavior between the vertically and horizontally trimmed specimens, or between the small diameter and large diameter specimens.

Values of  $\epsilon_{50}$ , the strain required to mobilize 50 % of the soil strength, were estimated from the triaxial stress strain curves. The estimated variation of  $\epsilon_{50}$  with depth is shown in Figure 5.1(f). The values increase with depth from about 0.005 in the stiff upper crust to 0.025 in the underlying softer soils. These are in good agreement with Reese et al.'s (1997) recommended  $\epsilon_{50}$  values of 0.005 for stiff clay and 0.020 for soft clay.

Stress-strain curves for the 10 UU tests performed on block sample specimens are included in Appendix B. The confining pressure for these tests ranged from 0 to 4 psi. Values of the initial tangent modulus,  $E_i$ , were estimated by transforming the stress-strain data using the hyperbolic formulation described by Duncan and Chang (1970). The transformation procedure is shown in Figures D.2, D.3, and D.4 for the natural soils. The estimated values of  $E_i$  are shown in Figure 5.3(a).  $E_i$  does not vary significantly over the range of confining pressures that were used. Consequently, an average value of  $E_i = 6,200$  psi was selected for use in the analyses.

**Effective stress parameters.** Summaries of the CU and CD test results are presented in Tables 5.4 and 5.5. Plots of effective stress,  $p'$  versus  $q$ , at failure for the CU and CD tests are shown in Figure 5.4. No variation of effective strength parameters with depth was apparent from the data. Values of  $\phi'$  and  $c'$  determined from these tests are as follows:

	$\phi'$ (deg)	$c'$ (psi)
lower bound	27	0
best fit	32	0
upper bound	32	4.9

## 5.3 BACKFILL SOILS

### 5.3.1 Soil Description and Index Properties

Two soil types were used as backfill in the lateral load tests: New Castle sand and crusher run gravel. These materials were selected because they are representative of the types of backfill materials often used for pile caps, footings, and other buried structures.

**New Castle sand.** New Castle sand is a relatively clean, fine sand consisting predominantly of subangular grains of quartz. Plots of 2 grain size distribution curves are shown in Figure D.5. About 70 % of the sand passes the No. 40 sieve and less than 1 % passes the No. 200 sieve. The coefficient of uniformity is 2.0, the coefficient of curvature is 2.8, and the Unified Classification is SP. The specific gravity of solids, determined in general accordance with ASTM D854, is 2.65. The maximum and minimum densities determined in general accordance with ASTM D4253 and ASTM D4254 are 105 and 87.3 pcf, respectively.

**Crusher run gravel.** Crusher run gravel was obtained from the Sisson and Ryan Stone Quarry, located in Shawsville, Virginia. The material is produced by processing and screening quartz and limestone rock to produce a well-graded mixture containing

angular to subangular grains that range in size from ¾-inch gravel to silt-size particles. The gravel is produced to meet the requirements of VDOT Road and Bridge Specification Section 205, Crusher Run Aggregate. The material obtained for this project also meets the more stringent gradation requirements of VDOT Road and Bridge Specification Section 208, 21B-Subbase and Base Material.

Plots of 4 grain size distribution curves are shown in Figure D.6. Approximately 40 to 50 % of the material passes the No. 4 sieve, 10 to 20 % passes the No. 40 sieve, and 5 to 10 % passes the No. 200 sieve. The soil passing the No. 200 sieve classifies as nonplastic silt, ML. The coefficient of uniformity is 23, the coefficient of curvature is 2.8, and the Unified Classification for the crusher run aggregate ranges between a GW-GM and a SW-SM. This material is referred to as gravel or crusher run gravel in this report.

### 5.3.2 Standard Density Relationships

**New Castle sand.** Moisture-density relationships were determined for the New Castle sand using the modified Proctor procedure (ASTM D1557). The maximum dry unit weight was found to be 107 pcf at an optimum water content of 12 %. The maximum and minimum densities determined in general accordance with ASTM D4253 and ASTM D4254 are 105 and 87.3 pcf, respectively.

**Crusher run gravel.** CD triaxial tests were performed using crusher run gravel that was scalped on the ½-inch sieve size. The grain size distribution curve for the scalped gravel is shown in Figure D.6. Density tests were performed on unscalped and scalped samples to provide a means of correlating field (unscalped) densities with lab (scalped) densities, as shown in Figure 5.5.

The maximum dry densities were determined using the wet method, Method 1B. The dry method, Method 1A, did not yield realistic results because of bulking and segregation of the material during placement into the mold. The minimum dry densities were determined by pouring soil into the mold using a hand scoop (Method A) and by

filling the mold by extracting a soil filled tube (Method B). The results were essentially the same, and an average value was used. Based on these results, Figure 5.5 was developed to correlate density values measured in the field on unscalped material with density values measured in the lab on scalped material. The line shown in Figure 5.5 can be represented by the following equation:

$$Drs = 1.053Dru - 6.4 \quad \text{Equation 5.1}$$

where  $Drs$  is the relative density of the scalped material, and  $Dru$  is the relative density of the unscalped material. The differences between the two becomes insignificant at relative densities greater than 60 %. For example, a field relative density measurement of 65 % ( $Dru = 65$  %) corresponds to a lab scalped value of  $Drs = 62$  %.

Moisture-density relationships were determined for the crusher run gravel using the Modified Proctor (ASTM D1557) and the Standard Proctor (ASTM D698) methods. The results are as follows:

<u>Modified Proctor</u>	<u>Unscalped</u>	<u>Scalped</u>
maximum dry density	147.4 pcf	146.1 pcf
optimum water content	4.9 %	5.1 %
<u>Standard Proctor</u>		
maximum dry density	135.7	-
optimum water content	7.6	-

### 5.3.3 In-Place Densities

Excavated zones around the pile caps and single piles were backfilled using two methods. The first method involved placing New Castle sand into the excavation in a loose condition. This was achieved by end-dumping and shoveling dry sand into the excavation with no additional compaction effort. The drop height was maintained at a constant level during sand placement.

The second method involved placing backfill in 8-inch-thick lifts and compacting it with a Wacker “jumping jack” compactor. This method was used to achieve a dense backfill condition for both the New Castle sand and the crusher run gravel. The soil water content was maintained near its optimum water content during placement.

Because of intermittent rains during construction, the natural soil at the bottom of the excavations was often wet, and medium to soft in consistency. A dryer and thicker lift of backfill (10 to 12 inches deep) was placed on the excavated surface to “bridge” over soft and wet soils. Consequently, the initial lift of backfill was less dense than the backfill in the upper lifts.

Nuclear density gauge and sand cone tests were performed during backfill placement in general accordance with ASTM D3017 and ASTM D1556, respectively. Nuclear density gauge tests were performed after compacting each lift of backfill. Sand cone tests were performed to calibrate the nuclear gage for both backfill materials. The statistical distribution of field density results are shown in Figure D.7. A summary of the average results from the moisture-density tests are shown in Table 5.6. The following values were selected for use in subsequent analyses:

<u>Backfill</u>	<u><math>\gamma_m</math> (pcf)</u>	<u><math>D_r</math> (%)</u>
compacted sand	104	60
uncompacted sand	92	10
compacted gravel	134	55

The densities were reduced from the values shown in Table 5.6, to account for the lower density soil in the bottom of the excavations. These reduced values represent the average density of the backfill in the excavations.

### 5.3.4 Strength Tests

Shear strength versus relative density relationships for the backfill soils were developed using the results of the CD triaxial tests, which were performed on reconstituted 2.8-inch-diameter specimens at low confining pressures. A suite of tests were performed at relative densities ranging from loose to very dense. Table 5.7 contains a summary of CD test results for New Castle sand samples that were tested at relative densities of 20, 60, and 80 percent. Table 5.8 contains a summary of CD test results for crusher run aggregate samples that were tested at relative densities of 50, 70, and 90 percent. Stress-strain curves for the 19 CD tests are shown in Figures D.8 through D.13.

Test specimens were prepared using the method of undercompaction developed by Ladd (1978). The advantages of this procedure is that it uses the same type of compaction energy that was used in the field, and it provides a means of obtaining consistent and repeatable results, with minimal particle segregation. Specimens are prepared to a target relative density by placing soil in layers, inside a forming jacket, and compacting each layer with a small tamper. The compaction density of each layer is varied linearly from the bottom to the top, with the bottom (first) layer having the lowest density. A nearly uniform density is achieved throughout the specimen because compaction of each succeeding layer further densifies the underlying lower layers, which are compacted initially to densities below the target density.

The results were normalized using the  $\phi_o - \Delta\phi$  approach (Duncan et al. 1980) to account for curvature of the failure envelope caused by changes in the level of confining stress. Equation 5.2 is used to determine the friction angle,  $\phi'$ :

$$f' = f'_o - \Delta f \log \left( \frac{s'_3}{p_a} \right) \quad \text{Equation 5.2}$$

where  $\phi_0$  is the friction angle at 1 atmosphere confining pressure,  $\Delta\phi$  is the change in  $\phi'$  over one log cycle,  $\sigma'_3$  is the effective confining pressure, and  $p_a$  is the atmospheric pressure.

Mathematical expressions were developed for calculating  $\phi_0$  and  $\Delta\phi$  based on the relative density of the soil. These expressions were developed using the following procedure:

1.  $\phi'$  was plotted on a semi-log scale as a function of the effective confining pressure, normalized by atmospheric pressure, as shown in Figure 5.6. The solid symbols represent CD test results. The 3 open symbols in Figure 5.6(a) represent the results of CU tests with pore pressure measurements.
2. Straight lines were fit through each set of data points to determine  $\phi_0$  and  $\Delta\phi$  values. These values are tabulated in Figure 5.6 for New Castle sand and crusher run gravel.
3. The  $\phi_0$  and  $\Delta\phi$  values were plotted as functions of relative density in Figure 5.7. Equations representing best fit straight lines were developed for the data as shown in Figure 5.7(a) for the sand and Figure 5.7(b) for the gravel.

Using these expressions and the relative density values presented in Section 5.3.3, the following estimates of  $\phi_0$  and  $\Delta\phi$  were calculated for the backfill materials.



<u>Backfill</u>	<u>D<sub>r</sub> (%)</u>	<u>φ<sub>o</sub> (deg)</u>	<u>Δφ (deg)</u>
compacted sand	60	40.3	7.8
uncompacted sand	10	32.1	4.5
compacted gravel	55	45.0	8.3

Effective stress friction angles were calculated using these values of  $\phi_o$  and  $\Delta\phi$ , and Equation 5.2. This was done for the backfill soils at depths of 0.75, 1.5, and 3 feet, as shown in Table 5.9. The effective cohesion is zero for the backfill soils.

Values of the initial tangent modulus,  $E_i$ , were estimated by transforming the stress-strain data using the hyperbolic formulation described by Duncan and Chang (1970). The transformed stress-strain plots are shown in Figures D.8, D.9, and D.10 for New Castle sand and Figures D.11, D.12, and D.13 for crusher run gravel.  $E_i$  values from the transformed stress-strain plots are shown as functions of relative density in Figure 5.3(b) for New castle sand and Figure 5.3(c) for crusher run gravel. Based on these plots, the following values of  $E_i$  will be used for the backfill soils:

<u>Backfill</u>	<u>E<sub>i</sub> (psi)</u>
compacted sand	9,700
uncompacted sand	5,000
compacted gravel	5,300

## 5.4 SUMMARY

The natural soils encountered at the Kentland Farms field test site consisted of sandy silt, sandy clay, and silty sand, with thin lenses of gravel. Two types of backfill soils were used: a poorly graded fine sand (New Castle sand) and a well graded silty gravel (crusher run gravel).

A laboratory testing program was developed to measure soil properties and to provide a basis for estimating the values of all the parameters that will be used to perform analyses of the full-scale lateral load tests. The results that will be used in the analyses described in Chapter 7, are summarized below:

- Distributions of  $\phi$ ,  $c$ ,  $\gamma_m$ , and  $\epsilon_{50}$  are shown in Figure 5.8, for the natural soils.
- Shear strengths parameters for the backfill soils ( $\phi'$  and  $\gamma_m$ ) are summarized in Table 5.9. The effective cohesion is zero for the backfill soils.
- Values of initial tangent modulus for the natural soil and backfill soils are shown in Figure 5.3.

Table 5.1. Summary of index test results on samples of natural soil.

Borehole and sample No.	Elevation (ft)	Finer than No. 200 Sieve <sup>a</sup> (%)	Liquid limit <sup>b</sup> (%)	Plasticity index <sup>c</sup> (%)	USCS <sup>d</sup>	Moist unit weight (pcf)	Natural moisture content (%)	Dry unit weight (pcf)
BH-1, cuttings	67.5 +/-	85.9	Non-viscous	Non-plastic	ML	-	20.6	-
BH-2, SS-1	95.0 – 93.5	59.8	40.5	21.8	CL	-	18.3	-
BH-2, SS-2	92.5 – 91.0	60.6	39.1	17.8	CL	-	22.2	-
BH-2, SS-3	90.0 – 88.5	51.5	34.0	8.6	ML	-	23.9	-
BH-2, SS-4	86.5 – 85.0	63.6	37.0	9.1	ML	-	27.8	-
BH-2, SS-5	82.0 – 80.5	30.7	29.5	9.0	SC	-	21.6	-
BH-2, SS-6	77.0 – 75.5	-	-	-	-	-	3.8	-
BH-3, SS-1	95.0 – 93.5	64.9	39.8	16.3	CL	-	21.3	-
BH-3, SS-2	92.0 – 90.5	63.3	35.0	6.2	ML	-	21.8	-
BH-3, SS-3	90.0 – 88.5	63.2	38.7	13.9	ML	-	24.2	-
BH-3, SS-4	87.0 – 85.5	61.4	35.3	12.3	ML	-	28.5	-
BH-3, SS-5	82.0 – 80.5	51.2	31.0	7.7	CL	-	26.1	-
BH-3, SS-6	77.0 – 75.5	52.2	15.0	3.9	CL-ML	-	10.8	-
BH-4, SS-1	95.5 – 94.0	73.4	33.5	9.0	ML	-	22.6	-
BH-4, cuttings	87.5 – 86.5	55.0	41.0	17.8	CL	-	26.2	-
BH-4, SS-4	87.7 – 86.2	72.9	32.1	9.1	CL	-	27.9	-
BH-4, SS-6	83.2 – 81.7	-	-	-	-	-	25.9	-
BH-4, cuttings	81.5 – 81.0	38.7	34.3	10.1	SC	-	27.7	-
BH-4, SS-7	81.0 – 79.5	68.0	21.1	1.6	ML	-	22.2	-
BH-4, ST-3	90.0-87.7	-	-	-	-	111	24.0	89.5
BH-4, ST-5	85.5-83.2	-	-	-	-	124	-	-

Table 5.1. Concluded.

Borehole and sample No.	Elevation (ft)	Finer than No. 200 Sieve <sup>a</sup> (%)	Liquid limit <sup>b</sup> (%)	Plasticity index <sup>c</sup> (%)	USCS <sup>d</sup>	Moist unit weight (pcf)	Natural moisture content (%)	Dry unit weight (pcf)
BH-5, cuttings	78.5 – 76.5	61.8	24.6	4.6	ML-CL	-	24.4	-
BH-5, ST-1	97.5-95.4	-	-	-	-	125	21.0	103.3
BH-5, ST-2	93.9 - 91.6	-	-	-	-	115	26.0	91.3
BH-5, ST-3	91.6 – 89.3	-	-	-	-	121-124	23.0*	98.4-100.8
BH-5, ST-4	89.3 – 87.0	-	-	-	-	115-119	26.0*	91.3-94.4
BH-5, ST-5	87.0 – 84.7	68.3	30.6	28.8	-	117	21.6	96.2
BH-5, ST-6	84.7 – 82.4	-	-	-	-	106-122	25.0*	84.5-98.6
BH-6, SS-1	97.0 – 95.5	34.2	37.8	10.0	SC	-	22.6	-
BH-6, ST-2	94.0 – 91.7	70.0	37.9	16.3	CL	-	21.6	-
Block 3	96.0 – 95.0	68.4	37.6	11.6	ML	121-125	20.0-22.6	99-104
<u>Notes</u>				<u>Type of sample</u>				
<sup>a</sup> ASTM D1140 <sup>b</sup> ASTM D 4318 <sup>c</sup> ASTM D 4318 (PI = LL – PL) <sup>d</sup> ASTM D 2487 (USCS = Unified Soil Classification System) <sup>e</sup> ASTM D 2216 * average moisture content				Cuttings (auger cuttings) SS (split spoon) ST (Shelby tube) Block (hand cut)				

Table 5.2. Summary of consolidation test results on samples of natural soil.

Sample	Elevation (ft)	P <sub>o</sub> (tsf)	P <sub>p</sub> (tsf)	OCR	C <sub>ec</sub>	C <sub>er</sub>	Permeability (cm/sec)
BH-5, ST-3*	90.5	0.42	5-10	-	0.13-0.14	0.025-0.040	K <sub>h</sub> =6.8x10 <sup>-7</sup>
BH-5, ST-4	87.5	0.60	5-10	8.3-16.7	0.14-0.17	0.030-0.035	k <sub>v</sub> =1.6x10 <sup>-7</sup>
BH-4, ST-5	84.5	0.78	5-10	6.4-12.8	0.17-0.18	0.013-0.030	k <sub>v</sub> =1.2x10 <sup>-6</sup>
* Sample BH-5, ST3 was trimmed horizontal.							

Table 5.3. Summary of UU test results on samples of natural soil.

Borehole No.	Sample	Elevation (ft)	Cell pressure (psi)	Strain rate (% / min)	$p_{max}$ (psi)	$q_{max}$ (psi)	Axial strain at failure (%)
BH-5	ST-2 #6	93.9 to 91.6	5	1.0	25.0	20.0	3.42
	ST-2 #4		10		38.4	28.4	2.43
	ST-2 #3		20		59.3	39.3	3.10
	ST-2 #1		30		71.9	41.9	6.52
BH-5	ST-3 #3	91.6 to 89.3	5	1.0	25.3	20.3	4.62
	ST-3 #6		10		33.5	23.5	5.88
	ST-3 #2		20		53.1	33.1	4.96
	ST-3 #4		30		67.4	37.4	5.35
BH-5	ST-4 #3	89.3 to 87.0	5	1.0	20.2	15.2	16.36
	ST-4 #2		10		27.3	17.3	14.53
	ST-4 #1		20		45.1	25.1	8.87
	ST-4 #4		30		57.0	27.0	4.62
Block 3	#2, vert., 1.4 in dia.	95.5	3	0.3	12.9	9.8	2.21
	#3, vert., 1.4 in dia.		2		19.6	17.6	2.72
	#4, vert., 1.4 in dia.		0		14.5	14.5	0.93
	#5, vert., 1.4 in dia.		4		24.6	20.6	1.91
	#6, horz., 1.4 in dia.	95.5	0	0.3	13.6	13.6	1.35
	#7, horz., 1.4 in dia.		4		25.0	21.0	2.31
	#8, horz., 1.4 in dia.		2		19.3	17.3	1.96
	#9, vert., 2.8 in dia.		95.5		2	0.3	29.71
Block 1	#10, vert., 2.8 in dia	95.5	4	0.3	22.21	18.21	3.57
	#11, vert., 2.8 in dia		0		13.67	13.67	1.89

Failure criterion: maximum deviator stress.

Table 5.4. Summary of CU test results on samples of natural soil.

Borehole No.	Sample	Elevation (ft)	B*	Cell pressure (psi)	Strain rate (% / min)	p' <sub>max</sub> (psi)	q <sub>max</sub> (psi)	Axial strain at failure (%)
BH-4	ST-3 #3	89.0	0.93	10	0.10	45.2	25.6	10.76
	ST-3 #4	88.5	0.95	20	0.08	41.9	23.5	5.33
	ST-3 #5	88.0	0.98	30	0.06	50.7	26.0	8.51
BH-5	ST-1 #2	96.5	0.93	-	-	-	-	-
	Stage 1	-	-	3.55	0.1	-	-	-
	Stage 2	-	-	8.96	0.1	-	-	-
	Stage 3	-	-	15.04	0.1	-	-	-
BH-5	ST-5 #3	86.0	0.95	-	-	-	-	-
	Stage 1	-	-	5	0.1	15.3	10.1	-
	Stage 2	-	-	10.1	0.1	22.6	13.9	-
	Stage 3	-	-	14.9	0.1	30.7	17.7	4.76
BH-5	ST-6 #1	84.5	0.97	10.3	0.1	9.0	4.5	20.67
	ST-6 #2	84.0	0.98	21.3	0.1	20.6	11.3	20.23
	ST-6 #5	83.0	0.97	30.2	0.07	39.6	21.6	14.09
BH-5	ST-6 #4	83.5	0.93	-	-	-	-	-
	Stage 1	-	-	5.04	0.07	15.5	9.9	-
	Stage 2	-	-	10.0	0.07	21.0	12.5	-
	Stage 3	-	-	15.03	0.07	31.6	17.8	7.46
<u>Notes</u> * B = Skempton's pore pressure coefficient. Failure criterion: maximum deviator stress.								

Table 5.5. Summary of CD test results on samples of natural soil.

<b>Borehole No.</b>	<b>Sample</b>	<b>Elevation (ft)</b>	<b>B*</b>	<b>Cell pressure (psi)</b>	<b>Strain rate (% / min)</b>	<b>p' max (psi)</b>	<b>q max (psi)</b>	<b>Axial strain at failure (%)</b>
BH-5	ST-5 #4	85.5	0.94	10.0	0.104	29.6	19.6	4.40
	ST-5 #5	85.1	0.95	20.0	0.060	48.2	28.2	7.94
	ST-5 #6	84.8	0.96	30.0	0.010	68.8	38.8	14.23
<p><u>Notes</u>                      * B = Skempton's pore pressure coefficient.                      Failure criterion: maximum deviator stress</p>								



Table 5.6. Average results from field moisture-density tests.

Soil type	Nuclear gage results			Corrected results based on sand cone tests		
	$\rho_n$ (pcf)	$w_c$ (%)	$\rho_{dry}$ (pcf)	$\rho_n$ (pcf)	$\rho_{dry}$ (pcf)	$D_r$ (%)
Crusher run gravel (unscalped)	141.0	4.7	134.7	134.1	128.1	67.4
Crusher run gravel (scalped)	-	-	-	-	-	64.6
New castle sand (compacted)	109.4	4.5	104.7	104.0	99.5	72.8
New castle sand (uncompacted)	92.1	3.6	88.9	88.9	88.9	10.6

Table 5.7. Summary of CD test results on compacted New Castle sand samples.

<b>Relative density (%)</b>	<b>Cell pressure (psi)</b>	<b>Maximum deviator stress (psi)</b>	<b>p' (psi)</b>	<b>q (psi)</b>	<b>Axial strain at failure (%)</b>
20	2.1	6.9	5.5	3.5	4.0
20	3.4	11.5	9.2	5.7	4.0
20	5.2	14.5	12.4	7.2	4.0
60	1.4	9.0	5.8	4.5	1.5
60	2.3	13.3	8.9	6.7	1.6
60	3.6	15.9	11.5	8.0	6.2
60	5.1	21.1	15.7	10.6	2.2
80	2.0	14.7	9.4	7.4	1.8
80	3.4	23.6	15.2	11.8	2.1
80	4.8	26.6	18.1	13.3	2.1

Table 5.8. Summary of CD test results on compacted crusher run gravel samples.

<b>Relative density (%)</b>	<b>Cell pressure (psi)</b>	<b>Maximum deviator stress (psi)</b>	<b>p' (psi)</b>	<b>q (psi)</b>	<b>Axial strain at failure (%)</b>
50	2.0	15.7	9.8	7.9	1.1
50	3.1	16.6	11.4	8.3	4.0
50	4.9	22.8	16.3	11.4	9.7
70	2.1	27.9	16.0	13.9	1.9
70	3.4	30.8	18.9	15.4	3.0
70	5.8	57.0	34.3	28.5	2.4
90	2.1	39.0	21.6	19.5	2.6
90	2.8	45.8	25.7	22.9	2.7
90	4.1	64.3	36.2	32.2	3.2

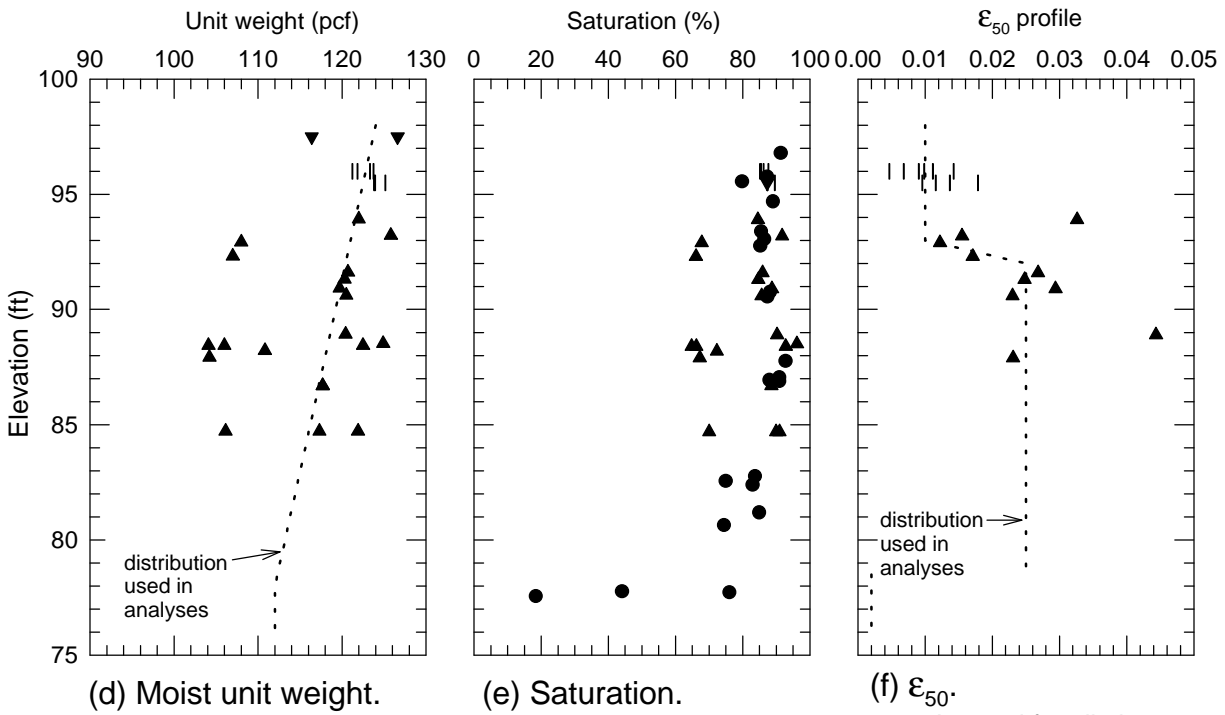
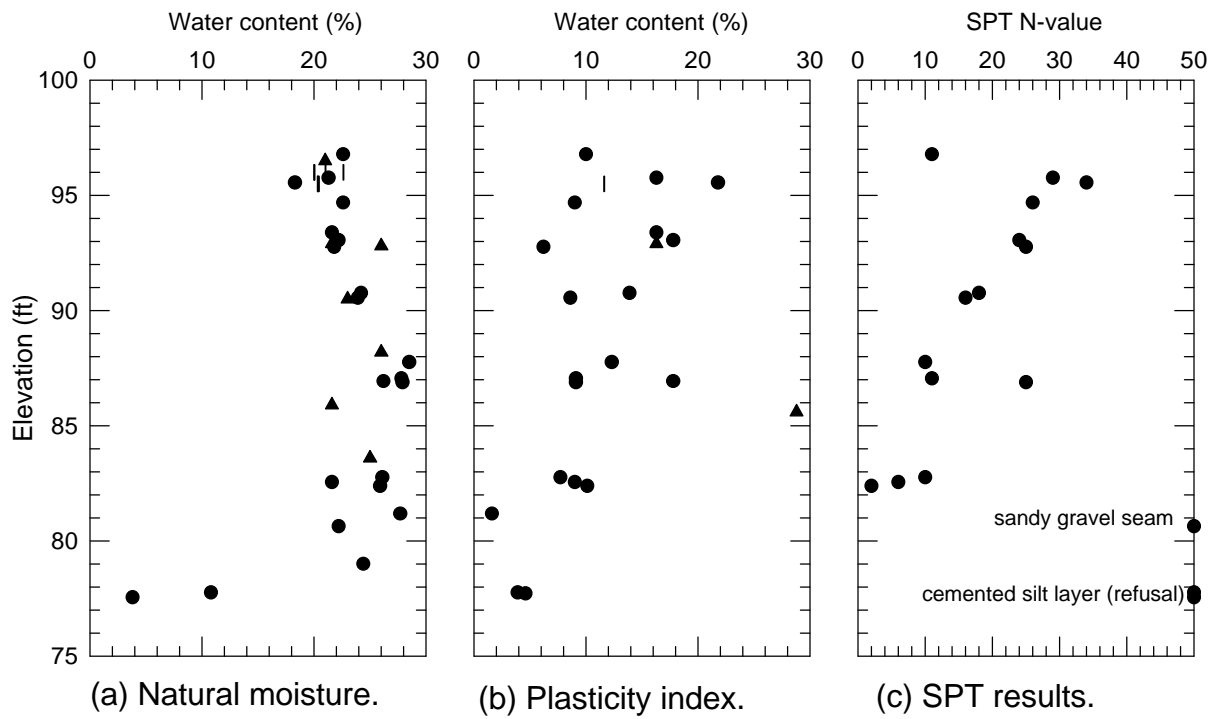
Table 5.9. Friction angles for New Castle sand and crusher run gravel.

Depth	Friction angle, $f_c$ (deg)		
	compacted sand $\gamma_m = 105$ pcf	uncompacted sand $\gamma_m = 92$ pcf	compacted gravel $\gamma_m = 138$ pcf
0.75	51	39	56
1.5	49	37	53
3	47	36	51

Note: 
$$f' = f_o - \Delta f \log \left( \frac{s_3}{p_a} \right)$$

$s_3$  = confining pressure

$p_a$  = atmospheric pressure (2117 psf)



Legend for all plots

- split spoon sample
- ▲ Shelby tube sample
- | block sample
- ▼ sand cone sample

Figure 5.1. Summary of index parameters for natural soils at the test facility.

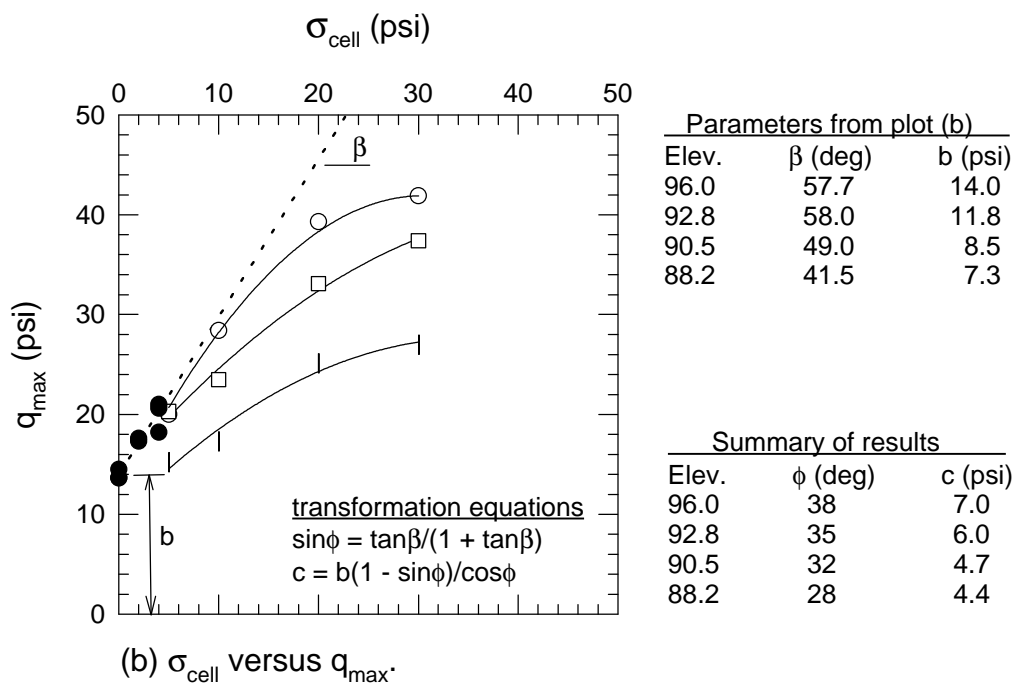
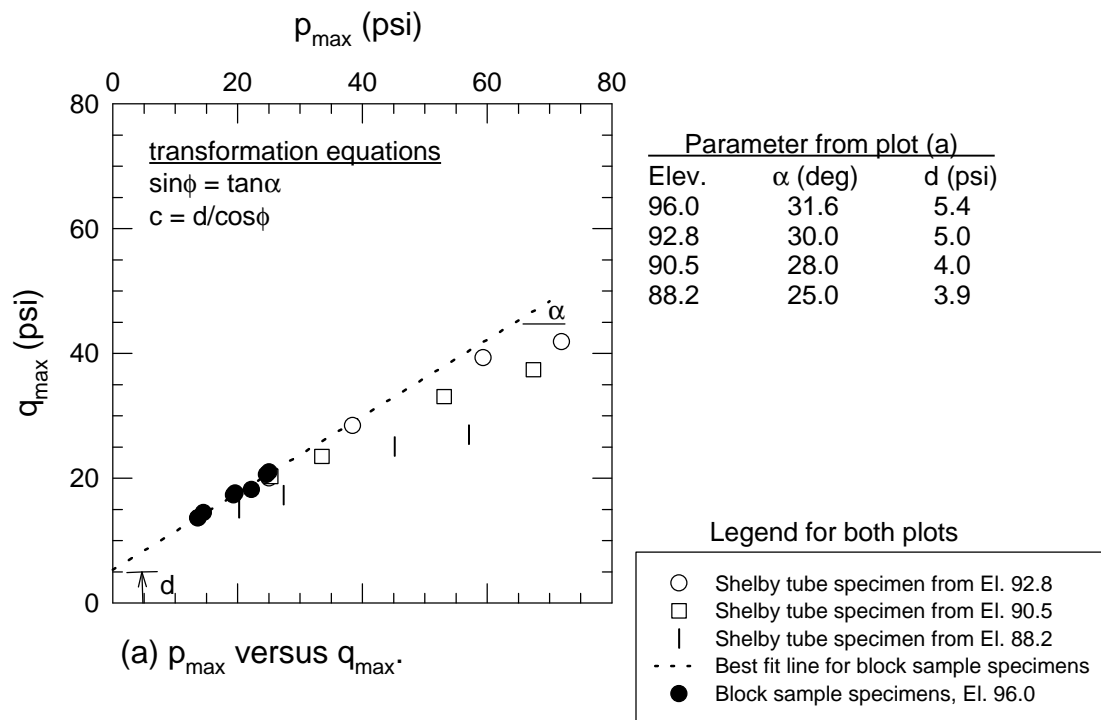


Figure 5.2. Natural soil strength parameters based on UU triaxial tests.

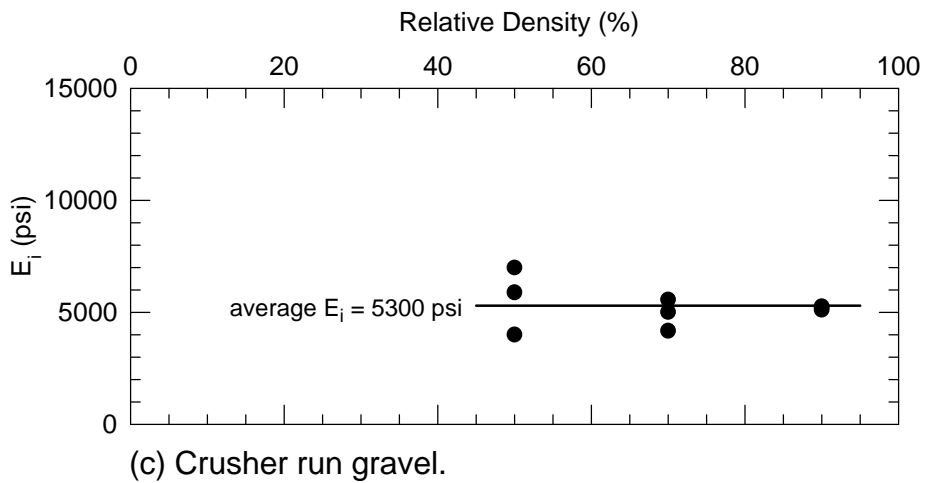
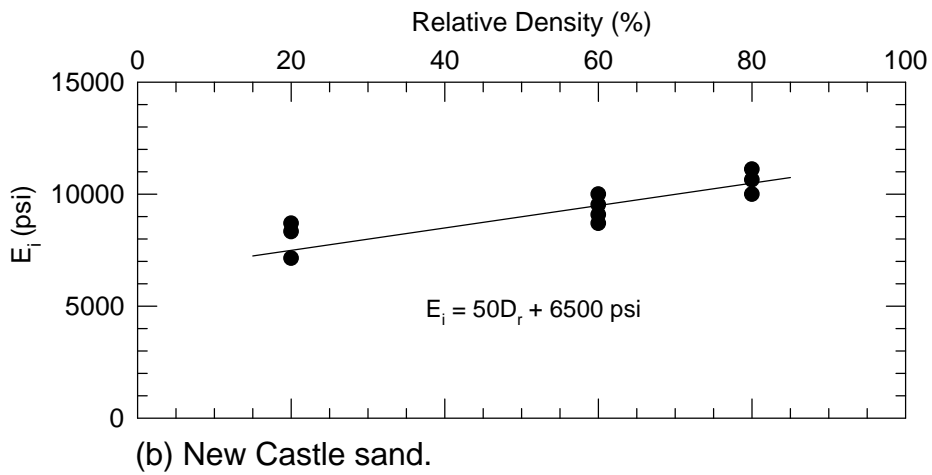
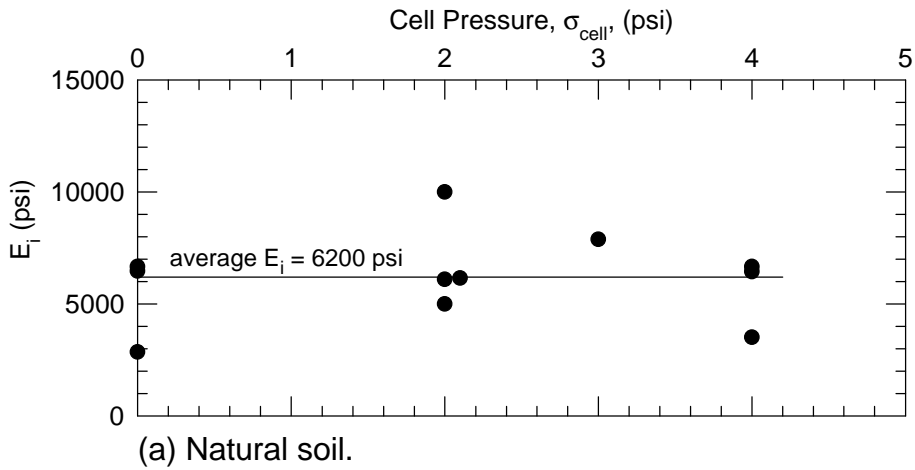


Figure 5.3. Initial tangent modulus ( $E_i$ ) for natural soil, New Castle sand, and crusher run gravel.

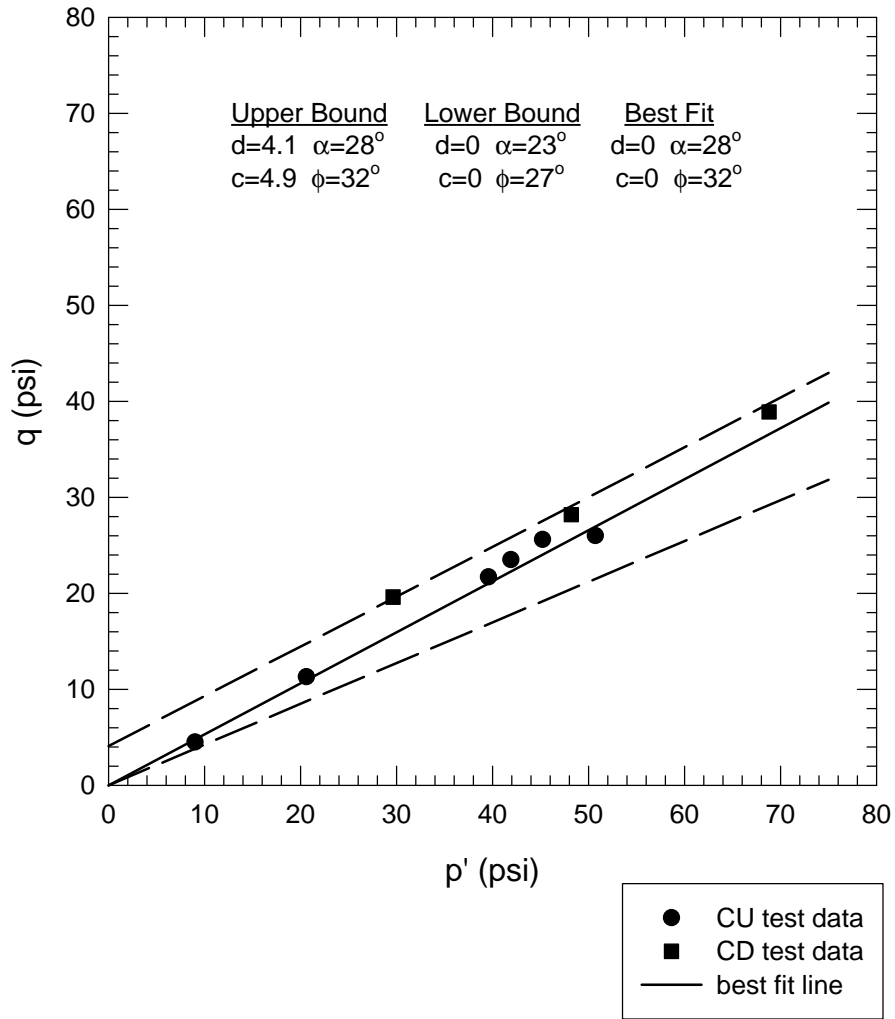


Figure 5.4. Maximum values of  $p'$  versus  $q$  for CU and CD triaxial tests on natural soil.



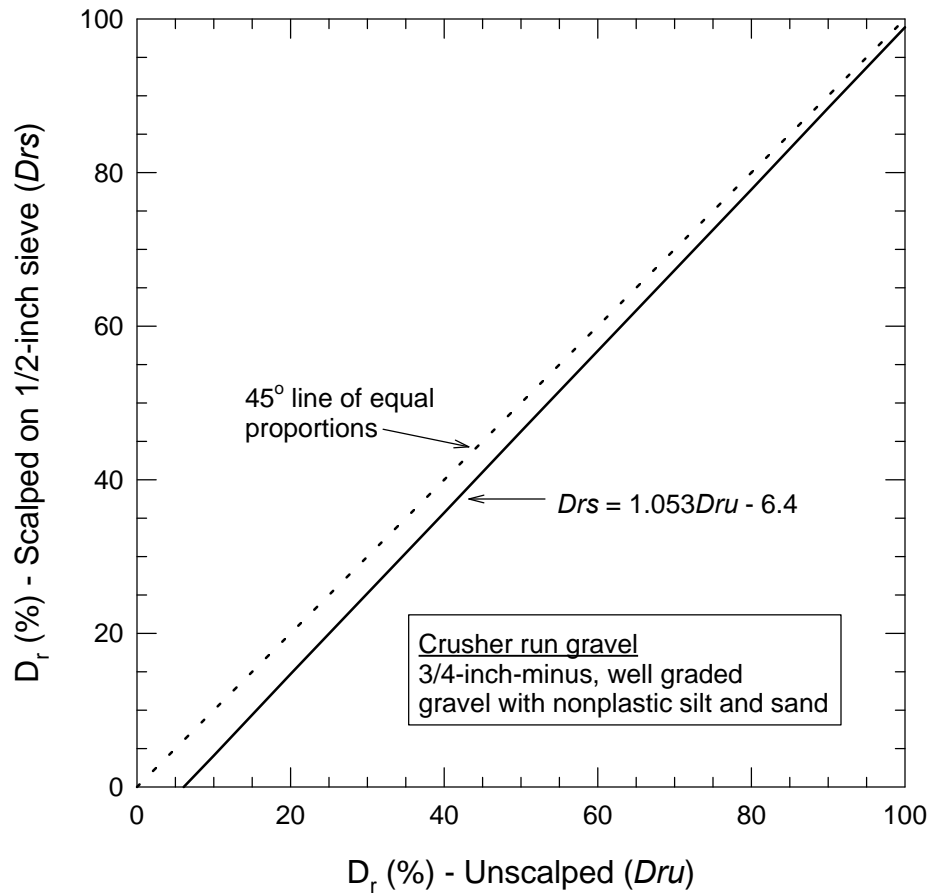
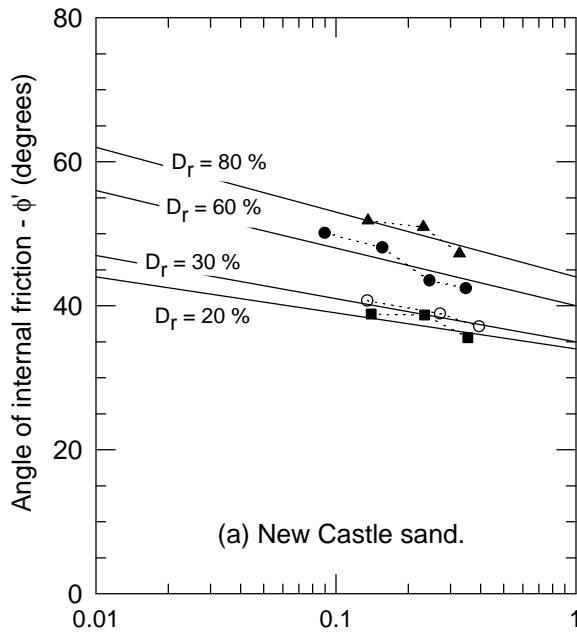


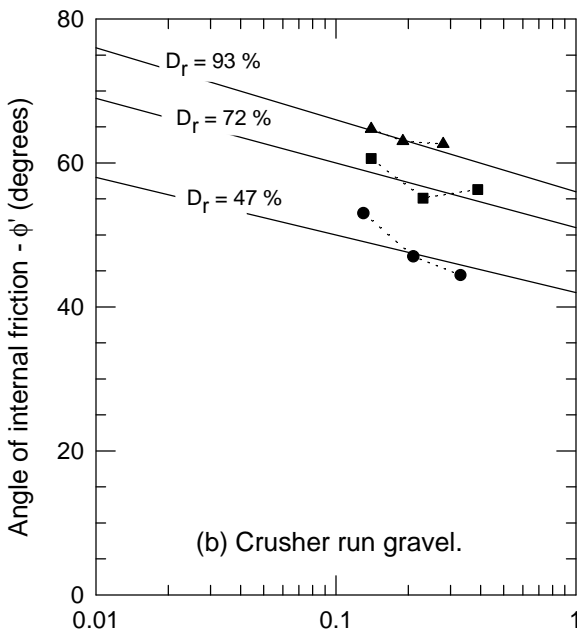
Figure 5.5. Relative density ( $D_r$ ) comparison of scalped and unscalped crusher run gravel.



New Castle Sand

$D_r$ (%)	$\phi_o$ (deg)	$\Delta\phi$ (deg)	Triaxial Test
20	34	5	CD
30	35	6	CU
60	40	8	CD
80	44	9	CD

Note: Solid symbols represent CD results, open symbols represent CU results.

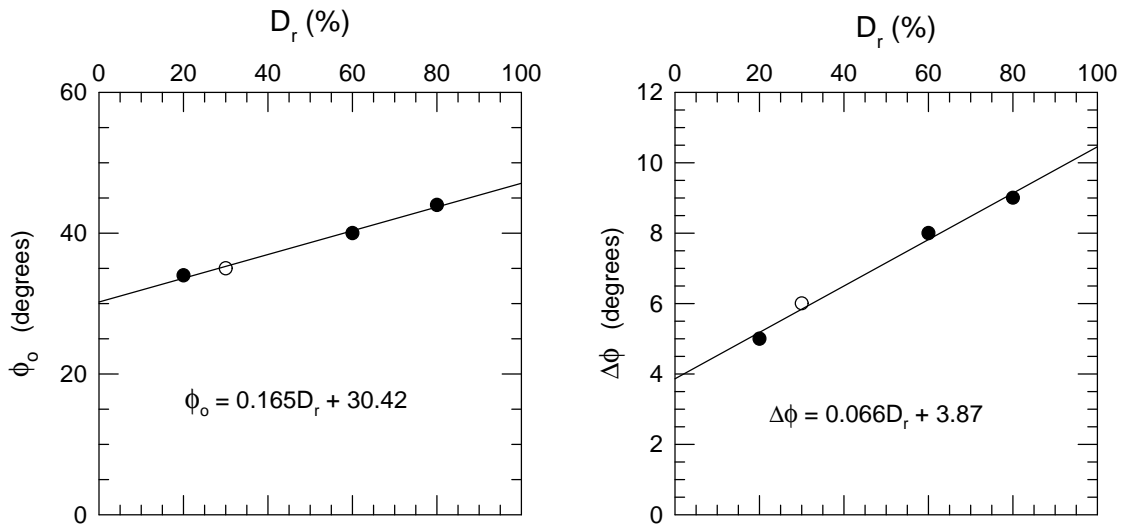


Crusher Run Gravel

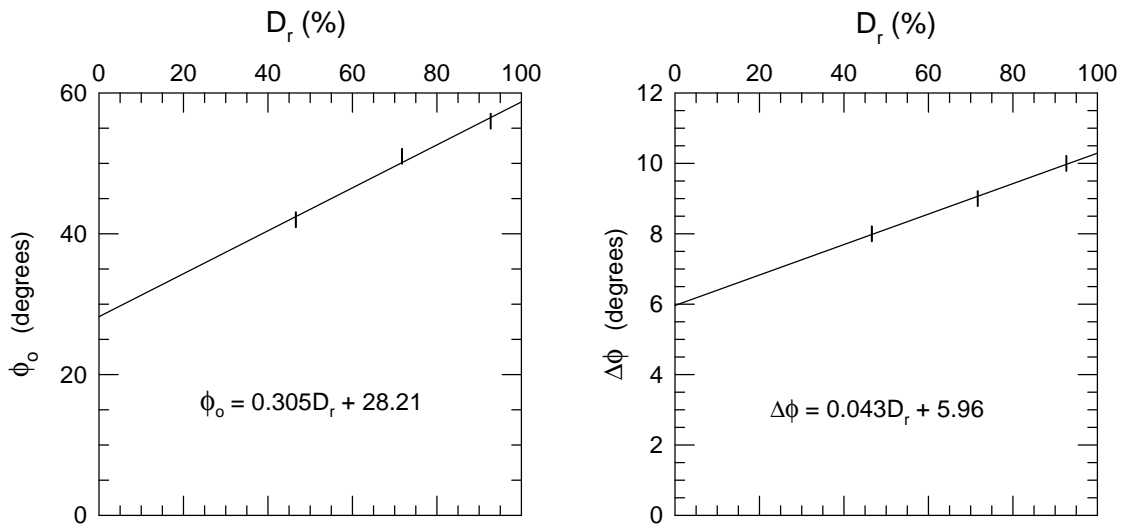
$D_r$ (%)	$\phi_o$ (deg)	$\Delta\phi$ (deg)	Triaxial Test
47	42	8	CD
72	51	9	CD
93	56	10	CD

Effective confining pressure  $(\sigma'_3/p_a)$  - log scale  
Atmospheric pressure

Figure 5.6. Effect of density on strength of New Castle sand and crusher run gravel.



(a.) New Castle sand.



(b.) Crusher run gravel.

Equation 5.2

$$\phi' = \phi_o - \Delta\phi \log_{10}(\sigma'_3/p_a)$$

where  $p_a$  = atmospheric pressure  
 $\sigma'_3$  = effective confining pressure

Note: Solid symbols represent CD results, open symbols represent CU results.

Figure 5.7. Distribution of  $\phi_o$  and  $\Delta\phi$  for New Castle sand and crusher run gravel.

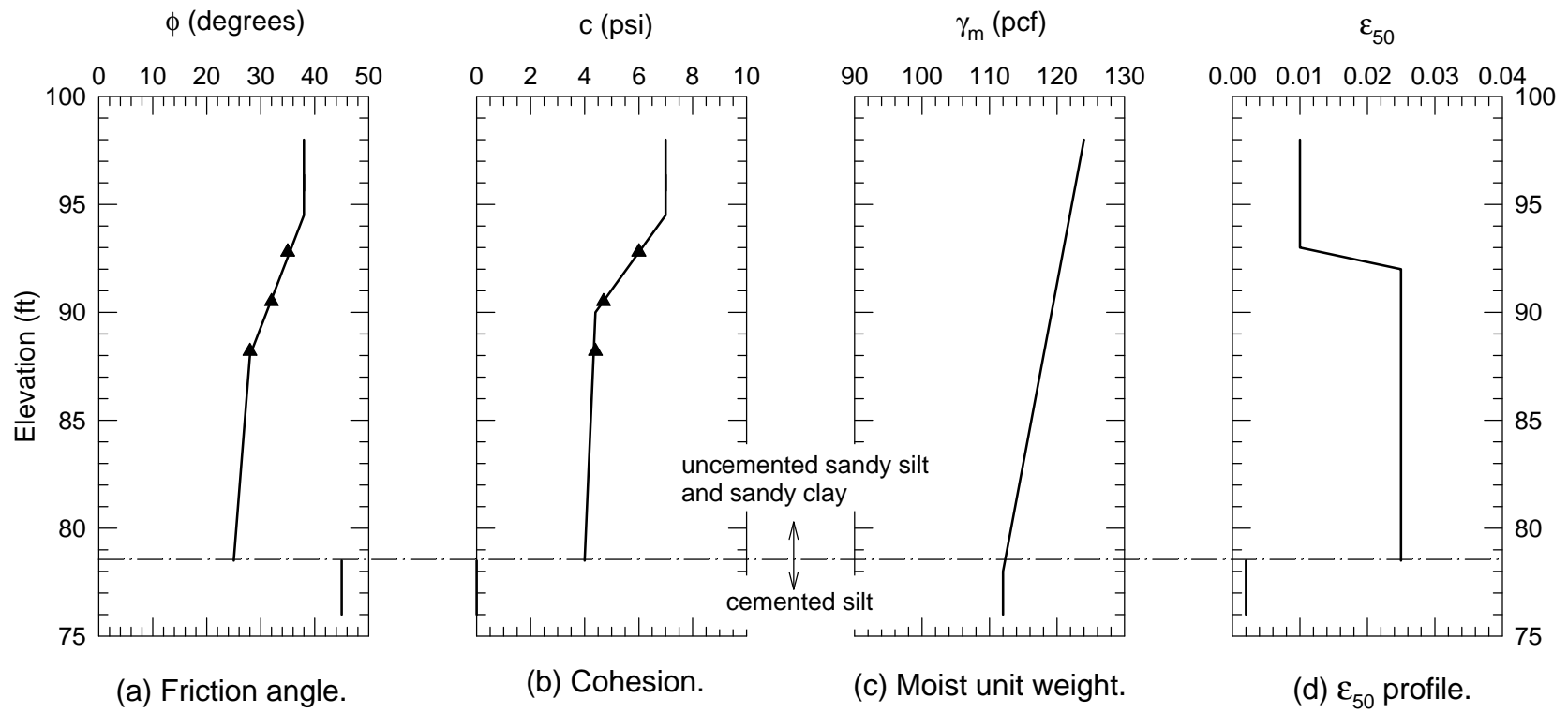


Figure 5.8. Soil parameter distributions for analytical models.

## CHAPTER 6

### LATERAL LOAD TESTS

#### 6.1 INTRODUCTION

Lateral load tests were conducted at the field test facility from early June through October, 1998. Thirty-one tests were performed on three groups of piles with embedded caps, two single piles, and a buried concrete bulkhead. The tests were conducted at locations A through D, identified in Figure 3.1.

The NE and NW piles were loaded against each other at location A. Tests conducted at this location are described in Table 6.1. The SE cap and the bulkhead were loaded against each other at location B. Tests conducted at this location are described in Table 6.2.

The north pile was tested in the direction of its strong axis using the NE cap as a counter reaction (location C). Tests conducted at this location are described in Table 6.3. The south pile was tested in its strong axis direction by loading it against the north pile (location D), which was embedded in concrete to increase its resistance. Tests on the south pile are described in Table 6.4.

#### 6.2 LOAD TESTS

In all the tests, compressive loads were applied through the vertical centroidal axis of the foundations. Tests were performed using incremental, cyclic, and sustained loading procedures, as described below.

The incremental procedure is historically the most recognized approach for performing lateral load tests on piles and drilled shafts. The procedure used in this study consisted of applying loads of increasing magnitude in 10 to 20 kip increments. A one-

minute-long pause was maintained between increments, at constant load. A typical distribution of data points obtained during the incremental procedure is shown in Figure 6.1(a). For easier viewing, intermediate points were filtered, and only the data at the end of each one-minute pause was plotted, as shown in Figure 6.1(b). A line or smooth curve was fit through the end points to facilitate comparisons among the various tests.

The cyclic procedure consisted of applying and releasing a large number of unidirectional loads. The time to complete one load cycle varied from approximately 40 seconds to 2 minutes. The loading and unloading frequency was controlled by the capacity of the hydraulic pump and the extended length of the ram plunger. After every 24 cycles the loading frequency was decreased. During the 25<sup>th</sup> cycle, loads were applied in 10 to 20 kip increments with a one-minute-long pause between increments. Readings were obtained during this cycle using same incremental procedure described in the previous paragraph.

Sustained loads were applied by incrementally increasing the load up to a predetermined level, and maintaining this level at a constant value over a 3 to 4 hour period.

The following two subsections describe the deformations and rotations that were observed during testing. Subsequent sections describe the results and their significance in more detail.

### **6.2.1 Deformations**

Examples of load versus deflection results for the south pile, SE cap, and bulkhead are shown in Figure 6.2. These plots cover the typical range of load and deflection values that were measured during the tests. Applied loads ranged from 0 to 140 kips, and maximum deflections ranged from 0.1 to almost 3 inches. For instance, the south pile deflected about 2.9 inches in loose sand, at a load of 45 kips (Figure 6.2a). While the SE pile cap in contact with natural soil deflected about 0.1 inches, at a load of

140 kips (Figure 6.2b). The bulkhead deflected approximately 1.6 inches at a load of 137 kips in natural soil and 90 kips in compacted gravel, as shown in Figure 6.2(c).

Pile cap deflections were relatively small, often less than 0.2 inches at the maximum load of 140 kips (the capacity of the loading system). This corresponds to a lateral load per pile of 35 kips, which exceeds typical design loads for HP 10 x 42 piles by a factor of three to four. These results are significant considering that many foundations are designed for maximum deflections of 0.5 to 1 inch, with no consideration of the resistance provided by the cap. This type of design approach is clearly over-conservative if cap resistance is ignored when the overall lateral resistance of the pile group is computed.

### 6.2.2 Rotations

Rotations at the tops of single piles depend on the magnitude of the applied load and the pile-head restraining condition. The maximum slope measured at the groundline during load testing was slightly less than 3 degrees for the north pile in dense sand. This occurred at a 45 kip load and a deflection of approximately 3.5 inches; a situation generally considered unsuitable in most practical applications.

Terms used to describe rotations of pile caps are defined in Figure 6.3 as follows:

$q$  = the angle of tilt in the direction of load (rotation about the horizontal axis), and

$t$  = the angle of twist or torsion of the cap about a vertical axis.

Rotations about a horizontal axis are primarily controlled by the stiffness of the cap, the stiffness of the pile-to-cap connection, and, for piles in groups, the axial capacity of the piles. Twisting of the cap may be caused by eccentricities in the applied load or non-heterogeneous conditions in the soil or backfill.

The angles of rotation ( $q$  and  $t$ ) measured during each test, are shown in Table 6.5 for the three caps and the bulkhead. The maximum value of  $t$  for the pile caps was 0.07 degrees, indicating that twisting or torsion of the pile caps was negligible in all of the tests. The angle of tilt,  $q$ , was also small. The SE pile cap, with soil removed from the cap sides and front, experienced the largest amount of tilt ( $q = 0.21$  degrees). In comparison,  $q$  was negligible (less than 0.001 degrees) for the NE cap embedded in natural soil.

The bulkhead experienced greater rotations because it was loaded to failure and was not supported on piles. The rotations of the bulkhead ranged from 0.07 degrees, for natural soil, to approximately 0.5 degrees for gravel backfill.

### 6.3 SINGLE PILE RESISTANCE

This section describes the results of lateral load tests performed on the north pile (described in Table 6.3) and the south pile (described in Table 6.4). The load versus deflection curves shown in this dissertation are based on pile deflections at the ground-line (or ground surface), as shown in Figure 6.4.

#### 6.3.1 Effect of Pile-Head Load Connection

Tests were performed on the north pile to evaluate the effect of two different connections on load-deflection behavior in various soils. The connections are identified as:

- 1) a pinned connection, which consisted of a unidirectional clevis that permitted rotation about the horizontal axis, as shown in Figure 6.5, and
- 2) a rigid strut connection, which consisted of a steel strut bolted rigidly to the pile, as shown in Figure 6.6.

Figure 6.7 shows the load versus deflection and load versus slope responses of the north pile, for both types of pile-head connectors, tested in natural soil and dense sand.



The pinned head tests were performed immediately after the rigid strut tests. As shown in the figure, the deflection and slope response curves are very similar for both connection devices. The slight concave upward shape in the early portion of clevis pin curve is believed to be caused by the testing sequence. The zone of soil immediately in front of the pile was preloaded or “hardened” during the initial rigid strut test. The similarity in response between the two connection devices is attributed to the following factors.

- 1) The clevis did not function as a true pin connection. It is believed that some resistance to rotation was developed because of tight clearances around the clevis pin and the steel plates that were used for the clevis tongue and yoke.
- 2) The rigid strut and clevis pin provided greater rotational restraint than the load cell because the load cell was free to rotate. Consequently, the rotational stiffness of the load cell controlled the level of rotational restraint that was provided in the loading system.

The difference in performance between the two connectors with regards to pile deflection and slope is negligible. For this reason, the remaining tests described in this chapter were performed using the rigid strut connection. This type of connection provides greater rotational restraint than a free-head connection, but less rotational restraint than a pure fixed-head connection. Although the strut was rigidly attached to the pile, bending at other more flexible locations in the loading train (primarily at the load cell) precluded a pure fixed-headed pile boundary condition. Consequently, the pile-head boundary conditions for these tests were only partially restrained.

Partially restrained boundary conditions are typically analyzed by measuring, computing, or estimating the rotational restraint, which was defined by Matlock and Reese (1961) as the moment divided by the rotation. The degree of rotational restraint involved in these tests is discussed in Section 6.3.3.

### 6.3.2 Effect of Soil Type and Density

The two single piles, identified as the north pile and south pile, were loaded in the direction of their strong axis at test locations C and D (Figure 3.1). The piles were initially tested in their as-driven condition, embedded in natural soil. As shown in Figure 6.8(a), the load-deflection curves for the two piles embedded in natural soil are nearly identical. This indicates quite uniform soil conditions at the site and good repeatability of testing procedures.

After testing the piles in their as-driven condition, the natural soil was excavated from around the piles and replaced with New Castle sand. The excavation and replacement extended to a depth of 7 feet at the north pile and 5.7 feet at the south pile. Tests were performed with the sand backfill in a loose condition,  $D_r = 10\%$ , and a dense condition,  $D_r = 60\%$ .

As shown in Figures 6.8(b) and 6.8(c), pile deflections increased noticeably when the natural soil was replaced by sand. At a deflection of 1/2-inch, the resistance of the north pile decreased by approximately 65% when the top 7 feet of natural soil was replaced by dense sand. The resistance of the pile in 7 feet of loose sand was reduced by approximately 80%.

At the same deflection (1/2-inch), the resistance of the south pile decreased by 60% when the top 5.7 feet of natural soil was replaced by dense sand. The resistance of the pile in 5.7 feet of loose sand was reduced by approximately 75%.

In summary, lateral load resistance increases with soil stiffness and density, as would be expected. An accurate evaluation of soil shear strength and stiffness, within the top 10 pile diameters, is necessary to analyze laterally loaded pile foundations reliably.

### 6.3.3 Effect of Pile-Head Rotational Restraint

The single piles were tested using rotationally restrained pile-head boundary conditions. Matlock and Reese (1961) quantified this type of boundary condition as the moment at the pile head divided by the rotation ( $M/\theta$ ). This type of connection provides greater rotational restraint than a free-head connection, but less rotational restraint than a fixed-head connection. In this dissertation, the term  $k_{m\theta}$  is used to represent the rotational stiffness,  $M/\theta$ .

The effects of pile head restraint were examined using the following three approaches, which are described in more detail in the following paragraphs.

- 1) the single pile response was compared to the measured response of a group pile restrained against rotation at the top by a concrete cap,
- 2) upper and lower bound response curves were calculated using free- and fixed-head boundary conditions, and
- 3) the value of rotational restraint,  $k_{mq}$  was determined through trial and error.

**Approach 1.** The measured response of the north pile was compared to the average response of a pile from the NE group, as shown in Figure 6.9(a). The NE group was constrained by a 36-inch-deep cap, which provided a highly restrained pile-head boundary condition. As would be expected, the NE group pile provides a stiffer response because it represents a boundary condition approaching complete restraint. (The NE group pile response curve represents the condition in which soil was removed from around the cap.)

**Approach 2.** The computer program *LPILE Plus3.0* (1997) was used to generate load deflection curves using free- and fixed-head boundary conditions. p-y curves were developed using the cubic parabola formulation with Brinch Hansen's (1961) ultimate theory for soils containing both friction and cohesion. Soil parameters were estimated from field and laboratory tests.

As shown in Figure 6.9(b), the calculated response curves establish upper and lower bounds of possible behavior. The calculated fixed-head response is stiffer than the measured response of the NE group pile, which is reasonable considering a pure fixed-head condition is rarely achieved in the field. The fixed-head response curve was calculated assuming 100 % group efficiency, and thus represents a true upper bound. The calculated response would be closer to the measured results if reductions for group efficiencies were incorporated into the calculations.

**Approach 3.** In this approach, the pile-head boundary condition was assumed to be partially restrained, and represented by  $k_{m\theta}$ . The magnitude of rotational restraint ( $k_{m\theta}$ ) at the pile-head was determined through a trial and error process. The value of  $k_{m\theta}$  was varied until the calculated load-deflection results matched the observed results. A value of  $k_{m\theta} = 2500$  ft-kips/rad was found to provide the best match between calculated and observed load-deflection responses. The calculated response curve for this value of  $k_{m\theta}$  is shown in Figure 6.10.

In summary, pile head rotational restraint significantly affects the performance of a laterally loaded pile. Three approaches were described that can be used for evaluating this effect, they are:

1. Perform field load tests using the same rotational restraint as planned for the production piles.
2. Calculate lower and upper bound limits using free and fixed head boundary conditions. Estimate a response

between these limits using experience and engineering judgement

3. Calculate response curves using a partially restrained boundary condition by back calculating, measuring, or estimating the rotational restraint,  $k_{m\theta}$ .

#### 6.3.4 Effect of Cyclic Loading

The two single piles were subjected to 150 cycles of monotonic loading to evaluate the effects of cyclic load on pile performance. Tests results for the north and south piles, embedded in natural soil, are shown in Figure 6.11. Results for the south pile embedded in dense sand are shown in Figure 6.12. The figures show the pile response every 25 cycles of load.

As shown in Figure 6.11, pile deflections in natural soil increased during the first 75 cycles, then gradually leveled off with no further change in deflection. An 80 % increase in deflection occurred as a result of cyclic loading. The maximum deflection reached at the end of loading was approximately 1.4 inches.

The south pile performance in dense sand was somewhat different, exhibiting a continual increase in deflections with load cycles, as shown in Figure 6.12(b). One hundred fifty cycles of load application resulted in a 60 % increase in deflection, at a 50 kip lateral load. The maximum deflection at the end of loading was almost 4 inches.

Increased deflections caused by cyclic loads are generally attributed to 1) gapping and subsequent scour of soil from around the pile or 2) cyclic soil degradation caused by the buildup of excess pore pressures from cyclically applied shear stresses (Brown and Reese 1985).

The first phenomenon does not apply to either of the soil conditions at this site because the water table was more than 12 feet below the ground surface.

The second phenomenon, cyclic soil degradation, occurs during undrained loading and includes a reduction of soil modulus and undrained shear strength (Poulos 1982). The natural fine-grained soils at the site may have experienced some degradation of strength caused by excess pore pressures. However, the low frequency cyclic loads used in these tests would not cause excess pore pressure development in the sand backfill.

In general, the cyclic behavior of a pile in sandy soil is usually similar to its static behavior. However, the results shown in Figures 6.11 and 6.12 indicate that cyclic loading significantly affected the single piles in both natural soil and dense sand backfill. These tests were performed at relatively large loads, resulting in deflections ranging from 10 % to almost 40 % of the pile diameter. These large loads and deflections may have exacerbated cyclic effects by stressing the soil and piles to conditions approaching their ultimate or yield strengths. Reese (1997) reported similar observations concerning load tests performed in stiff clay at a site near Manor, Texas.

In conclusion, the cyclic response observed in these tests overestimates the effects of cyclic load on the behavior of piles that are loaded at typical working stress levels. Detailed additional studies would be necessary to separate and quantify the different mechanisms that occur during cyclic loading.

## **6.4 PILE CAP RESISTANCE**

The results described in this section were obtained from lateral load tests performed on the NE and NW pile caps (described in Table 6.1) and the SE pile cap (described in Table 6.2).

### **6.4.1 Resistance With and Without Cap Embedment**

In the first series of tests, the pile groups were tested with the caps embedded in relatively undisturbed natural soil. The results from these tests are shown in Figure 6.13. Although loads as large as 140 kips were applied (35 kips per pile), the deflections were

small, less than 0.1 inches for the NE and NW caps, and approximately 0.13 inches for the SE cap.

As shown in Figures 6.13(a) and (b), the 18-inch-deep NW cap deflected less than the 36-inch-deep NE cap during the initial load tests in natural ground. This seemingly incongruous behavior is attributed to construction disturbances of the soil along the sides and front of the NE cap. During construction, soil was removed at three locations around the NE cap to provide room for embedding anchor rods, which were used in subsequent load tests at locations C and D (Figure 3.1). The excavations were backfilled with imported sandy soil before performing the load tests. In contrast, three sides of the 18-inch-deep NW cap were in full contact with undisturbed soil, which is stiffer than the sand backfill that was used in the trenches around the NE pile cap.

Subsequent tests were performed on the pile groups after soil was removed from the sides and front of the caps, as shown in Figure 6.14. By comparing the load-deflection responses from these tests with the initial tests in undisturbed ground, the contribution of cap resistance can readily be ascertained. As shown in Figure 6.13, the load-deflection curves clearly show that removing soil from the sides and front of the caps resulted in larger deflections at the same loads. Lateral deflections increased by approximately 150 % for the 36-inch-deep NE cap at 140-kip load, 400 % for the 18-inch-deep NW cap at 140-kip load, and 500 % for the 36-inch-deep SE cap at 90-kip load.

The percentage of overall lateral resistance provided by the pile caps are as follows:

- NE cap – 40 %, at 0.09 in deflection,
- NW cap – 50 %, at 0.05 in deflection, and
- SE cap – 50 %, at 0.125 in deflection

Results from these tests support the following conclusions:

1. The horizontal deflections of the pile caps are small considering the magnitude of the maximum lateral loads (approximately 35 kips per pile). This exceeds design loads that are often used for HP 10 x 42 piles by a factor of 3 to 4.
2. The fact that the 18-inch-deep cap deflected less than the 36-inch-deep cap is a result of trench construction disturbance along the sides and front of the 36-inch-deep cap. This indicates the important effect of cap resistance in the behavior of pile groups, and the significance of the strength and stiffness of soil around the caps in determining the magnitude of cap resistance.
3. Removing soil from the sides and front of the caps increased deflections by 150 to 500 %, further indicating the importance of the cap and the surrounding soil in resisting lateral loads.
4. Forty to fifty percent of the overall lateral load resistance was provided by the pile caps. This indicates that approximately  $\frac{1}{2}$  the lateral resistance of a pile group foundation can be developed in the soil around the pile cap.

#### **6.4.2 Resistance From Sides and Front of Caps**

Figure 6.15 shows load deflection responses for the NE, NW, and SE pile caps for the following three conditions:



1. cap in full contact with soil,
2. soil removed from the sides of the cap, and
3. soil removed from the sides and front of the cap.

The tests indicate that pile cap resistance is comprised of two elements: 1) shear resistance developed in soil along the sides of the cap and 2) passive resistance developed by soil in front of the cap. The contributions from these two components are shown in Table 6.6 for the three pile caps. The percent contributions shown in this table were determined at deflections of 0.09 in for the NE cap, 0.05 in for the NW cap, and 0.06 in for the SE cap.

At these small deflections, the side shear component for the NE and NW caps appear to be greater than the passive resistance developed in front of the cap. It is expected that at larger deflections, a greater percentage of passive resistance will be mobilized in front of the cap. Research by Clough and Duncan (1971) indicate that passive pressures are not fully mobilized until wall movements approach 2 to 4 % of the wall height. The comparisons provided in Table 6.6 are for deflections less than 0.25 % of the cap height. The resistance developed along the sides of the cap is not expected to change significantly with increased load. Consequently, the percent contribution from soil along the cap sides will decrease as deflections increase, and the passive pressure component will comprise a larger and more significant share of the overall resistance.

The response of the SE cap with soil removed from the cap sides (Figure 6.15c) is not representative because of disturbances that occurred during construction. A 2.5-foot-wide trench was excavated on the north side of the cap to make room for installing dowel anchor rods. The excavation was backfilled with sand prior to testing. These activities reduced the overall lateral capacity of the SE cap. Consequently, the contribution from the cap sides is most likely 1.5 to 2 times the value of 11 % shown in Table 6.6.

### 6.4.3 Effect of Repetitive Load Applications

Five load cycles were performed with the caps embedded in natural soil to examine the effect of repetitive load applications on the load-deflection response curves. Results from the first and fifth cycles are shown in Figure 6.16 for the NE and NW pile caps. The plots represent the load-deflection response after removing permanent set by resetting the deflection to zero, at the beginning of each load cycle. The same incremental load procedure was used in these tests, and the time lag between cycles (1 to 6 days) was representative of the time period between the different incremental tests. As shown in Figure 6.16, there is no discernable difference in behavior between the first and fifth cycles.

Therefore, it appears that the application of a small number of repetitive loads has no significant effect on the load-deflection behavior of the pile caps, particularly at the small deflections measured during this study.

### 6.4.4 Effect of Pile Cap Depth

The effect of cap depth or thickness on the lateral behavior of pile caps was examined by performing tests on two caps having the same plan dimensions (5 ft by 5 ft) and pile lengths (19 ft), but different depths. The piles were embedded more than 12 inches into the caps, which were heavily reinforced in both top and bottom faces. Cracking of concrete around the pile heads was not a factor because of the large amount of reinforcing steel, and the small deflections and rotations during testing. Load-deflection response curves for the NE 36-inch-deep and the NW 18-inch-deep pile caps are shown in Figure 6.17.

The response curves for the caps embedded in natural soil are shown in Figure 6.17(a). As previously described, the test on the NE cap in natural soil is not representative because of temporary trenches that were excavated at three locations around the cap during construction.

The results shown in Figure 6.17(b) were obtained from tests performed after soil was removed from around the caps. In this condition, the caps are isolated from the surrounding soil and, consequently, the lateral behavior is controlled by the resistance developed in the underlying piles. The two foundations behaved nearly identically in these tests, further indicating the presence of relatively homogeneous soil conditions around the piles. These results indicate that cap thickness has little to no effect on the lateral behavior of a pile group, if the cap is not embedded. A similar conclusion could be inferred for pile caps backfilled with very loose uncompacted soil.

The results of tests performed on the two caps backfilled with compacted crusher run gravel are shown in Figure 6.17(c). In this case, the 18-inch-deep NW cap deflected 20 % more than the 36-inch deep NE cap, at a lateral load of approximately 140 kips. This indicates that cap thickness influences the lateral response of a pile group. The magnitude of this effect depends on the shear strength and density of soil around the cap, the size of the cap, and the rotational restraint provided at the connection between the piles and cap.

In summary, a thicker pile cap is expected to deflect less than a thinner cap. As deflections increase, so will the disparity in performance between two caps of different size. This is because resistance developed by passive pressure in front of the caps will become increasingly significant at larger movements.

#### **6.4.5 Effect of Pile Length**

The effect of pile length on the lateral behavior of pile groups was examined by performing comparable tests on two caps having the same dimensions (5 ft by 5 ft by 3 ft deep), but different lengths of piles. Load-deflection responses for the NE cap with 19-foot-long piles and the SE cap with 10-foot-long piles are shown in Figure 6.18 for the following three conditions.

- 1. Pile caps embedded in natural soil, Figure 6.18(a):**

The resistance provided by the SE group (10-ft-long piles)

was 14 % less than the resistance provided by the NE group (19-ft-long piles), at 0.1 inches of deflection.

**2. Pile caps with no passive or side resistance,** Figure 6.18(b): The resistance provided by the SE group (10-ft-long piles) was 35 % less than the resistance provided by the NE group (19-ft-long piles), at 0.2 inches of deflection.

**3. Pile caps backfilled with compacted gravel,** Figure 6.18(c): The resistance provided by the SE group (10-ft-long piles) was 33 % less than the resistance provided by the NE group (19-ft-long piles), at 0.1 inches of deflection.

Pile group rotational stiffness, and, consequently, the lateral load behavior is affected by the vertical or axial capacity of piles in the group. The piles in the NE group were 19-feet-long, while the piles in the SE group were only 10-feet-long. As discussed in Chapter 7, rotational stiffness is primarily a function of pile side resistance. The longer piles in the NE group were able to develop larger side resistance forces than the shorter piles in the SE group. Consequently, the SE pile cap had a greater tendency to rotate as its leading piles were forced deeper into the ground and its trailing piles moved vertically upward. Larger cap deflections occurred as a result of these increased rotations. This explains the large difference in the load-deflection responses shown in Figure 6.18(b), when soil was removed from around the caps. As shown in Table 6.5, the SE cap rotated approximately 3 times as much as the NE cap during these tests.

#### **6.4.6 Effect of Backfill Type and Density**

Lateral load tests were performed on the NE, NW and SE caps to examine the effects of backfill type and density on pile cap lateral behavior. Response curves for tests in natural soil and gravel backfill are shown in Figure 6.19(a) for the NE cap, Figure 6.19(b) for the NW cap, and Figure 6.19(c) for the SE cap. In each case, caps embedded

in the stiff overconsolidated natural soils exhibited stiffer responses (smaller deflections) than caps backfilled with compacted gravel.

Tests were performed on the SE cap using four different backfill conditions, to further study the effect of soil strength on lateral load response. Direct comparisons are shown in Figure 6.20 for the following conditions:

1. Figure 6.20(a) – natural soil versus dense sand,
2. Figure 6.20(b) – dense sand versus loose sand,
3. Figure 6.20(c) – dense gravel versus dense sand, and
4. Figure 6.20(d) – loose sand versus no soil.

The most obvious trend in these comparisons is the direct relationship between backfill strength and lateral load behavior. Smaller deflections were observed in the stiffer, stronger soils, and deflections noticeably increased as soil strength and stiffness decreased. The stiffest, strongest soils are the natural undisturbed soils (smallest measured deflections) followed in decreasing order by dense gravel, dense sand, loose sand, and no soil (largest measured deflections).

These results further support the significance of cap resistance in the overall lateral behavior of pile groups. Not only does the cap provide a significant share of the resistance, but the magnitude of this resistance depends on the strength and stiffness of soil around the cap.

#### **6.4.7 Effect of Cyclic Loading**

The NE and NW pile groups were subjected to a large number of unidirectional loads to evaluate the effects of cyclic loading on the lateral resistance of caps backfilled with dense gravel. The load-deflection response at every 25 load cycles, and the deflection versus number of load cycles, is shown in Figure 6.21 for the NE and NW

caps. The effect of cyclic loading was small and appeared to level off after approximately 20 cycles. For instance, the NE cap deflections increased by 0.02 inches during the first 20 cycles and did not increase further over the following 130 cycles. The total increase in deflection for the NW cap was 0.035 inches, and 70 % of this occurred during the first 20 cycles.

Figure 6.22 shows the cyclic response of the SE cap embedded in natural soil. One hundred twenty unidirectional loads were applied during the test. The deflection versus load response for every 20 cycles of load is shown in Figure 6.22(a), and the deflection versus number of load cycles, is shown in Figure 6.22(b). As for the NE and NW caps, the effect of cyclic loading leveled off after approximately 20 cycles. The total increase in deflection was 0.034 in, and 80 % of this occurred during the first 20 cycles.

#### **6.4.8 Ground Surface Movements**

Vertical deflections of the backfill surface, in front of the NE cap, were monitored during the cyclic tests. Linear potentiometers were spaced 1 to 4 feet in front of the cap, as shown in Figure 6.23. Vertical deflections during the first load cycle (at 120 kip load and at zero load) are shown in Figure 6.23(a). Similar information is shown in Figure 6.23(b) for the 150<sup>th</sup> load cycle.

The vertical deflections were all in an upward direction, and the maximum values at peak load were observed in the potentiometers located one foot from the cap face. The vertical deflections were small, approximately 50 % of the horizontal cap deflections. The maximum permanent vertical deformation (the residual deflection after the 120 kip load was decreased to zero) was upward and occurred 2 feet in front of the cap.

Because the measured vertical deflections are very small, it is difficult to draw any firm conclusions from the results. The most significant observation is the upward movement of the backfill surface. This is caused by a combination of factors including dilatant behavior in the dense gravel backfill and the initial development of a passive soil wedge. As cap movements increase, the passive soil wedge will have a tendency to move

upward, as the cap rotates downward. The amount of this movement is controlled by the cap displacement and the interface friction between the front face of the cap and the backfill soil.

#### **6.4.9 Effect of Sustained Loading**

The effect of sustained lateral loads on pile cap performance was investigated for two soil conditions:

1. NE and NW caps backfilled with gravel (Figure 6.24)
2. SE cap embedded in natural ground (Figure 6.25).

Loads were incrementally increased to 135 kips and then held constant. As shown in Figures 6.24 and 6.25, there were no significant changes in horizontal deflections during sustained application of load. These results are comparable to the long-term performance of vertically loaded footings founded in dense granular soils or in overconsolidated low-plasticity fine-grained soils (same types of soil used in this study).

### **6.5 PASSIVE LOAD RESISTANCE WITHOUT PILES**

Lateral load tests were performed on the bulkhead, which was located at the west end of test trench B (Figure 3.1), to provide a means of experimentally studying passive pressure resistance without the influence of piles.

#### **6.5.1 Effect of Backfill Type on Passive Load Resistance**

The bulkhead was initially loaded against undisturbed natural ground. The load-deflection response curve for this test is shown in Figure 6.26. Loads were applied in 15 kip increments, up to a load of about 137 kips. Maintaining this load was difficult because the deflections did not stabilize over time, as shown in Figure 6.27. The resistance dropped off dramatically after about 90 minutes of loading, indicating failure within the soil mass. Cracks were observed extending outward from the lead corners of

the bulkhead, in a direction roughly parallel to the direction of loading. The cracks ranged in width from hairline to ¼-inch. The most visible crack was 45 inches long.

After completing the first series of tests, the natural soil was excavated from the front side of the bulkhead and replaced with compacted gravel backfill. The excavation extended to the bottom of the bulkhead, 3.5 feet, and extended outward in front of the bulkhead 7.5 feet. The bulkhead was then incrementally loaded to failure. As shown in Figure 6.26, failure occurred at a load of 90 kips and a deflection of approximately 1.6 inches.

In summary, the passive resistance of the bulkhead backfilled with dense gravel was 35 % less than the resistance obtained by the bulkhead embedded in natural soil.

### 6.5.2 Effect of Cyclic Loading

Figure 6.28 shows the response of the bulkhead backfilled with crusher run gravel and monotonically loaded 120 times at a 70 kip load. The deflection versus load response for every 20 cycles of load is shown in Figure 6.28(a) and the deflection versus number of load cycles, is shown in Figure 6.28(b) for every 20 cycles of 70 kip load. The effect of cyclic loading appeared to level off after approximately 20 cycles. The total increase in deflection was 0.33 in, and 70 % of this occurred during the first 20 cycles.

As shown in Figure 6.28(b), the deflections decreased after 120 cycles of load, at the maximum applied load of 100 kips. This is attributed to the soil preloading or “hardening”, which occurred during the application of 120 cycles of 70 kip load.

Vertical deflections of the backfill surface, on the front side of the bulkhead, were monitored during the cyclic tests. Linear potentiometers were spaced from 1 to 4.5 feet in front of the bulkhead, as shown in Figure 6.29(c). Vertical deflections during the first load cycle (at 70 kip load and zero load) are shown in Figure 6.29(a). Figure 6.29(b) shows similar deflection distributions for the 120<sup>th</sup> load cycle. The vertical deflections



were upward, and the maximum values at peak load were measured in the potentiometers located 4.5 feet from the front face of the bulkhead.

The vertical deflections were relatively large, approximately 60 % of the horizontal cap deflections. The maximum permanent vertical deformation (the measured deflection after the load was decreased to zero) was 0.47 inches, and occurred 4.5 feet from the cap face.

The backfill surface moved upward, similar to the pile cap tests, except the bulkhead displacements were considerably greater. A noticeable bulge developed on the surface of the backfill, extending 7.5 feet in front of the bulkhead, and parallel to the bulkhead face. Surface cracks extended from the front corners of the bulkhead out to the bulge. Based on the surface crack pattern and location of bulging soil, it appears that the failure surface intersected the ground surface approximately 7.5 feet in front of the bulkhead. The bulkhead and the passive failure wedge appeared to move in a lateral and upward direction, as the load was increased.

## **6.6 SUMMARY**

A field test facility was developed to perform full-scale lateral load tests on single piles, pile groups, and pile caps embedded in natural soil and backfilled with granular soil. The facility was designed specifically for this project to evaluate the lateral resistance provided by pile caps. A total of thirty-one tests were performed using incremental, cyclic, and sustained loading procedures.

Results from the testing program clearly support the research hypothesis that pile caps provide significant resistance to lateral load. The pile caps that were tested in this study provided approximately ½ of the overall lateral resistance of the pile group foundations.

The lateral resistance provided by a pile group/pile cap foundation depends on many interacting factors, which were isolated during this study to evaluate their significance. In order of importance, these are:

1. **Stiffness and density of soil in front of the cap.** The passive resistance that can be developed in front of a pile cap is directly related to the backfill strength. As shown in Figure 6.20, the lateral resistance increases as the stiffness and density of soil around the cap increases.
2. **Depth of cap embedment.** Increasing cap thickness or depth will result in smaller lateral deflections, as shown in Figure 6.17.
3. **Rotational restraint at the pile head.** The rotational restraint available at the pile head can most often be described as a partially restrained condition. As shown in Figure 6.9(b), this condition results in response that falls between that of a fixed-head and free-head boundary condition. Response curves can be calculated using partially restrained boundary conditions by calculating, measuring, or estimating the rotational restraint,  $k_{mq}$ , as shown in Figure 6.10.
4. **Pile group axial capacity.** Lateral behavior of a pile group is directly related to the vertical or axial capacity of the piles. As shown by the results in Figure 6.18, pile groups comprised of longer piles (greater axial capacity) have significantly greater lateral resistance than groups with shorter piles. The rotation of the cap and the passive resistance developed in front of the cap are both affected by the axial capacity of the piles.
5. **Stiffness and density of soil around the piles.** Lateral load resistance increases as the stiffness and density of soil around the piles increase, as shown in Figure 6.8. The soil within the top 10 pile diameters has the greatest effect on lateral pile response.

6. **Cyclic and sustained loads.** For the conditions tested in this study, the effects from cyclically applied loads and long-term sustained loads were minor, or secondary, in comparison to the other factors described above. In other situations, such as high groundwater or soft compressible soils, the effect of cyclic loading or long term sustained loading could be more significant.

In conclusion, the load tests performed in this study clearly indicate that pile caps provide considerable resistance to lateral loads. The lateral resistance of a pile group is largely a function of the passive resistance developed by the cap and the rotational restraint of the pile-cap system. The passive resistance of the cap is controlled by the stiffness and density of the backfill soil and the interface friction angle. The rotational restraint is a function of the pile-to-cap connection and the axial capacity of the piles.

Table 6.1. Summary of lateral load tests conducted at setup location A - NE pile cap versus NW pile cap.

Test No.	Test date	Foundation conditions	Type of test	Ground-water (ft)	Instrumentation comments
1	6/8/98	Both caps in full contact with natural ground	Baseline (no loads)	11.7	Evaluated instrumentation response over an 8 hour period.
2	6/12/98	Both caps in full contact with natural ground	Incrementally loaded to 134 kips	11.7	6 Celesco and 6 Longfellow transducers (some sticking noted in Longfellow's)
3	6/12/98	Both caps in full contact with natural ground	Cyclically loaded to 132.5 kips (10 cycles)	11.7	6 Celesco and 6 Longfellow transducers
4	6/12/98	Both caps in full contact with natural ground	Performed 10 load cycles to 100 kips	11.7	6 Celesco and 6 Longfellow transducers
5	6/18/98	Both caps in full contact with natural ground	Incrementally loaded to 136 kips	12.1	6 metal Celescos only, 3 per cap
6	6/18/98	Both caps in full contact with natural ground	Cyclically loaded to 137 kips (4 cycles)	12.1	6 metal Celescos only, 3 per cap
7	7/2/98	Soil removed from the sides of both caps	Incrementally loaded to 137 kips	13.1	12 Celesco transducers, 6 per cap
8	7/2/98	Soil removed from the sides of both caps	Cyclically loaded to 137 kips (4 cycles)	13.1	12 Celesco transducers, 6 per cap

Table 6.1. Concluded.

Test No.	Test date	Foundation conditions	Type of test	Ground-water (ft)	Instrumentation comments
9	7/9/98	Soil removed from sides and front of both caps	Incrementally loaded to 136 kips	13.4	12 Celesco transducers, 6 per cap
10	7/9/98	Soil removed from sides and front of both caps	Cyclically loaded to 137 kips (4 cycles)	13.4	12 Celesco transducers, 6 per cap
11	7/20/98	Sides and front of both caps backfilled with crusher run aggregate	Incrementally loaded to 136 kips	14.1	12 Celesco transducers, 6 per cap, and 4 Longfellows on NE cap backfill
12	7/20/98	Sides and front of both caps backfilled with crusher run aggregate	Performed 150 load cycles from 0 to 120 kips	14.1	12 Celesco transducers, 6 per cap, and 4 Longfellows on NE cap backfill
13	7/24/98	Sides and front of both caps backfilled with crusher run aggregate	Sustained load test at 135 kips for 190 min	14.4	12 Celesco transducers, 6 per cap, and 4 Longfellows on NE cap backfill

Table 6.2. Summary of lateral load tests conducted at setup location B - SE pile cap versus bulkhead.

Test No.	Test date	Foundation conditions	Type of test	Ground-water (ft)	Instrumentation comments
14	8/1/98	Pile cap and bulkhead in full contact with natural ground	Incrementally loaded to 135 kips	14.7	6 Celescos on cap, 4 on abutment, abutment failed at 135 kip sustained load (84 min)
15	8/26/98	Soil removed from sides of cap, bulkhead backfilled with crusher run aggregate	Incrementally loaded to 90 kips	14.8	6 Celescos on cap, 4 on abutment, and 4 Longfellow transducers on abutment backfill
16	8/29/98	Soil removed from sides and front of cap, bulkhead backfilled with crusher run aggregate	Incrementally loaded to 95 kips	15.0	6 Celescos on cap, 4 on abutment, and 4 Longfellow transducers on abutment backfill
17	8/31/98	Cap backfilled with uncompacted New Castle sand, bulkhead b/f with crusher run aggregate	Incrementally loaded to 100 kips	15.0	6 Celescos on cap, 4 on abutment, and 4 Longfellow transducers on abutment backfill
18	8/31/98	Cap backfilled with compacted New Castle sand, bulkhead b/f with crusher run aggregate	Incrementally loaded to 100 kips	15.0	6 Celescos on cap, 4 on abutment, and 4 Longfellow transducers on abutment backfill
19	9/3/98	Cap backfilled with compacted crusher run agg., bulkhead b/f with crusher run aggregate	Incrementally loaded to 100 kips	15.3	6 Celescos on cap, 4 on abutment, and 4 Longfellow transducers on abutment backfill
20	9/3/98	Cap backfilled with compacted crusher run agg., bulkhead b/f with crusher run aggregate	Performed 150 cycles from 0 to 60 kips	15.3	6 Celescos on cap, 4 on abutment, and 4 Longfellow transducers on abutment backfill

Table 6.3. Summary of lateral load tests conducted on the individual north pile.

Test No.	Test date	Foundation conditions	Type of test	Ground-water (ft)	Instrumentation comments
21	9/21/98	North pile with rigid strut connection in natural soil	Incrementally loaded to 50 kips	15.8	3 Celescosp mounted along pile C.L. and 3 mounted on tell-tale attached at G.S.
22	9/21/98	North pile with clevis pin connection in natural soil	Incrementally loaded to 50 kips	15.8	3 Celescosp mounted along pile C.L. and 3 mounted on tell-tale attached at G.S.
23	9/21/98	North pile with clevis pin connection in natural soil	Performed 150 cycles from 0 to 50 kips	15.8	3 Celescosp mounted along pile C.L. and 3 mounted on tell-tale attached at G.S.
24	9/30/98	North pile with rigid strut connection, top 7' of pile embedded in loose sand	Incrementally loaded to 20 kips	16.0	3 Celescosp mounted along pile C.L. and 3 mounted on tell-tale attached at G.S.
25	9/30/98	North pile with rigid strut connection, top 7' of pile embedded in compacted sand	Incrementally loaded to 40 kips	16.0	3 Celescosp mounted along pile C.L. and 3 mounted on tell-tale attached at G.S.
26	9/30/98	North pile with clevis pin connection, top 7' of pile embedded in compacted sand	Incrementally loaded to 40 kips	16.0	3 Celescosp mounted along pile C.L. and 3 mounted on tell-tale attached at G.S.

Table 6.4. Summary of lateral load tests conducted on the individual south pile.

<b>Test No.</b>	<b>Test date</b>	<b>Foundation conditions</b>	<b>Type of test</b>	<b>Ground-water (ft)</b>	<b>Instrumentation comments</b>
27	10/7/98	South pile with rigid strut connection in natural soil	Incrementally loaded to 74 kips	16.1	3 Celescros mounted along pile C.L. and 3 mounted on tell-tale attached at G.S.
28	10/7/98	South pile with rigid strut connection in natural soil	Performed 150 cycles from 0 to 50 kips	16.1	3 Celescros mounted along pile C.L. and 3 mounted on tell-tale attached at G.S.
29	10/9/98	South pile with rigid strut connection, top 5.7' of pile embedded in loose sand	Incrementally loaded to 45 kips	15.9	3 Celescros mounted along pile C.L. and 3 mounted on tell-tale attached at G.S.
30	10/9/98	South pile with rigid strut connection, top 5.7' of pile embedded in compacted sand	Incrementally loaded to 50 kips	15.9	3 Celescros mounted along pile C.L. and 3 mounted on tell-tale attached at G.S.
31	10/9/98	South pile with rigid strut connection, top 5.7' of pile embedded in compacted sand	Performed 150 cycles from 0 to 50 kips	15.9	3 Celescros mounted along pile C.L. and 3 mounted on tell-tale attached at G.S.

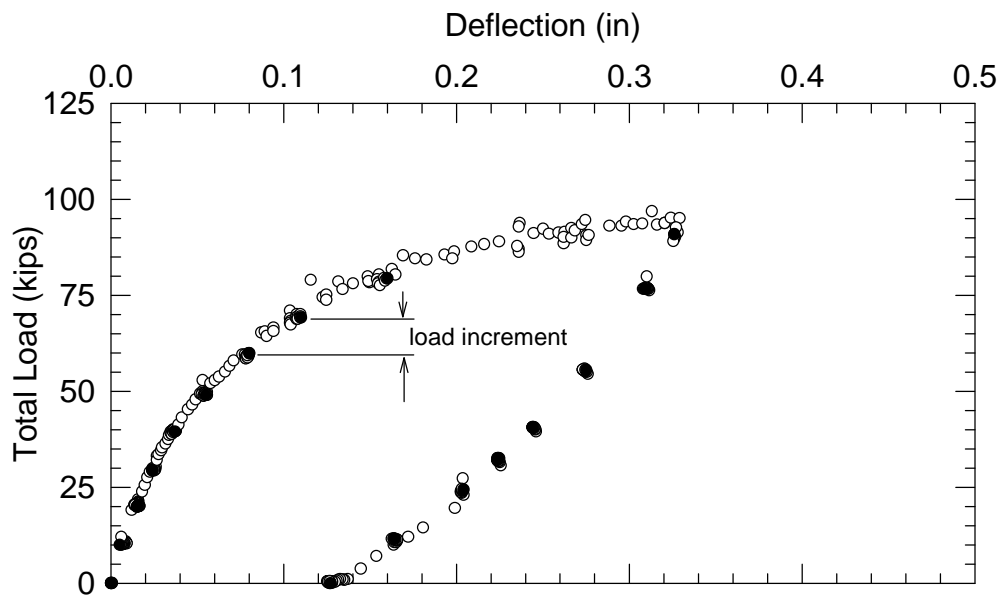


Table 6.5. Measured angular rotations.

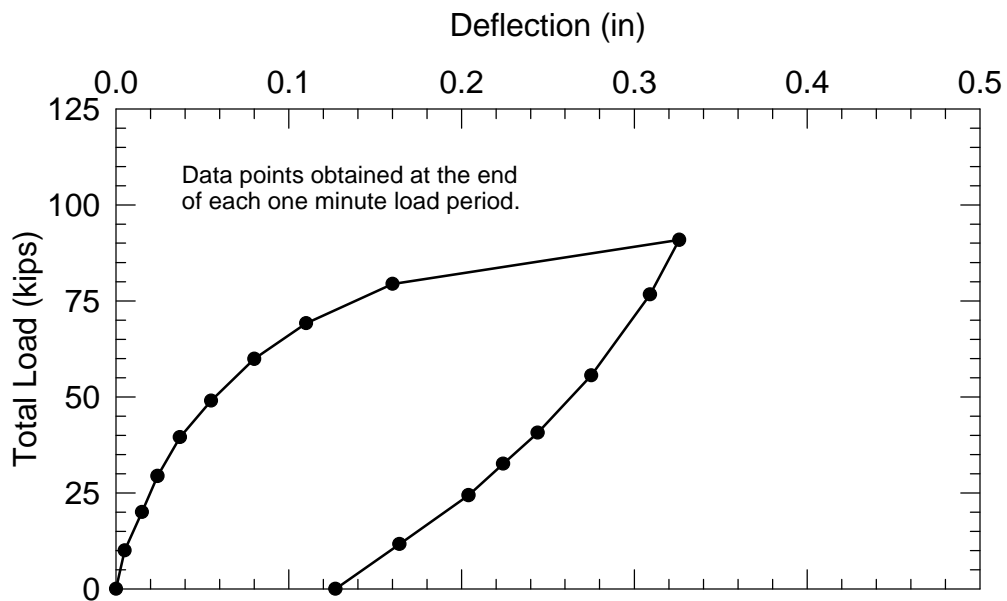
Foundation	Soil condition around cap	Load (kips)	Tilt in the direction of load $\mathbf{q}$ (deg)	Torsional rotation $\mathbf{t}$ (deg)
NE cap	natural soil	136	0.001	0.001
NE cap	gravel backfill	136	0.044	0.002
NE cap	no soil	136	0.072	0.003
NW cap	natural soil	136	0.069	0.001
NW cap	gravel backfill	136	0.044	0.002
NW cap	no soil	136	0.083	0.003
SE cap	natural soil	92	0.026	0.003
SE cap	gravel backfill	92	0.019	0.002
SE cap	dense sand	92	0.070	0.000
SE cap	loose sand	92	0.106	0.000
SE cap	no soil	92	0.209	0.016
Bulkhead	natural soil	92	0.192	0.073
Bulkhead	gravel backfill	92	0.56	0.21

Table 6.6. Distribution of pile cap lateral resistance in natural soil.

<b>Test location</b>	<b>Contribution from sides of cap (%)</b>	<b>Contribution from front of cap (%)</b>	<b>Contribution from pile group (%)</b>	<b>Deflection (in)</b>
NE cap	24	16	60	0.09
NW cap	37	13	50	0.05
SE cap	11	39	50	0.06

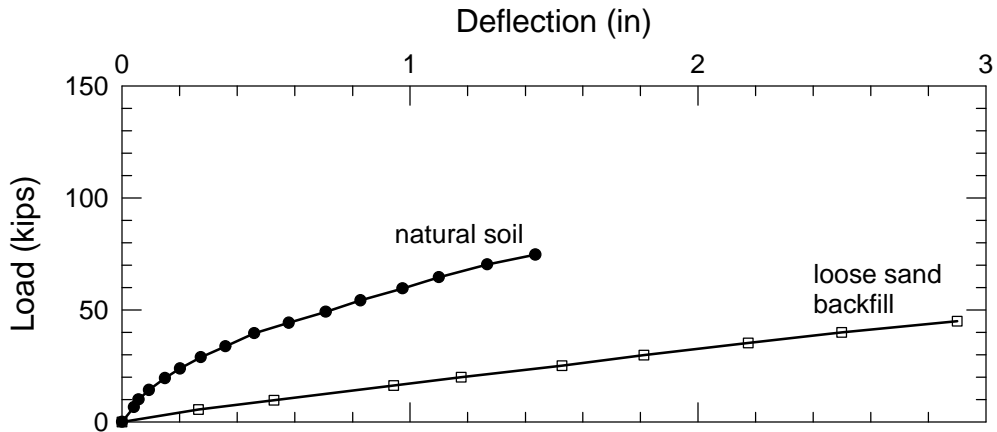


(a) Raw data from pile cap load test.

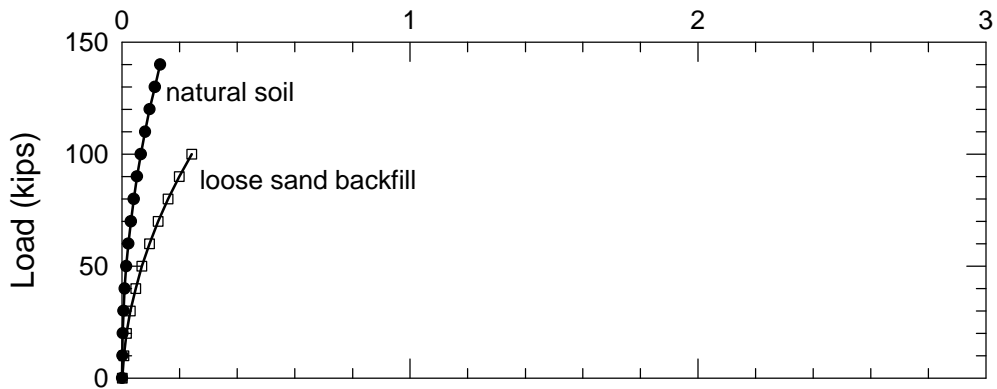


(b) Filtered data.

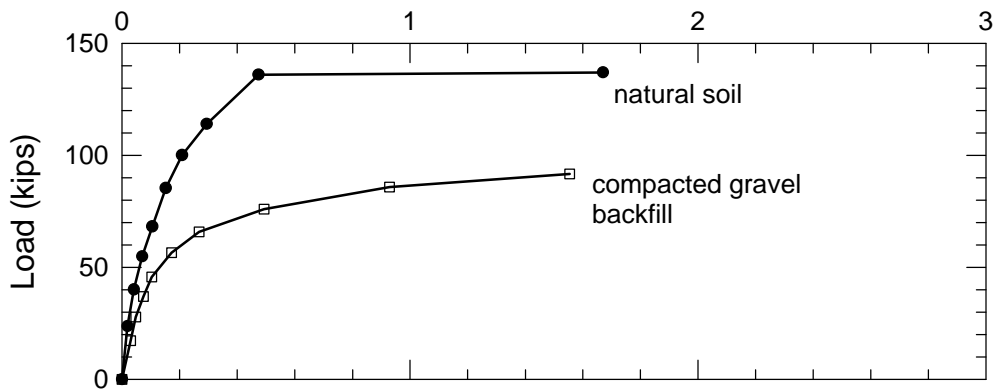
Figure 6.1. Typical load-deflection curve for SE pile cap backfilled with compacted gravel.



(a) South pile measured response.

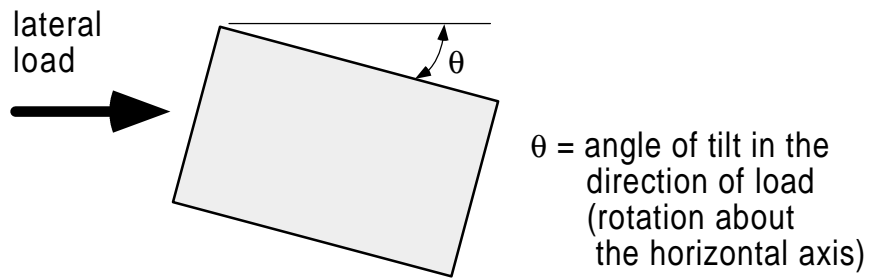


(b) SE pile cap measured response.

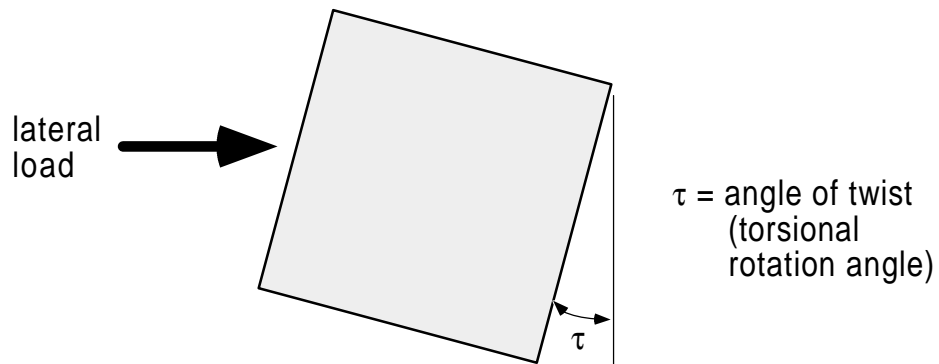


(c) Bulkhead measured response.

Figure 6.2. Typical results from lateral load tests performed at the field test facility.



(a) Cross-section of laterally loaded pile cap (exaggerated behavior).



(b) Plan view of laterally loaded pile cap (exaggerated behavior).

Figure 6.3. Description of pile cap rotation angles.

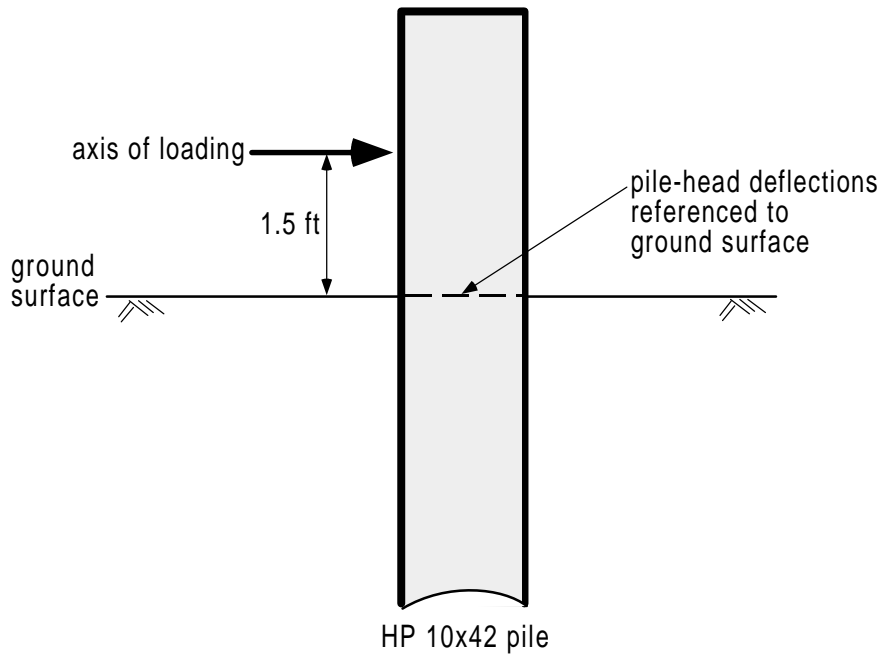


Figure 6.4. Single pile load testing arrangement.

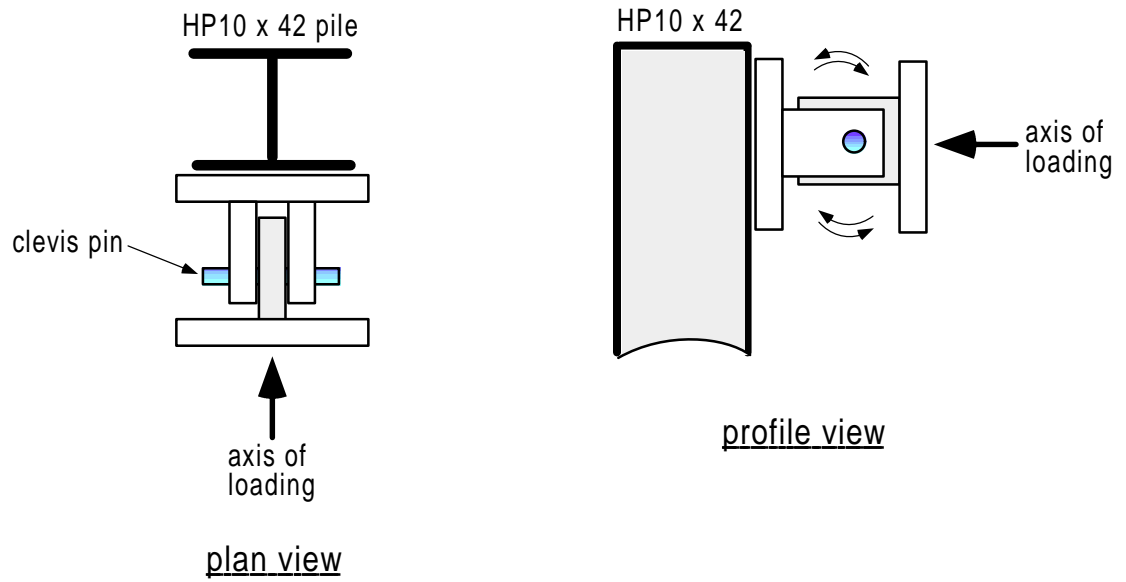


Figure 6.5. Pinned connection - clevis yoke and tongue.

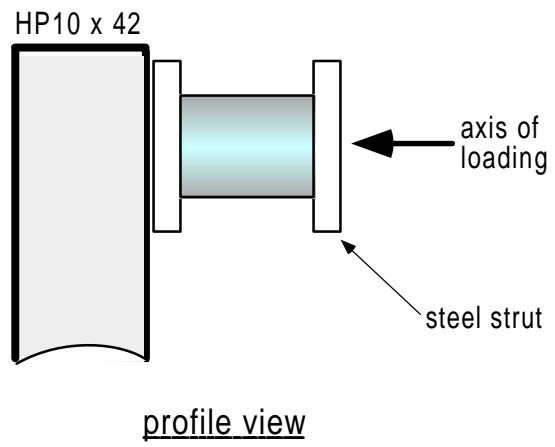


Figure 6.6. Rigid strut connection.



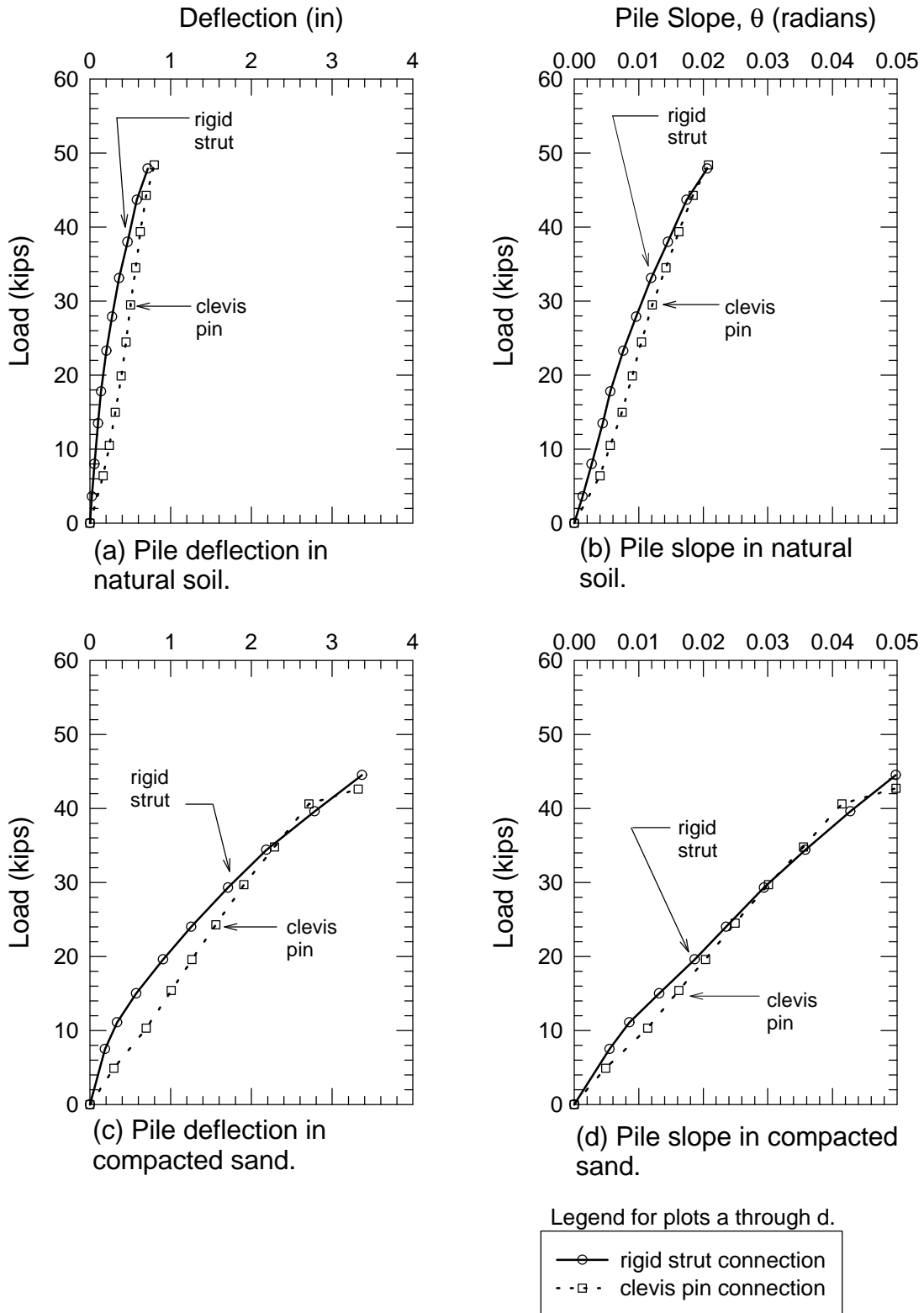


Figure 6.7. Comparison of load connectors used at the north pile.

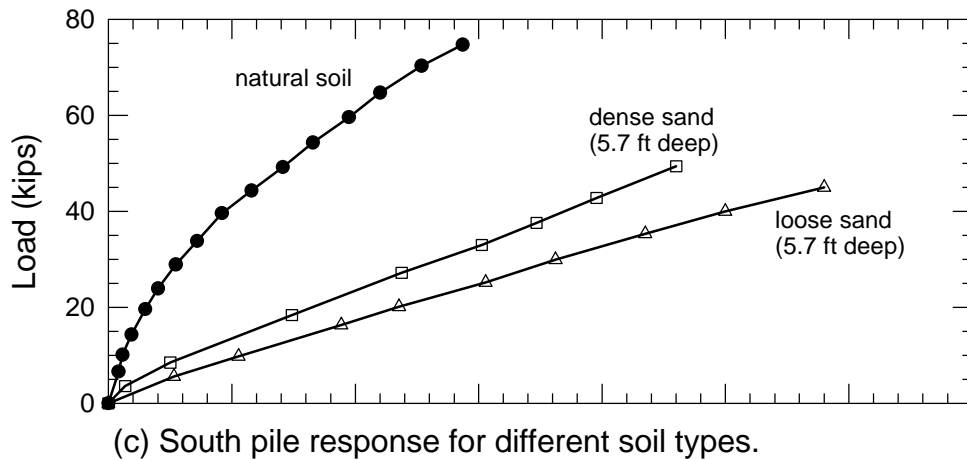
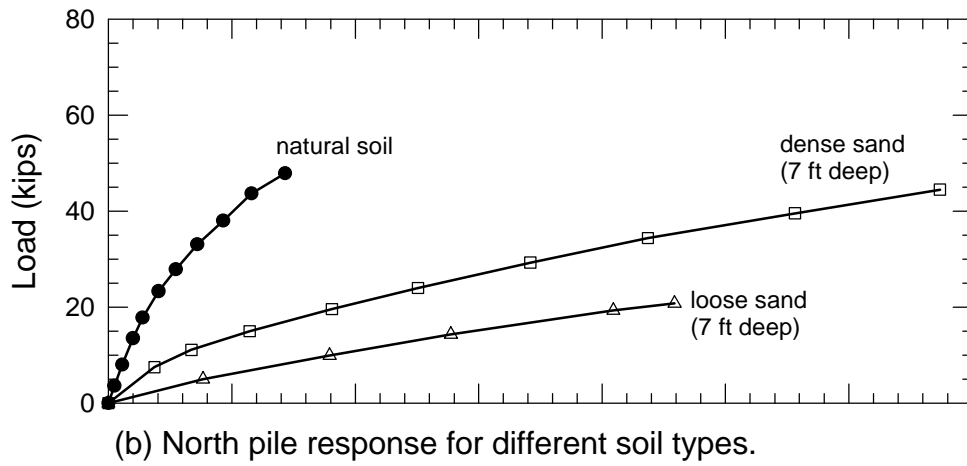
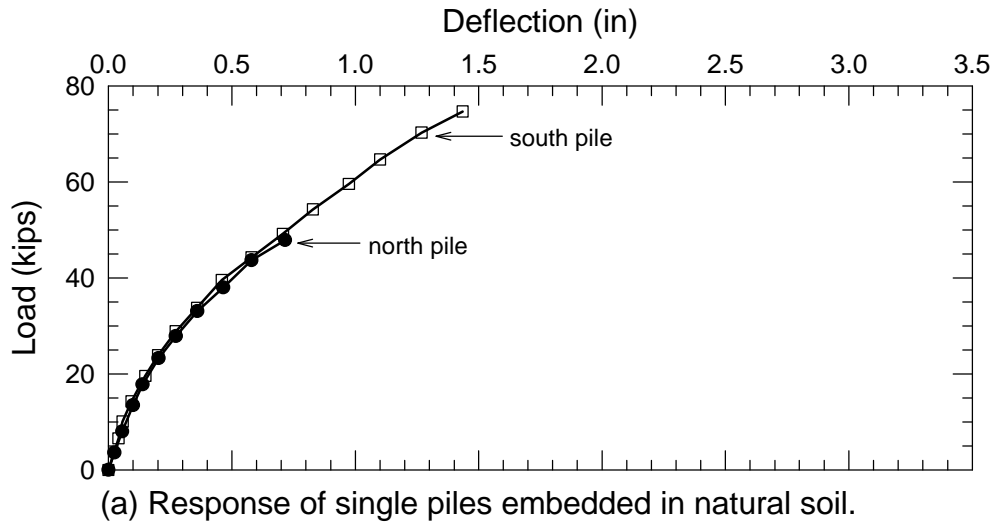


Figure 6.8. Effect of soil type and density on load deflection response of single piles.

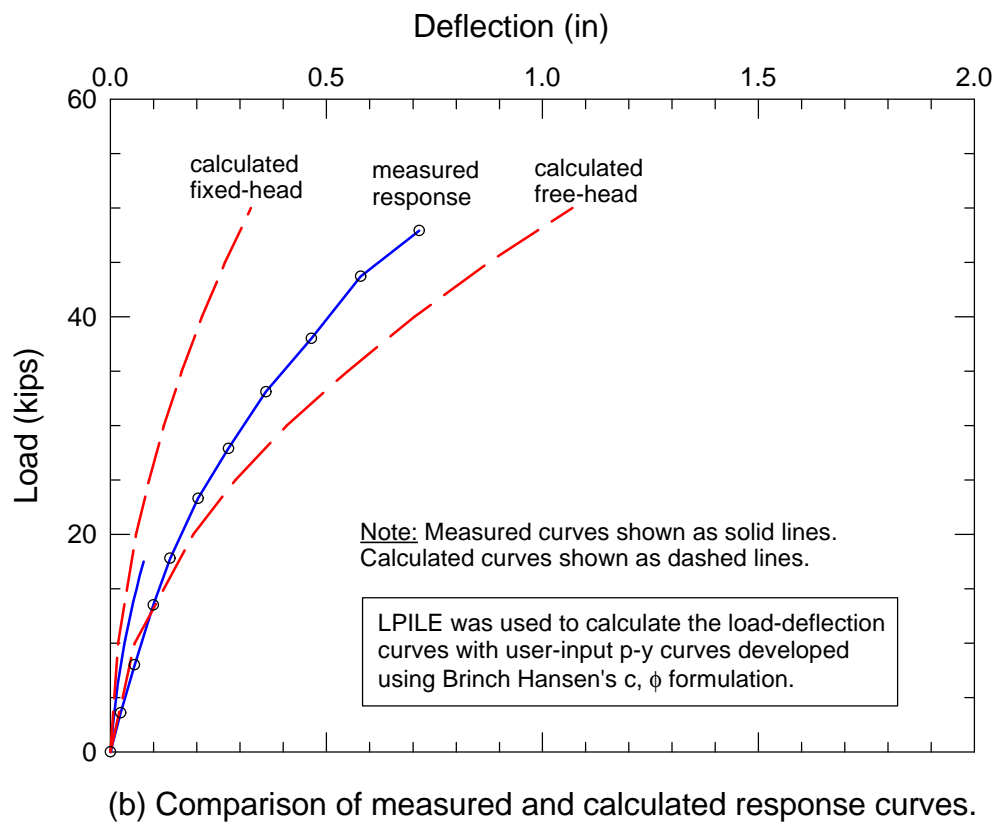
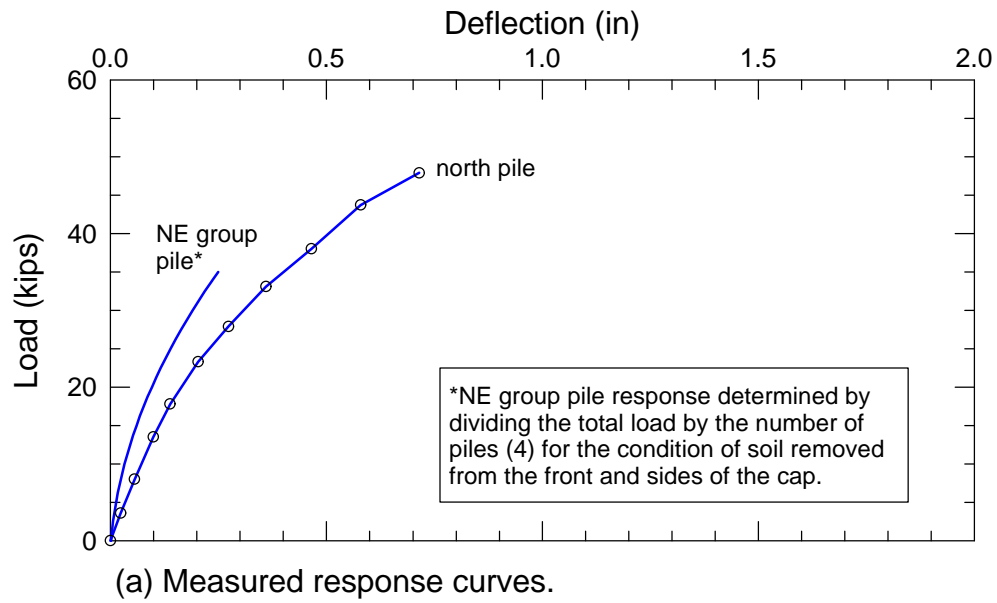


Figure 6.9. Effect of pile-head rotational restraint.

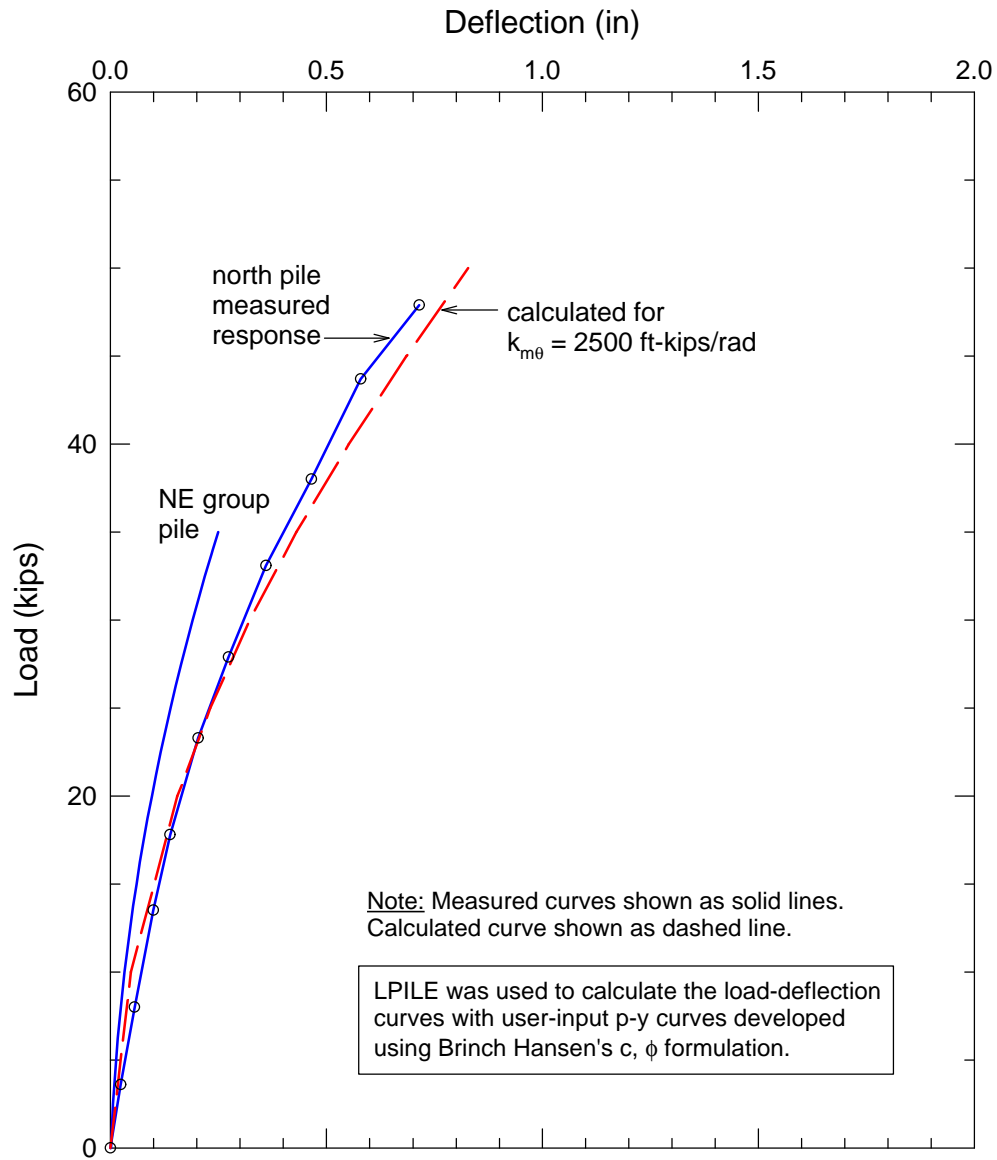


Figure 6.10. Response curve based on back calculated  $k_{mq}$  value for pile in natural soil.

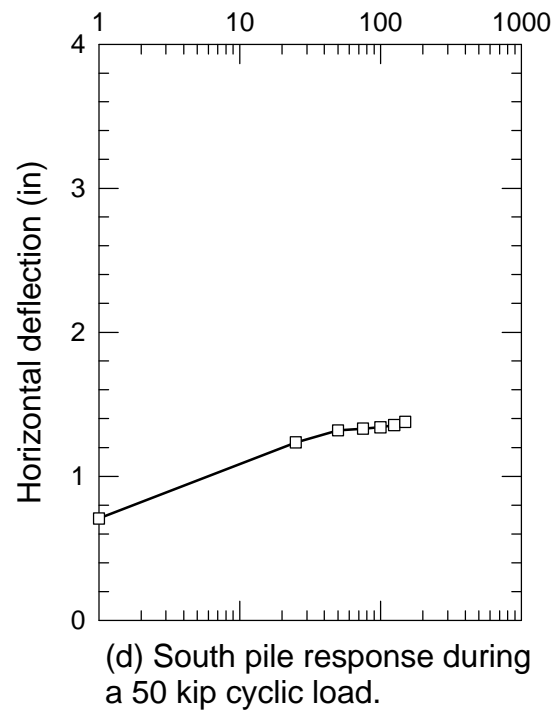
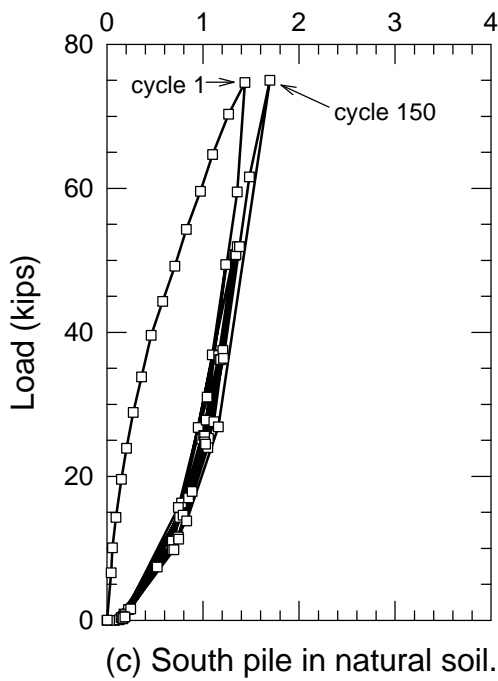
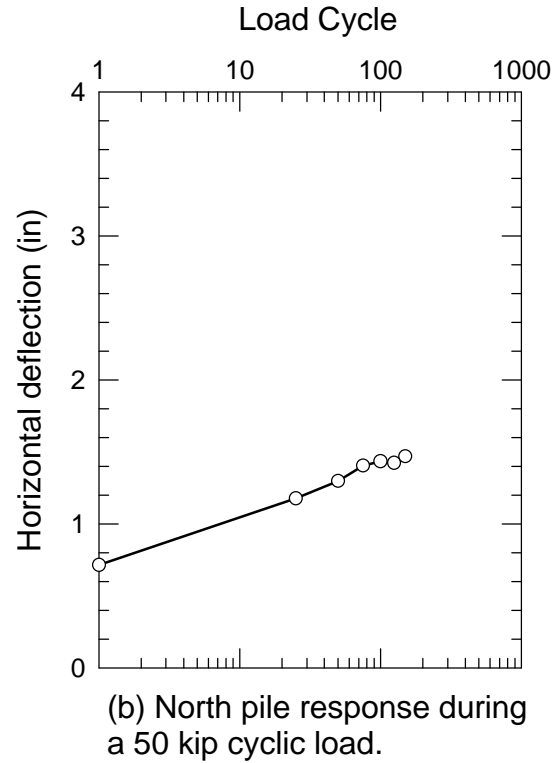
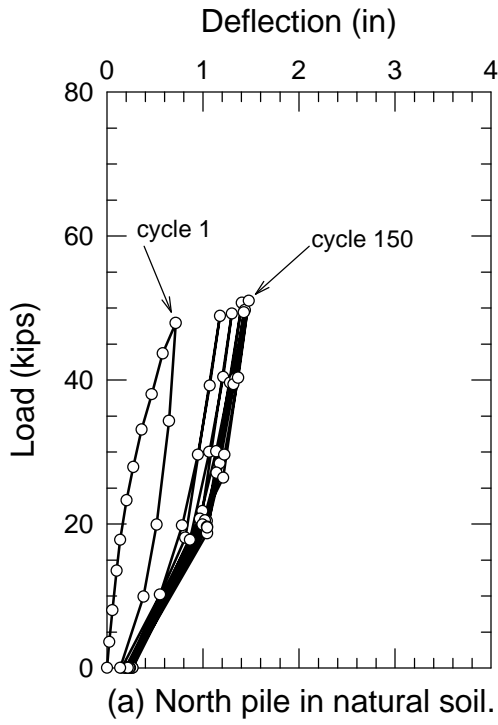
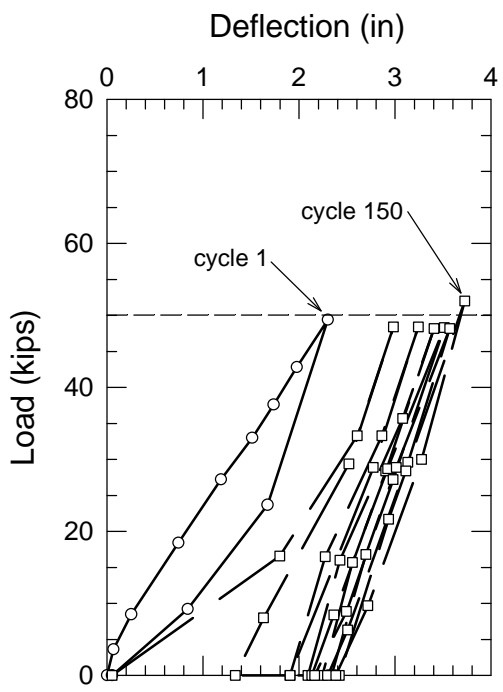
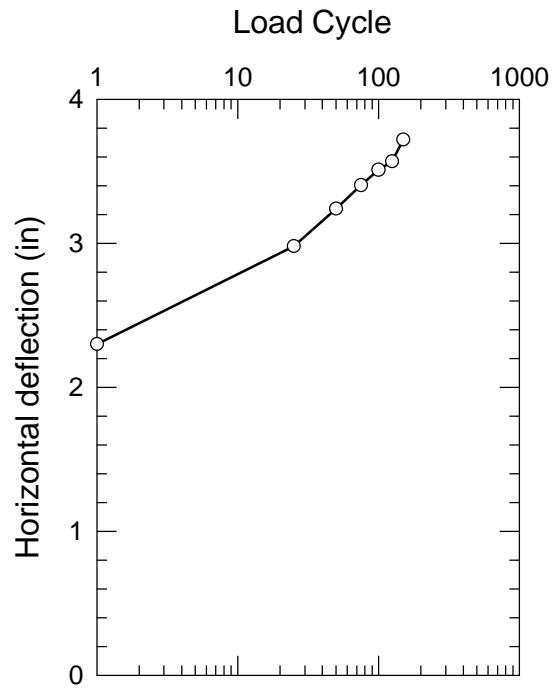


Figure 6.11. Effect of cyclic loading on single piles embedded in natural soil.



(a) South pile in dense sand.



(b) South pile response during a 50 kip cyclic load.

Figure 6.12. Effect of cyclic loading on south pile backfilled with 5.7 feet of compacted sand.

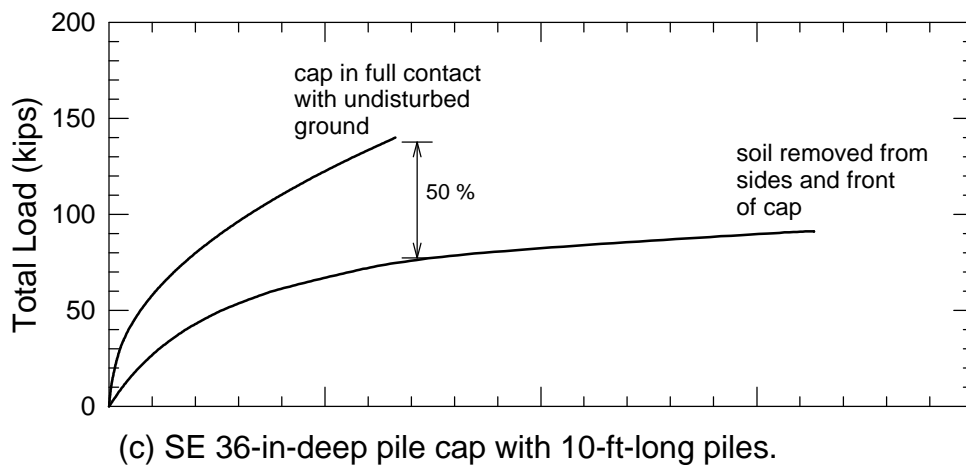
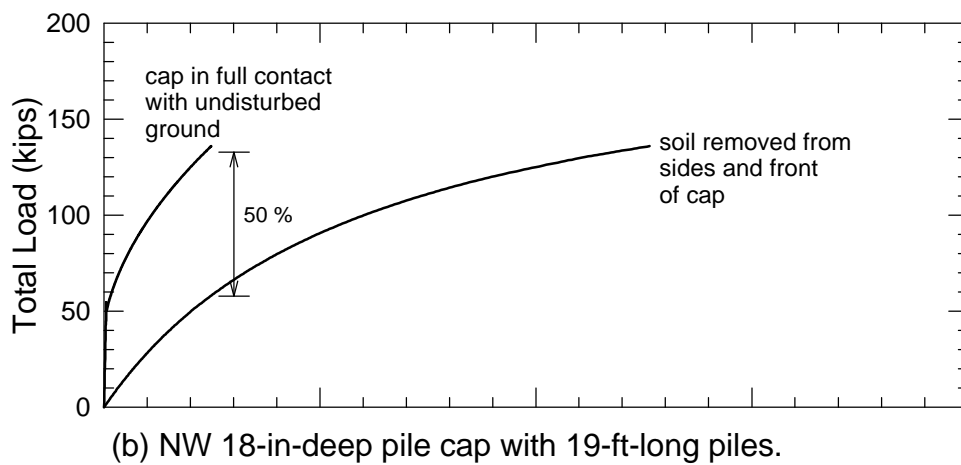
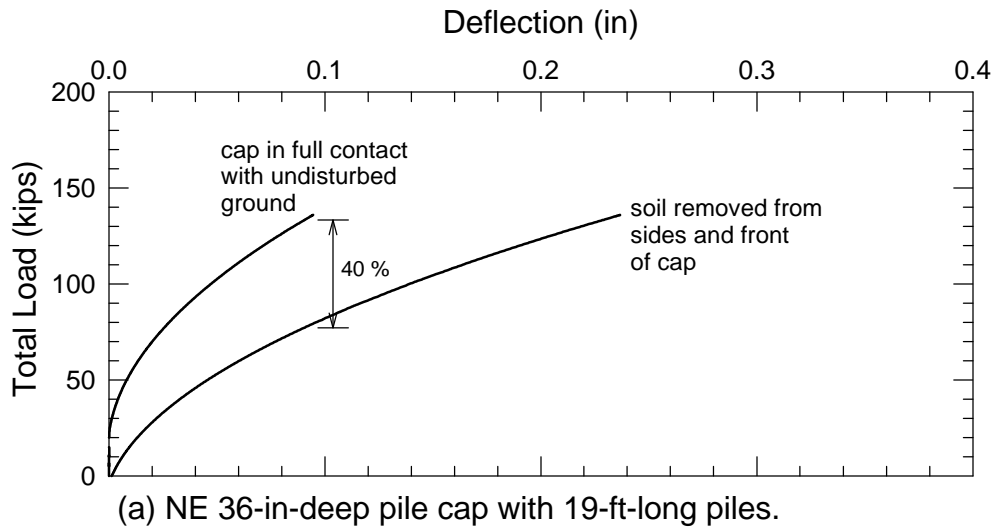
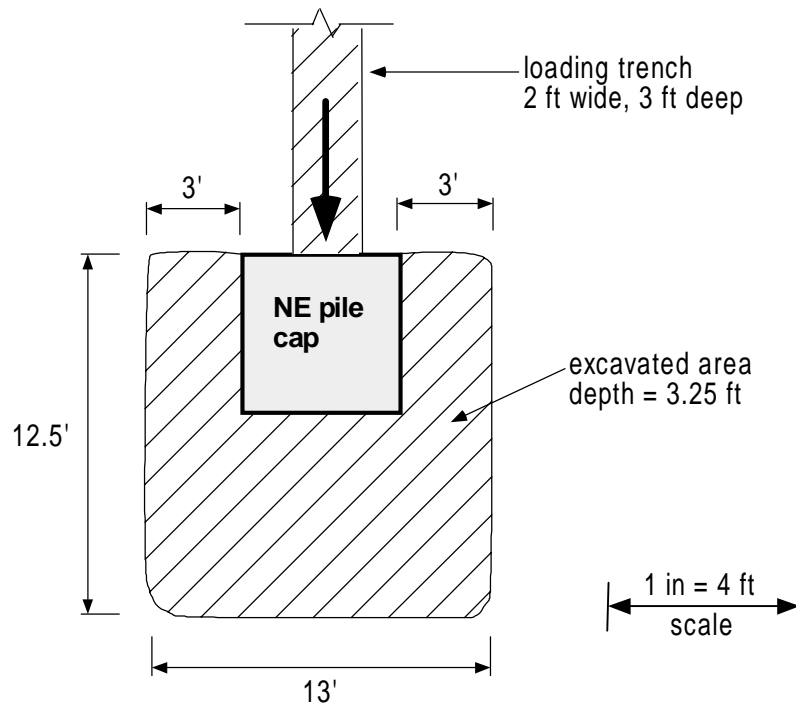


Figure 6.13. Load deflection response with and without pile cap embedment in natural soil.



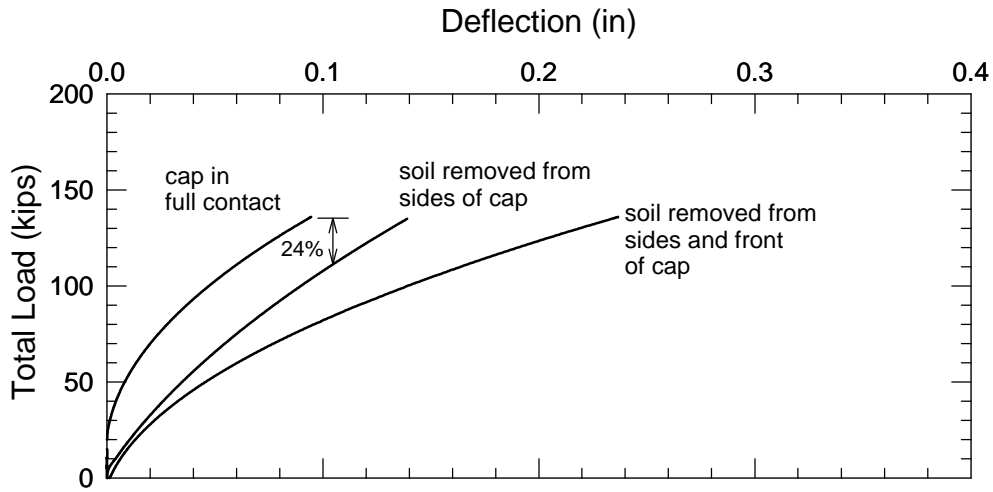
(a) Photograph of soil excavation around pile cap.



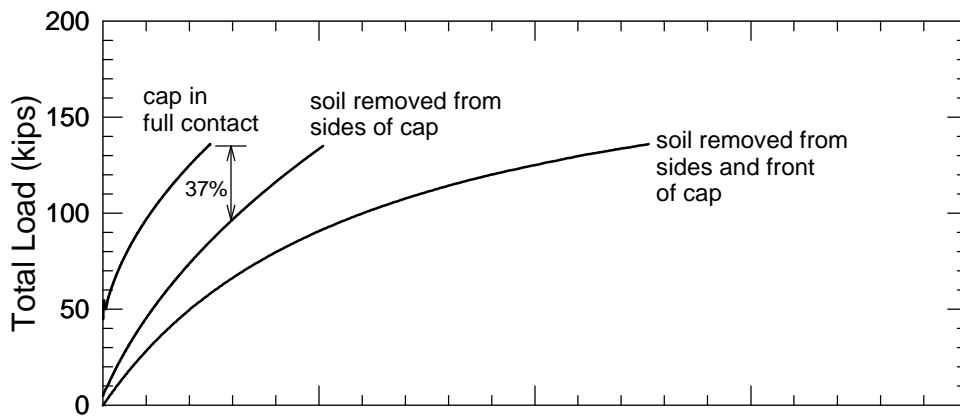
(b) Plan view of excavation around NE pile cap.

Figure 6.14. NE pile cap with soil excavated from sides and front.

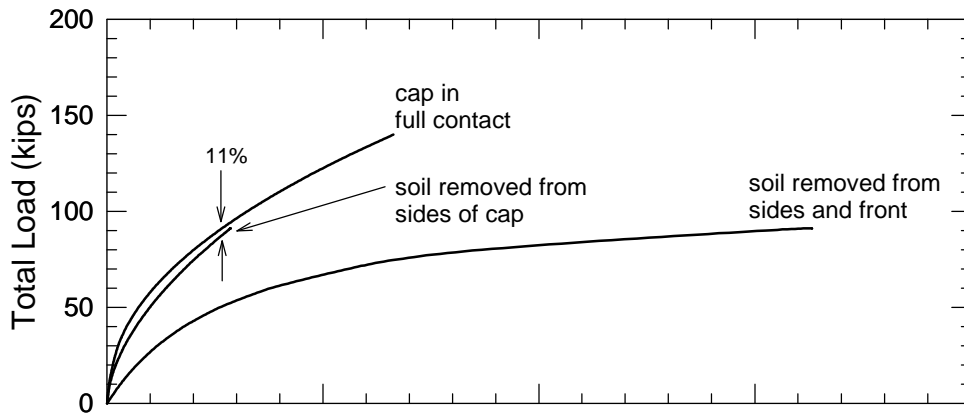




(a) NE 36-in-deep pile cap with 19-ft-long piles.

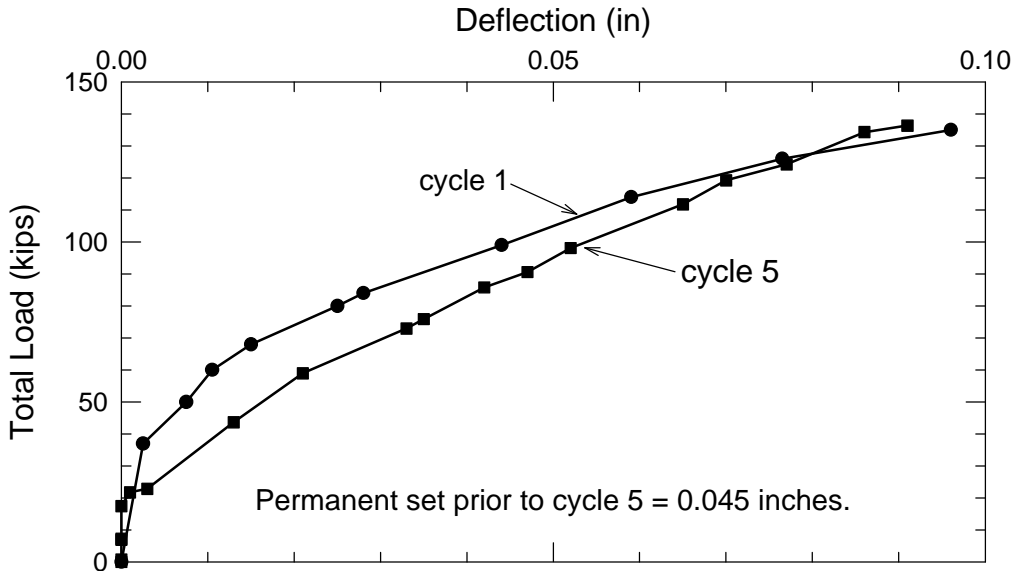


(b) NW 18-in-deep pile cap with 19-ft-long piles.

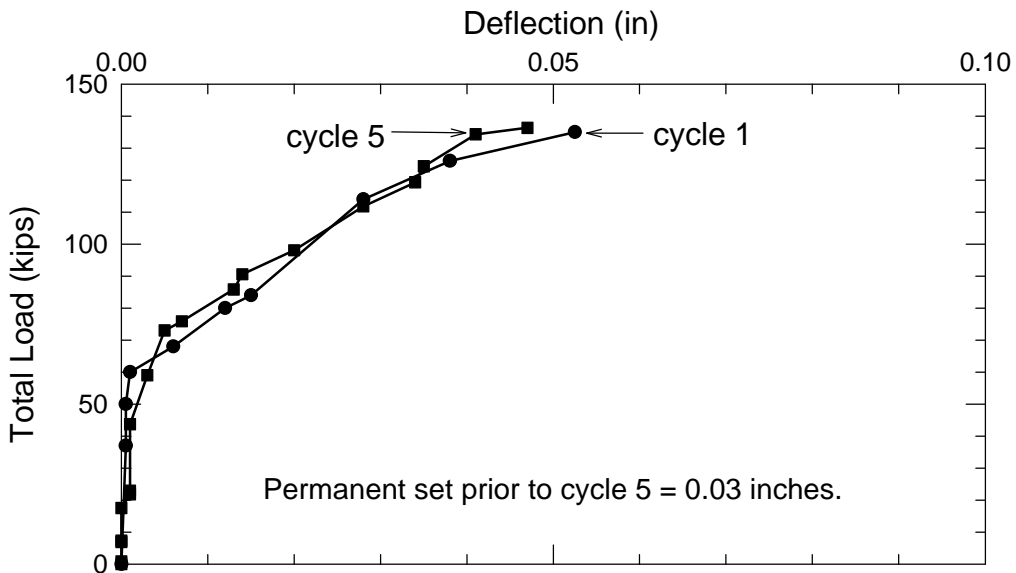


(c) SE 36-in-deep pile cap with 10-ft-long piles.

Figure 6.15. Effect of pile cap side resistance.



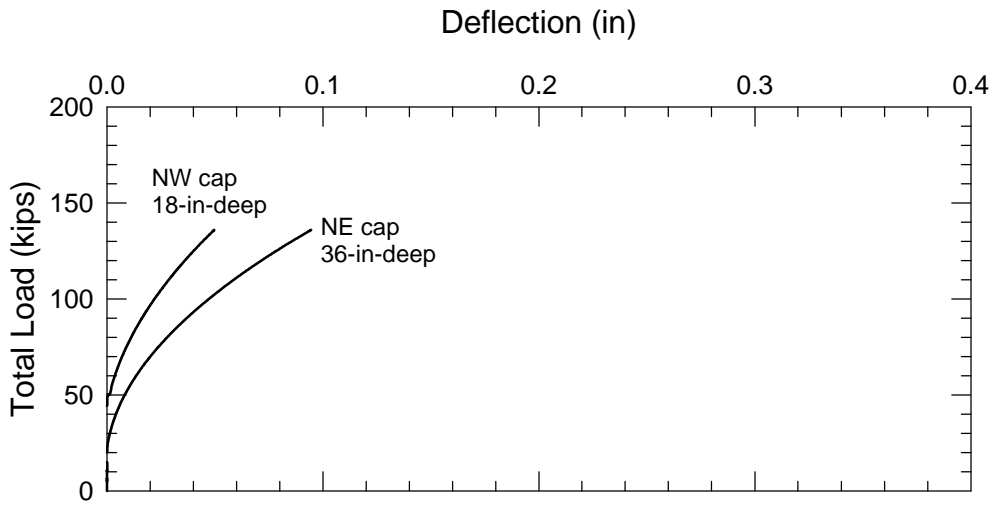
(a.) NE 36-in-deep cap in contact with natural soil.



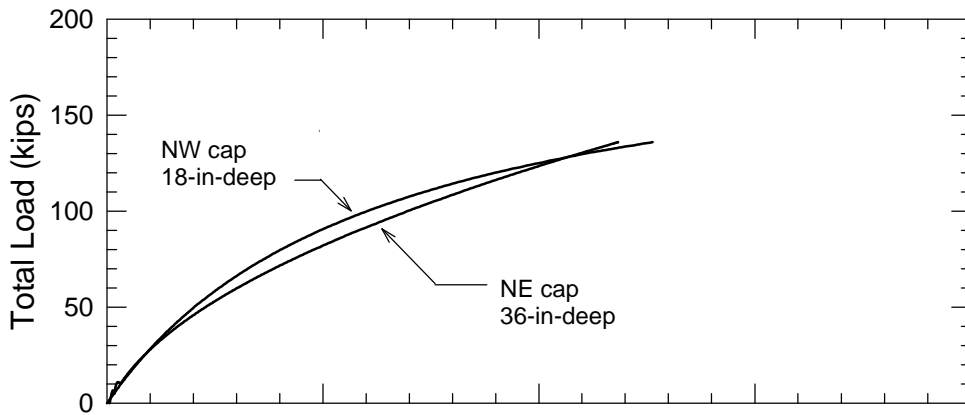
(b.) NW 18-in-deep cap in contact with natural soil.

Note: Load cycle 5 was applied six days after cycle 1. Cycle 5 was initiated at an assumed net deflection of zero. Permanent set prior to cycle 5 is noted in the plots.

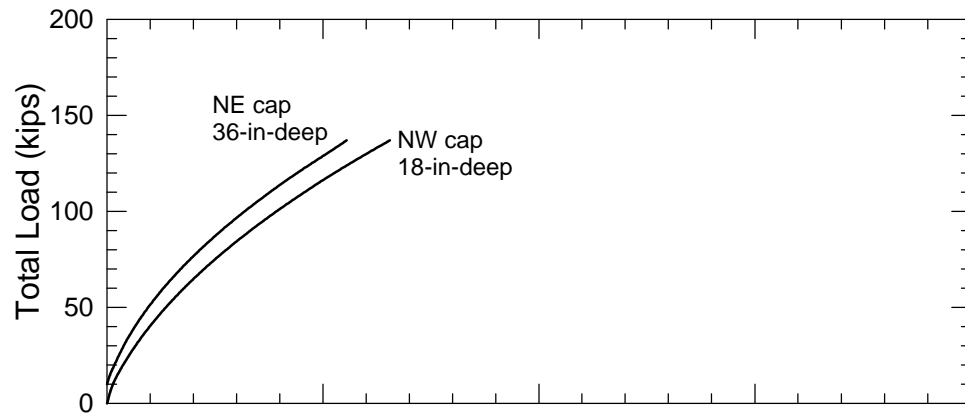
Figure 6.16. Effect of repetitive loading on pile cap deflections.



(a) Pile caps embedded in natural soil.

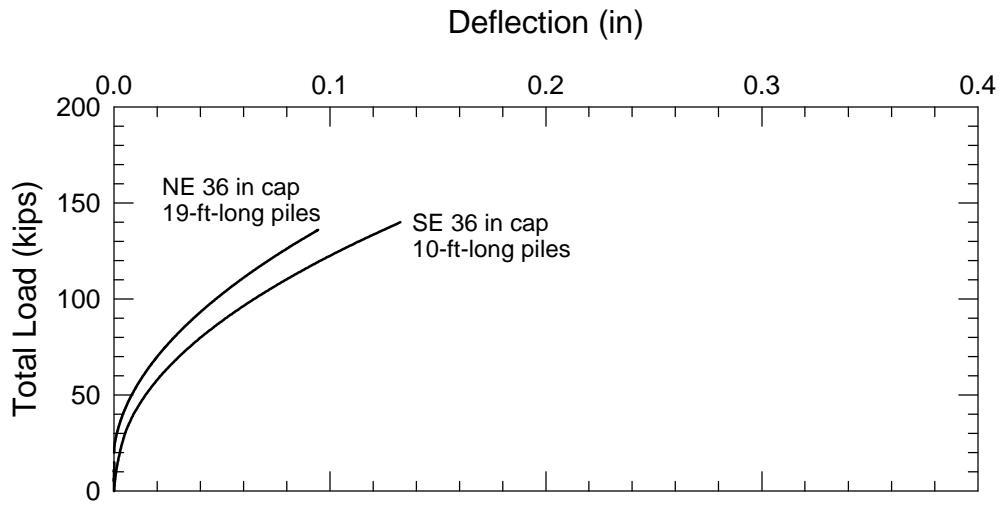


(b) Side and front resistance removed from pile caps.

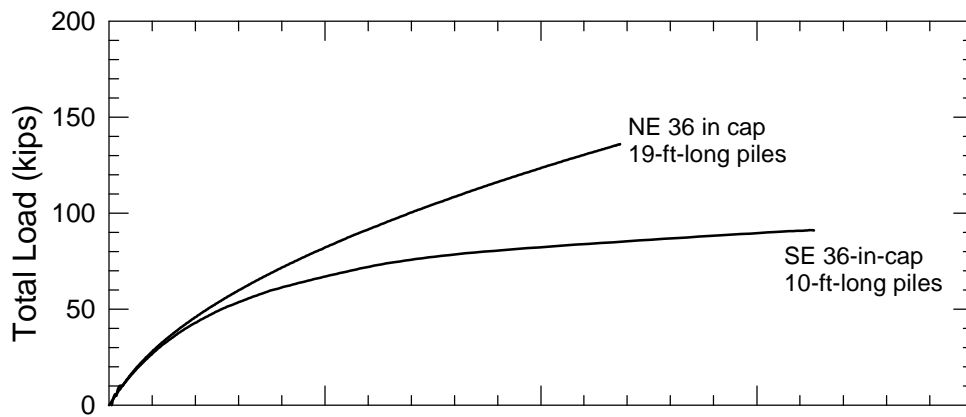


(c) Pile caps backfilled with very dense gravel.

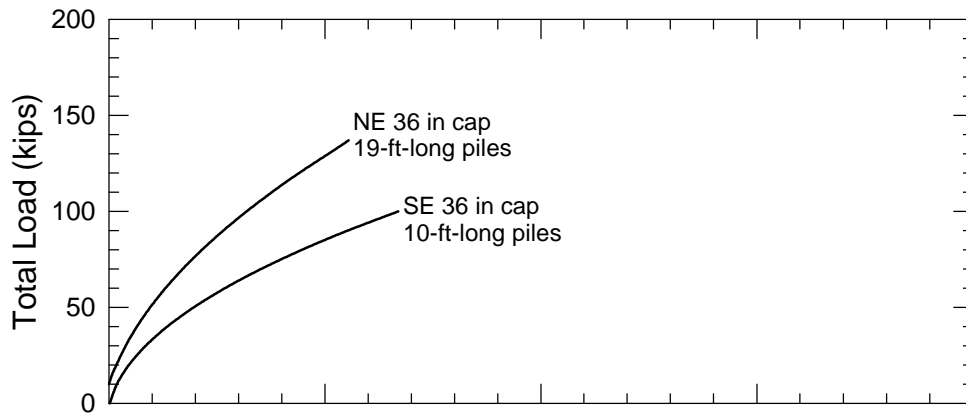
Figure 6.17. Effect of pile cap depth on load-deflection response.



(a) Pile caps embedded in natural soil.

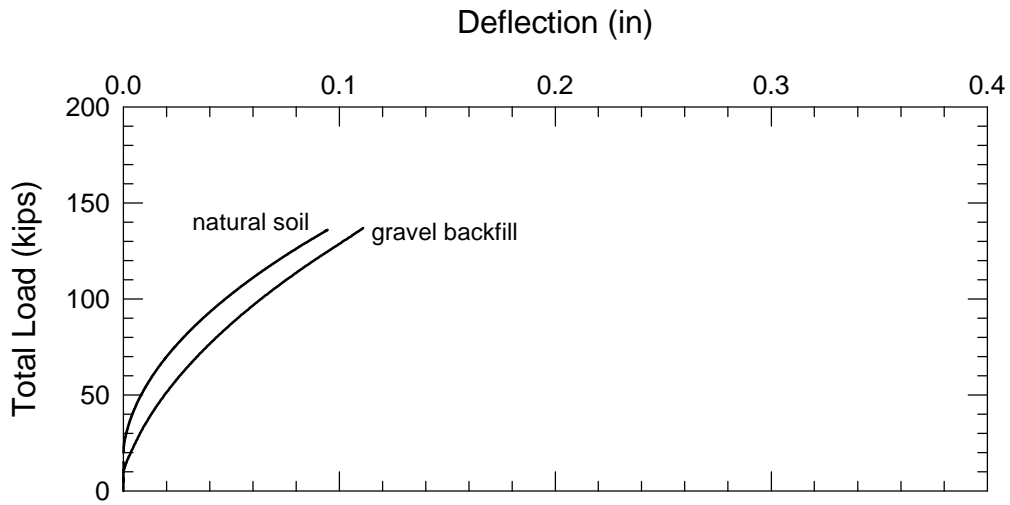


(b) Side and front resistance removed from pile caps.

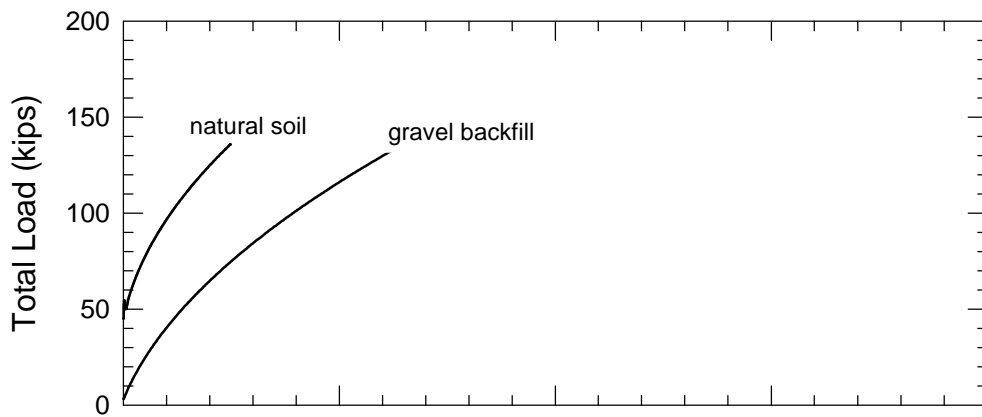


(c) Pile caps backfilled with compacted gravel.

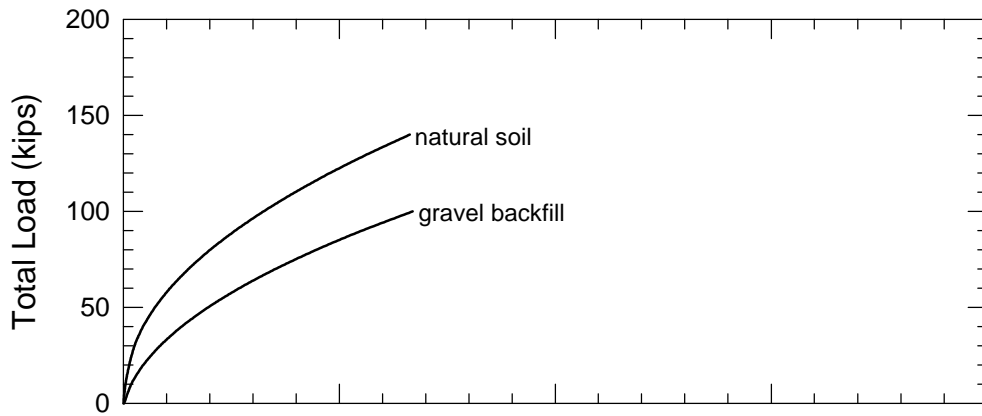
Figure 6.18. Effect of pile length on load-deflection response.



(a) NE 36-in-deep pile cap, 19-ft-long piles.

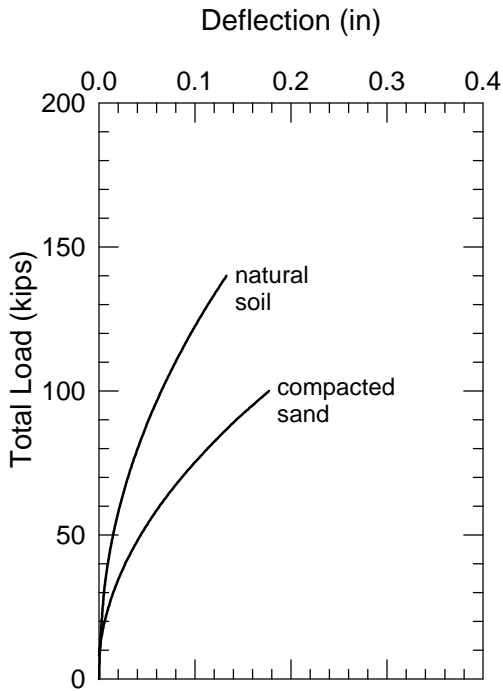


(b) NW 18-in-deep cap, 19-ft-long piles.

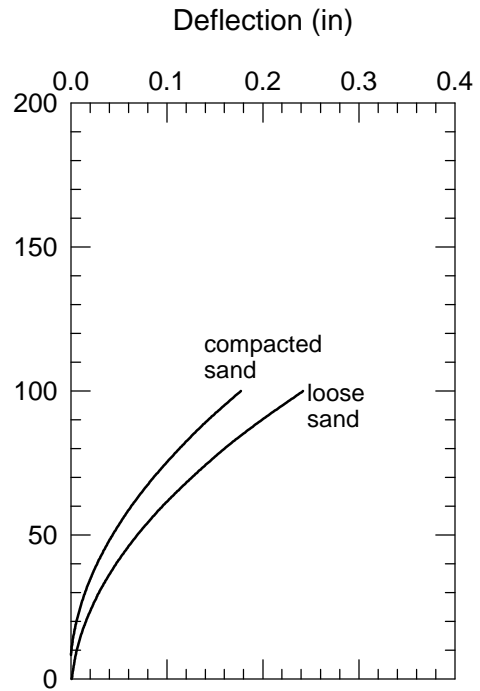


(c) SE 10-in-deep cap, 10-ft-long piles.

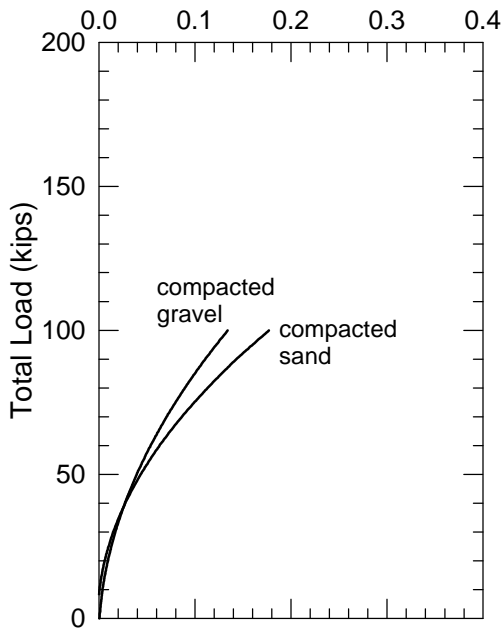
Figure 6.19. Comparison between natural soil and compacted gravel backfill.



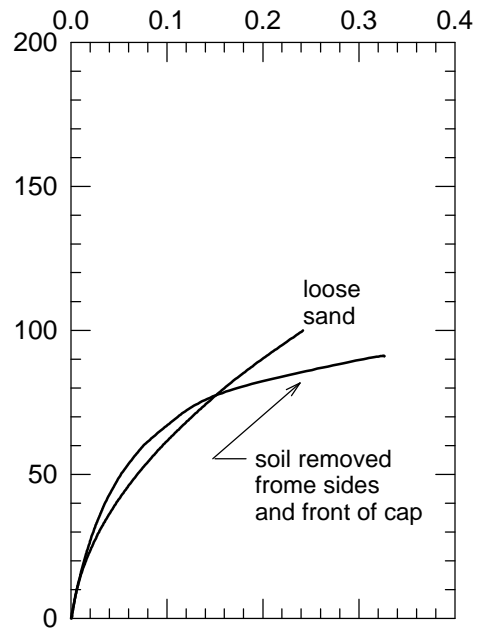
(a) Natural soil vs. compacted sand.



(b) Compacted sand vs. loose sand.

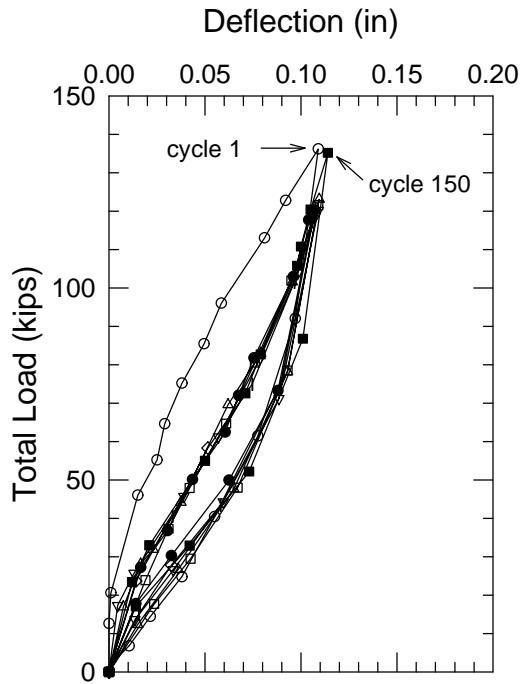


(c) Compacted gravel vs. dense sand.

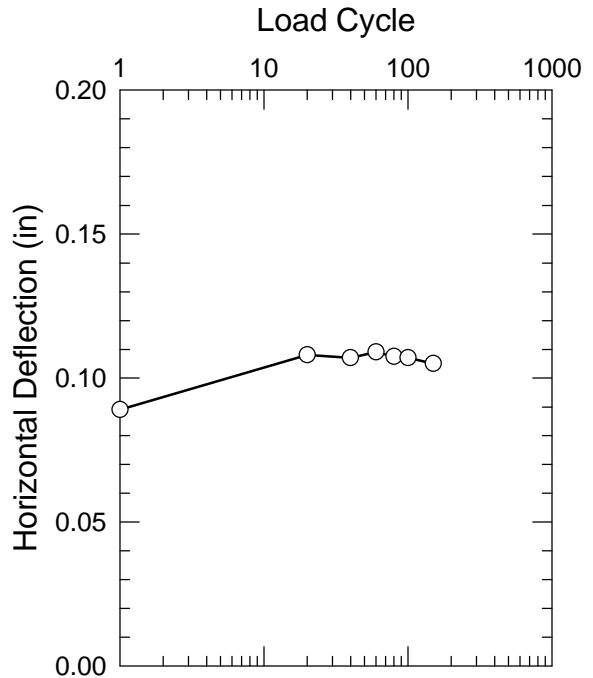


(d) Loose sand vs. no backfill.

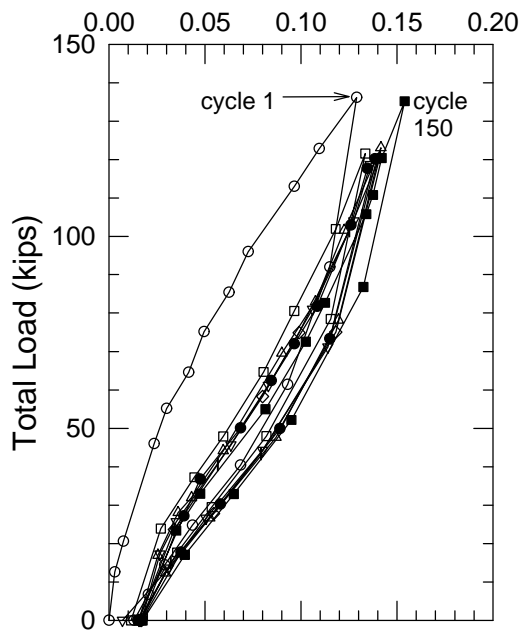
Figure 6.20. Effect of backfill type and density on load-deflection response of SE pile group.



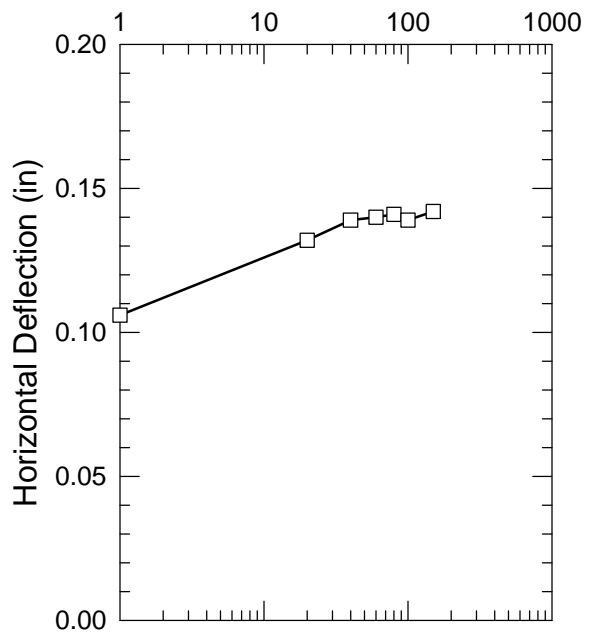
(a) NE 36-in-deep cap.



(b) NE cap response at 120 kip cyclic load.



(c) NW 18-in-deep cap.



(d) NW cap response at 120 kip cyclic load.

Figure 6.21. Cyclic response of NE and NW caps backfilled with compacted gravel.

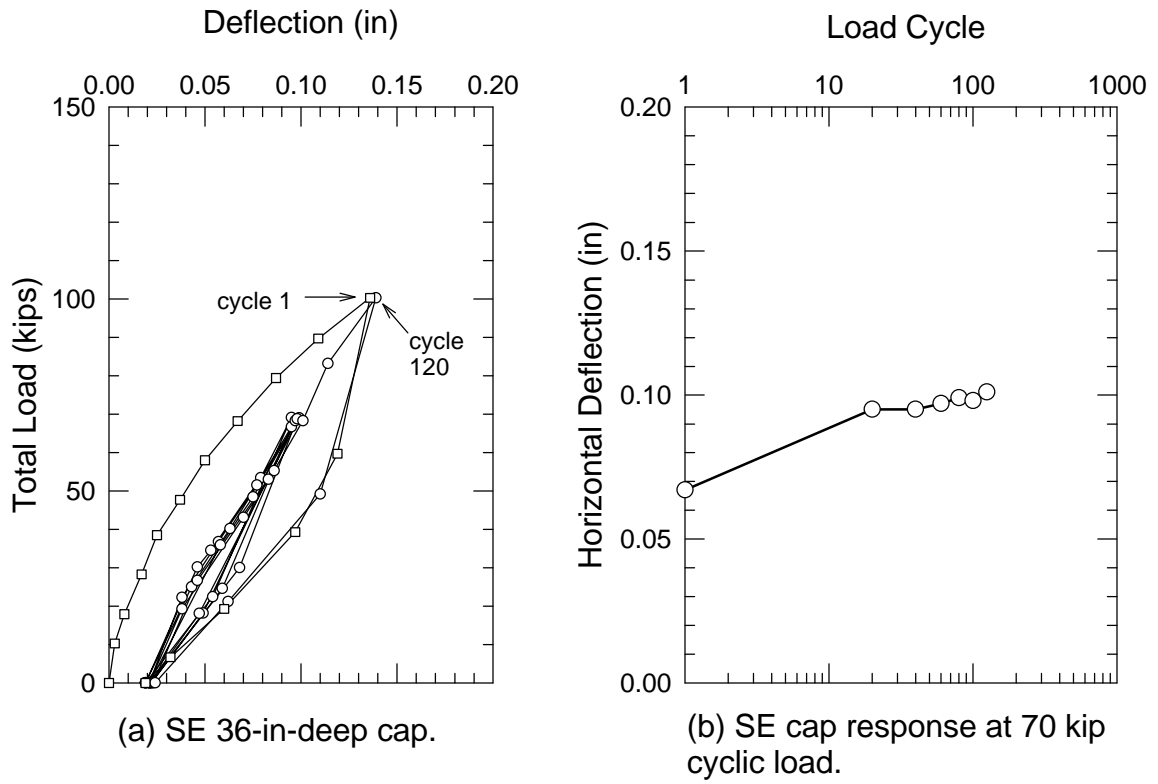
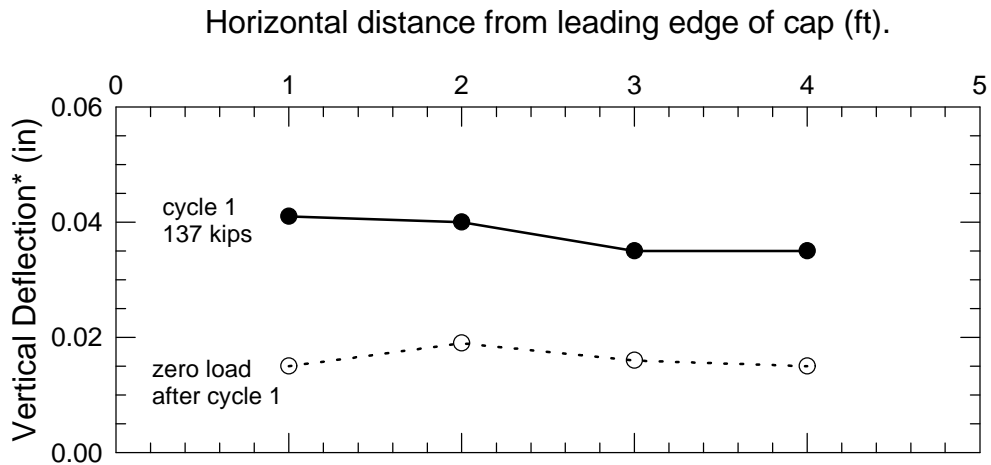
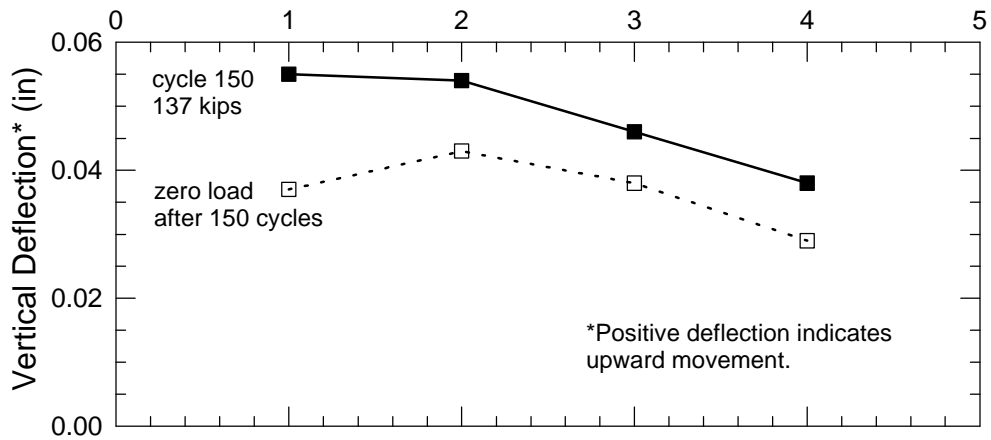


Figure 6.22. Cyclic response of SE cap backfilled with compacted crusher run gravel.

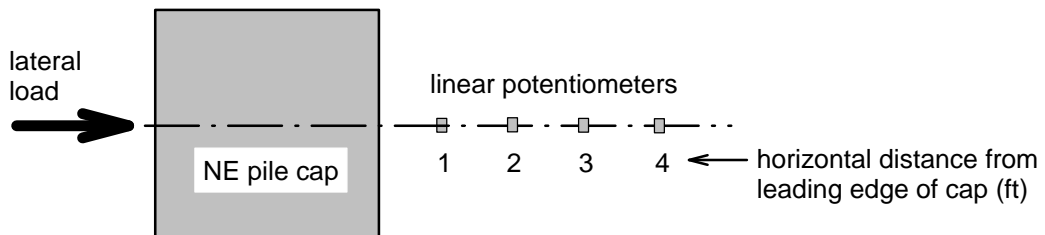




(a) Vertical movement caused by first load cycle.

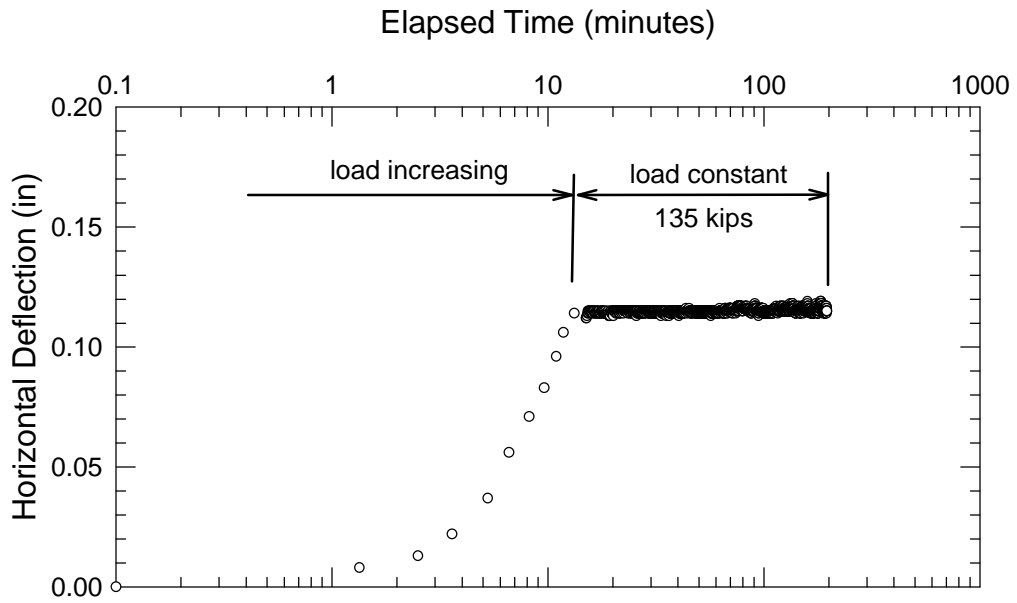


(b) Vertical backfill movement after 150 load cycles.

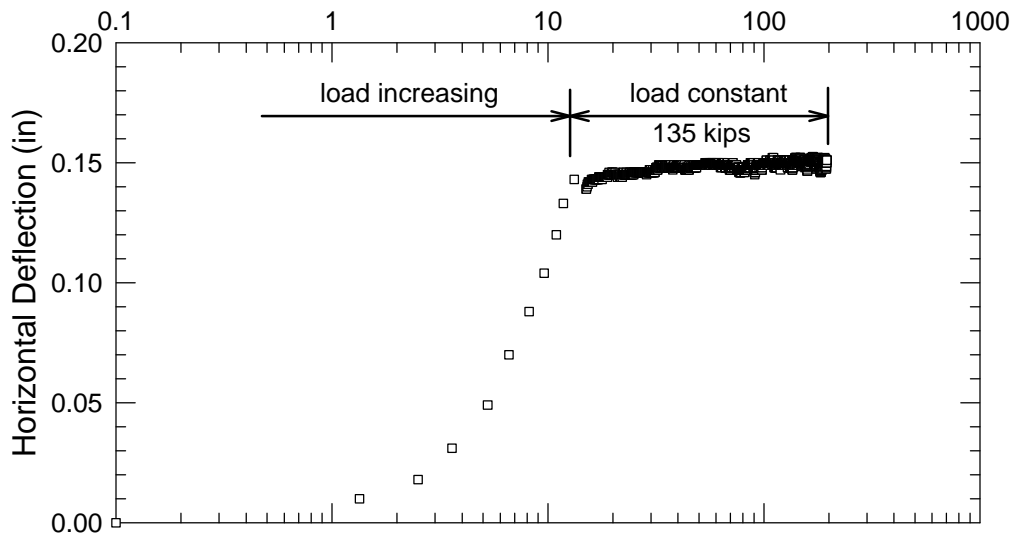


(c) Plan view of setup for measuring backfill surface deflection.

Figure 6.23. Vertical deflection of gravel backfill surface in front of NE 36-in-deep pile cap.



(a) NE pile cap response at a sustained load of 135 kips.



(b) NW pile cap response at a sustained load of 135 kips.

Figure 6.24. Effect of sustained load on NE and NW pile caps backfilled with compacted gravel.

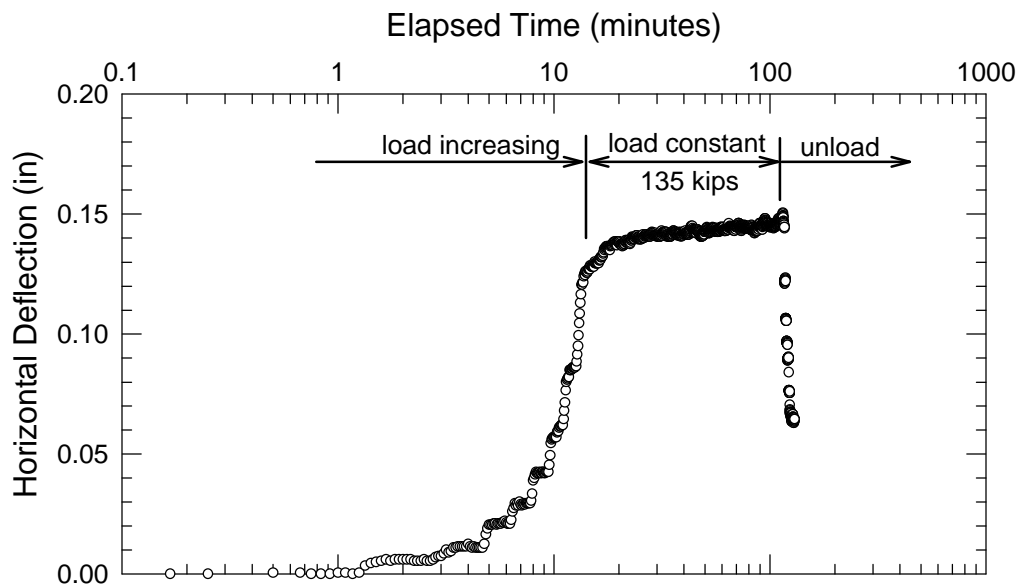


Figure 6.25. Effect of sustained load on SE cap embedded in natural soil.

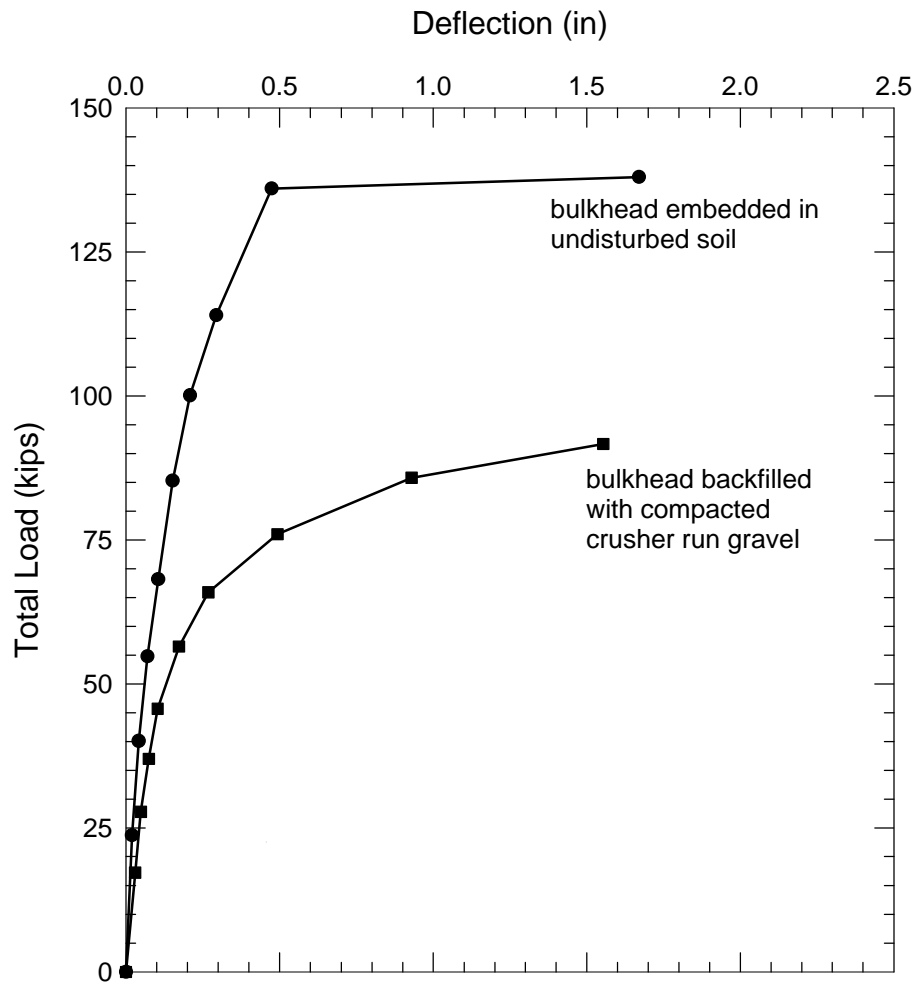


Figure 6.26. Passive resistance of embedded bulkhead in undisturbed soil and compacted gravel.

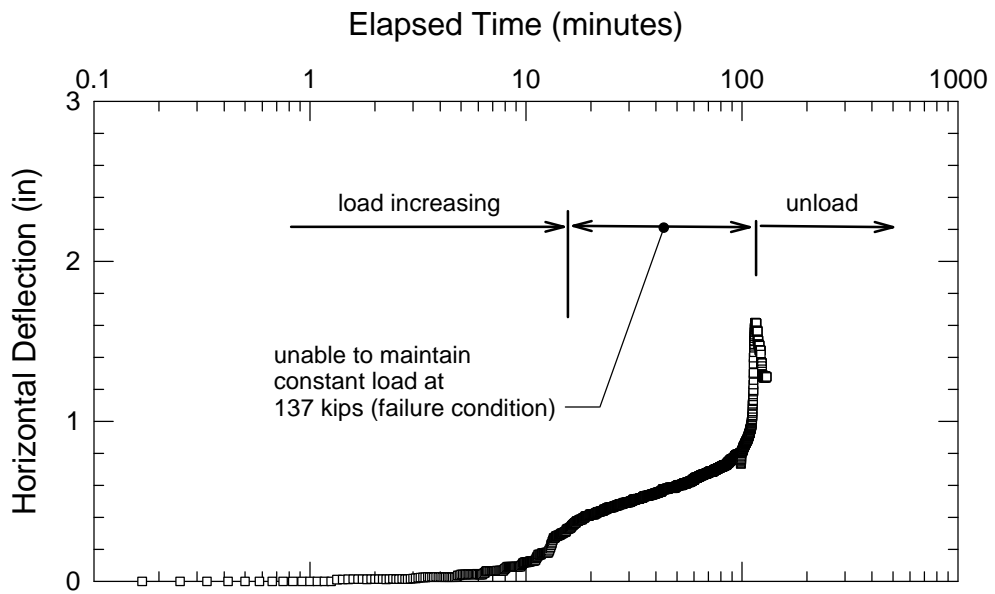
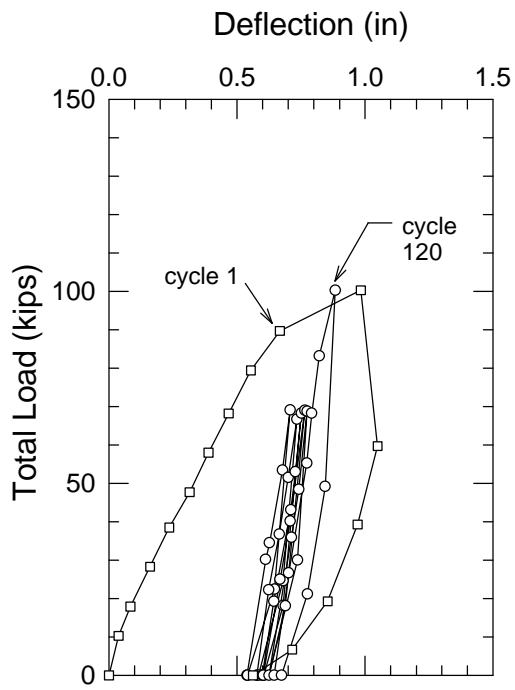
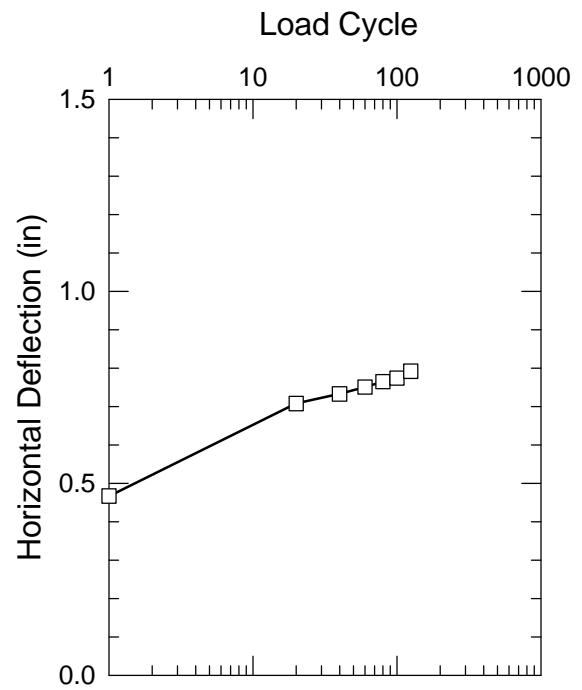


Figure 6.27. Effect of sustained load on bulkhead embedded in natural soil.

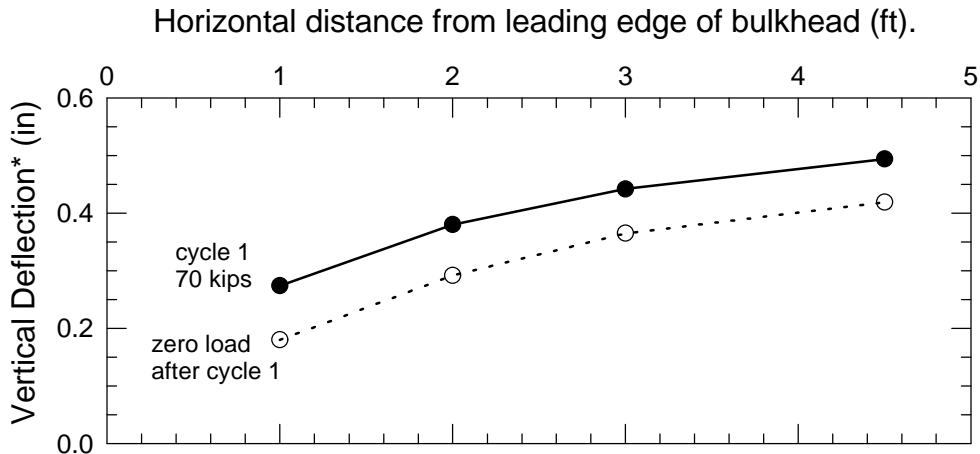


(a) Embedded bulkhead.

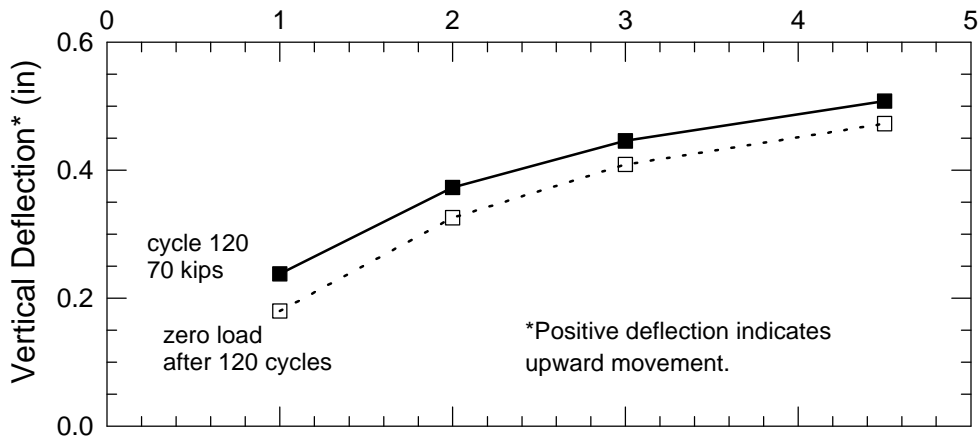


(b) Bulkhead response at 70 kip cyclic load.

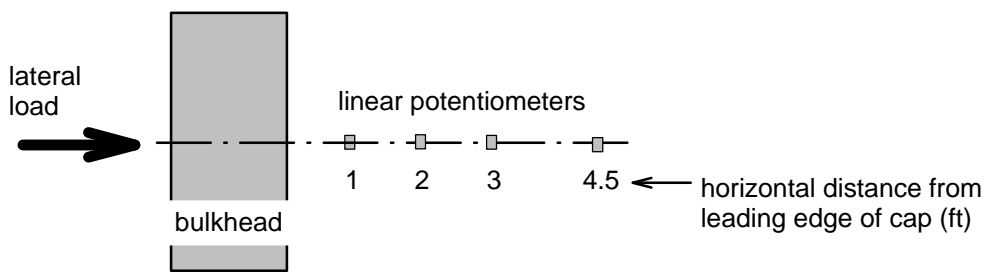
Figure 6.28. Cyclic response of bulkhead backfilled with dense crusher run gravel.



(a) Vertical movement caused by first load cycle.



(b) Vertical backfill movement after 120 load cycles.



(c) Plan view of setup for measuring backfill surface deflection.

Figure 6.29. Vertical deflection of gravel backfill surface in front of embedded bulkhead.

## CHAPTER 7

### ANALYSIS OF LATERALLY LOADED PILE GROUPS

#### 7.1 INTRODUCTION

This chapter describes a procedure for analyzing the response of pile groups to lateral loads. The accuracy of the procedure was evaluated by comparing the computed response of the pile groups at the Kentland Farms load test facility to the results of the load tests discussed in Chapter 6. The analyses were performed using the “group-equivalent pile” method, which was developed during the course of this research. The “group-equivalent pile” (abbreviated GEP) method makes it possible to analyze a pile group using computer programs developed for analyzing single piles, such as *LPILE Plus 3.0* (1997).

The GEP method involves the following elements:

- Step 1. A method for developing p-y curves for single piles in soils with friction, soils with cohesion, and soils with both friction and cohesion.
- Step 2. A method for modeling the resistance of pile groups to lateral loading, including group effects and rotational restraint due to the cap.
- Step 3. A method for computing p-y curves for pile caps in soils with friction, cohesion, or both friction and cohesion.

The development and application of the procedure are described in the following sections.



## 7.2 SINGLE PILE MODEL

### 7.2.1 Background

The laboratory tests described in Chapter 5 and the field load tests performed on two HP 10 x 42 piles provide a basis for development of p-y curves for the partly saturated silty and clayey soils (natural soils) at the field test facility. The soil parameters used to develop p-y curves for the natural soils are summarized in Figure 7.1.

The piles were analyzed using the computer program *LPILE Plus 3.0* (1997). This program uses finite difference numerical methods to solve the beam bending equation and nonlinear p-y curves to model the soil. *LPILE Plus 3.0* contains “default” p-y curve formulations that can be used for cohesive soils, cohesionless soils, and silts. These formulations are empirical, and are based on pile load tests performed in Texas by Matlock (1970), Reese et al. (1974), Reese and Welch (1975), and others.

As an alternative to “default” p-y curves, the program user can input p-y curves developed using other formulations, as was done in this study. The following subsection describes the procedure that was used to develop p-y curves for modeling the soil conditions encountered at the test site.

### 7.2.2 Single Pile p-y Curves

There are a number of formulations available for developing p-y curves. These are often empirically related to values of soil strength and stress-strain characteristics, which can be measured in the field or laboratory. Most of these methods use a cubic parabola to model the relationship between p and y. The general form of the cubic parabola relationship is expressed as follows:

$$p = 0.5 p_{ult} \left[ \frac{y}{(A \epsilon_{50} D)} \right]^n \quad \text{Equation 7.1}$$

where  $p$  is the soil resistance (force per length units);  $p_{ult}$  is the maximum value of  $p$  at large deflections (force per length units);  $y$  is the lateral deflection of a pile at a particular depth (length units);  $D$  is the diameter or width of the pile (length units);  $\epsilon_{50}$  is the strain required to mobilize 50 % of the soil strength (dimensionless);  $A$  is a parameter that controls the magnitude of deflections (dimensionless); and  $n$  is an exponent (dimensionless), which equals 0.33 for a cubic parabola.

The cubic parabola formulation was used to calculate  $p$ - $y$  curves in this study using the procedure developed by Mokwa et al. (1997) for evaluating the lateral response of piles and drilled shafts in partially saturated soils. This  $p$ - $y$  curve formulation was found by Mokwa et al. (1997) to be more accurate than the  $c$ - $\phi$  formulation developed by Reese (1997) for silty soils. Load-deflection curves computed using the Reese (1997) and the Mokwa et al. (1997)  $p$ - $y$  formulations are compared to measured load-deflection response curves in Section 7.2.4, for piles embedded in partially saturated natural soils at the Kentland Farms facility.

Brinch Hansen's (1961) ultimate load theory forms the basis of the Mokwa et al. (1997) procedure for developing  $p$ - $y$  curves, as described in the following paragraphs.

Evans and Duncan (1982) developed an approach based on Brinch-Hansen's (1961) ultimate load theory to determine values of  $p_{ult}$  for soils that have both cohesion and friction ( $c$ - $\phi$  soils). Field load tests performed by Helmers et al. (1997) showed that Brinch-Hansen's theory resulted in values of ultimate load capacity for drilled shafts that agreed well, on the average, with the results of field load tests performed in partially saturated soils at 5 sites in Virginia.

In some cases, Brinch-Hansen's theory underestimated the load capacity, and in other cases, it overestimated the capacity. To improve the reliability of Brinch-Hansen's theory for partly saturated silty and clayey soils, Helmers et al. (1977) recommended that theoretical values of soil resistance using Brinch-Hansen's theory should be reduced by 15 %, so that the actual capacities would not be overestimated for any of the test sites. This can be

accomplished by multiplying the theoretical values by a modification factor  $M$ , with  $M$  having a value of 0.85.

With this empirical adjustment to improve the reliability of the theory, Brinch-Hansen's (1961) theory can be used to express values of  $p_{ult}$  as follows:

$$p_{ult} = (\gamma x K_q + cK_c)MD \quad \text{Equation 7.2}$$

where  $M$  is an empirical modification factor = 0.85 (dimensionless);  $D$  is the pile width or diameter (length units);  $\gamma$  is the moist unit weight of foundation soil (force per volume units);  $x$  is the depth measured from the ground surface (length units);  $c$  is the cohesion of the foundation soil (force per area units);  $K_q$  is a coefficient for the frictional component of net soil resistance under 3D conditions (dimensionless); and  $K_c$  is a coefficient for the cohesive component of net soil resistance under 3D conditions (dimensionless).

The principal advancement made in Brinch-Hansen's (1961) theory was the development of expressions for  $K_q$  and  $K_c$ . These factors vary with depth below ground surface and depend on the values of the soil friction angle,  $\phi$ . The expressions used to evaluate  $K_q$  and  $K_c$  are given in Appendix E. It can be seen that these are quite complex. Once programmed in a spreadsheet, however, they can be evaluated easily.

### 7.2.3 Calculations for p-y Curves

The spreadsheet *PYSHEET* Mokwa et al. (1997) was developed to facilitate p-y curve calculations. *PYSHEET* has been renamed to *PYPILE*, and is included as a worksheet in the workbook named *PYCAP*, which is described in subsequent sections of this chapter. Printed output from *PYPILE* is shown in Figure 7.2. This spreadsheet incorporates Brinch Hansen's expressions for  $K_c$  and  $K_q$  and includes the modification factor,  $M$ , used by Helmers et al. (1997) to improve the reliability of Brinch-Hansen's (1961) theory. The studies described here were performed with  $M = 0.85$ , but the value of  $M$  can be varied in the spreadsheet if desired.

The spreadsheet can be used to calculate p-y curves for piles or drilled shafts of any size in c- $\phi$  soils, and the soil properties and the pile or shaft diameter can be varied with depth.

The parameter  $A$  is an empirical adjustment coefficient that can be determined by performing back analyses of field lateral load tests, or by estimating its value based on data for similar soils. The value of  $A$  can range from 0.35 to 2.65 (Evans 1982). Reese et al.'s (1974) p-y formulation for sand is based on other equations, but provides results that are comparable to the cubic parabola formulation using an  $A$  value of 2.5. Using the results from load tests performed at five sites around the state of Virginia, Mokwa et al. (1997) back-calculated a range of  $A$  values that varied from 0.72 to 2.65. An  $A$  value equal to 2.5 was found to provide the best overall match between calculated and measured load-deflection curves for the foundations tested at the Kentland Farms site. This value was used for all the p-y curve computations described in this chapter.

#### 7.2.4 Comparison of Measured and Calculated Deflections of Single Piles

Load-deflection response curves for the north and south piles were calculated using p-y curves computed using the computer spreadsheet *PYPILE*. Soil parameters used in the calculations were obtained from laboratory tests, which are summarized in Figure 5.8. Values for p-y curves were calculated using the pile model shown in Figure 7.1, and are plotted in Figure 7.3(a). The p-y values were input into *LPILE Plus 3.0* to calculate the response of single piles to lateral loading. Response curves generated by *LPILE Plus 3.0* include load versus deflection, load versus moment, and load versus shear distributions along the pile length.

All of the load-deflection curves shown in this chapter are referenced to pile deflections at the ground surface, as shown in Figure 7.4. The response curves shown in the following comparisons were obtained from the tests using the strut connection shown in Figure 6.6. As discussed in Chapter 6, tests were also performed using a clevis pin connection (Figure 6.5). Although the intent was to form a freely rotating connection with the clevis pin, the pinned connection was not effective. The spacing of the clevis tongue and yoke plates

were so close that they bound when loaded. Although modifications were attempted, an effective pin connection was not achieved. For this reason, there was no significant difference in the test results between the rigid strut and the clevis pin connection.

Measured load-deflection and load-rotation response curves for the south pile are shown in Figure 7.5. The north pile measured load-deflection curve is not shown because it was almost identical to that of the south pile (see Figure 6.8). Calculated load-deflection curves are compared to the measured response curve for the south pile in Figure 7.6. The calculated response curves were obtained using p-y curves from *PYPILE* with the Mokwa et al. (1997) formulation. As shown in Figure 7.6(a), the pile-head restraining condition falls between a pure fixed-head (zero slope) and a pure free-head (zero moment) condition. A third response curve was calculated for a rotationally restrained pile-head by back-calculating the rotational restraint  $k_{m\theta}$ . As shown in Figure 7.6(b), a  $k_{m\theta}$  value of  $5.5 \times 10^7$  in-lb/rad was found to provide the best match between calculated and observed load-deflection responses. This illustrates the importance of accurately quantifying the pile-head rotational stiffness.

The *LPILE Plus 3.0* analyses were repeated using the “default” silt p-y curve formulation that was developed by Reese (1997) for soils that possess both cohesion and friction. This p-y curve formulation is not a true c- $\phi$  method. It involves a combination of two separate formulations, one for sand (the contribution of  $\phi$ ) the other for clay (the contribution of c). The p-y curves are generated by adding the  $\phi$  resistance determined using the empirically based p-y formulation for sand with the c resistance determined using the empirically based method for soft clay below the water table. According to the *LPILE Plus 3.0* users manual, the procedure has not been validated by experimental data.

The soil parameters shown in Figure 7.1 were used to develop p-y curves in *LPILE Plus 3.0* using the default silt option. As shown in Figure 7.7(a), neither the fixed-head or free-head boundary conditions provide very accurate predictions of the load-deflection behavior. A third response curve was calculated for a rotationally restrained pile-head by back-calculating the rotational restraint  $k_{m\theta}$ . As shown in Figure 7.7(b), a  $k_{m\theta}$  value of  $4.0 \times$

$10^8$  in-lb/rad was found to provide the best match between calculated and observed load-deflection responses. This value is approximately 7 times as large as the value back calculated using p-y curves from *PYPILE* ( $k_{m\theta} = 5.5 \times 10^7$  in-lb/rad). A load-deflection curve calculated using  $k_{m\theta} = 5.5 \times 10^7$  in-lb/rad together with the *LPILE Plus 3.0* default p-y silt option is also shown in Figure 7.7(b).

### 7.2.5 Single Pile Rotational Restraint

The restraining moment (or the moment that resists pile rotation) can be calculated using the estimated value of  $k_{m\theta}$  and the measured rotation at the pile head, which was 0.029 radians at a load of about 75 kips. Based on the back-calculated value of  $k_{m\theta}$  determined using the p-y curves generated with *PYSHEET*, the restraining moment is calculated as follows:

$$k_{m\theta} = \frac{M}{\theta} = 4580 \frac{ft - kips}{rad} \quad \text{Equation 7.3a}$$

$$M = \left( 4580 \frac{ft - kips}{rad} \right) (0.0294 \text{ rad}) = 135 \text{ ft} - \text{kips} \quad \text{Equation 7.3b}$$

A conceptual diagram of the loading connections at the pile-head is shown in Figure 7.8(a). As can be seen in Figure 6.6, the strut was rigidly bolted to the pile. However, the load cell was not rigidly attached to the strut, but was held in place using four  $\frac{3}{4}$ -inch-diameter threaded rods. The threaded rods did not prevent the load cell from rotating. Consequently, as the pile deflected and tilted in the direction of load, the load cell rotated, causing a vertical force to develop at the end of the strut. This vertical force,  $V$ , created a moment at the pile of magnitude  $V \times w$ . Where  $w$  is the moment arm, as shown in the free body diagram, Figure 7.8(b).

Using the calculated value of  $M$ , and assuming  $V = P$ , the value of  $w$  can be calculated as follows:

$$w = \frac{M}{V} = \frac{135 \text{ ft} - \text{kips}}{75 \text{ kips}} = 1.8 \text{ ft} \quad \text{Equation 7.3c}$$

The load transfer mechanism between the load cell, threaded rods, and strut is difficult to quantify. Based on the diagrams shown in Figure 7.8, the calculated value of  $w = 1.8$  feet appears reasonable. This indicates that the back-calculated value of rotational restraint,  $k_{m\theta} = 5.5 \times 10^7$  in-lb/rad (based on *PYPILE* p-y values) provides a relatively accurate approximation of the boundary conditions at the pile head.

The same series of calculations were repeated using the results obtained from Reese's (1997) default silt p-y curves. A moment arm,  $w$ , of 13 feet was calculated from the best fit value of  $k_{m\theta} = 4.0 \times 10^8$  in-lb/rad (see Figure 7.7b). A 13-foot-log moment arm does not agree well with the actual load test configuration, and leads to a resisting moment that is larger than physically possible. The *LPILE Plus 3.0* analysis was repeated using Reese's default silt p-y curves with a more reasonable value of rotational restraint of  $k = 5.5 \times 10^7$  in-lb/rad. The resulting load-deflection curve shown in Figure 7.7(b) over-predicts the measured deflections by about 150 % at a load of 75 kips.

The measured rotation or slope at the pile head provides an alternate approach for evaluating the accuracy of the two different p-y formulations. The pile-head slope was measured during the load tests using the telltale shown in Figure 3.8. The measured load versus rotation results are shown in Figure 7.5(b). The best fit value of  $k_{m\theta}$  was determined for the two different p-y formulations using the same approach that was used for matching the measured load-deflection curves. The results for the Mokwa et al. (1997) *PYPILE* p-y curves are shown in Figure 7.9(a) and the results for the Reese (1997) *LPILE Plus 3.0* default p-y curves are shown in Figure 7.9(b). The values of  $k_{m\theta}$  determined by matching measured deflections and measured slopes are shown below for both p-y formulations.

<b>p-y curve formulation</b>	<b><math>k_{m\theta}</math> best match for deflection (in-lb/rad)</b>	<b><math>k_{m\theta}</math> best match for slope (in-lb/rad)</b>	<b>ratio of <math>k_{m\theta}</math>(deflection) to <math>k_{m\theta}</math>(slope)</b>
<i>PYPILE</i> Mokwa et al. (1997)	$5.5 \times 10^7$	$4.0 \times 10^7$	1.37
<i>LPILE Plus 3.0</i> default Reese (1997)	$4.0 \times 10^8$	$1.1 \times 10^8$	3.64

There is some discrepancy between the  $k_{m\theta}$  values determined using measured deflection as the fitting criteria and the  $k_{m\theta}$  values determined using measured slope as the matching criteria. This discrepancy can be expressed as a ratio of  $k_{m\theta}$ (deflection match) to  $k_{m\theta}$ (slope match). In principle, the p-y curves will provide a precise representation of the soil conditions when the ratio between  $k_{m\theta}$ (deflection match) to  $k_{m\theta}$ (slope match) equals 1.0. Based on the ratios shown above, neither of the p-y formulations provide an exact replication of the experimental data. There was a 37 % difference between the best-match  $k_{m\theta}$  values determined using the Mokwa et al. (1997) *PYPILE* p-y curves. As shown in Figure 7.10(a), a 37 % difference between  $k_{m\theta}$ (slope match) and  $k_{m\theta}$ (deflection match) leads to a relatively insignificant difference between calculated load-deflection response curves. However, as shown in Figure 7.10(b) for the *LPILE Plus 3.0* default p-y curves, a 260 % difference between  $k_{m\theta}$ (slope match) and  $k_{m\theta}$ (deflection match) results in a substantial difference between the calculated load-deflection response curves.

Based on the analyses and load test results described in the preceding paragraphs, it can be seen that Reese's (1997) default silt p-y curves result in a poor match with the response curves for the test piles at the Kentland Farms site. The p-y values generated using *PYPILE* provide more accurate load-deflection results for the partially saturated c- $\phi$  soils at the test site. *PYPILE* was therefore used for creating pile p-y curves for the remainder of the analyses in this report.



## 7.3 PILE GROUP MODEL

### 7.3.1 Background

The single pile model developed in Section 7.2 forms a part of the pile group model. The computer program *LPILE Plus 3.0* (1997) was used to analyze the pile groups at the test facility using the approach outlined below:

1. The piles in a four-pile group were modeled as a single pile with four times the moment of inertia of the actual pile, giving four times the flexural resistance of a single pile.
2. The “p” values for each pile were adjusted to account for group effects using the reduction factors shown in Figure 2.15.
3. The adjusted “p” values were summed to develop the combined “p” values for the group of piles.
4. The pile-head boundary condition of the “group-equivalent pile” was determined by estimating the rotational restraint provided by the pile cap.
5. The model created in steps 1 through 4 (the “group-equivalent pile” model) was analyzed using *LPILE Plus 3.0*, and the results were compared to the results of the load tests on the pile groups.

Details of these steps are described in the following sections.

### 7.3.2 Group Pile p-y Curves

The group-equivalent pile p-y curves were developed using the conditions and properties shown in Figure 7.1. The analytical approach for pile groups was similar to the single pile approach, except the single pile p-values were adjusted to account for the number of piles, and to account for reduced efficiencies caused by pile-soil-pile interactions. In other words:

$$p = \sum_{i=1}^N p_i f_{mi} \quad \text{Equation 7.4a}$$

where  $p_i$  is the p-value for the single pile,  $f_{mi}$  is the p-multiplier determined from Figure 2.15, and N is the number of piles in the group.

For the 4-pile groups at the Kentland Farms facility, with piles spaced equally at 4D, the p values equal:

$$p = (p \text{ single pile}) \times 3.2 \quad \text{Equation 7.4b}$$

The p-y curves calculated using this method are shown in Figure 7.3(b). The *EXCEL* spreadsheet *PYPILE* was used to create p-y curves for the NE, NW, and SE pile groups.

### 7.3.3 Pile-Head Rotations

Although piles in a group are restrained against rotation by a pile cap, the piles will experience a small amount of rotation during lateral loading. Rotation at the pile-head is caused primarily by: 1) deformation and possibly cracking of concrete at the pile connection to the cap, and 2) rotation of the cap and the pile group caused by vertical movement of the piles.

Flexural cracking of the concrete, in the caps at Kentland Farms, was minimized by using reinforcement in both the top and bottom faces of the cap and by providing a minimum of 5 inches of cover around the piles. Thus, for the pile groups tested in this study, pile-head

rotation caused by deformation or cracking of the concrete was negligible in comparison to the rotational effects associated with vertical movement of the piles.

Rotation of the cap caused by vertical movement of the piles can be significant, depending on the vertical capacities of the piles. During lateral loading, the front of the cap tends to move downward and the back of the cap tends to move upward. The amount of rotation depends primarily on the upward movement of the trailing piles, and is a function of the skin friction that is developed on the piles.

The pile group rotational stiffness concept is shown in Figure 7.11. The magnitude of vertical displacement,  $\Delta_t$ , is controlled by a number of factors, including skin friction or side resistance,  $Q_s$ , end resistance,  $Q_p$ , elastic shortening or lengthening of the piles, frictional resistance at the ends of the cap, and rotational resistance developed as the leading edge of the cap “toes” into the soil. Based on the load tests performed during this study, it appears that the largest contribution to restraint is that due to the frictional resistance of the piles.

The movement required to mobilize skin friction is considerably smaller than the movement required to mobilize end resistance, and is relatively independent of the pile size and soil type (Kulhawy 1984). There is no consensus in the literature regarding the amount of movement that is required to mobilize skin friction fully. However, a range from 0.1 to 0.3 inches is usually considered to be reasonable (Davisson 1975, Gardner 1975, and Kulhawy 1984). Values at the high end of this range are most likely associated with bored piles or drilled shafts, while values at the low end of the range are more representative of driven piles. For the purpose of back calculating  $\theta_{ult}$ , the value of  $\Delta_{ult}$  was assumed equal to 0.1 inches for the piles in this study.

### 7.3.4 Pile-Head Rotational Stiffness Calculations

The value of  $k_{m\theta}$  is defined as:

$$k_{m\theta} = \frac{M}{\theta} \quad \text{Equation 7.5}$$

where  $M$  is the restraining moment that resists rotation, and  $\theta$  is the angular rotation of the pile head. The value of  $k_{m\theta}$  approaches infinity for a pure fixed-head condition (zero slope), and  $k_{m\theta}$  is 0 for a pure free-head condition (zero restraining moment,  $M$ ).

Angular rotation of the pile head is assumed here to be equal to the rotation of the pile cap, which is a function of vertical pile movement. The amount of angular rotation can be determined from geometry as:

$$\theta = \tan^{-1} \frac{2\Delta_t}{S} \quad \text{Equation 7.6}$$

where  $S$  is the spacing between the leading and trailing rows of piles.

The ultimate value of bending moment that can be counted on to resist cap rotation,  $M_{ult}$ , is a function of the side resistance force from each pile,  $Q_{si}$ , and the moment arm,  $X_i$ , as follows:

$$M_{ult} = \sum_{i=1}^N Q_{si} X_i \quad \text{Equation 7.7}$$

where  $N$  is the number of piles in the group, and  $X_i$  is the moment arm, as shown in Figure 7.12(a).

There are a number of recognized methods for estimating  $Q_{si}$ , including rational approaches such as the  $\alpha$ -method (Tomlinson 1987),  $\beta$ -method (Esrig and Kirby 1979) and the  $\lambda$ -method (Vijayvergiya and Focht 1972). The computer program *SPILE* (1993), available from the FHWA, is useful for estimating pile skin resistance. *SPILE* uses the  $\alpha$ -method for performing total stress analyses of cohesive soils and the Nordlund (1963) method for performing effective stress analyses of noncohesive soils. In situ approaches are also available such as the SPT method developed by Meyerhof (1976) or the CPT method by Nottingham and Schmertmann (1975).

Estimates of skin resistance for the piles in this study were made using the  $\alpha$ -method (Tomlinson 1987), in which pile skin resistance,  $Q_s$ , is given by:

$$Q_s = \alpha S_u A_s \quad \text{Equation 7.8}$$

where  $\alpha$  is an adhesion factor that modifies the undrained shear strength,  $S_u$ , and  $A_s$  is the surface area of the pile shaft or perimeter area.  $\alpha$  values depend on the magnitude of  $S_u$ , the pile length and diameter, and the type of soil above the cohesive bearing stratum. Because the natural soil at the site is partially saturated, its shear strength consists of both cohesive ( $c$ ) and frictional ( $\phi$ ) components, as described in Chapter 5. An equivalent  $S_u$  value was estimated for this  $c$ - $\phi$  soil using the following expression:

$$S_u = c + \sigma_h \tan \phi \quad \text{Equation 7.9}$$

where  $\sigma_h$  is the horizontal stress at the depth of interest. Because the natural soil is overconsolidated and may contain residual horizontal stresses caused by pile driving, it was assumed that  $\sigma_h$  was equal to the vertical stress,  $\sigma_v$ .

Although the soils were relatively homogeneous at the Kentland Farms site,  $Q_{si}$  values varied between the three pile groups because of differences in the length of the piles in each group. Pile lengths used in the skin friction analyses were based on the distance from the bottom of the pile cap to the pile tip. There was a 9 inch difference in length between the NE and NW pile groups because the NE 36-inch-deep cap extended 9 inches deeper than the NW 18-inch-deep cap. The piles in the SE group were only driven 10 feet. Because the SE cap was 36 inches deep, the piles extended only 7 feet below the bottom of the cap. Calculated values of  $Q_{si}$  for the piles in the three test groups are summarized below.

<u>Foundation</u>	<u>Pile Length (ft)</u>	<u><math>Q_{si}</math> per pile (kips)</u>	<u>Avg. <math>S_u</math> (ksf)</u>	<u>Avg. <math>\alpha</math></u>
NE group	16.5	78	1.50	0.98
NW group	17.25	82	1.50	0.98
SE group	7	30	1.32	1.0

The average values of  $S_u$  and  $\alpha$  are based on weighted averages with respect to pile length. Skin resistance values ( $Q_{si}$ ) shown above were used with Equation 7.7 to estimate the limiting value of the restraining moment,  $M_{ult}$ . As shown in Figure 7.12(b), the relationship between  $M$  and  $\theta$  is expected to be nonlinear up to  $M_{ult}$ . The slope of a line drawn through any point along the  $M$ - $\theta$  distribution defines the value of  $k_{m\theta}$ . As shown in Figure 7.13(a), it was assumed the initial nonlinear portion of the  $M$ - $\theta$  curve could be represented by a cubic parabola. The actual shape of the curve is unknown, but a cubic parabola provides a reasonable approximation.

The relationship between  $M$  and  $\theta$  was simplified for the analyses by approximating the curve by a straight line, as shown in Figure 7.13(a). The corresponding value of  $k_{m\theta}$  (the slope of this line) can be computed as follows:

The cubic parabola shown in Figure 7.13(a) can be represented as;

$$M = M_{ult} \left( \frac{\theta}{\theta_{ult}} \right)^{0.33} \quad \text{Equation 7.10a}$$

rearranging terms;

$$\frac{M}{M_{ult}} = \left( \frac{\theta}{\theta_{ult}} \right)^{0.33} \quad \text{Equation 7.10b}$$

when  $\frac{\theta}{\theta_{ult}} = 0.5$

$$\frac{M}{M_{ult}} = (0.5)^{0.33} = 0.79 \quad \text{Equation 7.10c}$$

thus,  $M = 0.79M_{ult}$  for  $\theta = 0.5\theta_{ult}$

and, consequently,

$$k_{m\theta} = \frac{M}{\theta} = \frac{0.79M_{ult}}{0.5\theta_{ult}} = 1.6 \frac{M_{ult}}{\theta_{ult}} \quad \text{Equation 7.10d}$$

For the purpose of these analyses, it was assumed that the rotational restraint,  $k_{m\theta}$ , is constant up to the value of  $M_{ult}$ , as shown in Figure 7.13(b).

Using the relationships developed above,  $k_{m\theta}$  can be determined as follows:

$$k_{m\theta} = 1.6 \frac{M_{ult}}{\theta_{ult}} = 1.6 \frac{\sum_{i=1}^N Q_{si} X_i}{\tan^{-1}\left(\frac{2\Delta_t}{S}\right)} \quad \text{Equation 7.11}$$

The value of  $k_{m\theta}$  can be estimated using the iterative process described below:

**Step 1.** The rotational restraint calculated from Equation 7.11 is used as the initial pile head boundary condition.

**Step 2.** The calculated value of moment at the pile-head ( $M_{pile}$ ), obtained from the *LPILE Plus 3.0* analysis, is compared to the value of  $M_{ult}$  calculated using Equation 7.6.

- If  $M_{piles} > M_{ult}$ , the analysis is repeated using a smaller value of  $k_{m\theta}$ . This condition is represented by the square in Figure 7.13(b).
- If  $M_{piles} \leq M_{ult}$ , the solution is acceptable. This condition is represented by the solid circles in Figure 7.13(b).

Using the approach described in this section, the following values of  $M_{ult}$  and  $k_{m\theta}$  were calculated for the NE, NW, and SE pile groups.

<u>Foundation</u>	<u>M<sub>ult</sub> (in-lb)</u>	<u>k<sub>mθ</sub> (in-lb/rad)</u>
NE group	6.29 x 10 <sup>6</sup>	2.01 x 10 <sup>9</sup>
NW group	6.54 x 10 <sup>6</sup>	2.09 x 10 <sup>9</sup>
SE group	2.44 x 10 <sup>6</sup>	7.82 x 10 <sup>8</sup>

### 7.3.5 Comparison of Measured and Calculated Pile Group Deflections with No Cap Resistance

Load-deflection curves for the NE, NW, and SE pile groups at the Kentland Farms facility were calculated using *LPILE Plus 3.0* and the procedure described in this chapter, with the Mokwa et al. (1997) p-y curves. Calculated results were compared to the measured load-deflection curves for the pile groups. The first comparisons did not include cap resistance. The calculated results were compared to the load tests performed after soil was removed from the sides and the front of the pile caps.

**NE pile group.** The piles in the NE group extended 16.5 feet below the cap, which was 3 feet deep. p-y values for the “group-equivalent pile” for this group were computed using *PYPILE*. Calculated load-deflection curves for assumed fixed-head and free-head boundary conditions are shown in Figure 7.14(a). Neither of these conditions provides a reasonable estimate of the measured behavior. At a load of 135 kips, the fixed-head case under-predicts the deflection by 67 %, while the free-head case over-predicts the deflection by over 400 %.

The results obtained using a rotationally restrained pile-head boundary condition are in better agreement with the measured deflections, as shown in Figure 7.14(b). The rotational restraint,  $k_{m\theta} = 2.01 \times 10^9$  in-lb/rad, was estimated using the approach described in the previous section. In this case, at a load of 135 kips the calculated deflection was only 17 % greater than the measured deflection, a difference of only 0.04 inches.



**NW pile group.** The piles in the NW group extended 17.25 feet below the cap, which was 1.5 feet deep. *p-y* values for the equivalent NW-group-pile were computed using *PYPILE*. Calculated load-deflection curves for assumed fixed-head and free-head boundary conditions are shown in Figure 7.15(a). Neither of these conditions provides a reasonable estimate of the measured behavior. At a load of 135 kips, the fixed-head case under-predicts the deflection by 56 %, while the free-head case over-predicts the deflection by over 200 %.

The results obtained using a rotationally restrained pile-head boundary condition are considerably more accurate, as shown in Figure 7.15(b). The rotational restraint,  $k_{m\theta} = 2.09 \times 10^9$  in-lb/rad, was estimated using the approach described in the previous section. In this case, at a load of 135 kips the calculated deflection was only 13 % less than the measured deflection, a difference of only 0.03 inches.

**SE pile group.** The piles in the SE group extended 7 feet below the cap, which was 3 feet deep. *p-y* values for the SE group-pile were computed using *PYPILE*. Calculated load-deflection curves for assumed fixed-head and free-head boundary conditions are shown in Figure 7.16(a). Neither of these conditions provides a reasonable estimate of the measured behavior. At a load of 90 kips, the fixed-head case under-predicts the deflection by 53 %, while the free-head case was extremely over-conservative, predicting failure at a load of about 40 kips.

The results obtained using a rotationally restrained pile-head boundary condition are shown in Figure 7.16(b). The rotational restraint,  $k_{m\theta} = 7.82 \times 10^8$  in-lb/rad, was estimated using the approach described in the previous section. At a load of 135 kips, the calculated deflection was approximately 100 % greater than the measured deflection, a difference of about 0.34 inches. Although not as accurate as in the cases of the NE and NW pile groups, the calculations are more accurate than assuming fixed-head or free-head conditions, and provide a conservative approximation that would be reasonable for use in design.

In summary, the method that was developed for estimating the lateral capacity of pile groups provided results that were in reasonable agreement with full-scale lateral load tests at

the NE and NW pile groups. The largest difference between calculated and measured load-deflection results occurred for the SE group, which had the shortest piles. The author believes that as the pile lengths decrease, other factors begin to have greater effects on the rotational restraint of the pile head. Piles as short as 7 feet would not typically be used unless they were driven to refusal in a firm bearing strata. The short piles beneath the SE cap were not driven to refusal, and have very small axial capacities. The rotations of the cap will be controlled by the uplift capacity of the trailing piles. Consequently, the SE cap will experience larger rotations because of the small amount of skin resistance that can be developed by its shorter piles. It seems likely that the accuracy of the procedure could be improved by varying the value of  $k_{m\theta}$  to represent a nonlinear variation of  $M$  with  $\theta$ . However, this would complicate the procedure to such an extent that it would be too time-consuming for use in routine practice.

## **7.4 PILE CAP MODEL**

### **7.4.1 Background**

Load tests conducted during this study indicate that pile caps provide considerable resistance to lateral loads. This section describes the procedures that were developed for estimating cap resistance using an approach that can be readily coupled with the procedures for analyzing single piles and groups of piles. The approach provides a method for computing the cap resistance derived from passive earth pressures, and models the variation of this resistance with cap deflection using hyperbolic  $p$ - $y$  curves. As described in the following paragraphs, the hyperbolic  $p$ - $y$  curves are defined by the ultimate passive force and the initial elastic stiffness of the embedded pile cap.

### **7.4.2 Passive Earth Pressure Resistance**

The log spiral earth pressure theory was used to estimate the passive pressure developed on pile caps. The log spiral failure surface consists of two zones: 1) the Prandtl zone, which is bounded by a logarithmic spiral, and 2) the Rankine zone, which is bounded by a plane, as shown in Figure 7.17(a). The shape of the log spiral surface is shown in Figure

7.17(b). For large values of the wall friction angle,  $\delta$ , the theory is more accurate than Rankine or Coulomb's earth pressure theories, which apply only to simple states of stress, or use plane surfaces to approximate the failure surface. The log spiral, Rankine, and Coulomb theories provide identical results when the wall friction angle,  $\delta$ , is zero. However,  $K_p$  values estimated using Coulomb's theory are non-conservative, and can be very inaccurate for  $\delta$  values greater than about  $0.4\phi$ . On the other hand, Rankine's theory does not account for wall friction, and, consequently, may greatly underestimate passive earth pressures, especially at larger values of  $\delta$ .

The wall friction angle at the front face of a pile cap will be large because of the restraint against vertical movement of the cap that is provided by the piles. For this reason, the log spiral earth pressure theory is the most appropriate theory for estimating the ultimate passive pressure developed by pile caps.

Log spiral earth pressure forces can be determined using a trial and error graphical process based on the principle that a force vector acting on the log spiral failure surface makes an angle of  $\phi$  with the tangent to the spiral, and the lines of action of the force vectors pass through the center of the spiral, as shown in Figure 7.18. This approach can provide accurate results for any magnitude of wall friction, and can also account for cohesion in  $c-\phi$  soils. However, the graphical procedure is time-consuming, and is not adaptable to computer calculations. Caquot and Kerisel (1948) developed tables that can be used for estimating the earth pressure coefficient,  $K_p$ , based on the log spiral theory. These tables are available in many foundation engineering text books and manuals. The disadvantages of the tables are that they cannot be used in computer programs, and that they do not account for cohesion.

An *EXCEL* spreadsheet was developed by Dr. J.M. Duncan and the author to calculate passive earth pressures using the log spiral earth pressure theory, and was extended significantly during the course of this study. In its present form, the program accounts for friction, cohesion, and surcharge components of passive pressures, and any magnitude of wall friction. The program is coded in an *EXCEL* workbook named *PYCAP*, which was developed

for calculating p-y curves for embedded pile caps. The workbook *PYCAP* contains a number of different worksheets. The log spiral calculations are performed in the worksheet named *Log Spiral*. Details of the log spiral earth pressure theory, and the worksheet *Log Spiral*, are provided in Appendix F.

The magnitude of the interface wall friction angle and the effects of wall friction on passive earth pressures have been the focus of numerous studies including the classic retaining wall studies by Terzaghi (1932, 1934a, and 1934b), the interface tests performed on dense sands and concrete by Potyondy (1961), and the finite element studies by Clough and Duncan (1971). These studies and others indicate that wall friction is not an absolute value but depends on the amount of wall movement as well as on the soil properties and the properties of the soil/wall interface. In practice, average values of wall friction are often used based on engineering judgement and experience.  $\delta$  values used in practice most often fall within the range of about  $0.4\phi$  to  $0.8\phi$ . Recommended values of  $\delta$  for use in design are summarized in Table 7.1 for various types of soils and interface materials.

The passive earth pressure force,  $E_p$ , can be expressed in terms of its three primary components: 1) soil weight and friction,  $P_{p\phi}$ , 2) soil cohesion,  $P_{pc}$ , and 3) surcharge,  $P_{pq}$ .  $E_p$ , which is in units of force per unit length, can be expressed as:

$$E_p = (P_{p\phi} + P_{pc} + P_{pq}) \quad \text{Equation 7.12a}$$

or, in terms of earth pressure coefficients:

$$E_p = \frac{1}{2} \gamma H^2 K_{p\phi} + 2cHK_{pc} + qHK_{pq} \quad \text{Equation 7.12b}$$

where the earth pressure coefficient for friction and soil weight is defined as:

$$K_{p\phi} = \frac{2P_{p\phi}}{\gamma H^2} \quad \text{Equation 7.13a}$$

the earth pressure coefficient for cohesion is defined as:

$$K_{pc} = \frac{P_{pc}}{2cH} \quad \text{Equation 7.13b}$$

and the earth pressure coefficient for surcharge is defined as:

$$K_{pq} = \frac{P_{pq}}{qH} \quad \text{Equation 7.13c}$$

The  $K_{p\phi}$  value determined using the log spiral method approaches the Rankine value of  $K_p$  as  $\delta$  approaches zero. For this reason, and because numerical difficulties occasionally occur when  $\delta$  is less than 2 degrees, *PYCAP* automatically defaults to the Rankine value of  $K_p$  when  $\delta$  is less than 2 degrees. In this case, the ultimate passive force,  $E_p$ , is expressed in terms of force per unit length as:

$$E_p = \frac{1}{2} \gamma H^2 K_p + 2cH \sqrt{K_p} + qHK_p \quad \text{Equation 7.14}$$

where  $K_p$  is determined from Rankine theory as:

$$K_p = \tan^2 \left( 45 + \frac{\phi}{2} \right) \quad \text{Equation 7.15}$$

The value of  $E_p$  calculated using either of the approaches described above is modified by applying a factor to account for three-dimensional effects. This factor, called  $R$ , is discussed in Section 7.4.3. The 3-D passive earth pressure force,  $P_{ult}$  is thus determined from  $E_p$  as follows:

$$P_{ult} = E_p R b \quad \text{Equation 7.16}$$

where  $P_{ult}$  is the ultimate passive earth pressure force (force units),  $R$  is a correction factor for 3-D effects (dimensionless), and  $b$  is the width of footing or length of wall (length units).

When  $\phi = 0$ , *PYCAP* defaults to a different method for calculating passive earth pressure, which is called the  $\phi = 0$  sliding wedge method. The method closely follows the approach developed by Reese (1997) for modeling the failure zone in front of a laterally loaded pile. This approach assumes that the ground surface rises and translates in the direction of load. The failure wedge is represented as a plane surface, as shown in Figure 7.19. The semi-empirical equation used to calculate the passive earth pressure force is:

$$P_{ult} = \frac{cbH}{2} \left( 4 + \frac{\gamma H}{c} + \frac{0.25H}{b} + 2\alpha \right) \quad \text{Equation 7.17}$$

where  $\alpha$  is a factor that accounts for adhesion between the cohesive soil and the wall. Typical values of  $\alpha$  are shown in Table 7.2. Conservative values of  $\alpha$  should be used if there is a possibility that adhesion between the soil and wall could be lost or destroyed by water, frost action or remolding during cyclic loading.

The development of Equation 7.17 is described in Appendix G. This equation is based on full-scale test results, thus it implicitly includes three-dimensional and shape effects and, consequently, additional modifications using the 3-D shape factor are not necessary.

Appendices F and G describe the equations and approaches used to calculate the ultimate passive earth pressure force. As discussed in Section 7.4.3, for values of  $\phi > 0$ , this force is modified in *PYCAP* for three-dimensional effects using factors developed by Ovesen (1964) from experiments on embedded anchor blocks. This modified ultimate earth pressure force is incorporated into a hyperbolic formulation to develop pile cap p-y values for lateral load analyses. The entire process, including the generation of pile cap p-y values, is automated in the program *PYCAP*. The next section describes the procedure used to modify two-dimensional plane strain passive earth pressures to model three-dimensional behavior.

### 7.4.3 Three-Dimensional Effects

Load tests were performed on the bulkhead at the field test facility to study the relationship between passive pressures and deflections. Because the bulkhead had no piles, its

resistance to lateral load was provided almost entirely by passive pressure. Frictional resistance on its sides and base was negligibly small. Load tests were conducted to failure for the bulkhead embedded in natural ground, and after backfilling in front of it with crusher run gravel. Measured load versus deflection results are shown in Figure 7.20.

Various methods were examined for calculating the ultimate resistance of the bulkhead, using soil shear strength parameters that were developed from the laboratory tests. These methods included the classical Rankine, Coulomb, and log spiral earth pressure theories; the sliding wedge formulation described by Reese and Sullivan (1980); Brinch Hansen's (1961) ultimate load theory; and Ovesen's (1964) procedure to correct for three-dimensional effects. The most accurate results for both the  $c$ - $\phi$  natural soils and the cohesionless crusher run backfill were obtained using the log spiral earth pressure theory, modified for three-dimensional shape effects using Ovesen's (1964) procedure.

Pile cap resistance to horizontal movement is a function of the passive soil resistance developed at its front face, plus any sliding resistance on the sides and bottom of the cap, less any active earth pressure force on the back face of the cap. In the case of the bulkhead at Kentland Farms, the active force and the sliding resistance are small compared to the passive resistance, and they tend to offset each other. Passive earth pressure is thus the primary source of resistance to lateral load.

Conventional earth pressure theories consider only two-dimensional conditions, which correspond to a long wall moving against the soil. In the case of a bulkhead or pile cap, larger passive pressures are possible because of three-dimensional effects. A zone within the soil, which is wider than the face of the cap, is involved in resisting movement of the cap. The ratio between three-dimensional and two-dimensional soil resistance varies with the friction angle of the soil and the depth below the ground surface. Ovesen's theory provides a means of estimating the magnitude of this three-dimensional effect.

Ovesen (1964) conducted model tests on anchor blocks embedded in granular soils, and developed an empirical method for estimating the 3-D resistance of the embedded blocks.

Ovesen's expressions can be re-arranged to obtain a 3-D modifying factor (called R in this study) that can be calculated as follows:

$$R = 1 + (K_p - K_a)^{2/3} \left[ 1.1E^4 + \frac{1.6B}{1 + 5\frac{b}{H}} + \frac{0.4(K_p - K_a)E^3 B^2}{1 + 0.05\frac{b}{H}} \right] \quad \text{Equation 7.18}$$

where  $K_p$  and  $K_a$  are the passive and active earth pressure coefficients;  $b$  is the width of the cap measured horizontally in a direction normal to the applied load;  $H$  is the height of the cap;  $B$  is based on the spacing of multiple anchor blocks ( $B = 1$  for a single pile cap); and  $E$  is based on the depth of embedment of the pile cap, defined as:

$$E = 1 - \frac{H}{z + H} \quad \text{Equation 7.19}$$

where  $z$  is the depth of embedment measured from the ground surface to the top of the cap.

The value of  $K_{p\phi}$  determined in *PYCAP* is used in place of  $K_p$  in equation 7.11.  $K_a$  is determined using the Rankine earth pressure theory, which is approximately equivalent to the log spiral value because the active failure surface is very close to a plane.

The ultimate earth pressure force,  $P_{ult}$  (in units of force), can be determined by combining equations 7.12 and 7.18 as follows:

$$P_{ult} = RE_p b = R(P_{p\phi} + P_{pc} + P_{pq})b \quad \text{Equation 7.20}$$

where  $R$  is Ovesen's 3-D modifying factor (dimensionless),  $E_p$  is the two-dimensional or plane strain ultimate passive force (force per length units),  $b$  is the cap width or wall length (length units),  $P_{p\phi}$  is the earth pressure component due to soil weight and friction (force per length units),  $P_{pc}$  is the earth pressure component due to cohesion (force per length units),  $P_{pq}$  is the earth pressure component due to surcharge (force per length units).



These calculations are performed in the worksheet named *Log Spiral*, which is part of the workbook *PYCAP*. A copy of the output generated by *PYCAP* is shown in Figure 7.21. This output was generated in the worksheet titled *Summary*, which is used for specifying soil parameters and cap dimensions, and for displaying calculated results, including pile cap p-y values. The p-y values are formatted for copying and pasting directly into *LPILE Plus 3.0* or *GROUP* data files. The *GROUP* p-y values are not shown in Figure 7.21. They are the same as the *LPILE Plus 3.0* values, except the p and y columns are transposed.

Ovesen's tests were performed on compacted sand with friction angles ranging from  $\phi' = 32$  degrees to 41 degrees. The maximum difference in earth pressure coefficients ( $K_p - K_a$ ) was 5.7 in Ovesen's tests, and R did not exceed a value of about 2. As a conservative measure, a limit of 2.0 was placed on the value of R that is calculated in *PYCAP*.

Using *PYCAP*, the passive resistance of the bulkhead was calculated for natural soils at the site and for crusher run gravel backfill. Estimated values of the average soil parameters at the center of the bulkhead were used in the analyses. Even though the applied load was horizontal, a small amount of wall friction developed as soil within the passive failure wedge moved upward, due to the weight of the bulkhead as it moved with the soil. The magnitude of the resulting frictional force is limited to the weight of the bulkhead, which is about 10 kips. This force corresponds to a wall friction angle,  $\delta$ , of about 3.5 degrees for the natural soils, where the computed passive force was 160 kips, and  $\delta = 6.2$  degrees for the crusher run gravel, where the computed passive force was 92 kips.

Average parameters for the natural soils were obtained from Figure 5.8 and consisted of  $\phi = 37$  degrees,  $c = 970$  psf, and  $\gamma_m = 122$  pcf. For a wall friction angle of 3.5 degrees,  $K_{p\phi} = 4.65$ ,  $K_{pc} = 2.11$ ,  $K_{pq} = 0$ , and  $K_a = 0.25$ . Ovesen's R value was 1.43. Using these values, the calculated passive resistance,  $P_{ult}$ , was 160 kips for the bulkhead embedded in natural soil. As shown in Figure 7.20(a), the calculated ultimate resistance is in good agreement with the load test results. The *PYCAP* output sheet for this analysis shown in Figure 7.21

Parameters for the gravel backfill were determined using the data discussed in Chapter 5 and Appendix D. The measured  $\phi'$  values for this material are very high at low confining pressures.  $\phi'$  values as high as 53 degrees were determined at the center of the bulkhead, 1.75 feet below the ground surface. For these low confining pressures and high  $\phi'$  values, some degree of progressive failure seems inevitable as a result of the sharply peaked stress-strain curves, as can be seen in Appendix D. As an allowance for these anticipated progressive failure effects, it was decided to use  $\phi' = 50$  degrees for the compacted crusher run gravel.

For  $\phi' = 50$  degrees,  $c = 0$ ,  $\gamma_m = 134$  pcf, and a wall friction angle of 6.2 degrees (corresponding to the weight of the bulkhead):  $K_{p\phi} = 10.22$ ,  $K_{pc} = K_{pq} = 0$ , and  $K_a = 0.13$ . Ovesen's R value was 1.75. Using *PYCAP*, the calculated passive resistance,  $P_{ult}$ , was 92 kips for the bulkhead backfilled with crusher run gravel. As shown in Figure 7.20(b), the calculated ultimate resistance agrees quite well with the load test results, and is slightly conservative. The *PYCAP* output sheet for this analysis shown in Figure 7.22.

#### 7.4.4 Pile Cap Stiffness

The initial stiffness of the pile cap response corresponds to the initial slope of the load deflection curve. This value can be approximated using elasticity theory. The approach by Douglas and Davis (1964) for estimating the horizontal displacement of a vertical rectangle in a semi-infinite homogenous elastic mass was used in this study. The slope of the calculated load versus elastic displacement curve is called  $k_{max}$ , which is defined as the initial elastic stiffness with units of force divided by length.

The approach used to estimate  $k_{max}$  is somewhat approximate in that it is based on the average deflection of the corners of a flexible rectangular area. This approach slightly underestimates the deflection because the deflection at the corners of a flexible area is smaller than the deflection of a rigid area, which would be a closer approximation of the bulkhead or of a pile cap. However, the difference between the average corner deflection for a flexible rectangle and the deflection of a rigid rectangle is offset by the effect of shear on the sides and bottom of the cap, which are neglected in the elastic solution. Thus, the use of an elastic

solution based on a flexible loaded area is approximate, but it is believed to be sufficiently accurate for practical purposes.

The parameters needed to estimate  $k_{\max}$  include Poisson's ratio ( $\nu$ ), the initial tangent modulus of the soil ( $E_i$ ), and the dimensions and depth of the pile cap. A Poisson's ratio of 0.33 was assumed for the natural soils and a value of 0.30 was assumed for the granular backfill materials. The analysis is not sensitive to  $\nu$ , and reasonable estimates can be obtained from published correlations based on type of soil, such as those shown in Table 7.3.

Estimates of the initial tangent modulus,  $E_i$ , were obtained from laboratory triaxial stress-strain curves, as described in Chapter 5.  $E_i$  values for the natural soils and backfill materials are shown in Figure 5.3. When triaxial data is unavailable, values of  $E_i$  can be estimated using published correlations. Table 7.4 contains typical ranges of  $E_i$  for various types of soil, and Table 7.5 contains equations that can be used to calculate  $E_i$  based on in situ test results for coarse-grained soils, or undrained shear strengths ( $S_u$ ) for fine-grained soils.

The equations used to compute  $k_{\max}$  are given in Appendix H. These equations and associated influence factors are programmed in the worksheet called *Elasticity*, which is part of the *PYCAP* workbook. Figure 7.23 contains an example of the *Elasticity* worksheet that was used to compute  $k_{\max}$  for the natural soils.  $k_{\max}$  calculations are performed automatically when the *Summary* worksheet is activated. It is not necessary to enter the worksheet *Elasticity* to calculate pile cap p-y values, because the required soil parameters and cap dimensions are input in the *Summary* worksheet. The results, including the calculated  $k_{\max}$  value, are also displayed in the *Summary* worksheet.

Using this approach, values of  $k_{\max}$  were computed for the bulkhead embedded in natural soil ( $k_{\max} = 890$  kips/in) and for the bulkhead embedded in compacted gravel ( $k_{\max} = 760$  kips/in).

### 7.4.5 Pile Cap p-y Curves

Load-deflection curves for the pile caps and bulkhead were estimated using a hyperbolic equation of the same form as used by Duncan and Chang (1970) to represent stress-strain curves for soil. The hyperbolic load-deflection relationship is expressed as:

$$P = \frac{y}{\left( \frac{1}{k_{\max}} + R_f \frac{y}{P_{ult}} \right)} \quad \text{Equation 7.21}$$

where  $P$  is the load at any deflection  $y$ ,  $P_{ult}$  is the ultimate passive force (Section 7.4.2),  $k_{\max}$  is the initial stiffness (Section 7.4.4), and  $R_f$  is the failure ratio. The failure ratio is defined as the ratio between the actual failure force and the hyperbolic ultimate force, which is an asymptotic value that is approached as  $y$  approaches infinity. For soil stress-strain curves,  $R_f$  is always smaller than unity, and varies from 0.5 to 0.9 for most soils (Duncan et al. 1980). The value of  $R_f$  can be estimated by substituting  $P_{ult}$  for  $P$ , and by substituting the movement required to fully mobilize passive resistance,  $\Delta_{\max}$ , for  $y$ . Re-arranging the terms in Equation 7.21 results in the following expression for  $R_f$ :

$$R_f = 1 - \frac{P_{ult}}{\Delta_{\max} k_{\max}} \quad \text{Equation 7.22}$$

Calculations for  $R_f$  are performed in the *PYCAP* worksheet called *Hyperbola* using Equation 7.22. A copy of the *Hyperbola* worksheet is shown in Figure 7.24, for the bulkhead embedded in natural soil. Based on finite element and experimental studies by Clough and Duncan (1971),  $\Delta_{\max}$  was assumed to equal 4 % of the wall (or cap) height for the foundations in this study. As shown in Table 7.6, the value of  $R_f$  calculated using Equation 7.22 ranged from 0.67 to 0.97 for the pile caps and bulkhead at the Kentland Farms test facility, with an average value of 0.83.

Using Equation 7.21 with the values of  $P_{ult}$  and  $k_{\max}$  described in the previous sections, load versus deflection curves were computed for the bulkhead. Calculated results are

compared to observed responses for the bulkhead in natural soil (Figure 7.25a) and for the bulkhead backfilled with gravel (Figure 7.25b). As shown in the plots, the calculated results are in good agreement with the measured response curves over the full range of deflections.

Calculated load-deflection curves can readily be converted to p-y curves by dividing the load, P, by the cap height. This approach results in a constant value of resistance versus depth. A linear variation can also be assumed, but the difference between a constant value and a linear variation is negligible. Consequently, a constant value was assumed in the analyses conducted for this study.

All the components necessary for calculating pile cap p-y values have been described in the preceding pages. Soil parameters and cap dimensions are input in the *Summary* worksheet,  $P_{ult}$  is calculated in the *Log Spiral* worksheet, and  $k_{max}$  is calculated in the *Hyperbolic* worksheet. The hyperbolic equation is solved and p-y values are calculated in the *Hyperbolic* worksheet, and the output is displayed in the *Summary* worksheet.

Based on the approach described in this section, the computer spreadsheet named *PYCAP* was developed for calculating pile cap p-y curves. *PYCAP* includes the worksheets *Summary*, *Log Spiral*, *Hyperbola*, *Elasticity*, and *PYPILE*. (*PYPILE* is used to compute p-y curves for piles rather than caps, and works independently of the other sheets.) The cap p-y values are formatted for copying and pasting from the *Summary* worksheet directly into an *LPILE Plus3.0* or *GROUP* data input file. Computed results, such as the earth pressure coefficients (Rankine, Coulomb, and log spiral), Ovesen's 3-D factor (R),  $k_{max}$ , and  $P_{ult}$  are displayed in the *Summary* worksheet. An example of p-y curves calculated for the 36-in-deep cap in natural soil, compacted gravel, compacted sand, and loose sand are shown in Figure 7.26. The parameters used to develop the cap p-y curves are summarized in Table 7.7. A metric (or SI) units version of the *PYCAP* worksheet was also created, called *PYCAPSI*. *PYCAPSI* has all the same features as *PYCAP*, except SI units are used for the data and the computations.

The components necessary for creating soil models for pile groups and pile caps were described in the previous sections. These models, in the form of p-y curves, can be input into computer programs such as *LPILE Plus 3.0* (1997), *GROUP* (1996), or *Florida Pier* (1998) to compute the lateral response of the foundation system. *GROUP* and *Florida Pier* contain matrix structural analysis packages for computing reactions that are caused by interactions between the piles and pile cap. However, numerous problems were encountered when externally generated pile cap p-y curves were used with these programs, and it appears that they require further development and validation before they can be used with cap resistance.

For this reason, the simplified method described previously was developed for use in *LPILE Plus 3.0*. This method models the pile group as a “group-equivalent pile” (abbreviated GEP), with a rotationally restrained pile head boundary condition. The pile cap is modeled as an enlarged section with pile cap p-y values from *PYCAP*. This approach has been used to calculate the load-deflection responses of the foundations tested in this study. The results of the analyses are described in the following section.

## **7.5 COMPARISON OF MEASURED AND CALCULATED LOAD-DEFLECTION RESULTS**

### **7.5.1 Background**

Load-deflection response curves were calculated for the 3 pile groups described in Chapter 6. The response curves were developed for pile caps embedded in natural soil, and for pile caps backfilled with granular material (crusher run gravel or New Castle sand). The analyses were performed using the following procedure:

1. **Estimate soil parameters** (Chapter 5). Values are listed in Figure 5.8 for the natural soil and Table 5.9 for the granular backfill.
2. **Calculate single pile p-y curve** (Section 7.2). For c- $\phi$  soils, use Brinch-Hansen’s ultimate theory together with

the cubic parabola formulation for p-y curves. This is done in the spreadsheet *PYPILE*.

3. **Modify the single pile curve for group effects** (Section 7.3.2). The “group-equivalent pile” p-y curves are developed in *PYPILE* by multiplying the p-values by the term  $\sum_{i=1}^N f_{mi}$ . Values of  $f_m$  can be obtained from Figure 2.15. The “group-equivalent pile” p-y curves can be copied and pasted from *PYPILE* directly into *LPILE Plus 3.0*.
4. **Estimate the pile-head rotational restraint** (Section 7.3.4). Evaluate  $k_{m\theta}$  based on the axial capacities of the piles and their spacings in the group.
5. **Determine  $P_{ult}$  for the pile cap** (Section 7.4.3). Use the log spiral earth pressure theory in conjunction with Ovesen’s 3-D factor. Calculation are performed using *PYCAP*.
6. **Determine the initial cap stiffness,  $k_{max}$**  (Section 7.4.4). Use elasticity theory by Douglas and Davis (1964). Calculation are performed using *PYCAP*.
7. **Develop p-y curves for the pile cap** (Section 7.4.5). Use the hyperbolic formulation with  $P_{ult}$  and  $k_{max}$ . The cap p-y curves can be copied and pasted from the spreadsheet *PYCAP* directly into *LPILE Plus 3.0*.
8. **Perform the analysis** (use *LPILE Plus 3.0*). Analyze the load-deflection behavior of the “group-equivalent pile”

(GEP) to determine deflections, moments, and shear forces for the pile group.

Steps 2 through 7 are automated in the spreadsheet *PYCAP*. Step 8 can be performed using lateral analysis computer programs such as *LPILE Plus 3.0*, *GROUP*, or *Florida Pier*. The analyses conducted during this study were performed using the GEP approach with *LPILE Plus 3.0*. The input parameters that were used to calculate pile cap p-y values are summarized in Table 7.7.

The procedure outlined above was used to calculate load-deflection curves for the three pile groups at the Kentland Farms test facility. These curves were compared to the observed responses measured during the load tests, as described in the following sections.

### 7.5.2 Pile Caps Embedded in Natural Soil

Analyses were performed for the NE, NW, and SE pile groups with their caps embedded in natural soils. These caps were constructed by pouring concrete against undisturbed natural ground. Intimate, uniform contact was achieved between the cap and natural soil, thus, a relatively high value of wall friction ( $\delta = 0.8\phi$ ) was assumed. The values of soil parameters that were used in the analyses are shown in Table 7.7. Calculated load-deflection plots are compared to measured response curves in Figure 7.27. The  $k_{m\theta}$  values used in the analyses are shown in the plots. Details pertaining to these values are described in Section 7.3.4.

As shown in the plots in Figure 7.27, the calculated deflections for the three groups were larger than the measured responses and are therefore somewhat conservative. The discrepancy between calculated and measured deflections indicates that the strength of the natural soil in the top 3 feet may have been underestimated. This soil was highly desiccated, making it difficult to obtain undisturbed samples, even using block sampling techniques. Consequently, the triaxial strength tests may have resulted in estimates of shear strength that are smaller than the actual in situ strengths, because of sample disturbance.



The difference between observed and calculated results could also be affected by construction-related factors that are difficult to account for in any analytical method. For example, the method of cap construction can affect the rotational stiffness of the system. The caps were constructed at this test facility by pouring concrete against carefully excavated, undisturbed trench sidewalls. Consequently, cap rotations were probably less than the calculated values. This may explain, in part, the conservative nature of the calculated response curves shown in Figure 7.27.

### 7.5.3 Pile Caps Backfilled with Granular Backfill

Load tests were performed on the NE, NW, and SE pile caps backfilled with compacted crusher run gravel. The SE cap was also tested using uncompacted and compacted New Castle sand backfill. A comprehensive laboratory program was conducted to develop soil parameters for the backfill materials, based on measured field densities. These parameters are described in Chapter 5. The soil parameters used in the analyses are summarized in Table 7.7.

The backfill was placed and compacted around the caps after the natural soil was excavated and removed. During construction, backfill along the cap face was most likely not compacted as well as the backfill in the remainder of the excavation because of difficulties in compacting immediately adjacent to the vertical concrete face. For this reason, the wall friction angle,  $\delta$ , was assumed equal to  $0.5\phi$ .

Results calculated using *PYCAP* are shown in Table 7.6. Calculated load-deflection curves are compared to measured results in Figure 7.28 for the pile caps backfilled with gravel, and in Figure 7.29 for the SE cap backfilled with sand.

As shown in Figures 7.28 and 7.29, the agreement between measured and calculated results is quite good for the pile caps in granular backfill. For the most part, the differences between calculated and observed deflections were less than 30 %. In the case of the NW cap, the calculated load-deflection curve is virtually identical to the measured response (Figure

7.28b). The calculated results are conservative in all cases except the SE cap backfilled with New Castle sand. In this case, the calculated deflections are greater than the observed deflections at loads below 70 kips, and the calculated deflections are less than the observed deflection at loads above 70 kips (Figure 7.29).

## **7.6 COMPARISONS WITH RESULTS OF LOAD TESTS PERFORMED BY OTHERS**

### **7.6.1 Background**

Four studies were described in Chapter 2 in which the responses of pile groups with and without cap resistance were compared. The analytical approach described in the previous sections of this chapter was used to analyze foundation responses for the Zafir and Vanderpool (1998) load tests. The study by Beatty (1970) did not contain sufficient information regarding soil conditions and foundation size. The study by Rollins et al. (1997) was excluded because a rapid impact loading was used in their test. Kim and Sing's (1974) work was excluded because the pile cap was not embedded in their study, but was constructed on the ground surface and was not backfilled.

### **7.6.2 Zafir and Vanderpool (1998) Case Study**

The load tests reported by Zafir and Vanderpool (1998) were associated with a construction project at a new interstate interchange (I-15/US95) in Las Vegas, Nevada. The pile group consisted of four 2-foot-diameter drilled shafts, each 33 feet long, and spaced at 2D center to center. The cap consisted of an 11-foot-diameter reinforced cap, drilled to a depth of about 10 feet. Subsurface conditions at the site consisted of interlayers of sandy clay, silty clay, and clayey sand. Very stiff caliche deposits occurred at depths of 14 to 18.5 feet and 35 to 38 feet. Groundwater was reported at 13 feet below the ground surface. Soil parameters used to perform the analyses were obtained from Zafir and Vanderpool's (1998) report, and are shown in Table 7.8.

Group-equivalent pile (GEP) p-y curves were developed using the procedure described in Section 7.2 with the spreadsheet *PYPILE* and the soil parameters shown in Table 7.8. p-y curves for the stiff clay layers are shown in Figure 7.30(a), and p-y curves for the caliche layers are shown in Figure 7.30(b). Pile cap soil resistance was modeled using cap p-y curves calculated using *PYCAP*. The *PYCAP Summary* worksheet for this analysis is shown in Figure 7.31. The cap resistance versus deflection relationship (p-y curve) was developed for a calculated ultimate passive force,  $P_{ult}$ , of 1096 kips and an initial elastic stiffness,  $k_{max}$ , of 6700 kips/in. The cap p-y curve is shown in Figure 7.30(a).

Three boundary conditions were used in the analyses: fixed-head (zero rotation), free-head (zero moment), and rotationally restrained ( $k_{m\theta}$  value) pile head. As shown in Figure 7.32(a), the calculated response based on a fixed-head boundary condition underestimated the observed deflection by approximately 90 %, at a load of 1500 kips. In contrast, the calculated deflection based on a free-head boundary condition was over-conservative by over 300 %.

Excellent agreement between calculated and observed load-deflection response was obtained by assuming a rotationally restrained pile-head boundary condition, as shown in Figure 7.32(b). Pile-head rotational stiffness was estimated using  $k_{m\theta}$  calculated from Equation 7.11. A value of  $k_{m\theta} = 1.93 \times 10^{10}$  in-lb/rad was determined based on an estimated skin friction,  $Q_s$ , of 262 tons per pile, mobilized at a vertical movement of 0.1 inches. The ultimate bending moment resisting cap rotation,  $M_{ult}$ , was estimated to be 4200 ft-kips. The measured response was well predicted by the analytical approach. The plots in Figure 7.32 demonstrate the importance of pile-head boundary conditions in the analyses.

## 7.7 SUMMARY OF DESIGN METHOD

The preceding sections describe the details of the approach developed for analyzing laterally loaded pile groups. The approach can be summarized in a step-by-step design method, as described below.

### **Step 1. Estimate soil parameters.**

The soil parameters required for the analyses are:  $\phi$ ,  $c$ ,  $\delta$ ,  $\alpha$ ,  $\nu$ ,  $E_i$ , and  $\gamma_m$ .

Undrained (total stress) values of  $\phi$  and  $c$  should be used for fine-grained soils. These values can be obtained from UU triaxial tests or estimated using correlations with in situ test results, such as those obtained from SPT, CPT or vane shear tests. Drained (effective stress) values should be used for cohesionless soils. Values of  $\phi'$  can be estimated using correlations with in situ test results, such as SPT or CPT, or by performing CD triaxial tests.  $c'$  is usually assumed equal to zero for effective stress analyses. Figure 7.33 or other correlations can be used to approximate  $\phi'$  if the soil type and relative density, or dry unit weight are known..

Wall friction,  $\delta$ , and the adhesion factor,  $\alpha$ , can be estimated based on type of soil and type of interface material using Table 7.1 and Table 7.2, respectively.

Poisson's ratio can be estimated from correlations based on type of soil (Table 7.3).

Values of initial tangent modulus,  $E_i$ , can be obtained using stress-strain results from triaxial tests or estimated based on type of soil (Table 7.4) or based on SPT  $N$  values, CPT  $q_c$  values, or  $S_u$  values (Table 7.5).

Soil unit weight,  $\gamma_m$ , can be measured in the lab or estimated from correlations based on type of soil and relative density or consistency (see Figure 7.33).

### **Step 2. Calculate single pile p-y curves.**

For  $c$ - $\phi$  soils, use Brinch-Hansen's ultimate theory together with the cubic parabola formulation to develop p-y curves. This is done in the spreadsheet *PYPILE*, which is a separate worksheet in *PYCAP*. *PYPILE* can also be used for  $c = 0$  or for  $\phi = 0$  soils, or the "default" p-y formulations in *LPILE Plus 3.0* can be used. (Step 2 is discussed in Section 7.2.)

### **Step 3. Modify the single pile p-y curves for group effects.**

The group-equivalent pile (GEP) p-y curves are developed in *PYPILE* by multiplying the p-values by the term  $\sum_{i=1}^N f_{mi}$ . Values of  $f_m$  can be obtained from Figure 2.15. The GEP p-y curves can be copied and pasted from *PYPILE* directly into *LPILE Plus 3.0*. (Step 3 is discussed in Section 7.3.2.)

**Step 4. Estimate the pile-head rotational restraint,  $k_{m\theta}$ .**

The rotational restraint is a function of the side resistance of the piles, the deflection required to mobilize skin friction, and the corresponding moment on the pile cap.  $k_{m\theta}$  is determined using Equation 7.11. The pile skin friction capacity,  $Q_{si}$ , can be calculated using rational approaches such as the  $\alpha$ -method (Tomlinson 1987),  $\beta$ -method (Esrig and Kirby 1979) and the  $\lambda$ -method (Vijayvergiya and Focht 1972). In situ approaches are also available, such as the SPT method developed by Meyerhof (1976) or the CPT method by Nottingham and Schmertmann (1975). The computer program *SPILE* (1993), available from the FHWA, is useful for computing values of  $Q_{si}$ . (Step 4 is discussed in Section 7.3.4.)

**Step 5. Determine  $P_{ult}$  for the pile cap.**

The ultimate lateral load resistance of the pile cap is determined using the log spiral earth pressure theory and Ovesen's 3-D correction factor. Calculations for  $P_{ult}$  are performed using the *EXCEL* workbook named *PYCAP*. *PYCAP* contains the worksheets *Summary*, *Log Spiral*, *Hyperbola*, *Elasticity*, and *PYPILE*. Soil parameters and cap dimensions are specified in worksheet *Summary*.  $P_{ult}$  calculations are performed in worksheet *Log Spiral*. The results are displayed in the *Summary* worksheet. (Step 5 is discussed in Section 7.4.3, and the log spiral theory is described in Appendix F.)

**Step 6. Determine the cap stiffness,  $k_{max}$ .**

The initial stiffness of the pile cap is approximated using elasticity theory.  $k_{max}$  is calculated using the worksheet *Elasticity*, which is part of the *PYCAP* workbook. Soil parameters needed for  $k_{max}$  calculations ( $E_i$  and  $\nu$ ) and cap dimensions are specified in the

*Summary* worksheet. Calculations for  $k_{\max}$  are performed automatically when worksheet *Summary* is activated. (Step 5 is discussed in Section 7.4.4, and the elastic equations used in the *Elasticity* worksheet are described in Appendix H.)

### Step 7. Develop p-y curves for the pile cap

Pile cap p-y values are developed using the hyperbolic formulation with  $P_{\text{ult}}$  and  $k_{\max}$ . Parameters are specified in the *Summary* worksheet, calculations are performed in the *Hyperbolic* worksheet, and the results, p-y values, are displayed in the *Summary* worksheet. The cap p-y values can be copied and pasted from the *Summary* worksheet directly into *LPILE Plus 3.0*. (Step 7 is discussed in Section 7.4.5.)

### Step 8. Perform the analysis.

The lateral response of the pile group is analyzed using *LPILE Plus 3.0*. p-y curves developed for the GEP (Step 3) and for the pile cap (Step 7) are used to represent the soil resistance. The pile group is modeled as a single pile with EI equal to the sum of the EI values for all of the piles in the group. The cap is modeled by enlarging the top portion of the GEP based on the cap dimensions. A rotationally restrained pile-head boundary condition is specified using the value of  $k_{m\theta}$  calculated during Step 6.

### Step 9. Evaluate the results.

The calculated displacements of the GEP correspond to the displacements of the actual pile group. However, to determine the shear forces (V) and moments (M) of the piles within the group, the shear forces and moments of the GEP are factored based on the pile's row multiplier,  $f_{mi}$  and the EI value for each pile. This is done as follows:

$$V_i = V_{\text{gep}} \left( \frac{f_{mi} EI_i}{\sum_{i=1}^N (f_{mi} EI_i)} \right) (f_{mc}) \quad \text{Equation 7.22}$$

where  $V_i$  is the shear in pile  $i$ ,  $V_{gep}$  is the total shear for the GEP,  $N$  is the number of piles,  $f_{mi}$  is the  $p$ -multiplier for the row containing the pile of interest ( $f_m$  is obtained from Figure 2.15),  $EI_i$  is the flexural stiffness of pile  $i$ , and  $f_{mc}$  is a multiplier for corner piles. Corner piles in the leading row carry a larger share of the load than non-corner piles. Consequently, the corner piles will have larger shear forces and bending moments. The multiplier,  $f_{mc}$ , is an adjustment factor to account for larger values of  $V_i$  and  $M_i$  in the corner piles. Based on 1g model tests by Franke (1988), the following values are recommended for  $f_{mc}$ :

Pile spacing measured normal to direction of load	$f_{mc}$ factor
non-corner piles	1.0
$\geq 3D$	1.0
2D	1.2
1D	1.6

The moment in pile  $i$  is computed as:

$$M_i = M_{gep} \left( \frac{f_{mi} EI_i}{\sum_{i=1}^N (f_{mi} EI_i)} \right) (f_{mc}) \tag{Equation 7.23}$$

where  $M_i$  is the moment in pile  $i$  and  $M_{gep}$  is the moment computed for the GEP.

Equations 7.22 and 7.23 can be simplified using a distribution coefficient called  $D_i$ , which is defined as:

$$D_i = \left( \frac{f_{mi} EI_i}{\sum_{i=1}^N (f_{mi} EI_i)} \right) \quad \text{Equation 7.24}$$

Thus, the shear and moment in pile  $i$  are determined using the following equations:

$$V_i = V_{gep} D_i f_{mc} \quad \text{Equation 7.25a}$$

$$M_i = M_{gep} D_i f_{mc} \quad \text{Equation 7.25b}$$

## 7.8 SUMMARY

An analytical approach was developed for evaluating the lateral response of pile groups with embedded caps. The approach involves creating p-y curves for single piles, pile groups, and pile caps using the computer spreadsheets *PYPILE* and *PYCAP*.

Single pile p-y curves are developed using Brinch Hansen's (1961) ultimate load theory for soils that possess both cohesion and friction. The approach is programmed in *PYPILE*, which can be used to calculate p-y curves for piles of any size, with soil properties that are constant or that vary with depth.

“Group-equivalent pile” (abbreviated GEP) p-y curves are obtained by multiplying the “p” values of the single pile p-y curves by a modification factor that accounts for reduced capacities caused by group interaction effects, and summing the modified p-values for all the piles in the group. The p-multiplier curves developed in Chapter 2 are used for this purpose. The pile group is modeled in the computer program *LPILE Plus 3.0* using these GEP p-y curves. The flexural resistance of the GEP pile is equal to the sum of the flexural resistances of all the piles in the group.

A rotationally restrained pile-head boundary condition is used in the analysis. The rotational stiffness is estimated from the axial skin friction of the piles, the deflection required to mobilize skin friction, and the corresponding moment on the pile cap.



Pile cap resistance is included in the analysis using cap p-y curves. A method of calculating cap p-y curves was developed during this study, and has been programmed in the spreadsheet *PYCAP*. The approach models the passive earth pressures developed in front of the cap. These passive pressures are represented by p-y curves developed from a modified hyperbolic formulation, which is defined by the ultimate passive force and the initial elastic stiffness of the embedded pile cap. The ultimate passive force is determined using the log spiral earth pressure theory in conjunction with Ovesen's (1964) three-dimensional correction factors.

The GEP approach for creating pile group and pile cap p-y curves provides a means of modeling the soil in a way that is compatible with established approaches for analyzing laterally loaded single piles. *LPILE Plus 3.0* was used to calculate load-deflection curves for the pile groups tested in this study, and for a load test described in the literature. Comparisons between measured and calculated load-deflection responses indicate that the analytical approach developed in this study is conservative, reasonably accurate, and suitable for design purposes. Deviations between calculated and measured load-deflection values fall well within the practical range that could be expected for analyses of the lateral response of pile groups. This approach represents a significant improvement over current design practices, which often completely ignore the cap resistance.

The author believes it would be difficult to obtain more accurate estimates of pile group behavior, even with more complex analytical methods, because of the inevitable uncertainties and variations in soil conditions, unknown or uncontrollable construction factors, and the complex structural and material interactions that occur between the piles, pile cap, and soil.

Table 7.1. Friction angles,  $\delta$ , between various soils and foundation materials (After NAVFAC, 1982.)

<b>Interface material</b>	<b>Friction angle, <math>\delta</math> (degrees)</b>
<i>Mass concrete or masonry on the following soils:</i>	
clean sound rock	35
clean gravel, gravel-sand mixtures, coarse sand	39 to 31
clean fine to medium sand, silty medium to coarse sand, silty or clayey gravel	24 to 29
fine sandy silt, nonplastic silt	17 to 19
very stiff and hard residual or preconsolidated clay	22 to 26
medium stiff and stiff clay and silty sand	17 to 19
<i>Formed concrete or concrete sheet piling against the following soils:</i>	
clean gravel, gravel-sand mixtures, well-graded rock fill with spalls	22 to 26
clean sand, silty sand-gravel mixture, single size hard rock fill	17 to 22
silty sand, gravel or sand mixed with silt or clay	17
fine sandy silt, nonplastic silt	14

Table 7.2. Typical values of the soil adhesion factor,  $\alpha$ . (After NAVFAC, 1982.)

<b>Interface soil</b>	<b>Soil cohesion c (psf)</b>	<b>Adhesion factor a</b>
Very soft cohesive soil	0 to 250	1.0
Soft cohesive soil	250 to 500	1.0
Medium stiff cohesive soil	500 to 1000	1.0 to 0.75
Stiff cohesive soil	1000 to 2000	0.75 to 0.5
Very stiff cohesive soil	2000 to 4000	0.5 to 0.3

Table 7.3. Typical range of values for Poisson's ratio. (After Bowles, 1982.)

Type of soil	Poisson's ratio, $\nu$
Sand (dense)	0.2 to 0.4
coarse-grained (void ratio = 0.4 to 0.7)	0.15
fine-grained (void ratio = 0.4 to 0.7)	0.25
Silt	0.3 to 0.35
Loess	0.1 to 0.3
Sandy Clay	0.2 to 0.3
Clay	
saturated	0.4 to 0.5
unsaturated	0.1 to 0.3
Rock (depends on rock type)	0.1 to 0.4
Concrete	0.15
Ice	0.36

Table 7.4. Typical range of  $E_i$  values for various soil types. (After Bowles, 1982.)

Type of soil	$E_i$	
	(ksf)	(Mpa)
Sand silty loose dense	150 to 450 200 to 500 1000 to 1700	7 to 21 10 to 24 48 to 81
Sand and Gravel loose dense	1000 to 3000 2000 to 4000	48 to 144 96 to 192
Glacial Till loose dense very dense	200 to 3200 3000 to 15,000 10,000 to 30,000	10 to 153 144 to 720 478 to 1440
Silt	40 to 400	2 to 20
Loess	300 to 1200	14 to 57
Clay very soft soft medium hard sandy	50 to 250 100 to 500 300 to 1000 1000 to 2000 500 to 5000	2 to 15 5 to 25 15 to 50 50 to 100 25 to 250
Shale	3000 to 300,000	144 to 14,400
Silt	40 to 400	2 to 20

Table 7.5. Equations for  $E_i$  by several test methods. (After Bowles, 1982.)

Type of soil	SPT ( $E_i$ in units of ksf)	CPT ( $E_i$ in units of $q_c$ )	Undrained shear strength, $S_u$ ( $E_i$ in units of $S_u$ )
sand	$E_i = 100(N + 15)$ $E_i = 360 + 15N$ $E_i = (300 \text{ to } 440)\ln(N)$	$E_i = (2 \text{ to } 4)q_c$ $E_i = 2(1 + D_r^2)q_c$	
clayey sand	$E_i = 6.4(N + 15)$	$E_i = (3 \text{ to } 6)q_c$	
silty sand	$E_i = 6(N + 6)$	$E_i = (1 \text{ to } 2)q_c$	
gravelly sand	$E_i = 24(N + 6)$		
soft clay		$E_i = (6 \text{ to } 8)q_c$	
clay, $PI > 30$ or organic			$E_i = (100 \text{ to } 500)S_u$
clay, $PI < 30$ or stiff			$E_i = (500 \text{ to } 1500)S_u$
clay, $1 < OCR < 2$			$E_i = (800 \text{ to } 1200)S_u$
clay, $OCR > 2$			$E_i = (1500 \text{ to } 2000)S_u$

Notes:

1. Multiply ksf by 47.88 to obtain  $E_i$  in units of kPa.
2.  $q_c$  = cone penetrometer (CPT) tip resistance
3.  $D_r$  = relative density
4.  $PI$  = plasticity index =  $LL - PL$
5.  $OCR$  = overconsolidation ratio
6.  $S_u$  = undrained shear strength

Table 7.6. Summary of results from *PYCAP* analyses.

<b>Foundation</b>	<b>Soil around pile cap</b>	<b>Hyperbolic <math>R_f</math></b>	<b><math>K_{pf}</math></b>	<b><math>K_{pc}</math></b>	<b><math>K_{pq}</math></b>	<b>3-D factor R</b>	<b><math>k_{max}</math> (kips/inch)</b>	<b><math>P_{ult}</math> (kips)</b>
Bulkhead	natural soil	0.89	4.65	2.11	0	1.43	891	160
Bulkhead	gravel backfill	0.93	10.22	0	0	1.75	756	92
NE 36-inch cap	natural soil	0.70	12.51	4.42	0	1.91	733	322
NE 36-inch cap	gravel backfill	0.82	26.46	0	0	2.00	623	160
NW 18-inch cap	natural soil	0.67	12.71	4.41	7.66	1.87	619	148
NW 18-inch cap	gravel backfill	0.89	26.46	0	0	1.80	462	36
SE 36-inch cap	natural soil	0.70	12.51	4.42	0	1.91	733	322
SE 36-inch cap	gravel backfill	0.82	26.46	0	0	2.00	623	160
SE 36-inch cap	compacted sand	0.95	16.92	0	0	2.00	1147	79
SE 36-inch cap	loose sand	0.97	7.58	0	0	1.65	590	26

Table 7.7. Parameters used to calculate pile cap p-y curves.

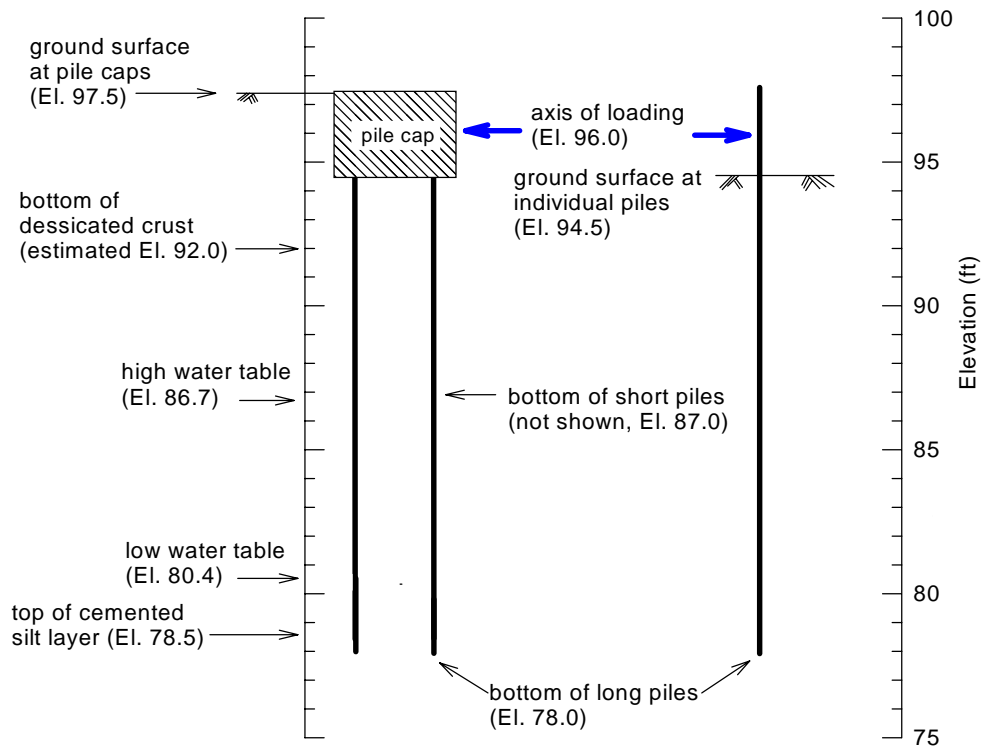
Parameter	Natural soil	Compacted gravel	Compacted sand	Loose sand
$\phi$ (deg)	38	50	46	37
$\delta$ (deg)	30	25	23	18.5
c (psi)	7	0	0	0
$\alpha$	1	0	0	0
$\gamma_m$ (pcf)	123	134	104	92
$E_i$ (ksf)	890	760	1400	720
$\nu$	0.33	0.30	0.30	0.30



Table 7.8. Soil parameters used in the Zafir and Vanderpool case study.

Depth (ft)	Soil type	$g$ (pcf)	$k$ (pci)	$S_u$ (psf)	$e_{50}$
0.0 to 10.0	stiff clay	125	1,000	3,000	0.0050
10.0 to 14.0	stiff clay	120	600	1,300	0.0066
14.0 to 18.5	caliche	140	> 2,000	566,000	0.0010
18.5 to 35.0	stiff clay	125	2,000	6,000	0.0040
35.0 to 38.0	caliche	140	> 2,000	560,000	0.0005

Note: The parameters shown in this table were obtained from Zafir and Vanderpool's (1998) report.



Elevation (ft)	Moist unit weight, $\gamma_m$ (pcf)	Cohesion total stress, $c$ (psi)	Friction angle total stress, $\phi$ (degrees)	Strain at 50% $\sigma_{dmax}$ $\epsilon_{50}$
97.5	123.7	7.0	38.0	0.01
96.0	122.8	7.0	38.0	0.01
94.5	121.9	7.0	38.0	0.01
92.0	120.4	6.0	35.0	0.025
88.0	118.0	5.0	28.0	0.025
87.0	117.4	4.3	27.0	0.025
80.0	112.4	4.0	25.0	0.025
79.0	112.3	0.0	45.0	0.002
78.0	112.0	0.0	45.0	0.002

Figure 7.1. Soil parameters for calculating p-y curves.

## Soil Resistance vs. Deflection (p-y) Calculation Sheet for Single Pile

Date: 8/9/99  
 Project: Single pile natural soil  
 Engineer: rlm

Input (red lettering)								Calculated Values		
Brinch-Hansen (1961)								Brinch-Hansen (1961)		
Slope Angle (deg), $i =$	0									
Depth, x (ft)	D (ft)	$\gamma$ (pcf)	c (psf)	$\phi$ (deg)	$\epsilon_{50}$	A	M	$K_c$	$K_q$	$p_{ult}$ (lb/in)
0.00	0.83	121.9	1008	38	0.01	2.5	0.85	10.57	9.07	626
2.50	0.83	120.4	864	35	0.01	2.5	0.85	42.13	11.87	2,350
6.50	0.83	118	720	28	0.025	2.5	0.85	34.93	8.87	1,879
14.50	0.83	50	576	25	0.025	2	0.85	31.84	8.01	1,420
15.50	0.83	50	0	45	0.002	2.5	0.85	344.75	72.66	3,311
16.50	0.83	50	0	45	0.02	2.5	0.85	356.23	75.21	3,648
0.00	0	0	0	0	0.02	2.5	0.85	#DIV/0!	0.00	#DIV/0!
0.00	0	0	0	0	0.002	2.5	0.85	#DIV/0!	0.00	#DIV/0!
0.0	0	0	0	0	0.002	2.5	0.85	#DIV/0!	0.00	#DIV/0!

Definition of Parameters			
x =	depth below ground surface (ft)	K <sub>c</sub> =	cohesive resistance coefficient
D =	shaft diameter (ft)	K <sub>q</sub> =	friction resistance coefficient
$\gamma$ =	soil unit weight (pcf)	p <sub>ult</sub> =	ultimate soil resistance (in-lb/in <sup>2</sup> )
c =	soil cohesion (psf)	p =	soil resistance (in-lb/in <sup>2</sup> )
$\phi$ =	soil friction angle (deg)	y =	shaft deflection
$\epsilon_{50}$ =	strain required to mobilize 50% of the soil strength		
A =	p-y curve shape factor		
M =	ultimate lateral load reduction factor		

The p-y values calculated below (shaded cells) are formatted for cutting and pasting directly into LPILE plus 3.0 input files.

Brinch-Hansen p-y values			
Depth (in)	p/p <sub>ult</sub>	y (in)	p (lb/in)
Depth (in) =====>	0.0	0.000	0.0
	0.1	0.002	62.7
	0.2	0.016	125.3
	0.3	0.054	187.9
	0.4	0.127	250.5
	0.5	0.249	313.1
	0.7	0.683	438.2
	0.9	1.452	563.2
	1.0	1.992	625.7
	1.0	24.900	626.1
Depth (in) =====>	30.0	0.000	0.0
	0.1	0.002	235.4
	0.2	0.016	470.5
	0.3	0.054	705.4
	0.4	0.127	940.3
	0.5	0.249	1175.1
	0.7	0.683	1644.5
	0.9	1.452	2113.9
	1.0	1.992	2348.5
	1.0	24.900	2350.1
Depth (in) =====>	78.0	0.000	0.0

Figure 7.2. Example of p-y calculations using spreadsheet PYPILE (1 of 2).

<b>Depth (in) =====&gt;</b>	<b>78.0</b>	<b>10</b>	<b>&lt;=====</b>	<b>No. of data points</b>
0.0	<b>0.000</b>	<b>0.0</b>		<b>defining p-y curve</b>
0.1	<b>0.005</b>	<b>188.2</b>		
0.2	<b>0.040</b>	<b>376.0</b>		
0.3	<b>0.134</b>	<b>563.8</b>		
0.4	<b>0.319</b>	<b>751.6</b>		
0.5	<b>0.623</b>	<b>939.3</b>		
0.7	<b>1.708</b>	<b>1314.5</b>		
0.9	<b>3.630</b>	<b>1689.7</b>		
1.0	<b>4.980</b>	<b>1877.2</b>		
1.0	<b>62.250</b>	<b>1878.5</b>		
<b>Depth (in) =====&gt;</b>	<b>174.0</b>	<b>10</b>	<b>&lt;=====</b>	<b>No. of data points</b>
0.0	<b>0.000</b>	<b>0.0</b>		<b>defining p-y curve</b>
0.1	<b>0.004</b>	<b>142.2</b>		
0.2	<b>0.032</b>	<b>284.2</b>		
0.3	<b>0.108</b>	<b>426.1</b>		
0.4	<b>0.255</b>	<b>568.0</b>		
0.5	<b>0.498</b>	<b>709.8</b>		
0.7	<b>1.367</b>	<b>993.4</b>		
0.9	<b>2.904</b>	<b>1276.9</b>		
1.0	<b>3.984</b>	<b>1418.7</b>		
1.0	<b>49.800</b>	<b>1419.6</b>		
<b>Depth (in) =====&gt;</b>	<b>186.0</b>	<b>10</b>	<b>&lt;=====</b>	<b>No. of data points</b>
0.0	<b>0.000</b>	<b>0.0</b>		<b>defining p-y curve</b>
0.1	<b>0.000</b>	<b>331.6</b>		
0.2	<b>0.003</b>	<b>662.8</b>		
0.3	<b>0.011</b>	<b>993.8</b>		
0.4	<b>0.025</b>	<b>1324.6</b>		
0.5	<b>0.050</b>	<b>1655.4</b>		
0.7	<b>0.137</b>	<b>2316.8</b>		
0.9	<b>0.290</b>	<b>2978.0</b>		
1.0	<b>0.398</b>	<b>3308.5</b>		
1.0	<b>4.980</b>	<b>3310.8</b>		
<b>Depth (in) =====&gt;</b>	<b>198.0</b>	<b>10</b>	<b>&lt;=====</b>	<b>No. of data points</b>
0.0	<b>0.000</b>	<b>0.0</b>		<b>defining p-y curve</b>
0.1	<b>0.004</b>	<b>365.4</b>		
0.2	<b>0.032</b>	<b>730.2</b>		
0.3	<b>0.108</b>	<b>1094.9</b>		
0.4	<b>0.255</b>	<b>1459.4</b>		
0.5	<b>0.498</b>	<b>1823.9</b>		
0.7	<b>1.367</b>	<b>2552.6</b>		
0.9	<b>2.904</b>	<b>3281.1</b>		
1.0	<b>3.984</b>	<b>3645.3</b>		
1.0	<b>49.800</b>	<b>3647.8</b>		

Figure 7.2-Continued. Example of p-y calculations using spreadsheet *PYPILE* (2 of 2).

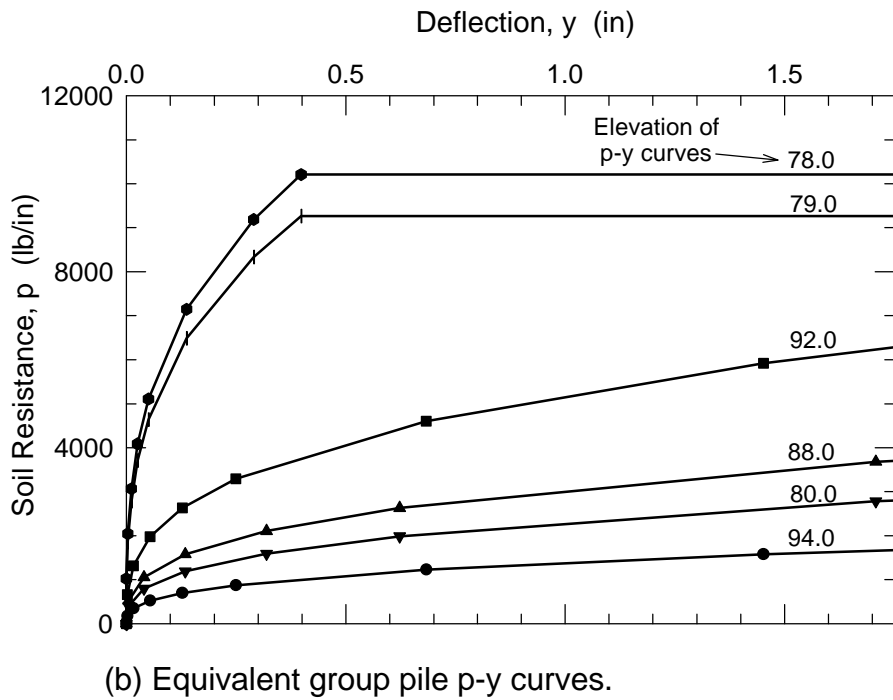
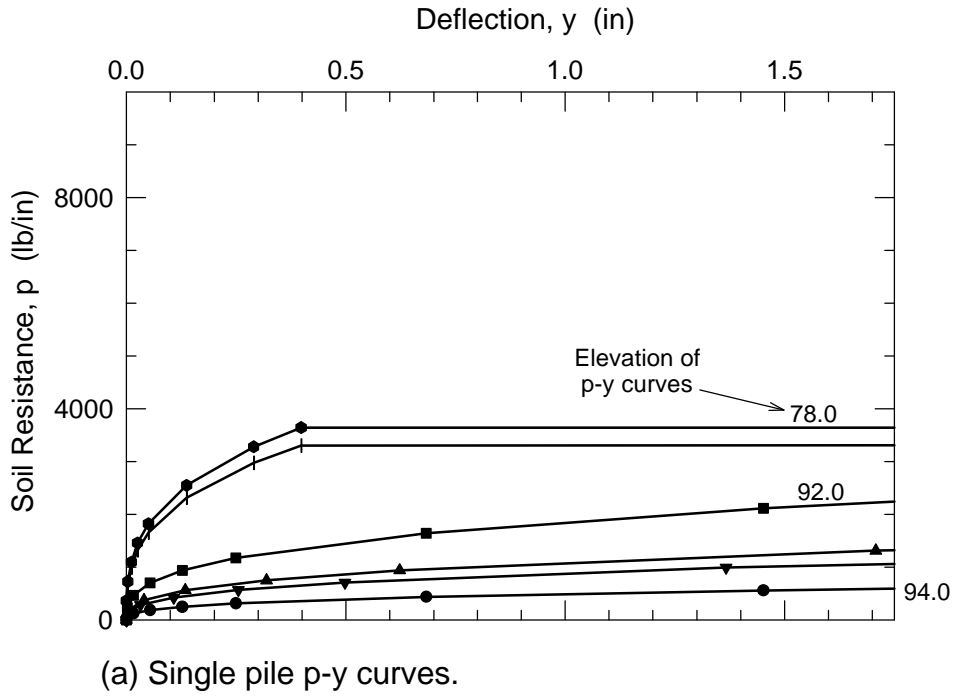


Figure 7.3. p-y curves for LPILE Plus 3.0 analyses.

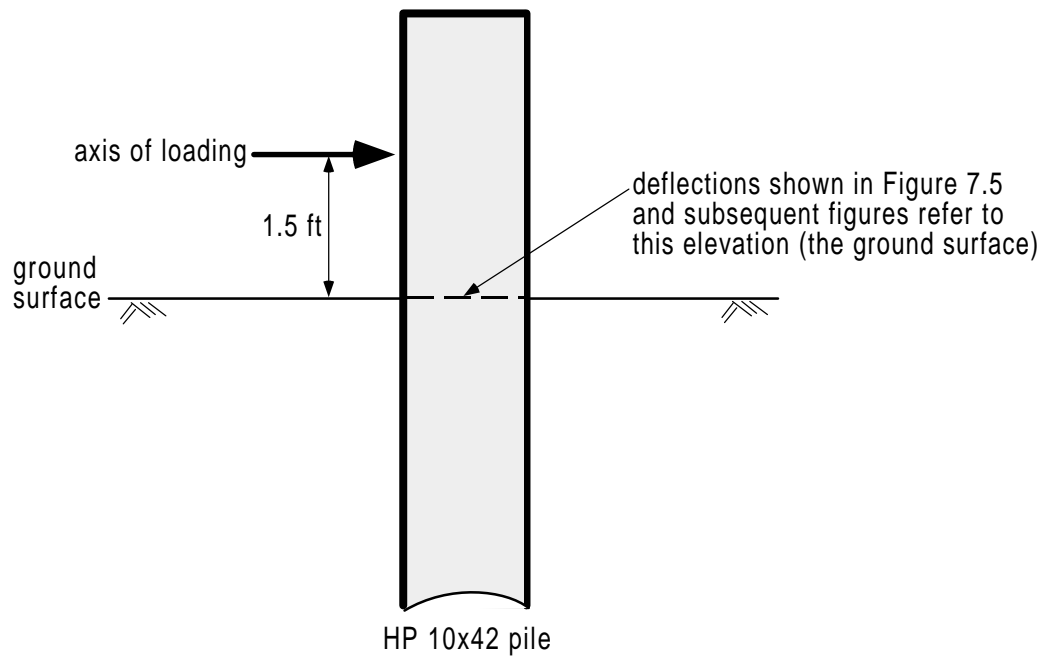
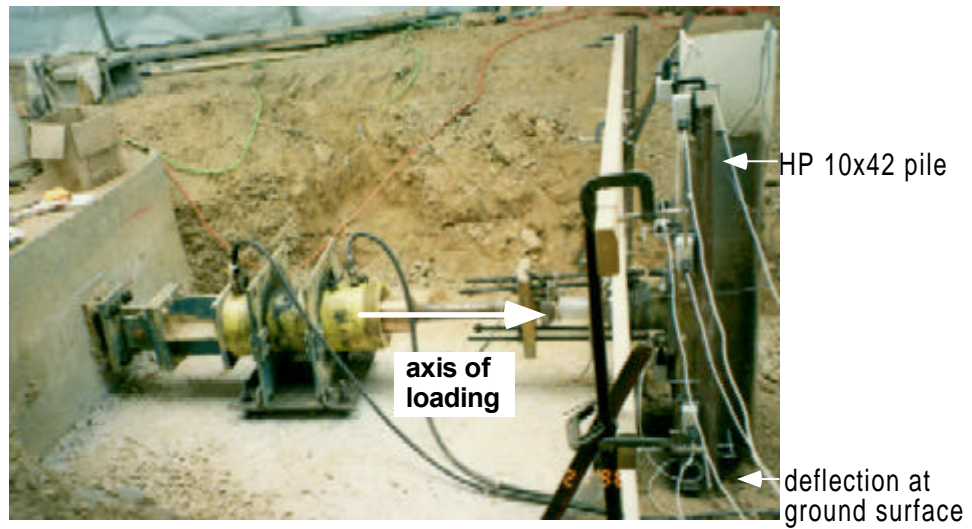
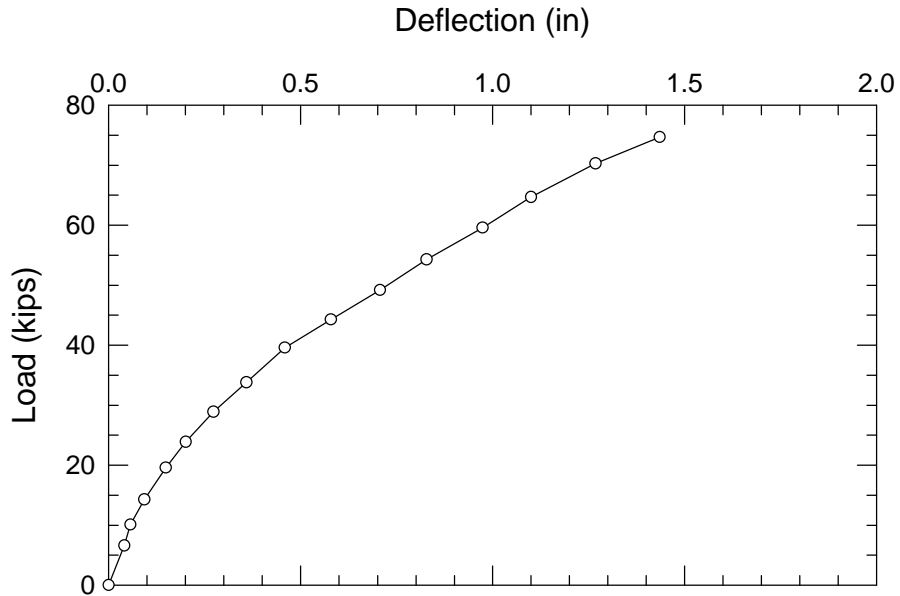
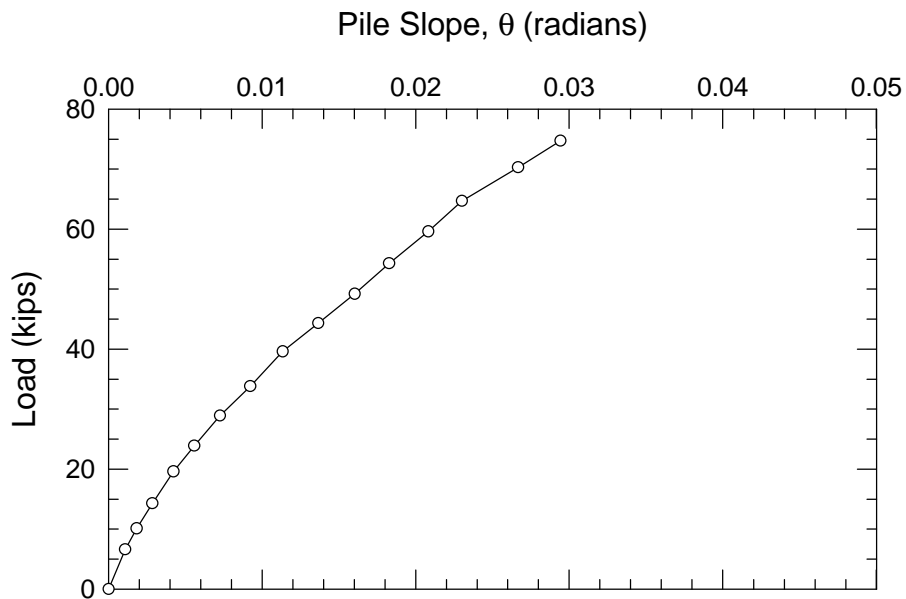


Figure 7.4. Single pile load testing arrangement.

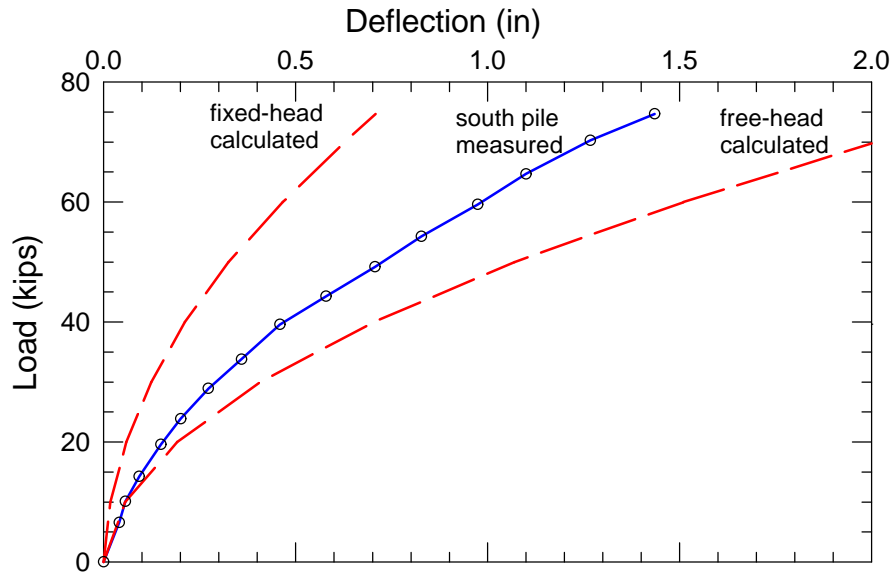


(a) Measured load versus deflection response.

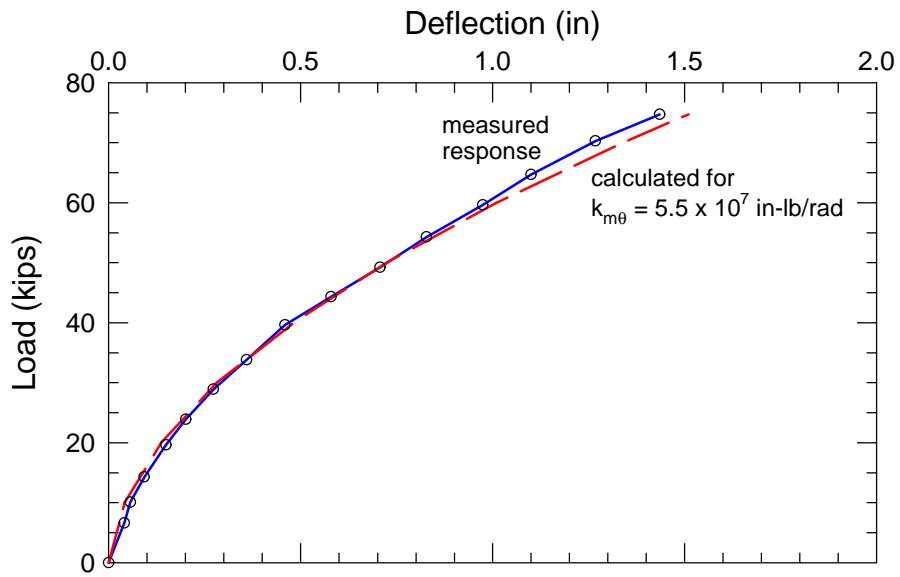


(b) Measured load versus pile-head rotation.

Figure 7.5. Measured response of south pile in natural soil.



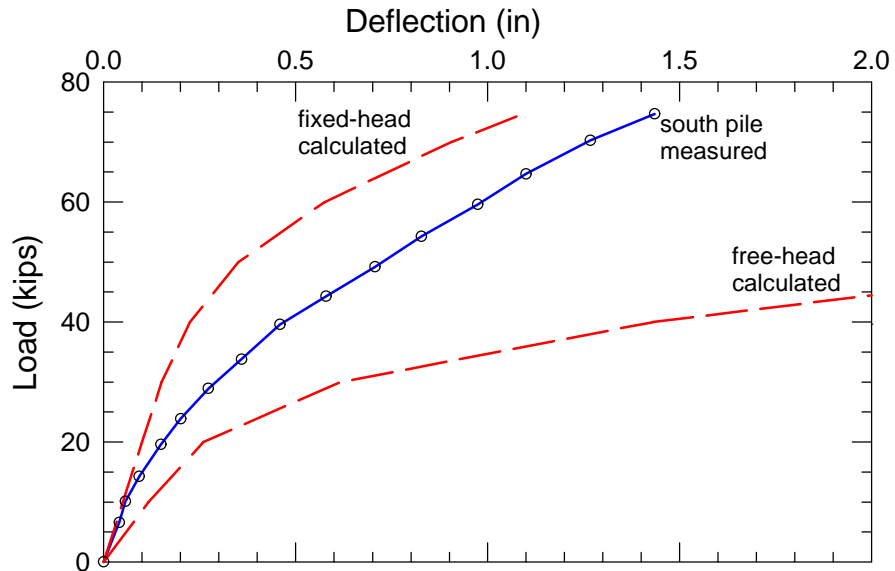
(a) Fixed-head and free-head boundary conditions.



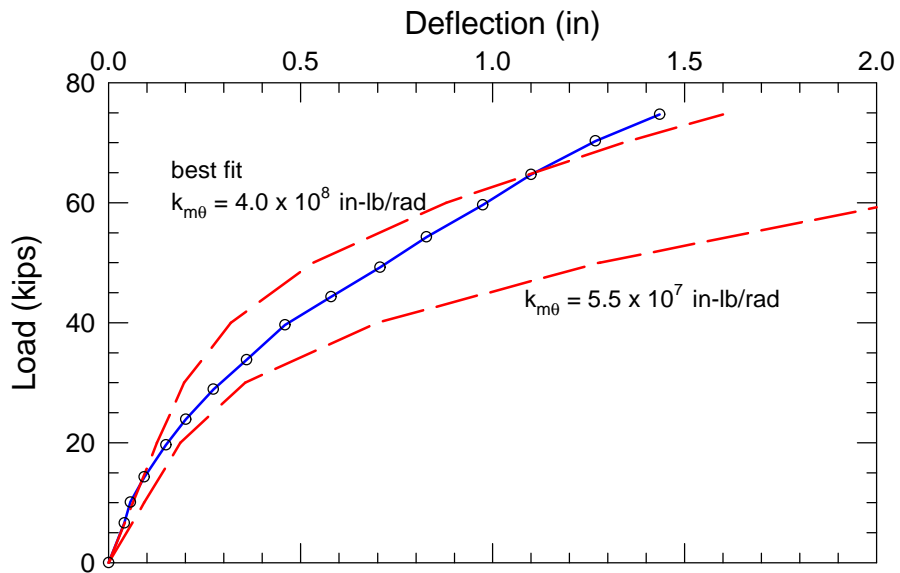
(b) Rotationally restrained pile-head boundary condition, best fit  $k_{m\theta}$  value.

Figure 7.6. Calculated load-deflection curves for the south pile in natural soil, using p-y curves from *PYSHEET*.



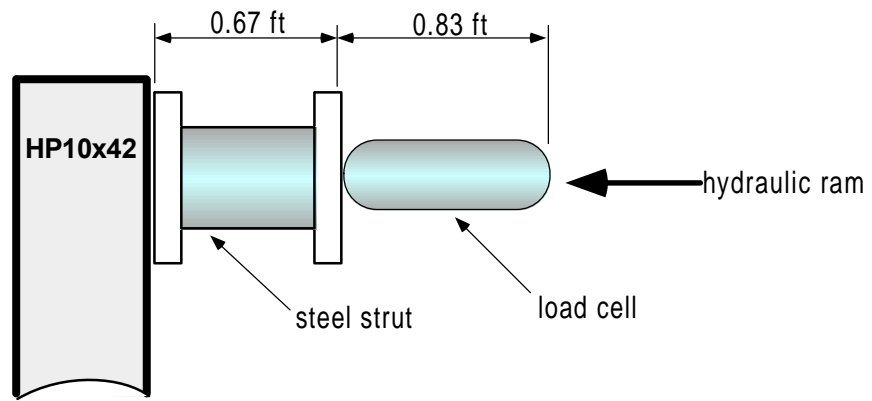


(a) Fixed-head and free-head boundary conditions.

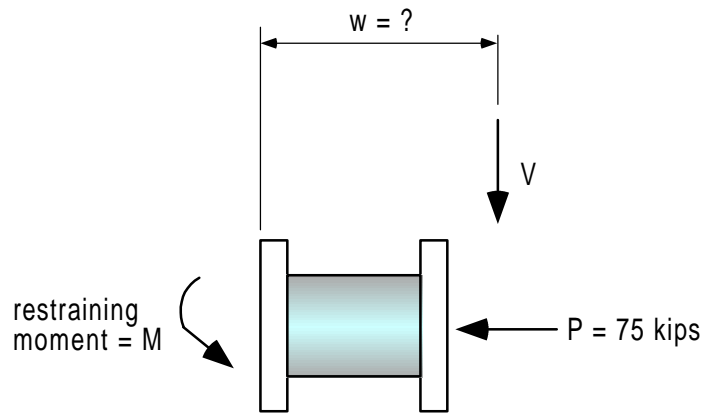


(b) Rotationally restrained pile-head boundary condition.

Figure 7.7. Calculated load-deflection curves for the south pile in natural soil, using *LPILE Plus 3.0* default p-y curves.

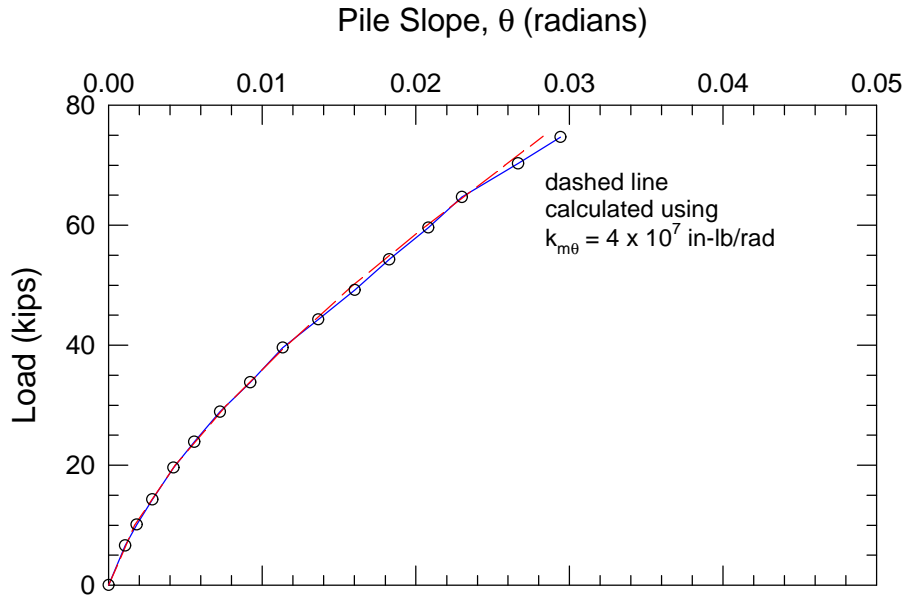


(a) Conceptual diagram of load connections.

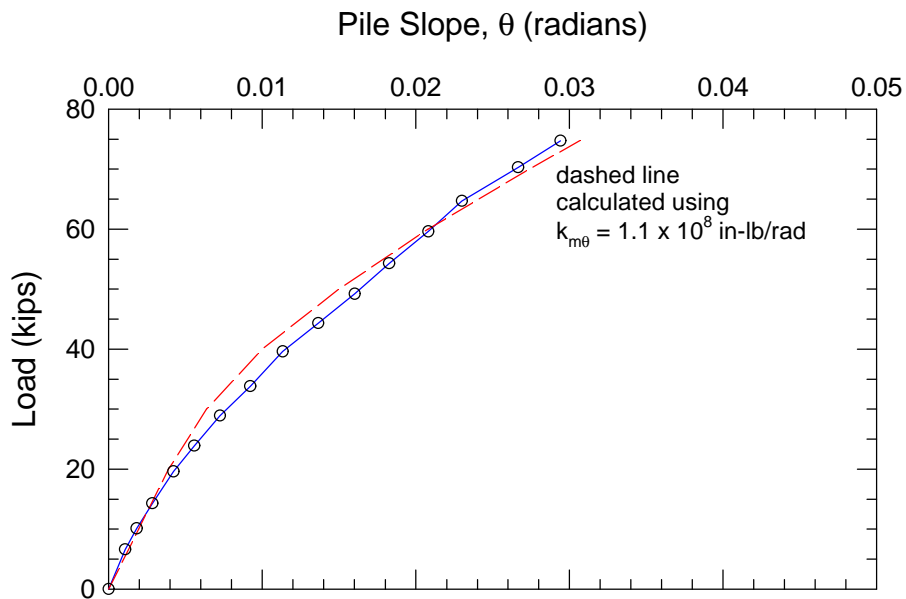


(b) Free-body-diagram of rigid strut connection.

Figure 7.8. Pile-head loading connection.

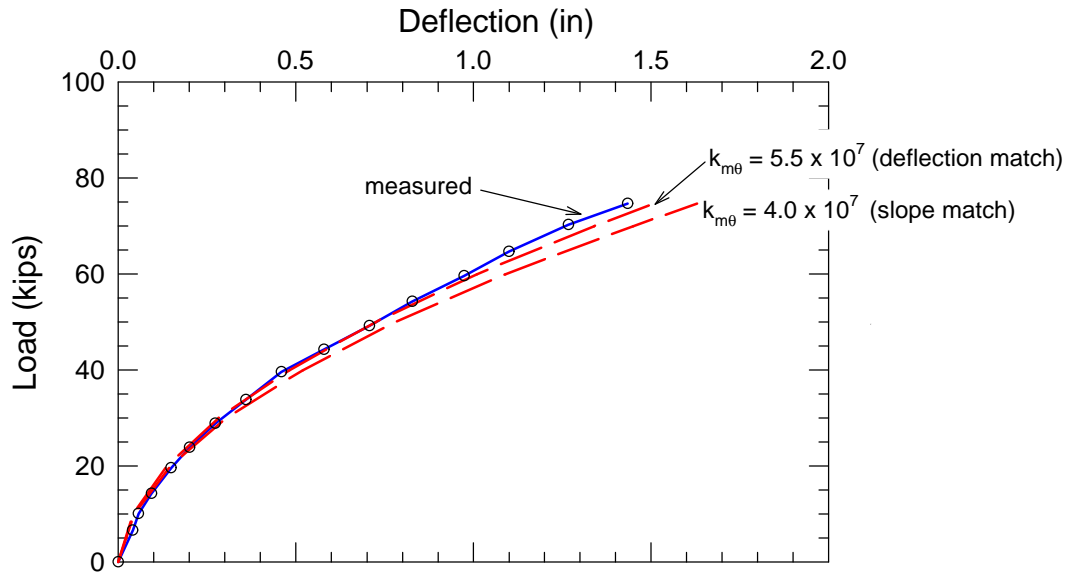


(a) Calculated response using Mokwa et al. (1997) p-y curves from *PYSHEET*.

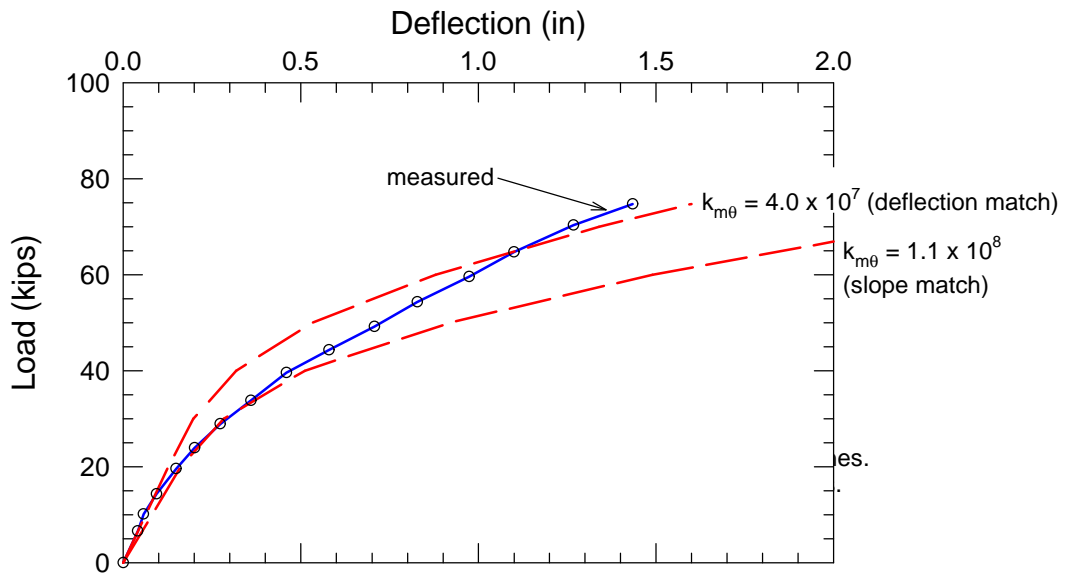


(b) Calculated response using Reese (1997) "default" p-y curves from *LPILE Plus 3.0*.

Figure 7.9. Calculated slope versus deflection curves for the south pile using best match  $k_{m\theta}$  values.

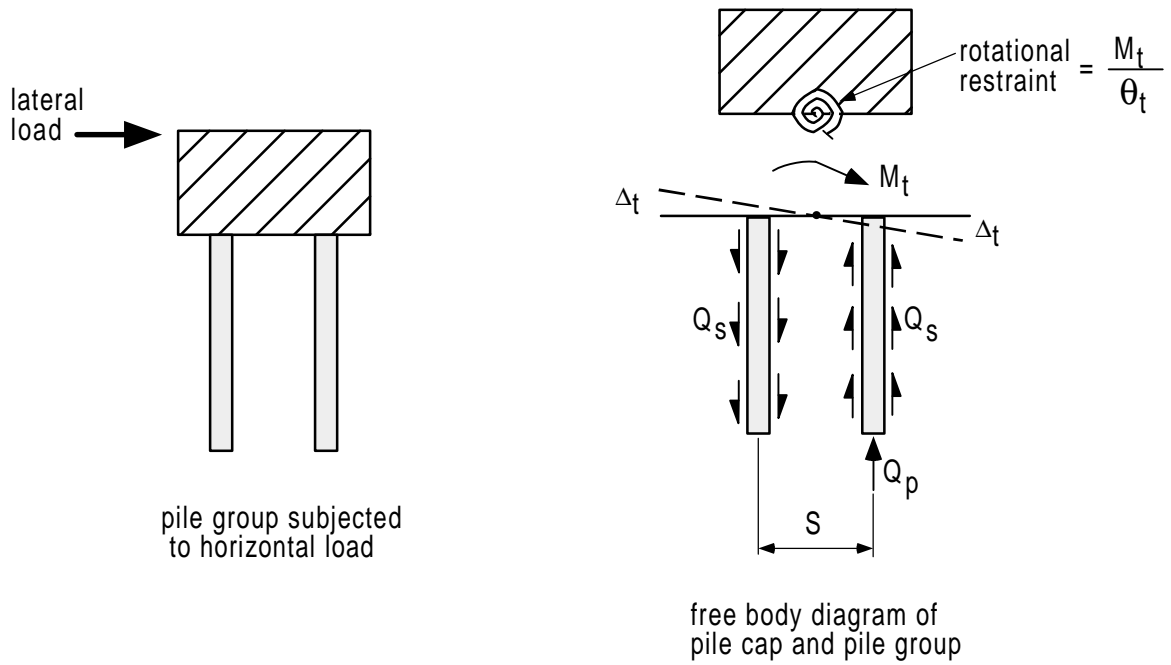


(a) Calculated response using Mokwa et al. (1997) p-y curves from *PYSHEET*.



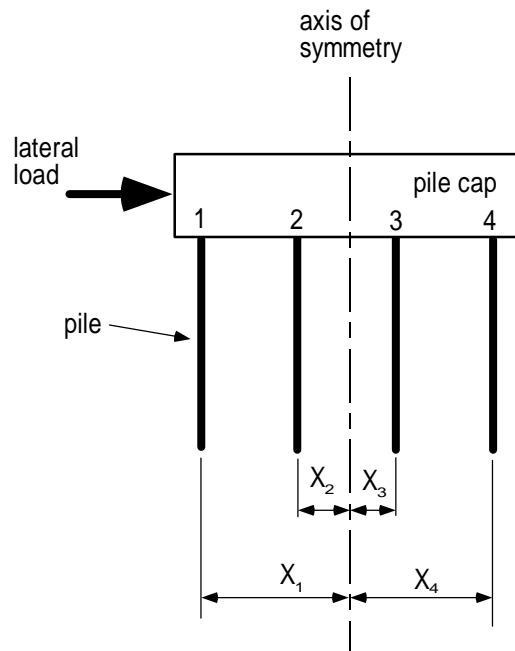
(b) Calculated response using Reese (1997) "default" p-y curves from *LPILE Plus 3.0*.

Figure 7.10. Comparison of calculated load versus deflection curves using best fit  $k_{m\theta}$  ratios.

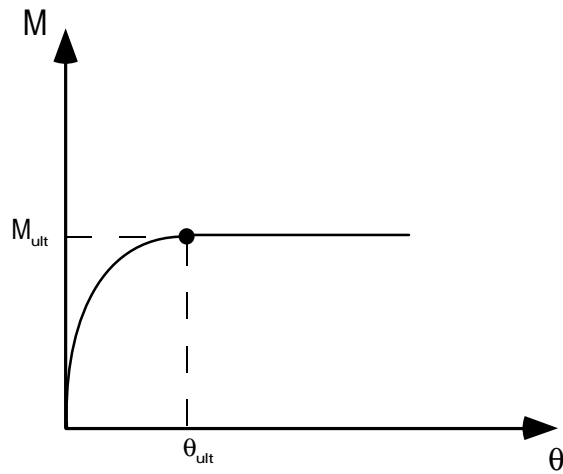


- $M_t$  = moment resisting rotation
- $\Delta_t$  = vertical displacement
- $Q_s$  = pile side resistance force
- $Q_p$  = pile end resistance force
- $S$  = spacing between leading and trailing rows
- $\theta_t$  = angular rotation of cap and pile head

Figure 7.11. Conceptual model for estimating pile group rotational restraint.

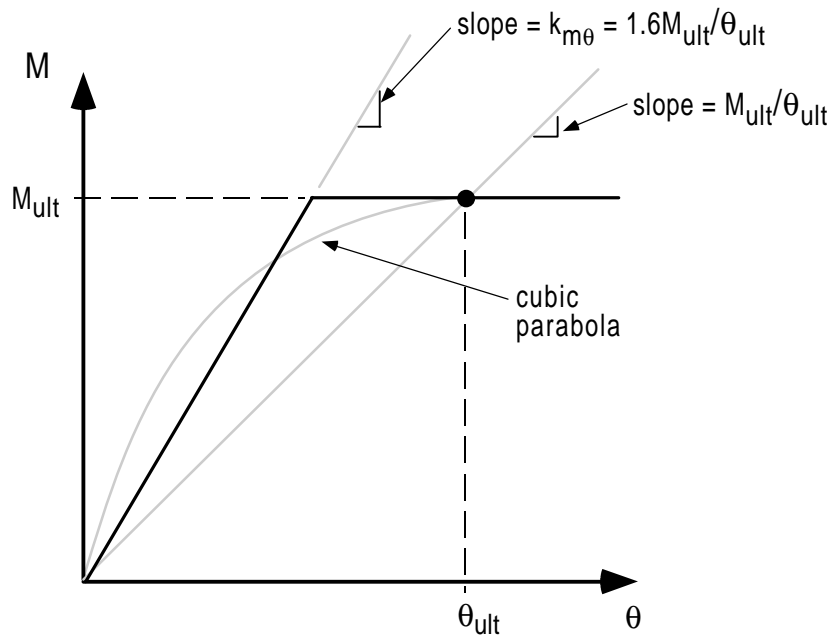


(a) Cross-section through a 4 by 4 pile group.

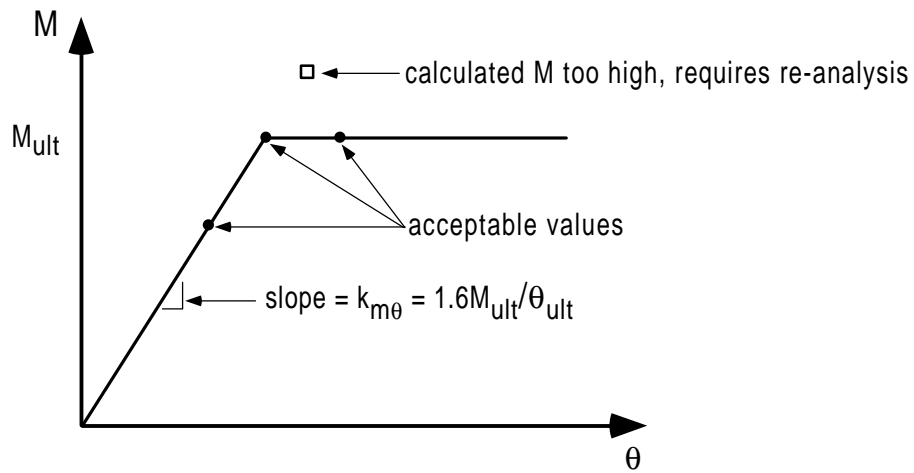


(b) Assumed relationship between  $M$  and  $\theta$ .

Figure 7.12. Details for rotational restraint calculations.

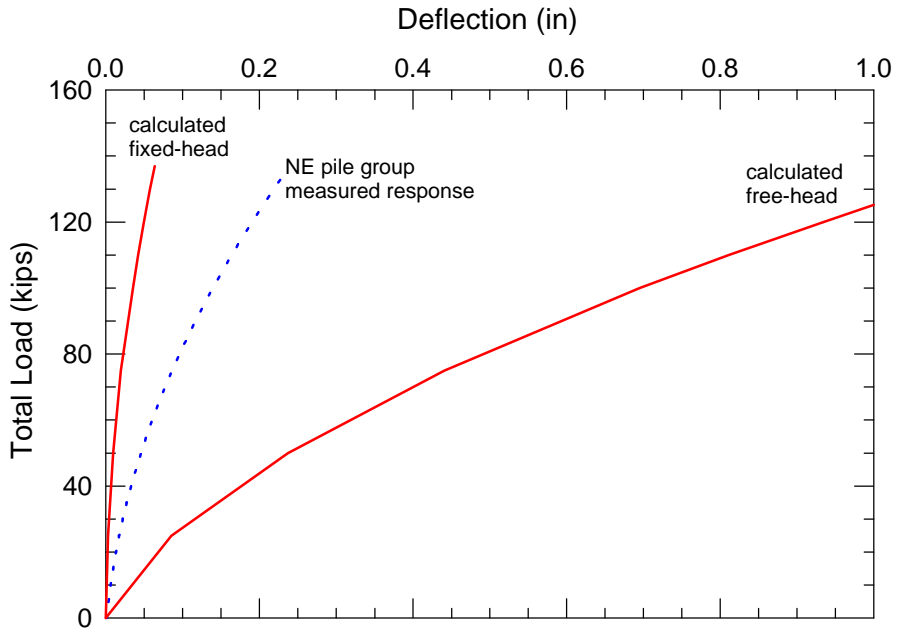


(a) Graphical illustration of  $k_{m\theta}$  approximation.

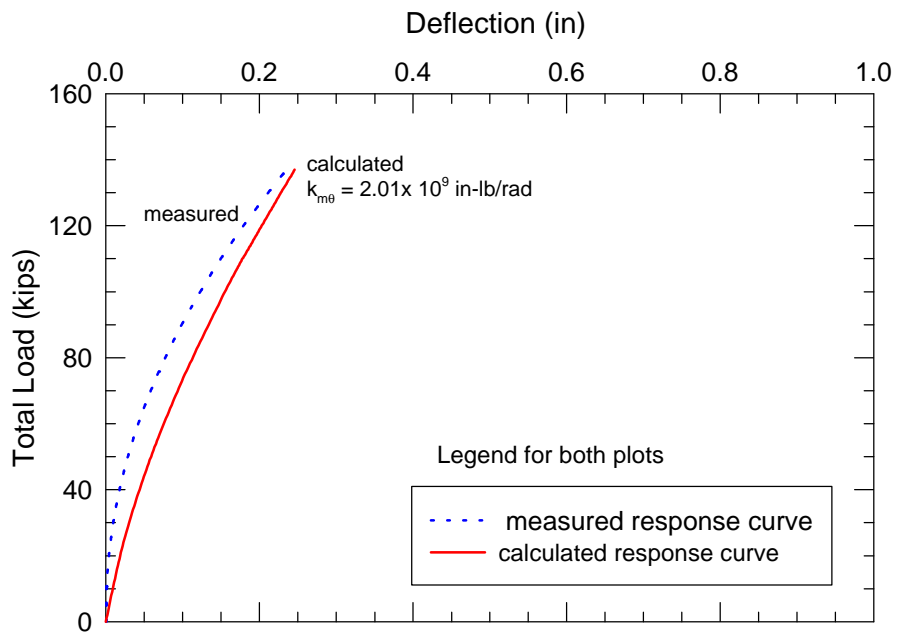


(b) Assumed  $k_{m\theta}$  distribution for analysis and design

Figure 7.13.  $k_{m\theta}$  approximation.



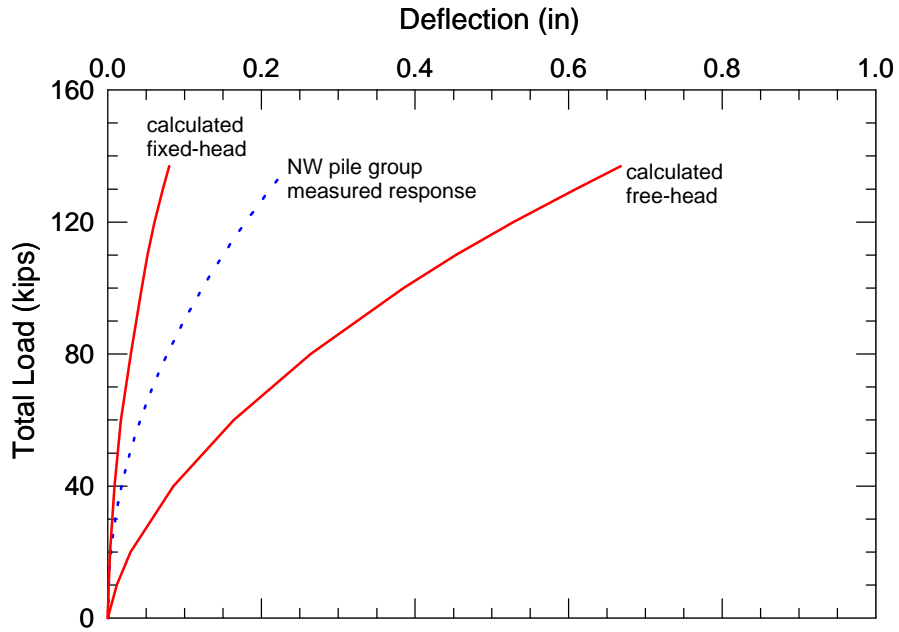
(a) Calculated response for fixed-head and free-head boundary conditions.



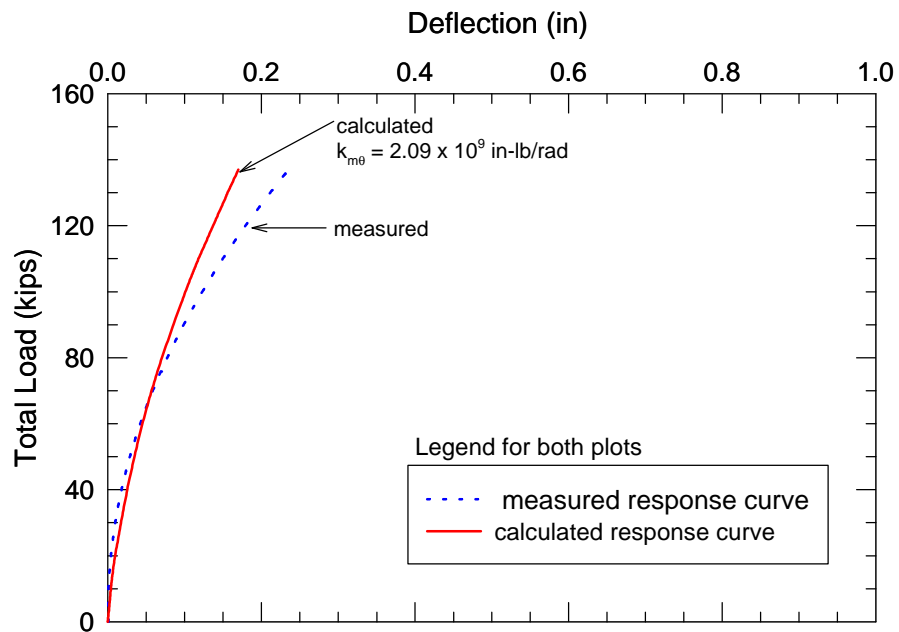
(b.) Calculated response for rotationally restrained pile head boundary condition.

Figure 7.14. Calculated response for the NE pile group with no cap resistance.



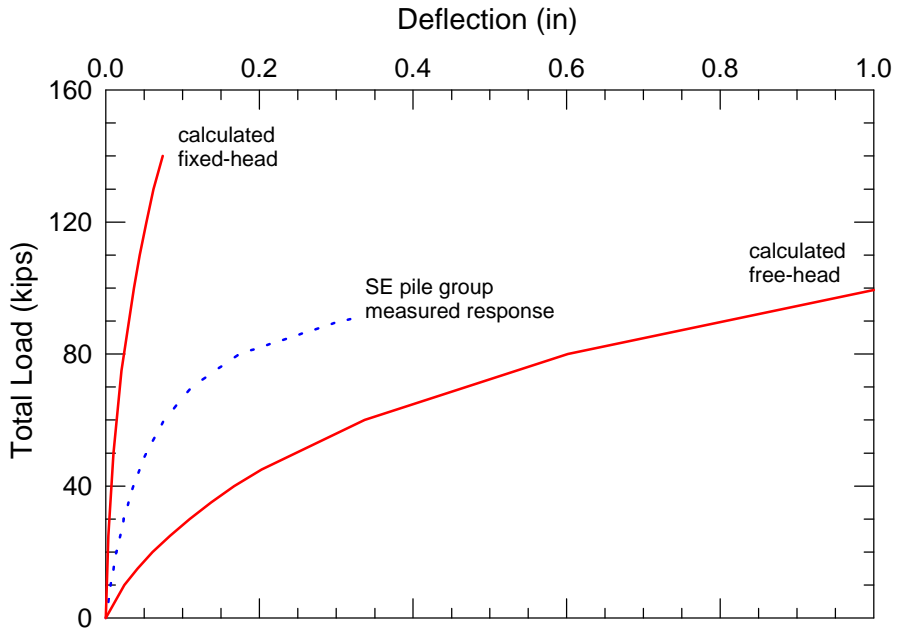


(a) Calculated response for fixed-head and free-head boundary conditions.

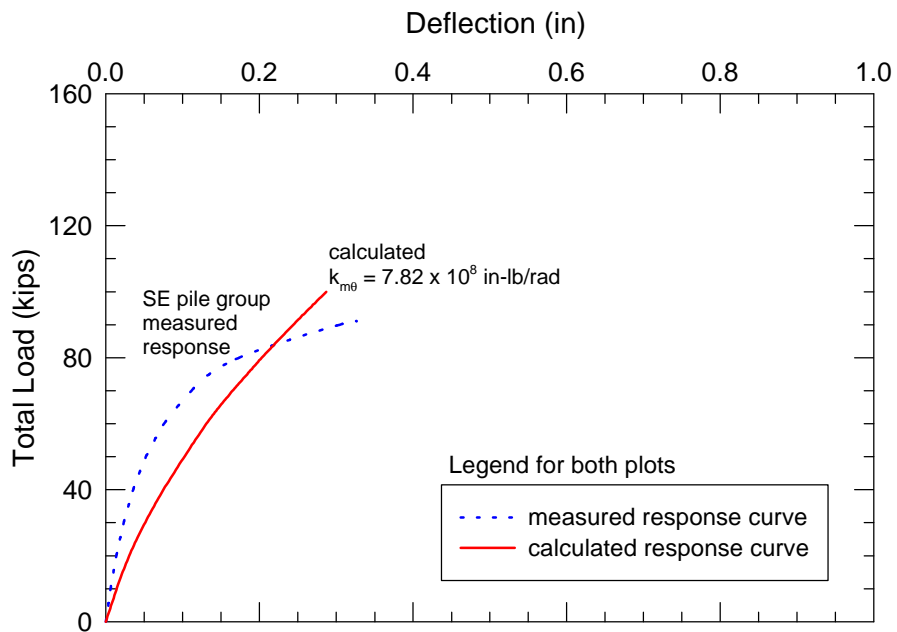


(b.) Calculated response for rotationally restrained pile head boundary condition.

Figure 7.15. Calculated response for the NW pile group with no cap resistance.

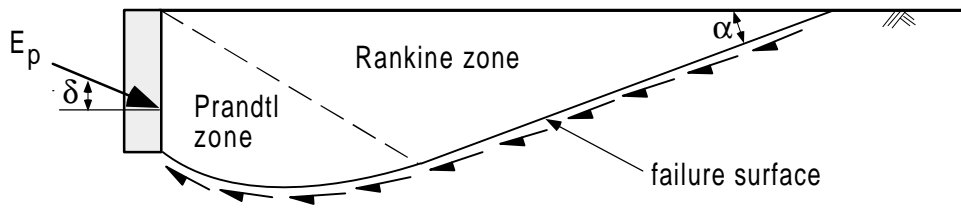


(a) Calculated response for fixed-head and free-head boundary conditions.



(b.) Calculated response for rotationally restrained pile head boundary condition.

Figure 7.16. Calculated response for the SE pile group with no cap resistance.

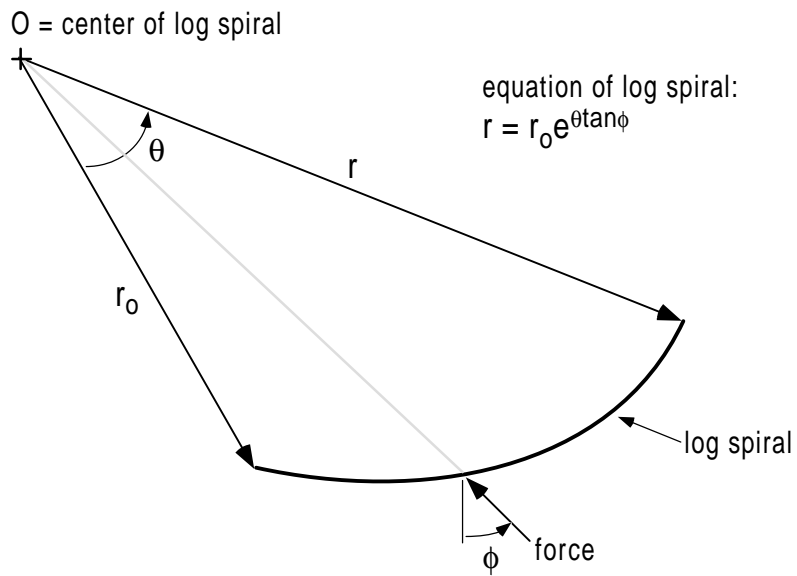


$E_p$  = passive earth pressure

$\delta$  = wall friction angle

$\alpha = 45 - \phi/2$

(a) Theoretical shape of passive failure zone.



(b) Log spiral.

Figure 7.17. Log spiral approximation.

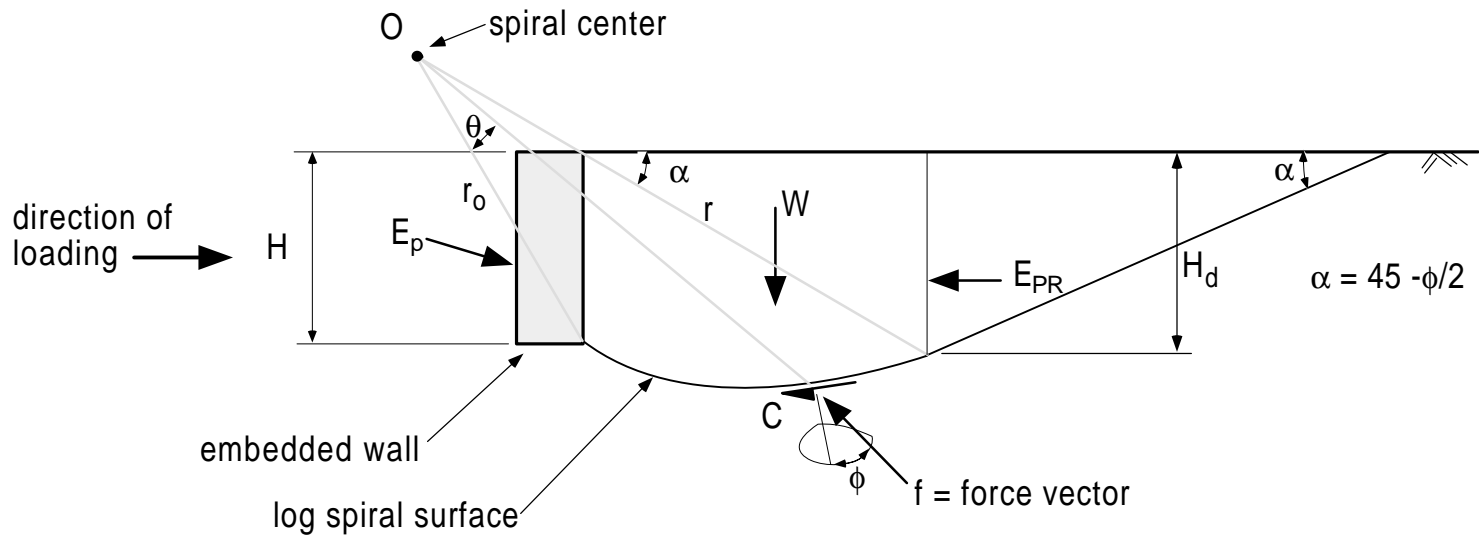
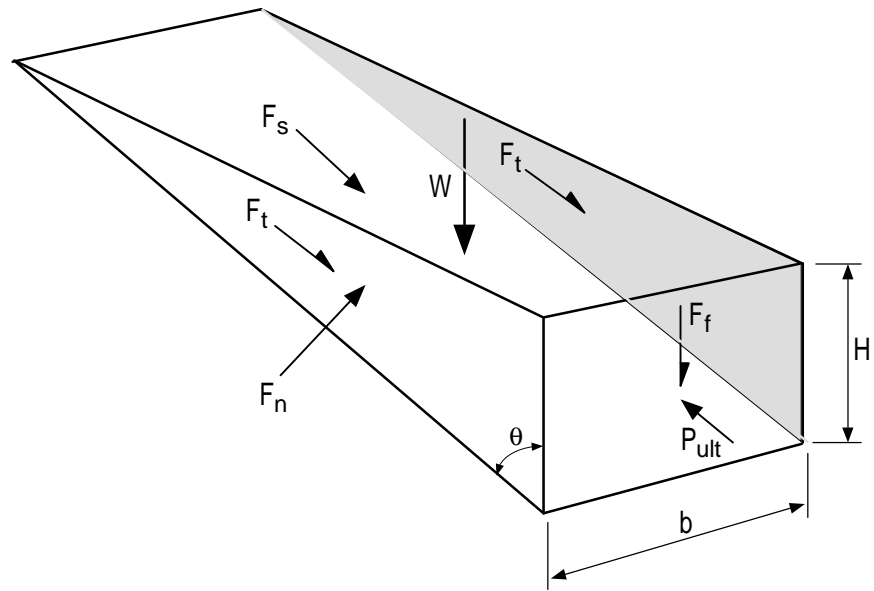
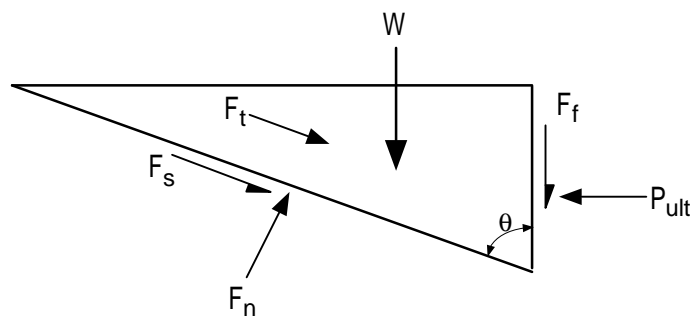


Figure 7.18. Graphical representation of the log spiral earth pressure method.

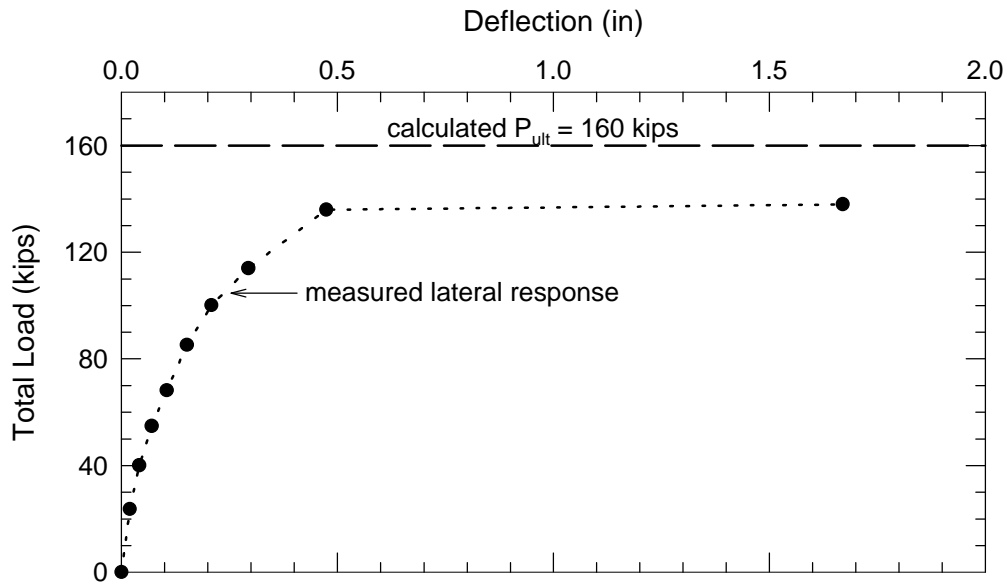


Orthogonal view of failure wedge

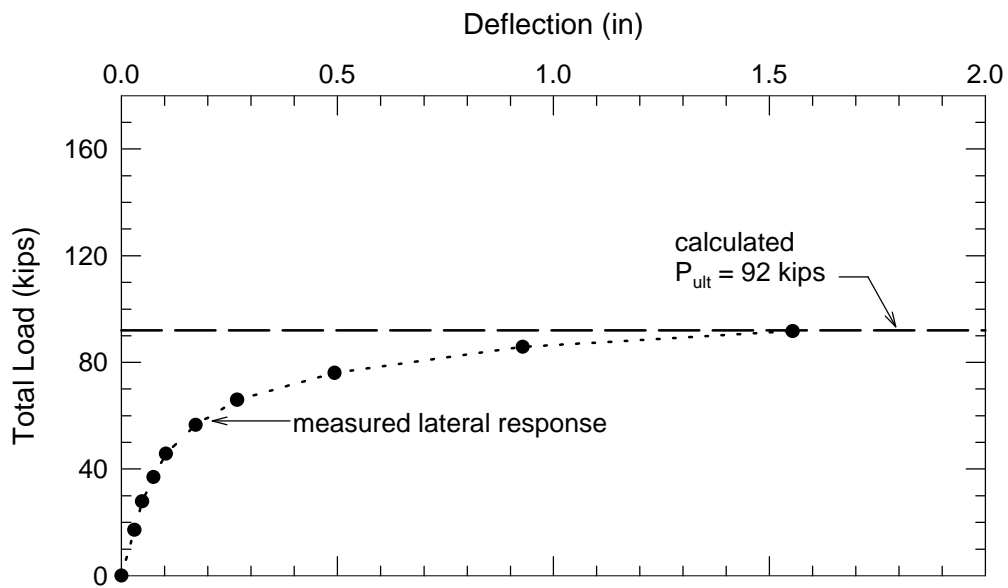


Side view of failure wedge

Figure 7.19.  $\phi = 0$  passive wedge model.



(a) Bulkhead embedded in natural soil.



(b) Bulkhead backfilled with compacted crusher run gravel.

Figure 7.20. Comparison of measured and calculated passive resistance for bulkhead in natural soil and gravel.

## **Ultimate Capacity Calculation Sheet**

*Created by R.L. Mokwa and J.M. Duncan - August 1999*

Date: 9/1/99  
 Description: Bulkhead in natural soil  
 Engineer: RLM

### **Input Values (red)**

cap width,	b (ft) =	<b>6.30</b>
cap height,	H (ft) =	<b>3.50</b>
embedment depth,	z (ft) =	<b>0.00</b>
surcharge,	$q_s$ (psf) =	<b>0.0</b>
cohesion,	c (psf) =	<b>970.0</b>
soil friction angle,	$\phi$ (deg.) =	<b>37.0</b>
wall friction,	$\delta$ (deg.) =	<b>3.5</b>
initial soil modulus,	$E_i$ (kip/ft <sup>2</sup> ) =	<b>890</b>
poisson's ratio,	$\nu$ =	<b>0.33</b>
soil unit weight,	$\gamma_m$ (pcf) =	<b>122.0</b>
adhesion factor,	$\alpha$ =	<b>0.00</b>
$\Delta_{max}/H$ , (0.04 suggested, see notes) =		<b>0.04</b>
<b>Calculated Values (blue)</b>		
$K_a$ (Rankine) =		<b>0.25</b>
$K_p$ (Rankine) =		<b>4.02</b>
$K_p$ (Coulomb) =		<b>4.56</b>
$K_{p\phi}$ (Log Spiral, soil weight) =		<b>4.65</b>
$K_{pq}$ (Log Spiral, surcharge) =		<b>0.00</b>
$K_{pc}$ (Log Spiral, cohesion) =		<b>2.11</b>
$E_p$ (kip/ft) =		<b>17.81</b>
Ovesen's 3-D factor, R =		<b>1.43</b>
$k_{max}$ , elastic stiffness (kip/in) =		<b>890.5</b>
<b><math>P_{ult}</math> (kips) =</b>		<b>160.4</b>

Figure 7.21. *PYCAP Summary* worksheet for bulkhead in natural soil.

## **Ultimate Capacity Calculation Sheet**

*Created by R.L. Mokwa and J.M. Duncan - August 1999*

Date: 9/1/99  
 Description: Bulkhead backfilled with compacted gravel  
 Engineer: RLM

### **Input Values (red)**

cap width,	b (ft) =	<b>6.30</b>
cap height,	H (ft) =	<b>3.50</b>
embedment depth,	z (ft) =	<b>0.00</b>
surcharge,	q <sub>s</sub> (psf) =	<b>0.0</b>
cohesion,	c (psf) =	<b>0.0</b>
soil friction angle,	φ (deg.) =	<b>50.0</b>
wall friction,	δ (deg.) =	<b>6.2</b>
initial soil modulus,	E <sub>i</sub> (kip/ft <sup>2</sup> ) =	<b>760</b>
poisson's ratio,	ν =	<b>0.3</b>
soil unit weight,	γ <sub>m</sub> (pcf) =	<b>134.0</b>
adhesion factor,	α =	<b>0.00</b>
Δ <sub>max</sub> /H, (0.04 suggested, see notes) =		<b>0.04</b>
<b>Calculated Values (blue)</b>		
K <sub>a</sub> (Rankine) =		<b>0.13</b>
K <sub>p</sub> (Rankine) =		<b>7.55</b>
K <sub>p</sub> (Coulomb) =		<b>10.41</b>
K <sub>pφ</sub> (Log Spiral, soil weight) =		<b>10.22</b>
K <sub>pq</sub> (Log Spiral, surcharge) =		<b>0.00</b>
K <sub>p<sub>c</sub></sub> (Log Spiral, cohesion) =		<b>0.00</b>
E <sub>p</sub> (kip/ft) =		<b>8.39</b>
Ovesen's 3-D factor, R =		<b>1.75</b>
k <sub>max</sub> , elastic stiffness (kip/in) =		<b>756.4</b>
<b>P<sub>ult</sub> (kips) =</b>		<b>92.3</b>

Figure 7.22. PYCAP Summary worksheet for bulkhead backfilled with compacted gravel.



## Elasticity Solution for Horizontal Loading on a Vertical Rectangle

Created by R.L. Mokwa - August 1999

Reference: Douglas, D.J. and Davis, E.H. (1964). *Geotechnique*, Vol.14(3), p. 115-132.

**Description:** Bulkhead in natural soil

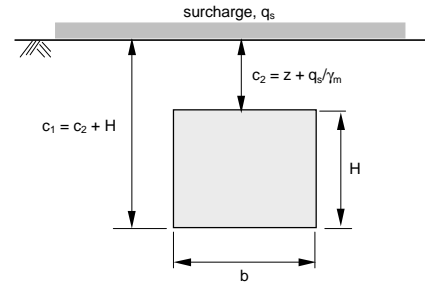
**Date:** 9/1/99

### Equations

$$y_1 = \frac{P(1+\nu)(l_1)}{16\pi HE(1-\nu)} \quad y_2 = \frac{P(1+\nu)(l_2)}{16\pi HE(1-\nu)}$$

### Input Parameters

$y_1$ = horizontal deflection at upper corner of rectangle	$y_{avg} = (y_1 + y_2)/2$
$y_2$ = horizontal deflection at lower corner of rectangle	$k_{max}$ = Initial elastic stiffness
P = applied force	= slope of P versus $y_{avg}$ line
$\nu$ = Poisson's ratio	$k_{max} = P/y_{avg}$
$E_i$ = Initial tangent soil modulus	
H = rectangle height	
$F_1, F_4, F_5$ = influence factors	
$c_1, c_2, d$ = dimensions defined in diagram	
$l_1 = \{ (3-4\nu)F_1 + F_4 + 4(1-2\nu)(1-\nu)F_5 \}$	
$l_2 = \{ (3-4\nu)F_1 + F_2 + 4(1-2\nu)(1-\nu)F_3 \}$	



### Input from Summary Sheet

$\nu$ =	0.33
$E_i$ (kip/ft <sup>2</sup> ) =	890
h (ft) =	3.50
b (ft) =	6.30
$c_1$ (ft) =	3.50
$c_2$ (ft) =	0.00

### Calculated Values

$K_1 = 2c_1/b$ =	1.111
$K_2 = 2c_2/b$ =	0.000
$F_1$ =	2.561
$F_2$ =	1.474
$F_3$ =	0.625
$F_4$ =	2.561
$F_5$ =	1.703
$l_1$ =	8.416
$l_2$ =	6.346

### Results

Initial elastic stiffness, $k_{max}$	
$k_{max}$ =	<b>890.5 kips/inch</b>

Figure 7.23. Elasticity worksheet for the bulkhead in natural soil.

# Hyperbolic Calculation Sheet

Created by R.L. Mokwa - August 1999

**Description:** Bulkhead in natural soil

**Hyperbolic equation:**  $P = y / \{ (1/k_{max}) + (yR_f/P_{ult}) \}$

$R_f = \{ (\Delta_{max}/P_{ult}) - (1/k) \} (P_{ult}/\Delta_{max})$

**Input values - Use "Summary" worksheet for data entry.**

$k_{max}$  (kips/in) = 890.5  
 H (ft) = 3.50  
 $P_{ult}$  = 160.4

$\Delta_{max}/H$  = 0.04  
 $\Delta_{max}$  (in) = 1.68  
 $R_f$  = 0.89

**Calculated values using hyperbolic formulation**

Def. (in)	Load (kips)
y	P
0	0.00
0.01	8.48
0.03	23.26
0.05	35.68
0.1	59.54
0.15	76.62
0.2	89.45
0.25	99.43
0.3	107.43
0.35	113.98
0.4	119.44
0.45	124.06
0.5	128.02
0.55	131.46
0.6	134.46
0.65	137.12
0.7	139.48
0.75	141.59
0.8	143.49
0.85	145.21
0.9	146.78
0.95	148.21
1	149.51
1.05	150.72
1.1	151.83
1.15	152.86
1.2	153.82
1.25	154.71
1.3	155.54
1.35	156.32
1.4	157.05
1.45	157.73
1.5	158.38
1.55	158.99
1.6	159.56
1.65	160.10
1.7	160.62
1.75	161.11
1.8	161.57
1.85	162.01

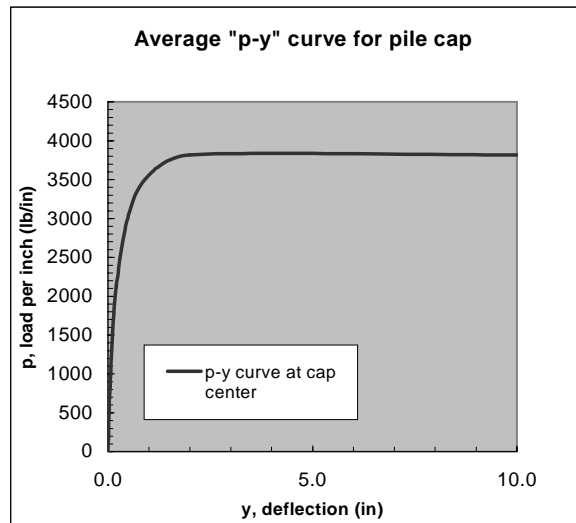
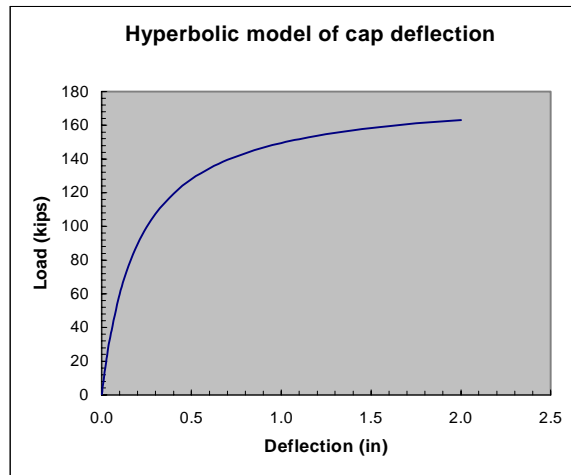
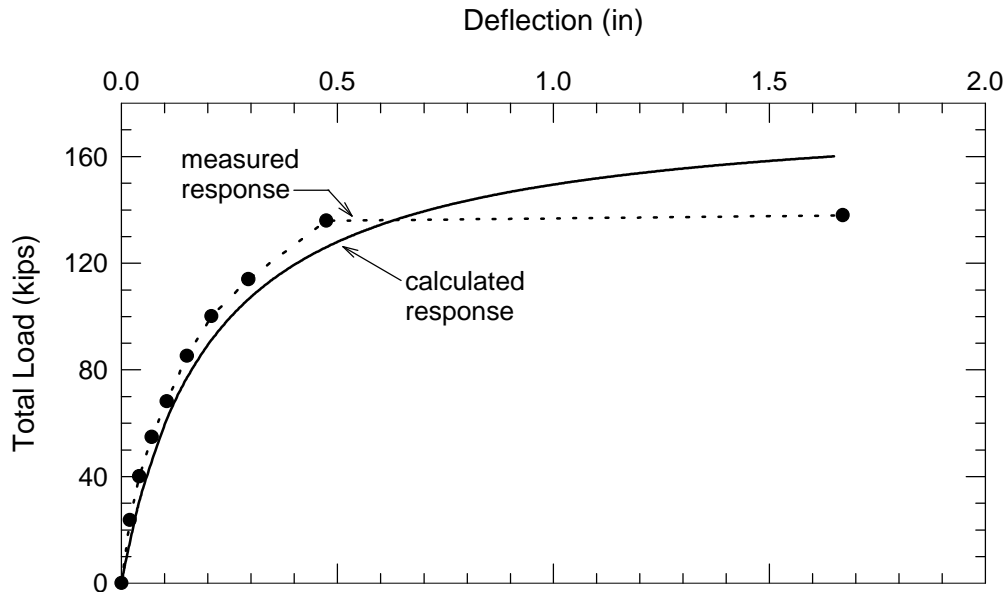
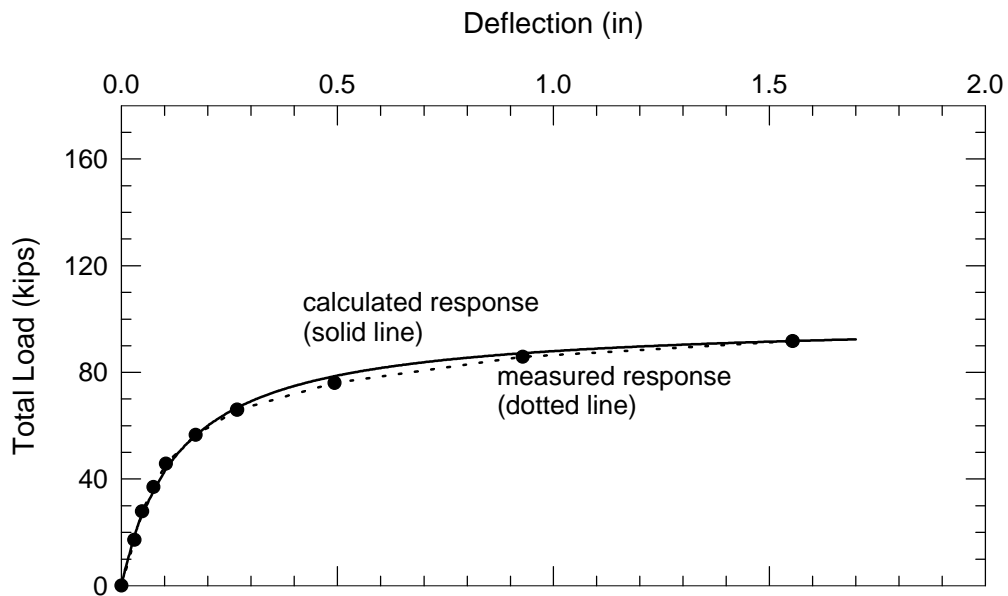


Figure 7.24. *Hyperbola* worksheet for the bulkhead in natural soil.



(a) Bulkhead embedded in natural soil.



(b) Bulkhead backfilled with compacted crusher run gravel.

Figure 7.25. Comparison of calculated versus observed load-deflection behavior of bulkhead in natural soil and gravel.

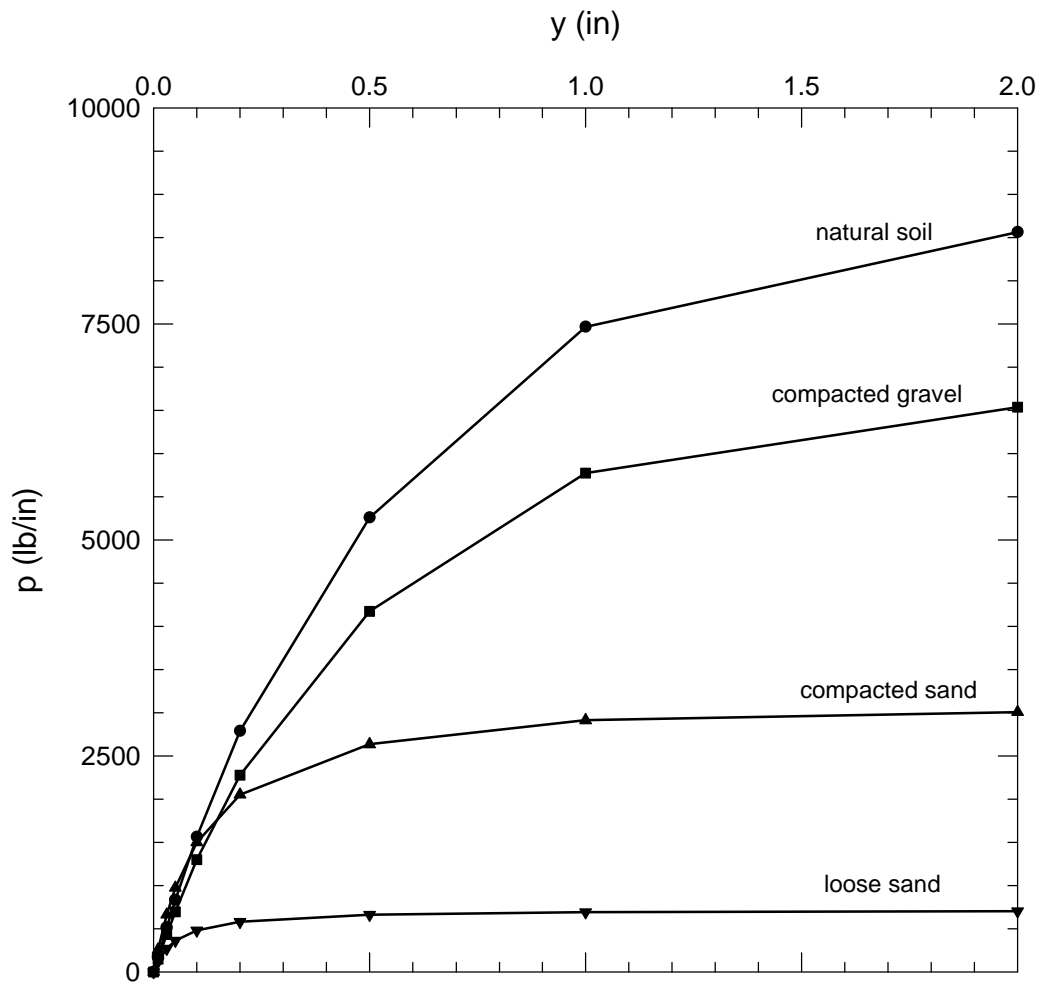
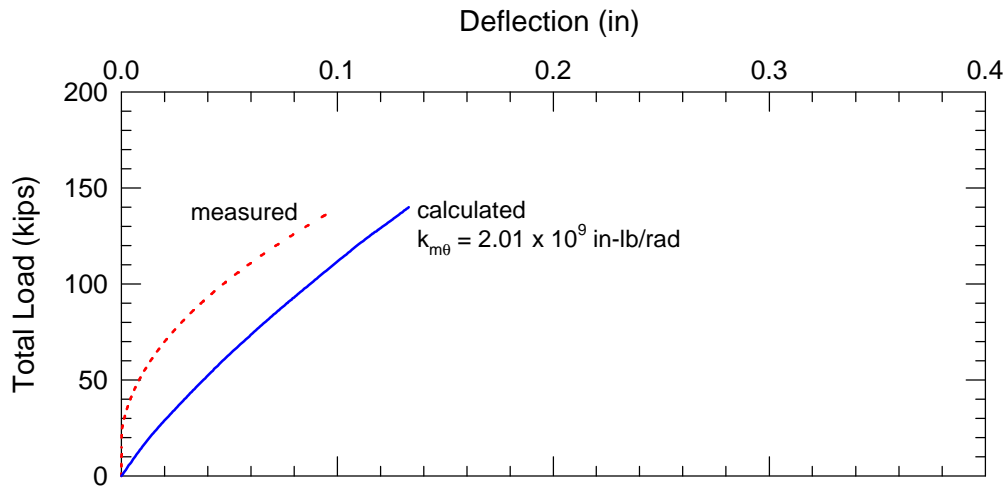
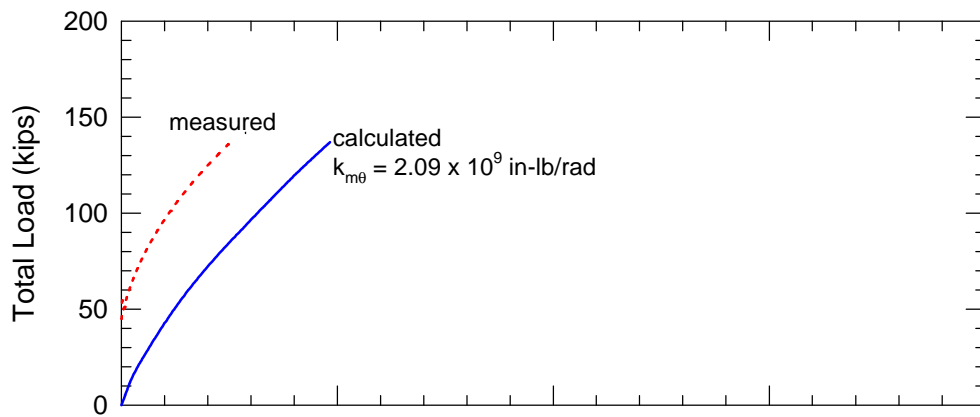


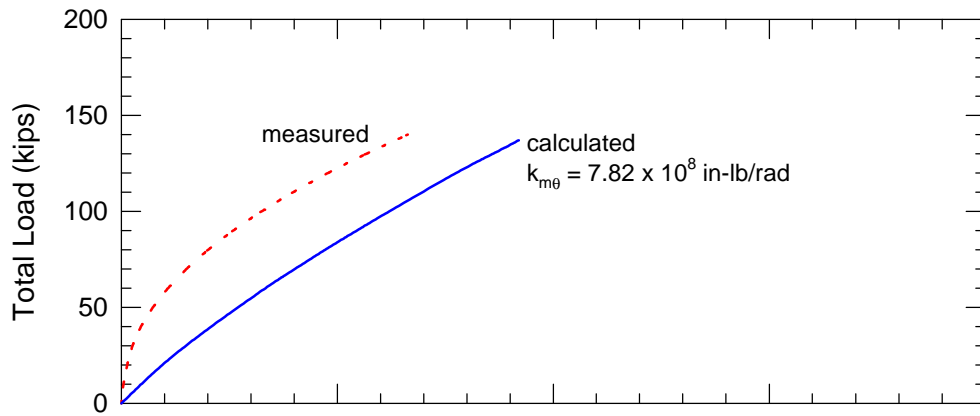
Figure 7.26.  $p$ - $y$  curves for 36-in-deep pile cap in four different soils.



(a) NE 36-inch-deep cap.

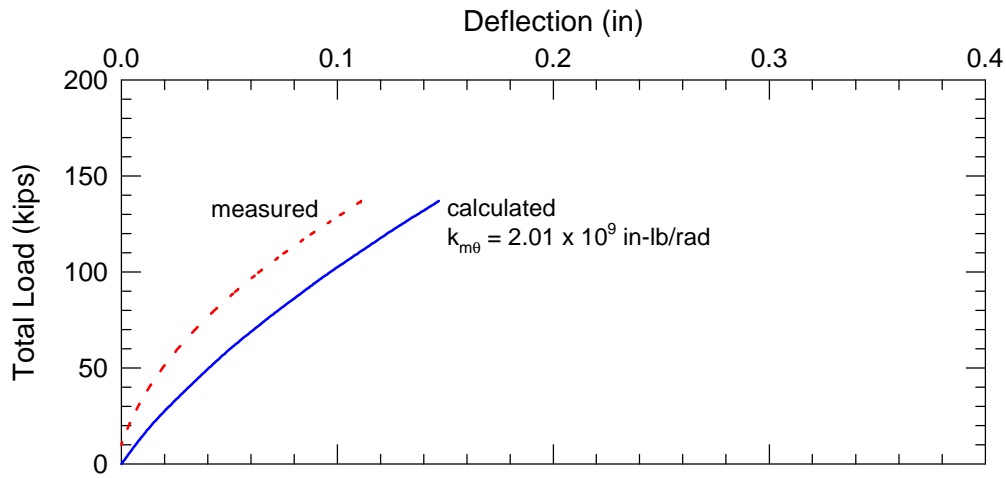


(b) NW 18-in-deep.

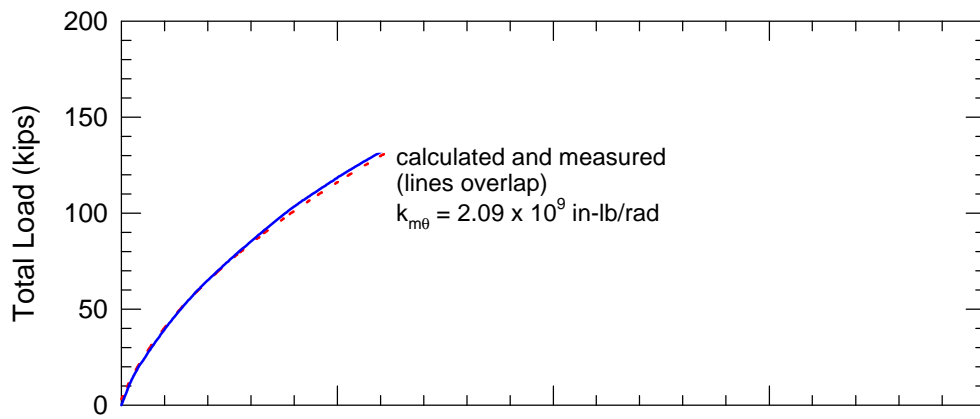


(c) SE 36-inch-deep cap.

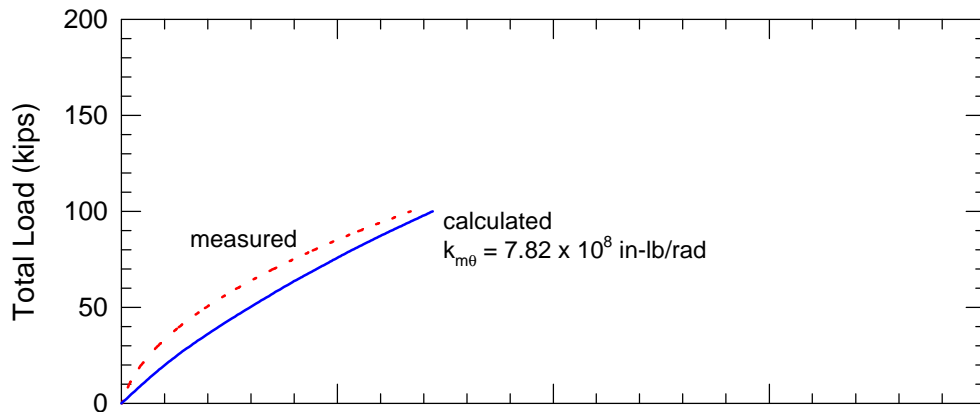
Figure 7.27. Comparison between calculated and measured responses for pile caps in natural soil.



(a) NE 36-inch-deep pile cap.



(b) NW 18-inch-deep cap.



(c) SE 36-inch-deep cap.

Legend for all plots

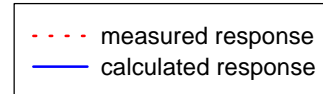
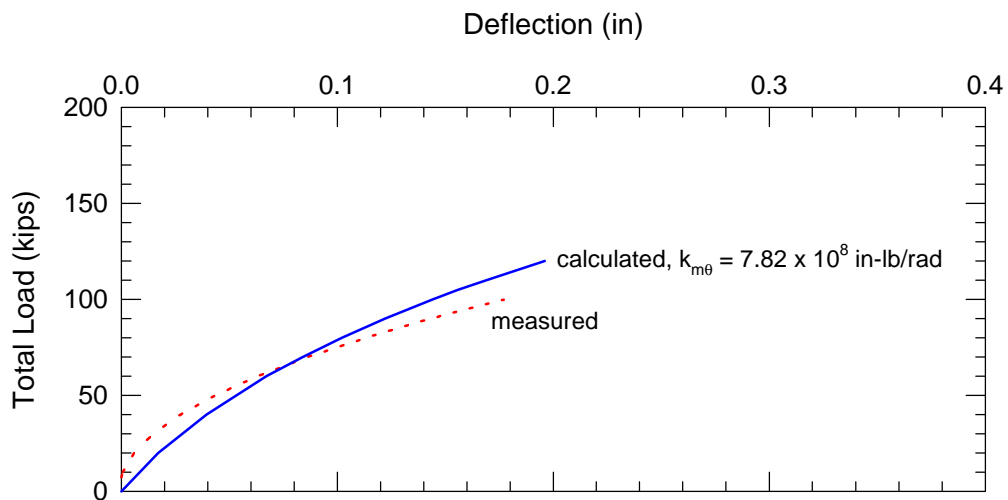
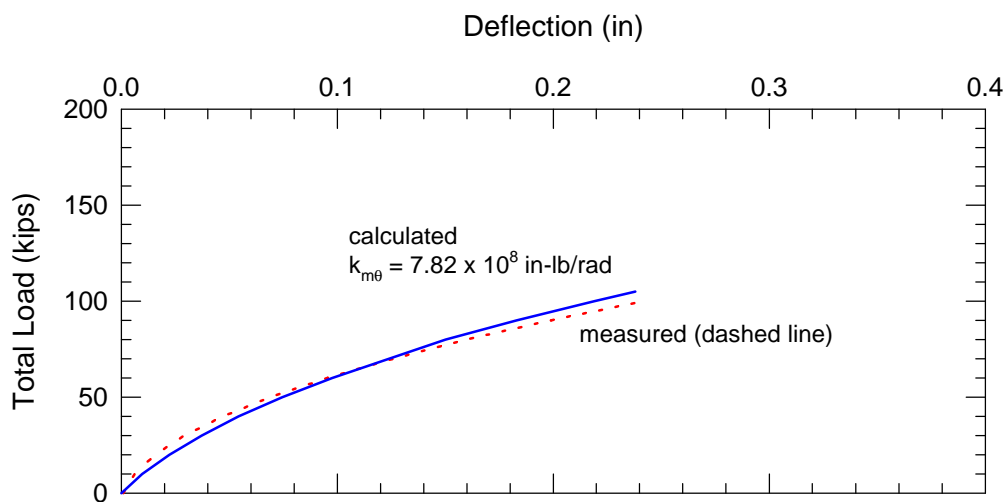


Figure 7.28. Comparison between calculated and measured responses for pile caps backfilled with crusher run gravel.



(a) SE cap backfilled with compacted sand.



(b) SE cap backfilled with loose sand.

Legend for both plots

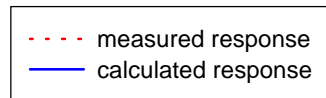
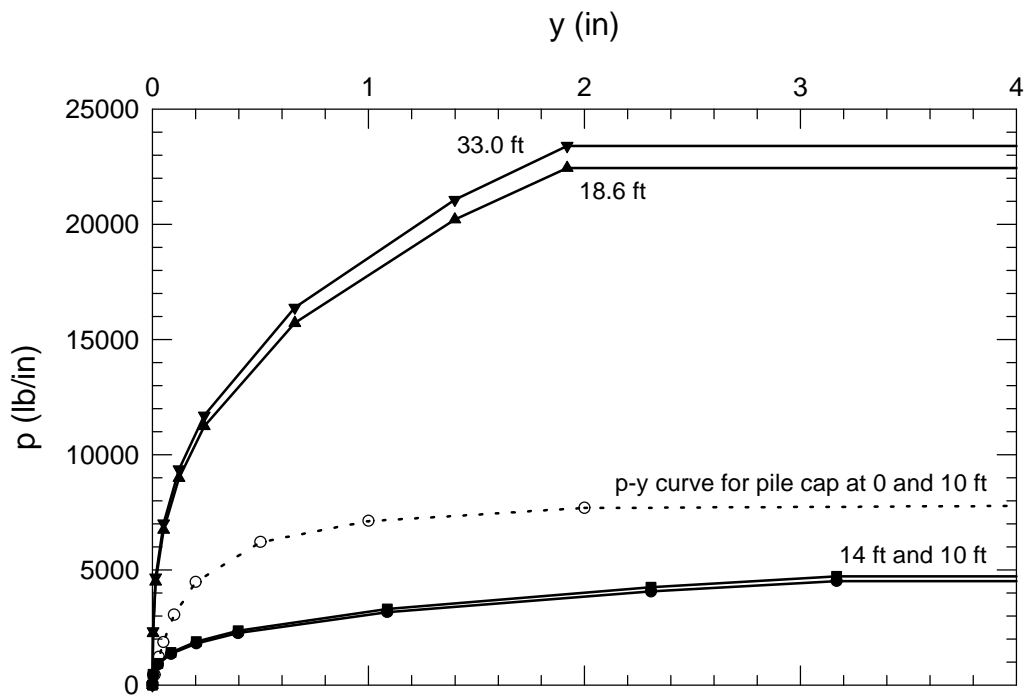
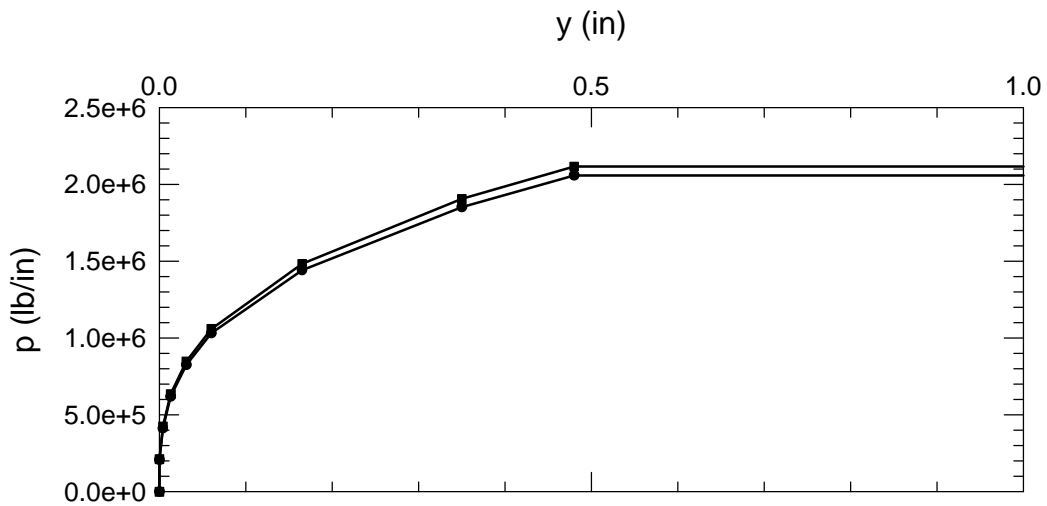


Figure 7.29. Comparison between calculated and measured responses of SE cap backfilled with New castle sand.



(a) p-y curves for stiff clay at 0, 10, 14, 18.6, and 33 feet below grade.



(b) p-y curves for caliche layer at 14.1 and 18.5 feet below grade.

Figure 7.30. "Group-equivalent pile" (GEP) p-y curves for the Zafir and Vanderpool (1998) case study.



## **Ultimate Capacity Calculation Sheet**

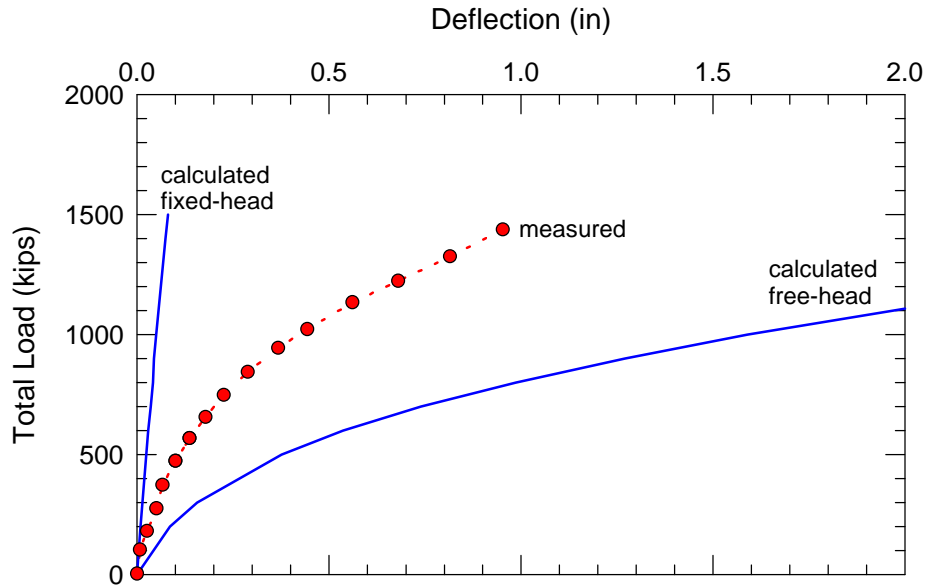
*Created by R.L. Mokwa and J.M. Duncan - August 1999*

Date: 9/1/99  
 Description: Zafir and vanderpool case study  
 Engineer: RLM

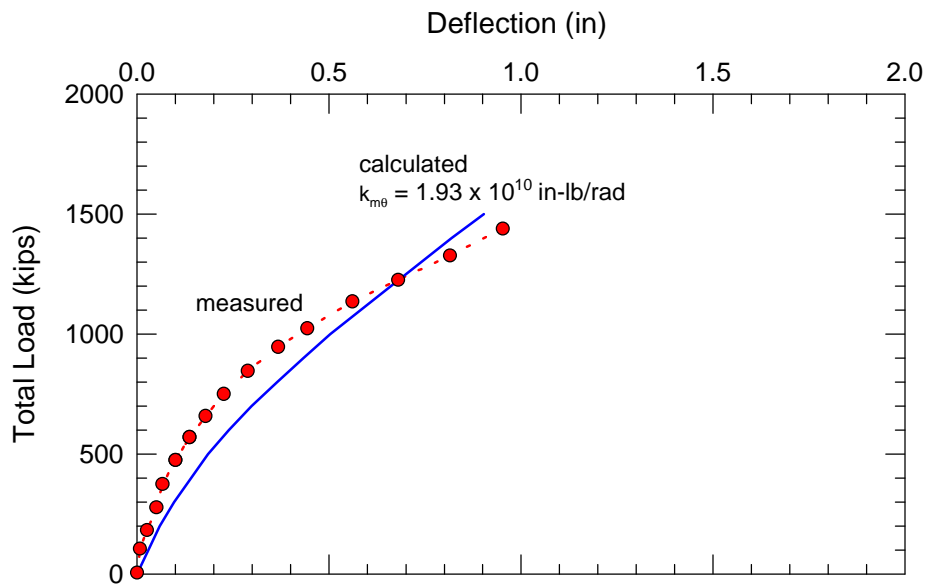
### **Input Values (red)**

cap width,	b (ft) =	<b>11.00</b>
cap height,	H (ft) =	<b>10.00</b>
embedment depth,	z (ft) =	<b>0.00</b>
surcharge,	q <sub>s</sub> (psf) =	<b>0.0</b>
cohesion,	c (psf) =	<b>3000.0</b>
soil friction angle,	φ (deg.) =	<b>0.0</b>
wall friction,	δ (deg.) =	<b>0</b>
initial soil modulus,	E <sub>i</sub> (kip/ft <sup>2</sup> ) =	<b>3000</b>
poisson's ratio,	v =	<b>0.33</b>
soil unit weight,	γ <sub>m</sub> (pcf) =	<b>125.0</b>
adhesion factor,	α =	<b>1.00</b>
Δ <sub>max</sub> /H, (0.04 suggested, see notes) =		<b>0.04</b>
<b>Calculated Values (blue)</b>		
K <sub>a</sub> (Rankine) =		<b>1.00</b>
K <sub>p</sub> (Rankine) =		<b>1.00</b>
K <sub>p</sub> (Coulomb) =		<b>1.00</b>
K <sub>pφ</sub> (Log Spiral, soil weight) =		<b>Rankine Kp</b>
K <sub>pq</sub> (Log Spiral, surcharge) =		<b>Rankine Kp</b>
K <sub>pc</sub> (Log Spiral, cohesion) =		<b>Rankine Kp</b>
E <sub>p</sub> (kip/ft) =		<b>66.25</b>
Ovesen's 3-D factor, R =		<b>1.00</b>
k <sub>max</sub> , elastic stiffness (kip/in) =		<b>6708.4</b>
<b>phi = 0 Solution</b>		
<b>P<sub>ult</sub> (kips) =</b>		<b>1096.3</b>

Figure 7.31. Summary worksheet from PYCAP for the Zafir and Vanderpool case study.

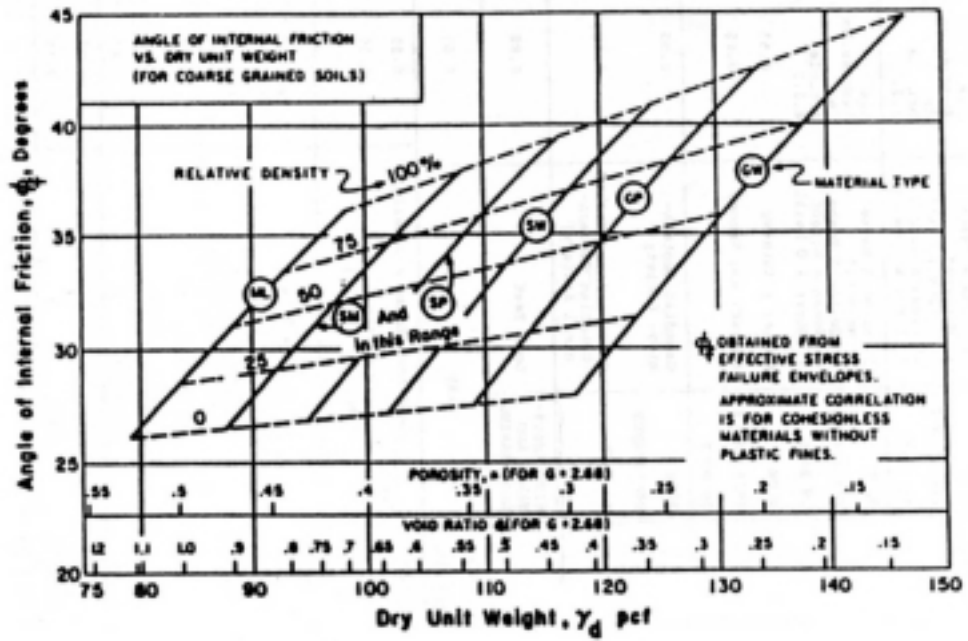


(a) Fixed-head and free-head boundary conditions.



(b) Rotationally restrained pile-head boundary condition.

Figure 7.32. Calculated responses for the Zafir and Vanderpool (1998) case study.



where

- ML: Silt
- SM: Silty sand
- SP: Poorly graded sand
- SW: Well-graded sand
- GP: Poorly graded gravel
- GW: Well-graded gravel

Figure 7.33. Approximate relationship between the friction angle and dry unit weight of granular soils. (After NAVFAC 1982)

## **CHAPTER 8**

### **SUMMARY AND CONCLUSIONS**

It is clear, from examples in the literature and from the field tests performed on pile groups at Virginia Tech's field test site, that pile caps provide considerable resistance to lateral loads on deep foundation systems. Neglecting this resistance in design results in excessive estimates of pile group deflections and bending moments under load, and underestimates the foundation stiffness. In many situations, neglecting cap resistance introduces inaccuracies of one hundred percent or more. There is a need for rational procedures for including cap resistance in the design of pile groups to resist lateral loads. This research has made it possible to quantify many important aspects of pile group and pile cap behavior under lateral loads due to wind, waves, and thermal expansions and contractions of bridge decks.

The program of work accomplished in this study includes performing a detailed literature review on the state of knowledge of pile group and pile cap resistance to lateral loads, developing a full-scale field test facility, conducting 31 lateral load tests on pile groups and individual piles, performing laboratory tests on natural soils obtained from the site and on imported backfill materials, and developing an analytical method for including the lateral resistance of pile caps in the design of deep foundation systems.

#### **8.1 LITERATURE REVIEW**

A comprehensive literature review was conducted to examine the current state of knowledge regarding pile cap resistance and pile group behavior. Over 350 journal articles and other publications pertaining to lateral resistance, testing, and analysis of pile caps, piles, and pile groups were collected and reviewed. Pertinent details from these studies were evaluated and, whenever possible, summarized in tables and charts.

Of the publications reviewed, only four papers were found that described load tests performed to investigate the lateral resistance of pile caps. These studies indicate that the lateral resistance of pile caps can be quite significant, especially when the cap is embedded beneath the ground surface.

A review of the most widely recognized techniques for analyzing laterally loaded single piles was performed. These techniques provide a framework for methods that are used to evaluate the response of closely spaced piles, or pile groups. Modifications of single pile techniques are often in the form of empirically or theoretically derived factors that are applied, in various ways, to account for group interaction effects.

Piles in closely spaced groups behave differently than single isolated piles because of pile-soil-pile interactions that take place in the group. Deflections and bending moments of piles in closely spaced groups are greater than deflections and bending moments of single piles, at the same load per pile, because of these interaction effects.

The most widely used method of adjusting for group interaction effects is the group efficiency factor,  $G_e$ , which is defined as the average lateral capacity per pile in a group divided by the lateral capacity of a single pile. The value of  $G_e$  is always less than or equal to unity.

The current state of practice regarding pile group behavior was reviewed from an experimental and analytical basis. Thirty-seven experimental studies were reviewed in which the effects of pile group behavior on the group efficiency,  $G_e$ , were observed and measured. These included 15 full-scale field tests, 16 1g model tests, and 6 geotechnical centrifuge tests. Thirty analytical studies were reviewed that addressed pile group lateral load behavior. These studies included closed-form analytical approaches, elasticity methods, hybrid methods, and finite element methods. Based on these studies, a number of factors were evaluated to determine the influence that pile group behavior has on the

group efficiency,  $G_e$ . These factors, listed in order of importance are: pile spacing, group arrangement, group size, pile-head fixity, soil type and density, and pile displacement.

Measurements of pile displacements and stresses during full-scale and model tests indicate that piles in a group carry unequal lateral loads, depending on their location within the group and the spacing between piles. This unequal distribution of load among piles is caused by “shadowing”, which is a term used to describe the overlap of shear zones and consequent reduction of soil resistance.

Shadowing is accounted for in the p-y method of analysis using p-multipliers, which are empirical reduction factors that are experimentally derived from load tests on pile groups. The p-multiplier ( $f_m$ ) values depend on pile position within the group and pile spacing. The procedure follows the same approach used in the p-y method of analysis for single piles, except a multiplier, with a value less than one, is applied to the p-values of the single pile p-y curve. This reduces the ultimate soil resistance and softens the shape of the p-y curve. Because they are determined experimentally, the multipliers include both elasticity and shadowing effects.

The results from 11 experimental studies were reviewed in which p-multipliers for pile groups of different sizes and spacings were developed. In these studies, which include 29 separate tests, values of  $f_m$  were determined through a series of back-calculations using results from instrumented pile-groups and single pile load tests.

Group efficiency factors ( $G_e$ ) and p-y multipliers ( $f_m$ ) represent two approaches for quantifying group interaction effects. Because these approaches represent the same phenomenon, the factors listed above for empirically derived  $G_e$  values apply equally as well to the empirically derived  $f_m$  values. Three additional factors that are more specific to the  $f_m$  approach are:

1. **Row position.** The lateral capacity of a pile in a group is significantly affected by its row position (leading row, first trailing row, etc.) and the center to center pile

spacing. The leading row carries more load than subsequent rows; consequently, it has the highest multiplier. Multipliers decrease going from the leading to the trailing row, which has the lowest multiplier.

2. **Corner pile effects.** At spacings less than  $3D$ , the outer corner piles will take a greater share of load than interior piles, and consequently, will experience greater bending moments and stresses. Ignoring this behavior is unconservative, and could result in overstressed corner piles. Recommendations were presented for modifying bending moments computed for the corner piles if the spacing normal to the direction of load (side-by-side spacing) is less than  $3D$ .
3. **Depth.** Although a single value of  $f_m$  for all depths is commonly used for the sake of simplicity, it is possible to use values of  $f_m$  that vary with depth, to achieve improved agreement between computed and measured group response.

Design lines were developed for estimating pile group efficiency values and  $p$ -multipliers as functions of pile arrangement and pile spacing. The design lines are presented in chart form in Chapter 2.

These design lines represent state-of-the-art values for use in analysis and design of laterally loaded pile groups. The writer believes that these lines are suitable for all except the largest projects, where lateral load behavior of pile groups is an extremely critical issue. For projects where the expense can be justified, these lines can be verified or improved by performing on-site full-scale load tests on groups of instrumented piles.

## 8.2 FIELD LOAD TESTS

A field test facility was developed to perform full-scale lateral load tests on single piles, pile groups, and pile caps embedded in natural soil and backfilled with granular soil. The facility was designed specifically for this project to evaluate the lateral resistance provided by pile caps. The test facility is located at Virginia Tech's Kentland Farms, approximately 10 miles west of Blacksburg, Virginia. Test foundations that were constructed at the facility consisted of three groups of four piles each, one with a cap 18 inches deep and two with 36-inch-deep caps, two individual test piles, and an embedded bulkhead with no piles.

Details of the facility including the in-ground appurtenances, the loading equipment and connections that were used to apply horizontal compressive loads to the foundations, the instrumentation that was used for monitoring displacements and slopes of the single piles, pile caps, and bulkhead, and the data acquisition system are described in Chapter 4.

A total of thirty-one tests were performed at the facility using incremental, cyclic, and sustained loading procedures.

Results from the testing program clearly support the research hypothesis that pile caps provide significant resistance to lateral load. The pile caps that were tested in this study provided approximately 50 % of the overall lateral resistance of the pile group foundations.

The lateral resistance provided by a pile group/pile cap foundation depends on many interacting factors, which were isolated during this study to evaluate their significance. In order of importance, these are:

1. **Stiffness and density of soil in front of the cap.** The passive resistance that can be developed in front of a pile cap is directly related to the backfill strength. As



was demonstrated during the load tests, the lateral resistance increases as the stiffness and density of soil around the cap increases.

2. **Depth of cap embedment.** Increasing cap thickness or depth results in smaller lateral deflections.
3. **Rotational restraint at the pile head.** The rotational restraint available at the pile head can most often be described as a partially restrained condition. This condition results in response that falls between that of a fixed-head and free-head boundary condition. Response curves can be calculated using partially restrained boundary conditions by calculating, measuring, or estimating the rotational restraint,  $k_{mq}$ .
4. **Pile group axial capacity.** Lateral behavior of a pile group is directly related to the vertical or axial capacity of the piles. Pile groups comprised of longer piles (greater axial capacity) have significantly greater lateral resistance than groups with shorter piles. The rotation of the cap and the passive resistance developed in front of the cap are both affected by the axial capacity of the piles.
5. **Stiffness and density of soil around the piles.** Lateral load resistance increases as the stiffness and density of soil around the piles increase. The soil within the top 10 pile diameters has the greatest effect on lateral pile response.

6. **Cyclic and sustained loads.** For the conditions tested in this study, the effects from cyclically applied loads and long-term sustained loads were minor, or secondary, in comparison to the other factors described above. In other situations, such as high groundwater or soft compressible soils, the effect of cyclic loading or long term sustained loading could be more significant.

In conclusion, the load tests performed in this study clearly indicate that pile caps provide considerable resistance to lateral loads. The lateral resistance of a pile group is largely a function of the passive resistance developed by the cap and the rotational restraint of the pile-cap system. The passive resistance of the cap is controlled by the stiffness and density of the backfill soil and the interface friction angle. The rotational restraint is a function of the pile-to-cap connection and the axial capacity of the piles.

### 8.3 SOIL PARAMETERS

The natural soils encountered at the Kentland Farms field test site consisted of sandy clay, sandy silt, and silty sand with thin layers of gravel. Two soil types were used as backfill in the lateral load tests: a poorly graded fine sand (New Castle sand) and a well graded silty gravel (crusher run gravel). These materials were used because they are representative of the types of backfill materials often used for pile caps, footings, and other buried structures.

Various in situ techniques were used to determine soil stratification, shear strength, soil modulus, state of stress in the ground, and groundwater levels. The subsurface investigation included solid-stem auger borings with standard penetration tests, dilatometer soundings, groundwater piezometer installation, and backhoe test pits. Split spoon samples, Shelby tube samples, and hand-excavated block samples were obtained during the investigation for subsequent laboratory testing.

A comprehensive suite of laboratory tests were conducted on these materials to measure soil properties and to provide a basis for estimating the values of parameters that were used in the analyses. The laboratory testing program included soil classification, unit weight, strength (UU, CU, and CD triaxial tests), and consolidation. Parameters required for the pile group analyses included:  $\phi$ ,  $c$ ,  $\delta$ ,  $\alpha$ ,  $\nu$ ,  $E_i$ , and  $\gamma_m$ . The testing program and the measured values of these parameters are discussed in Chapter 5. Correlation charts and tables from published sources are provided in Chapter 7 for many of these parameters. The correlations are useful as a supplement to laboratory and in situ tests.

#### 8.4 ANALYTICAL METHOD

An analytical method was developed for evaluating the lateral response of pile groups with embedded caps. The approach involves creating p-y curves for single piles, pile groups, and pile caps using the computer spreadsheets *PYPILE* and *PYCAP*.

Single pile p-y curves are developed using Brinch Hansen's (1961) ultimate load theory for soils that possess both cohesion and friction. The approach is programmed in *PYPILE*, which can be used to calculate p-y curves for piles of any size, with soil properties that are constant or that vary with depth.

A method called the "group-equivalent pile" (abbreviated GEP) approach was developed for creating pile group and pile cap p-y curves in a way that is compatible with established approaches for analyzing laterally loaded piles. GEP p-y curves are obtained by multiplying the "p" values of the single pile p-y curves by a modification factor that accounts for reduced capacities caused by group interaction effects, and summing the modified p-values for all the piles in the group. The p-multiplier curves developed in Chapter 2 are used for this purpose. The pile group is modeled in the computer program *LPILE Plus 3.0* using these GEP p-y curves. The flexural resistance of the GEP pile is equal to the sum of the flexural resistances of all the piles in the group.

A rotationally restrained pile-head boundary condition can be modeled in the analysis. The rotational stiffness is estimated from the axial skin friction of the piles, the deflection required to mobilize skin friction, and the corresponding moment on the pile cap.

Pile cap resistance is included in the analysis using cap p-y curves. A method for calculating cap p-y curves was developed during this study, and has been programmed in the spreadsheet *PYCAP*. The approach models the passive earth pressures developed in front of the cap. The relationship between passive pressure and the cap deflection is represented by p-y curves developed using a hyperbolic formulation, which is defined by the ultimate passive force and the initial elastic stiffness of the embedded pile cap. The ultimate passive force is determined using the log spiral earth pressure theory in conjunction with Ovesen's (1964) three-dimensional correction factors.

The commercially available computer program *LPILE Plus 3.0* (Reese et al. 1997) was used in conjunction with the GEP approach to calculate load-deflection curves for the pile groups tested in this study, and for a load test described in the literature. Comparisons between measured and calculated load-deflection responses indicate that the analytical approach developed in this study is conservative, reasonably accurate, and suitable for use in design. Deviations between calculated and measured load-deflection values fall well within the practical range that can be expected for analyses of the lateral response of pile groups. This approach represents a significant improvement over current design practices, which often completely ignore the cap resistance.

The author believes it would be difficult to obtain more accurate estimates of pile group behavior, even with more complex analytical methods, because of the inevitable uncertainties and variations in soil conditions, unknown or uncontrollable construction factors, and the complex structural and material interactions that occur between the piles, pile cap, and soil.

## 8.5 RECOMMENDATIONS FOR FUTURE RESEARCH

The response of piles to lateral loading has been the focus of numerous analytical and experimental studies over the past 60 years. However, the response of the pile cap, and the interaction between the pile cap and the pile group have received little attention, in these studies. The results of this research project represent a significant initial contribution in the area of pile cap response to lateral loads. In addition, the analytical approach and computer program developed during this study are expected to be a valuable asset to practicing engineers. It is recommended that future research be conducted to support and refine the results of this study.

The following recommendations for future research include additional experimental studies, as well as advanced analytical and numerical studies.

1. Research is needed to investigate further the rotational stiffness concept that was used in this study. Additional experimental studies are needed to explore the relationship between pile skin friction and pile group rotational restraint. These studies should include the effect that the pile cap and the pile cap backfill conditions (soil type, density, and interface shear strength) have on rotational restraint. The geotechnical centrifuge may be a good tool for performing these studies, because it provides a relatively inexpensive means of varying test conditions. The experimental studies would be enhanced by finite element analyses to supplement interpretations based on direct observations.
2. The technique developed in this study for estimating the pile cap initial elastic stiffness could be further explored, and possibly improved, using finite element

analyses. Additional experimental work could be performed to verify the suitability of the analyses.

3. The concept of modifying the plane strain log spiral solution for three-dimensional effects was developed during this study. Three-dimensional modification factors were obtained from Ovesen's (1964) research on embedded anchor blocks. Additional research would be useful to refine the modification factors for different soil types, including cohesive soils and soils that have both cohesion and frictional shear strength components.
4. Little is known about the performance of pile caps during dynamic or vibratory loading. Research, including full-scale experimental studies, is needed in this area to evaluate the effect the pile cap has on the stiffness and lateral response of pile groups subjected to these types of loads.

## REFERENCES

- AASHTO (1994). "LRFD Bridge Design Specifications." American Association of State Highway and Transportation Officials, Washington, D.C.
- Adachi, T. and Kimura, M. (1994). "Analyses of ultimate behavior of lateral loading cast-in-place concrete piles by 3-dimensional elasto-plastic FEM." 8th Intl. Conf. on Computer Methods and Advances in Geomechanics, Morgantown, WV, 2279-2284.
- Adachi, T., Kimura, M., and Kobayashi, H. (1994). "Behavior of laterally loaded pile groups in dense sand." *Intl. Conf. Centrifuge 94*, Singapore, 509-514.
- Alizadeh, M., and Davisson, M. T. (1970). "Lateral load test on piles - Arkansas River Project." *ASCE J. of Geotechnical Engineering*, SM5, 1583-1603.
- Ashour, M., Pilling, P., Norris, G., and Perez, H. (1996). "Development of a strain wedge model program for pile group interference and pile cap contribution effects." *Report No. CCEER-94-4, Federal Study No. F94TL16C, FHWA/CA/TL-96/28*, Submitted to State of California Department of Transportation, Department of Civil Engineering, University of Nevada, Reno.
- Baguelin, F., and Frank, R. (1980). "Theoretical studies of piles using the finite element method." *Institution of Civil Engineers (ICE). Numerical Methods in Offshore Piling*, London, 83-91.
- Baguelin, F., Jezequel, J. F., and Meimon, Y. (1985). "Chargements lateraux sur un groupe des pieux (static and cyclic lateral loads on a pile group)." *Proceedings of the 11th International Conference on Soil mechanics and Foundation Engineering, Vol. 3*, Balkema, Rotterdam, The Netherlands, 1587-1588.
- Banerjee, P. K., and Davies, T. G. (1979). "Analysis of some reported case histories of laterally loaded pile groups." *Institution of Civil Engineers (ICE). Numerical Methods in Offshore Piling*, London, 83-90.
- Barton, Y. O. (1984). "Response of pile groups to lateral loading in the centrifuge." *Proceeding of a Symposium on the Application of Centrifuge Modeling to Geotechnical Design*, A.A. Balkema, Rotterdam, The Netherlands.
- Beatty, C. I. (1970). "Lateral test on pile groups." *Foundation Facts*, VI(1), 18-21.
- Bhushan, K., and Askari, S. (1984). "Lateral-load tests on drilled pier foundations for solar plant heliostats." *Laterally Loaded Deep Foundations: Analysis and Performance. American Society for Testing and Materials*, STP 835, 140-156.
- Blaney, G. W., and O'Neill, W. O. (1989). "Dynamic lateral response of a pile group in clay." *Geotechnical Testing Journal*, 22-29.

- Blaney, G. W., and O'Neill, W. O. (1991). "Procedures for prediction of dynamic lateral pile group response in clay from single pile tests." *Geotechnical Testing Journal*, 3-12.
- Bogard, D., and Matlock, H. (1983). "Procedures for analysis of laterally loaded pile groups in soft clay." *Proceedings, Specialty Conf. of Geotechnical Engineering in Offshore Practice*, ASCE, 499-535.
- Bowles, J. E. (1982). *Foundation Analysis and Design*, McGraw-Hill Book Company, New York, NY.
- Broms, B. B. (1964a). "Lateral resistance of piles in cohesionless soils." *ASCE Journal of the Soil Mechanics and Foundation Division Proceedings (JSMFD)*, 90(SM3), 123-156.
- Broms, B. B. (1964b). "Lateral Resistance of Piles in Cohesive Soils." *ASCE Journal of the Soil Mechanics and Foundation Division Proceedings (JSMFD)*, 90(SM2), 27-63.
- Brown, D. A., and Bollman, H. T. (1991). "Pile-supported bridge foundations designed for impact loading." *Transportation Research Record*, Report No. 1331, Washington D.C. 87-91.
- Brown, D. A., Morrison, C., and Reese, L. C. (1988). "Lateral load behaviour of pile group in sand." *ASCE Journal of Geotechnical Engineering*, 114(11), 1261-1276.
- Brown, D. A., and Reese, L. C. (1985). "Behavior of a large-scale pile group subjected to cyclic lateral loading." Report to the Minerals Management Services, U.S. Dept. of Interior, Reston, VA. Dept. of Research, FHWA, Washington DC and U.S. Army Engineer Waterways Experiment Station, Vicksburg, Mississippi.
- Brown, D. A., Reese, L. C., and O'Neill, M. W. (1987). "Cyclic lateral loading of a large-scale pile group." *ASCE Journal of Geotechnical Engineering*, 113(11), 1326-1343.
- Brown, D. A., and Shie, C. F. (1991). "Modification of p-y curves to account for group effects on laterally loaded piles." *Geotechnical Engineering Congress*, (G.S.P. No. 27), 479-490.
- Caquot, A. I., and Kerisel, J. (1948). "Tables for the calculation of passive pressure, active pressure and bearing capacity of foundations." Libraire du Bureau des Longitudes, de L'ecole Polytechnique, Paris Gauthier-villars, Imprimeur-Editeur, 120.
- Chen, L. T., Poulos, H. G., and Hull, T. S. (1996). "Model tests on pile groups subjected to lateral soil movement." *Research Report No. R729*, Univ. of Sydney, Dept. of CE.
- Clark, J. I., Mckeown, S., Lester, W. B., and Eibner, L. J. (1985). "The lateral load capacity of large diameter concrete piles." *38th Canadian Geotechnical Conference, Theory and Practice in Foundation Engineering*, Bolton, England.
- Clark, J. L. (1973). "Behavior and design of pile caps with four piles." *Technical Report for the Portland Cement Association*, UDC 624.154.155.



- Clemente, J. L., and Sayed, S. M. (1991). "Group efficiency of piles driven into sands: a simple approach." *Geotechnical Engineering Congress*, (G.S.P. No. 27), 346-355.
- Clough, G. W., and Duncan, J. M. (1971). "Finite element analyses of retaining wall behavior." *ASCE Journal of the Soil Mechanics and Foundations Division*, 97(SM12), 1657-1672.
- COM624 (1993). "Laterally loaded pile analysis program for the microcomputer." *FHWA-SA-91-048*, Computer program documentation, by S. T. Wang and L. C. Reese.
- Cox, W. R., Dixon, D. A., and Murphy, B. S. (1984). "Lateral-load tests on 25.4-mm (1-in.) diameter piles in very soft clay in side-by-side and in-line groups." *Laterally Loaded Deep Foundations: Analysis and Performance*, ASTM STP 835, 122-139.
- Davisson, M. T. (1975). "Pile load capacity." *Design Construction and Performance of Deep Foundations*, San Francisco, CA, 1-49.
- Davisson, M. T., and Salley, J. R. (1970). "Model study of laterally loaded piles." *ASCE Journal of the Soil Mechanics and Foundations Division*, 96(SM5), 1605-1627.
- Desai, C. S., and Kuppusamy, T. (1980). "Application of a numerical procedure for laterally loaded structures." *Institution of Civil Engineers (ICE). Numerical Methods in Offshore Piling*, London, 93 - 99.
- Douglas, D. J., and Davis, E. H. (1964). "The movements of buried footings due to moment and horizontal load and the movement of anchor plates." *Geotechnique*, 14(2), 115-132.
- Duncan, J. M., Byrne, P., Wong, K. S., and Mabry, P. (1980). "Strength, stress-strain and bulk modulus parameters for finite element analysis of stress and movements in soil masses." *UCB/GT/80-01*, College of California, Berkeley, California.
- Duncan, J. M., and Chang, C. Y. (1970). "Nonlinear analysis of stress and strain in soils." *Journal of the Soil Mechanics and Foundations Division ASCE*, 96(SM5), 1629-1653.
- Duncan, J. M., Evans, L. T., and Ooi, P. S. (1994). "Lateral load analysis of single piles and drilled shafts." *ASCE Journal of Geotechnical Engineering*, 120(6), 1018-1033.
- Dunnavant, T. W., and O'Neill, M. W. (1986). "Evaluation of design-oriented methods for analysis of vertical pile groups subjected to lateral load." *Numerical Methods in Offshore Piling*, Inst. Francais du Petrole, Laboratoire Central des ponts et Chaussées, 303-316.
- Esrig, M. E., and Kirby, R. C. (1979). "Advances in general effective stress method for the prediction of axial capacity for driven piles in clay." *11th Annual Offshore Technology Conference*, Houston, Texas, 437-449.

- Evans, L. T., and Duncan, J. M. (1982). "Simplified analysis of laterally loaded piles." *UCB/GT/82-04*, University of California Berkely.
- Feagin, L. B. (1937). "Lateral pile-loading tests." *Transactions*, ASCE, Vol. 102, 236-254.
- Feagin, L. B. (1948). "Performance of pile foundations of navigation locks and dams on the upper Mississippi River." *Proceedings of the Second International Conference on Soil Mechanics and Foundation Engineering, Vol. IV*, Rotterdam, 98-106.
- Feagin, L. B. (1953). "Lateral load tests on groups of battered and vertical piles." *Symposium on Lateral Load Tests on Piles*, ASTM Special Publication (154), 12-29.
- Florida Pier (1998). "User's manual for Florida Pier." NT Version 1.27, Prepared by the Department of Civil Engineering, University of Florida, Gainesville, Florida.
- Focht, J. A., and Koch, K. J. (1973). "Rational analysis of the lateral performance of offshore pile groups." *Fifth Annual Offshore Technology Conference*, Houston, Texas, 701-708.
- Franke, E. (1988). "Group action between vertical piles under horizontal loads." W.F. Van Impe, ed., A.A. Balkema, Rotterdam, The Netherlands, p. 83 - 93.
- Gabr, M. A., Lunne, T., and Powell, J. J. (1994). "p-y analysis of laterally loaded piles in clay using DMT." *ASCE Journal of Geotechnical Engineering*, 120(5), 816-837.
- Gandhi, S. R., and Selvam, S. (1997). "Group effect on driven piles under lateral load." *ASCE Journal of Geotechnical and Geoenvironmental Engineering*, 123(8), 702-709.
- Garassino, A. (1994). "Some developments on laterally loaded piles with particular reference to p-y subgrade reaction method." *Proceedings of the 4th International Conference on Piling and Deep Foundations*, A.A. Balkema, Rotterdam, The Netherlands, 759-770.
- Gardner, W. S. (1975). "Considerations in the design of drilled piers." *Design Construction and Performance of Deep Foundations*, San Francisco, CA, 1-32.
- Georgiadis, M. and Butterfield, R. (1982). "Laterally loaded pile behavior." *ASCE Journal of the Geotechnical Engineering Division*, 108(GT1).
- Gill, H. L. and Demars, K. R. (1970). "Displacement of Laterally Loaded Structures in Nonlinearly Responsive Soil." Technical Report R-670, U.S. Naval Civil Engineering Laboratory, California.
- Gleser, S. M. (1953). "Discussion to lateral load tests on groups of battered and vertical piles by L.B. Feagin." *Symposium on Lateral Load Tests on Piles*, ASTM Special Publication (154), 21-29.

- Gleser, S. M. (1984). "Generalized behavior of laterally loaded vertical piles." *Laterally Loaded Deep Foundations: Analysis and Performance*. ASTM STP 835. *American Society for Testing and Materials*, 72-96.
- GROUP (1996). "A program for the analysis of a group of piles subjected to axial and lateral loading." Version 4.0, by Lymon Reese, Shin Tower Wang, Jose A. Arellaga, and Joe Hendrix. ENSOFT, Inc., Austin, Texas.
- Hansen, B. (1961). "The ultimate resistance of rigid piles against transversal forces." *Bulletin No. 12*, Danish Geotechnical Institute, Copenhagen.
- Hariharan, M., and Kumarasamy, K. (1982). "Analysis of pile groups subjected to lateral loads." *Proceedings of the International Conf. on the Behavior of Off-Shore Structures, V. 2*, Trondheim, Norway: Norwegian Institute of Technology, 383-390.
- Helmers, M. J., Duncan, J. M., and Filz, G. M. (1997). "Use of ultimate load theories for design of drilled shaft sound wall foundations." The Charles E. Via, Jr. Department of Civil Engineering, Virginia Tech, Blacksburg, VA.
- Hetenyi, M. (1946). *Beams on Elastic Foundation*, The University of Michigan Press, Ann Arbor, Michigan.
- Hoit, M., Hays, C., and McVay, M. (1997). "Florida pier. Methods and models for pier analysis and design." *Transportation Research Board*, TRB 97-0554, 76th Meeting.
- Holloway, D. M., Moriwaki, Y., Stevens, J. B., and Perez, J. Y. (1981). "Response of a pile group to combined axial and lateral loading." *International Conference on Soil Mechanics and Foundation Eng.*
- Horvath, J. S. (1984). "Simplified elastic continuum applied to the laterally loaded pile problem - part 1: theory." *Laterally Loaded Deep Foundations: Analysis and Performance*, *American Society for Testing and Materials*, 112-121.
- Hughes, J. M., Fendall, H. D., and Goldsmith, P. R. (1980). "Model pile groups subject to lateral loading." *Australia-New Zealand Conference on Geomechanics*.
- Iyer, P. K., and Sam, C. (1991). "3-D elastic analysis of three-pile caps." *Journal of Engineering Mechanics*, 117(12).
- Jamiolkowski, M., and Garassino, A. (1977). "Soil modulus for laterally loaded piles." *Proceedings of the IX International Conf. on Soil Mechanics and Foundation Engineering*, Tokyo, Japan.
- Johnson, S. S. (1993). "Geologic Map of Virginia - Expanded Explanation." *Virginia Division of Mineral Resources*, Charlottesville, Virginia.

- Kim, J. B. (1984). "Pile caps subjected to lateral loads." *Analysis and Design of Pile Foundations*, ASCE symposium proceedings, Geotechnical Engineering Division, ASCE National Convention, San Francisco, California.
- Kim, J. B., Kindia, C. H., and Bhattacharya, S. (1969). "Lateral stability of pile groups." *69-1*, Bucknell University, Lewisburg, PA.
- Kim, J. B., and Singh, L. P. (1974). "Effect of pile cap - soil interaction on lateral capacity of pile groups," Master of Science, Bucknell University, Lewisburg, PA.
- Kim, J. B., Singh, L. P., and Brungraber, R. J. (1979). "Pile cap soil interaction from full-scale lateral load tests." *ASCE Journal of Geotechnical Engineering*, 105(5), 643-653.
- Kimura, M., Adachi, T., Kamei, H., and Zhang, F. (1995). "3-D finite element analyses of the ultimate behavior of laterally loaded cast-in-place concrete piles." *5th Intl. Symposium on Numerical Models in Geomechanics*, 589-594.
- Kishida, H., and Nakai, S. (1977). "Large deflection of a single pile under horizontal load." *Proceedings of the IX International Conf. on Soil Mechanics and Foundation Engineering*, Tokyo, Japan, 87-92.
- Kondner, R. L. (1963). "Hyperbolic stress-strain response: cohesive soils." *ASCE Proceedings of the Soil Mechanics and Foundation Division*, 89(SM1), 115-143.
- Kotthaus, M., Grundhoff, T., and Jessberger, H. L. (1994). "Single piles and pile rows subjected to static and dynamic lateral load." *Centrifuge 94*, editors: Leung, Lee and Tan, Balkema, Rotterdam, The Netherlands, 497-502.
- Kulhawy, F. H. (1984). "Limiting tip and side resistance." *Analysis and Design of Pile Foundations*, ASCE National Convention, San Francisco, CA, 80-98.
- Lieng, J. T. (1989). "A model for group behavior of laterally loaded piles." *Offshore Technology Conference*, Houston, TX, 377-394.
- Liu, J. L. (1991). "Comprehensive effect coefficients calculating method for lateral bearing capacity of pile groups." *Asian Regional Conference on Soil Mechanics and Foundation Engineering*, 247-250.
- LPILE (1997). "A program for the analysis of piles and drilled shafts under lateral loads." by Lymon Reese, Shin Tower Wang, Jose A. Arrellaga, and Joe Hendrix, ENSOFT, Inc., Houston, TX.
- Matlock, H. (1970). "Correlations for design of laterally loaded piles in soft clay." *Proceedings, Offshore Technology Conference, Vol. I, Paper No. 1204*, Houston, Texas, 577-594.

- Matlock, H., Ingram, W. B., Kelley, A. E., and Bogard, D. (1980). "Field tests of the lateral-load behavior of pile groups in soft clay." *12th Offshore Technology Conference, Vol. IV*, Houston, TX, 163-174.
- Matlock, H., and Reese, L. C. (1960). "Generalized solutions for laterally loaded piles." *ASCE Journal of Soil Mechanics and Foundations Division*, 86(SM5), 63-91.
- Matlock, H., and Reese, L. C. (1961). "Foundation analysis of offshore pile supported structures." *Proceedings of the 5th International Conference on Soil Mechanics and Foundation Engineering*, Paris, France.
- McClelland, B., and Focht, J. A. (1956). "Soil Modulus for laterally loaded piles." *Journal of the Soil Mechanics and Foundation Division*, Proceedings Paper (101), 1049-1063.
- McVay, M., Bloomquist, D., Vanderlinde, D., and Clausen, J. (1994). "Centrifuge modeling of laterally loaded pile groups in sands." *ASTM Geotechnical Testing Journal*, 17, 129-137.
- McVay, M., Casper, R., and Shang, T. (1995). "Lateral response of three-row groups in loose to dense sands at 3D and 5D pile spacing." *ASCE Journal of Geotechnical Engineering*, 121(5), 436-441.
- McVay, M., Zhang, L., Molnit, T., and Lai, P. (1997). "Centrifuge testing of large laterally loaded pile groups in sands." *ASCE Journal of Geotechnical and Geoenvironmental Engineering*, 124(10), 1016 - 1026.
- Meimon, Y., Baguelin, F., and Jezequel, J. F. (1986). "Pile group behaviour under long time lateral monotonic and cyclic loading." *Proceedings of the 3rd International Conference on Numerical Methods on Offshore Piling*, Inst. Francais Du Petrole, Nantes, France, 285-302.
- Meyerhof, G. G. (1976). "Bearing capacity and settlement of pile foundations." *ASCE Journal of the Geotechnical Engineering Division*, 102(GT3), 196-228.
- Mokwa, R. L., Duncan, J. M., and Helmers, M. J. (1997). "Deflections and bending moments in drilled shaft sound wall foundations under working load conditions." The Charles E. Via, Jr. Department of Civil Engineering, Virginia Tech, Blacksburg, VA.
- Morrison, C., and Reese, L. C. (1986). "A lateral-load test of full-scale pile group in sand." *GR86-1*, FHWA, Washington D.C.
- Najjar, Y. M., and Zaman, M. M. (1988). "Effect of loading sequence and soil non-linearity on the response of a pile group foundation using a three-dimensional finite element analysis." *Numerical Methods in Geomechanics*, Innsbruck, 1127-1135.
- Narasimha, R. (1995). "Behavior of pile supported dolphins in marine clay under lateral loading."

- NAVFAC (1982). "Foundations and earth structures design manual 7.2." Dept. of the Navy, Naval Facilities Engineering Command, Alexandria, VA.
- Nordlund, R. L. (1963). "Bearing capacity of piles in cohesionless soils." *ASCE Soil Mechanics and Foundation Journal*, SM(3).
- Nottingham, L., and Schmertmann, J. (1975). "An investigation of pile capacity design procedures." Final Report D629 to FDOT from the Dept. of Civil Engineering, Univ. of Florida, September, 159.
- Novak, M. (1980). "Soil-pile interaction under dynamic loads." *Institution of Civil Engineers (ICE). Numerical Methods in Offshore Piling*, London, 59-68.
- Novak, M., and Janes, M. (1989). "Dynamic and static response of pile groups." *XII ICSMFE*, 1175-1178.
- Ochoa, M., and O'Neill, W. (1989). "Lateral pile interaction factors in submerged sand." *ASCE Journal of Geotechnical Engineering*, 115(3), 359-378.
- O'Halloran, J. (1953). "The lateral load capacity of timber pile groups." No. 154, ASTM Special Publication.
- O'Neill, M. (1991). "Construction practices and defects in drilled shafts." *Transportation Research Record, TRB, National Research Council*, Report No. 1331 Washington D.C.
- O'Neill, M. W. (1983). "Group action in offshore piles." *Proc. Specialty Conference on Geotechnical Eng. in Offshore Practice, ASCE*, Houston, TX, 25-64.
- O'Neill, M. W., Ghazzaly, O. I., and Ha, H. B. (1977). "Analysis of three-dimensional pile groups with non-linear soil response and pile-soil-pile interaction." *Proceedings of the 9th Offshore Technology Conference, Vol. II*, Houston, TX.
- O'Neill, M. W., Reese, L. C., and Cox, W. R. (1990). "Soil behavior for piles under lateral loading." *22nd Annual Offshore Technology Conf.*, Houston, TX, 279-287.
- Ooi, P. S., and Duncan, J. M. (1994). "Lateral load analysis of groups of piles and drilled shafts." *ASCE Journal of Geotechnical Engineering*, 120(6), 1034-1050.
- Oteo, C. S. (1977). "Horizontally loaded piles. Deformation influence." *Proceedings of the IX International Conf. on Soil Mechanics and Foundation Engineering*, Tokyo, Japan, 101-106.
- Ovesen, N. K. (1964). "Anchor slabs, calculation methods and model tests." *Bulletin No. 16*, The Danish Geotechnical Institute, Copenhagen.
- Paduana, J., and Yee, W. S. (1974). "Lateral load tests on piles in bridge embankment." *Transportation Research Record, Transportation Research Board, National Research Council, No. 517*, 77-92.

- Potyondy, J. G. (1961). "Skin friction between various soils and construction materials." *Geotechnique*, 11(1), 339-353.
- Poulos, H. G. (1971a). "Behavior of laterally loaded piles: Part I-single piles." *ASCE Journal of the Soil Mechanics and Foundations Division*, 97(SM5), 711-731.
- Poulos, H. G. (1971b). "Behavior of laterally loaded piles: Part II - group piles." *ASCE Journal of the Soil Mechanics and Foundations Division*, 97(SM5), 733-751.
- Poulos, H. G. (1980). "Comparisons between theoretical and observed behavior of pile foundations." *Australia-New Zealand Conference on Geomechanics*, 95-104.
- Poulos, H. G. (1981). "Behavior of single piles subjected to cyclic lateral loads." Report No. R385, School of Civil Engineering, Univ. of Sydney, Australia.
- Poulos, H. G., and Davis, E. H. (1980). *Pile Foundation Analysis and Design*, John Wiley and Sons, New York.
- Poulos, H. G., and Lee, C. Y. (1989). "Behavior of grouted piles in offshore calcareous sand." *12th International Conf. on Soil Mechanics and Foundation Engineering*, Rio de Janeiro, 955-958.
- Prakash, S. (1962). "Behavior of pile groups subjected to lateral loads," Doctor of Philosophy, University of Illinois, at Urbana, IL.
- Prakash, S., and Saran, D. (1967). "Behavior of laterally loaded piles in cohesive soils." *Proceedings, Third Asian Conference on Soil Mechanics*, 235-238.
- Prakash, S., and Sharma, H. D. (1990). *Pile Foundations in Engineering Practice*, John Wiley and Sons, New York.
- Randolph, M. F. (1981). "The response of flexible piles to lateral loading." *Geotechnique*, 31(2), 247-259.
- Rao, S. N., Ramakrishna, V. G., and Raju, G. B. (1996). "Behavior of pile-supported dolphins in marine clay under lateral loading." *ASCE Journal of Geotechnical Engineering*, 122(8), 607-612.
- Reddy, J. N. (1993). *An Introduction to the Finite Element Method, 2nd edition*, McGraw-Hill, Inc., NY.
- Reese, L. C. (1977). "Laterally loaded piles: program documentation." *ASCE Journal of Geotechnical Engineering*, 103(GT4), 287-305.
- Reese, L. C., and Allen, J. D. (1977). "Drilled shaft design and construction guidelines manual, vol.2. structural analysis and design for lateral loading." U.S. Department of Transportation, FHWA, Office of Research and Development.

- Reese, L. C., Cox, W. R., and Koop, F. D. (1974). "Analysis of laterally loaded piles in sand." *Offshore Technology Conference*, Vol. II, Paper No. 2080, Houston, Texas, 473-484.
- Reese, L. C., and Sullivan, W. R. (1980). "Documentation of computer program COM624." University of Texas, Austin, TX.
- Reese, L. C., and Wang, S. T. (1997). "LPILE Plus 3.0 Technical manual of documentation of computer program." Ensoft, Inc., Austin, Texas.
- Reese, L. C., and Welch, R. C. (1975). "Lateral loading of deep foundations in stiff clay." *Journal of the Geotechnical Engineering Division, ASCE*, 101(GT7), 633-649.
- Robertson, P. K., and Campanella, R. G. (1985). "Design of axially loaded and laterally loaded piles using in-situ tests: A case history." *Soil Mechanics Series No. 86*, Dept. of Civil Engineering, University of B.C., Vancouver, Canada.
- Rollins, M., K., Weaver, T. J., and Peterson, K. T. (1997). "Statnamic lateral load testing of a full-scale fixed-head pile group." *Report*, UDOT, FHWA.
- Rollins, K. P., Peterson, K. T., and Weaver, T., J. (1998). "Lateral Load Behavior of Full-Scale Pile Group in Clay." *ASCE Journal of Geotechnical and Geoenvironmental Engineering*, 124(6), 468-478.
- Ruesta, P. F., and Townsend, F. C. (1997). "Evaluation of laterally loaded pile group." *ASCE Journal of Geotechnical and Geoenvironmental Engineering*, 123(12), 1153-1174.
- Sarsby, R. W. (1985). "The behavior of model pile groups subjected to lateral loads." *38th Canadian Geotechnical Conference, Theory and Practice in Foundation Engineering*, Bolton, England.
- Schmertmann, J. H. (1986). "Suggested method for performing the flat dilatometer test." *Geotechnical Testing Journal*, 9(2), 93-101.
- Schmertmann, J. H. (1988). "Guidelines for using the CPT, CPTU, and Marchetti DMT for geotechnical design, Volume III (of IV) - DMT test methods and data reduction." Report Number FHWA PA 87-024-84-24.
- Schmidt, H. G. (1981). "Group action of laterally loaded bored piles." *Proceedings of the 10th International Conference on Soil Mechanics and Foundation Eng.*, Vol. 10 (2), Stockholm, Sweden, 833-838.
- Schmidt, H. G. (1985). "Horizontal load tests on files of large diameter bored piles." *Proceedings of the Eleventh International Conference on Soil Mechanics and Foundation Engineering*, Vol. 3, San Francisco, CA, 1569-1573.
- Schofield, A. N. (1980). "Cambridge geotechnical centrifuge operations." *Geotechnique*, 30(3), 227-268.



- Selby, A. G., and Poulos, H. G. (1984). "Lateral load tests on model pile groups." *Australia-New Zealand Conference on Geomechanics*, 154-158.
- Shibata, T., Yashima, A., and Kimura, M. (1989). "Model tests and analyses of laterally loaded pile groups." *Soils and Foundations*, 29(1), 31-44.
- Singh, A., Hu, R. E., and Cousineau, R. D. (1971). "Lateral load capacity of piles in sand and normally consolidated clay." *ASCE Engineer's Notebook*. August.
- Singh, A., and Prakash, S. (1971). "Model pile group subjected to cyclic lateral load." *Soils and Foundations*, 11(2), 51-60.
- Sogge, R. L. (1984). "Microcomputer analysis of laterally loaded piles." *ASTM STP 835, American Society for Testing and Materials*, 35-48.
- SPILE (1993). "A microcomputer program for determining ultimate vertical static pile capacity - users manual." by Alfredo Urzua, U.S. Dept. of Transportation, FHWA-SA-92-044, June, 43 pages.
- Stose, G. W. (1913). "The Cambro-Ordovician limestone of the Appalachian Valley in Southern Pennsylvania." *Journal of Geology*, 16, 698-714.
- Tamura, A., Sunami, S., Ozawa, Y., and Murakami, S. (1982). "Reduction in horizontal bearing capacity of pile group." *Proceedings of the Fourth International Conference on Numerical Methods in Geomechanics*, Edmonton, Canada, 865-874.
- Terzaghi, K. (1932). "Record earth-pressure testing machine." *Engineering News Record*, 109, September, 365-369.
- Terzaghi, K. (1934). "Large retaining wall tests. Part V. Pressure of glacial till." *Engineering News Record*, III, 503-508.
- Terzaghi, K. (1934a). "Large retaining wall tests. Part I. Pressure of dry sand." *Engineering News Record*, February, 136-140.
- Terzaghi, K. (1955). "Evaluation of coefficient of subgrade reaction." *Geotechnique*, 5(4), 297-326.
- Tomlinson, M. J. (1987). "Pile Design and Construction." *Viewpoint Publication*, 415 pages.
- Tshebotarioff, G. P. (1953). "The resistance to lateral forces of single piles and pile groups." *ASTM STP 154, American Society for Testing and Materials*, 38 pages.
- Vijayvergiya, V. N., and Focht, J. A. (1972). "A new way to predict the capacity of piles in clay." *4th Annual Offshore Technology Conference*, Houston, Texas, Vol. 2, 865-874.

- Wen, R. K. (1955). "Model studies of laterally loaded pile foundations." *Proceedings of the U.S. National Research Council Highway Research Board Annual Meeting*, 104-152.
- Zafir, Z., and Vanderpool, W. E. (1998). "Lateral response of large diameter drilled shafts: I-15/US 95 load test program." *Proceedings of the 33rd Engineering Geology and Geotechnical Engineering Symposium*, University of Nevada, Reno, 161-176.
- Zhang, L., and Hu, T. (1991). "Modeling of residual stresses of large piles in centrifuge." *Centrifuge 91*, Balkema, Rotterdam, The Netherlands, 237-243.

**APPENDIX A**  
**LITERATURE REVIEW TABLES**

Table A.1. Summary of pile group lateral load tests.

Reference	Lateral Load Test Description	Foundation Soil	Principal Findings
Feagin, L.B. (1937) and Feagin, L.B. (1948) and Feagin, L.B. (1953) and Gleser, S.M. (1953)	Conducted <b>full-scale field tests</b> on pile-supported locks and dams at locations along the Mississippi River. Tested groups of 14-in.-dia. timber piles driven vertically and battered at 3D to 4D spacing. Vertical piles were driven 30 ft and pile heads were constrained with concrete caps.	fine to coarse sand with occasional gravel	Observed that lateral movements of large pile groups is greater than that indicated by equivalent load tests on individual piles. Determined that groups combining both vertical and battered piles were more resistant than groups containing only vertical piles. The resistance increased as batter ratio increased. The greatest resistance was measured when vertical and lateral loads were combined, with the direction of lateral load the same as the direction of batter.
O'Halloran, J. (1953)	Conducted <b>full-scale field tests</b> (in 1928) on 2 pile groups in conjunction with the Anglo-Canadian Pulp and Paper Mill Project on the St. Charles River in Quebec City, Canada. The groups consisted of 4 fixed-head, 13 to 16-in.-dia., 21-ft-long timber piles.	sand fill, no strength data available	This constitutes one of the oldest group load tests on record. Group interaction effects were only qualitatively considered in the tests. The author and reviewers were surprised at the uncharacteristically high resistance of the 4-pile group, based on the load per pile in the group. They neglected passive resistance of the embedded 4-ft-deep pile cap.
Tschebotarioff, G.P. (1953)	Conducted <b>1g model tests</b> on 3-pile and 7-pile groups using 2-in.-dia., 29-in.-long wood piles, battered at 5 to 10 degrees.	14 in of well-graded fine sand underlain by 15 in of very soft silty clay	Determined that the magnitude and nature of stresses in a laterally loaded pile are related to the pile location within a group and the size of the group. Concluded that more experimental and analytical work is needed in this area.

Table A.1. Continued.

Reference	Lateral Load Test Description	Foundation Soil	Principal Findings
Wen, R.K. (1955)	Conducted <b>1g model tests</b> using three 45-in-long, 1.5 –in-square, white oak timber piles.	dry sand placed in a 2.5 by 6 by 4 ft deep wood tank	Observed that at high lateral loads, the front piles took the greatest portion of load and were the most severely stressed by bending.
Prakash, S. Saran, D. (1967)	Conducted <b>1g model tests</b> on 4-pile and 9-pile groups at spacings ranging from 3D to 5D. Model piles were 9-mm-dia., 11.4-in-long aluminum tubes. Pile heads were constrained by a 1-in-thick concrete pile cap. Test tank size was 10 by 6 by 12 in deep.	cohesive soil (ML) placed by dropping from a height of 4 ft, piles were pushed into tank	Determined that as pile spacing decreases in the direction of load, group rotation and deflection increases. Concluded that pile group effects vanish at spacings exceeding 6 pile diameters.
Alizadeh, M. Davisson, M.T. (1970)	Conducted 37 <b>full-scale field tests</b> in conjunction with the Arkansas River Navigation Project at Lock and Dam 1, 3, and 4 in the Arkansas River Valley. A variety of pile types including timber, prestressed concrete, steel pipe, and steel H-piles were tested free-headed.	alluvial soils consisting of fine sand and silty sand	Determined that a reasonable approximation can be obtained by assuming a triangular variation of the horizontal subgrade modulus ( $n_h$ ) with depth. Determined that $n_h$ is insensitive to deflections for deflections > 0.25 in, and strongly dependent on deflections when deflections are < 0.25 in. Small changes in $D_r$ can cause large changes in $n_h$ .

Table A.1. Continued.

Reference	Lateral Load Test Description	Foundation Soil	Principal Findings
Davisson, M.T. Salley, J.R. (1970)	Conducted <b>1g model tests</b> in conjunction with the Arkansas River Navigation Project on vertical and battered fixed-headed piles fabricated from 0.5-inch-O.D. aluminum tubing. Tested a 6-pile group constrained at the top by a cap, 2 scaled model lock walls supported on piles, and 3 scaled model dam monoliths supported on battered piles.	sand in a 4 by 4 by 4-ft.-deep tank, piles were embedded 21 in	Examined a variety of pile spacings. Determined that group effects decreased the effective value of the coefficient of subgrade reaction, $n_h$ , and increased the relative stiffness factor, $T$ . Measured normalized $T$ values of 1.25 at 4D spacing and 1.30 at 3D spacing. Observed that, in general, cyclic loading caused deflections to approximately double.
Singh, A. Prakash, S. (1971)	Conducted <b>1g model tests</b> on 4-pile groups spaced at 4D. Model piles were 0.5-in-square aluminum tubes, 24-in-long. Conditions of free rotation and no rotation were imposed at the pile heads. The model tank size was 47 by 47 by 47 in deep.	clean sand, $D_r=80\%$ and $\phi=46^\circ$	Determined that cyclic response of the 4-pile group was similar to the individual pile in terms of pile head deflection. However, piles in the group were observed to be more sensitive to changes in moment than the single pile. Restraining the cap from rotation reduced the percentage increase in deflections and moments caused by cyclic loading. Applying a vertical load to the pile group did not effect the lateral behavior.

Table A.1. Continued.

Reference	Lateral Load Test Description	Foundation Soil	Principal Findings
Kim, J.B. Singh, L.P. Brungraber, R.J. (1979)	Conducted <b>full-scale field tests</b> on three groups of fixed-headed 10BP42 piles at 4.8D and 3.6D c/c spacings. Two groups were vertical and one group contained battered piles. The pile cap was constructed on the ground surface, with its soffit in contact with the soil.	Piles were driven to refusal through 40 ft of uniform clay to fractured limestone.	Measured lateral group efficiencies ( $G_e$ ) greater than unity. $G_e$ was determined by comparing the response of a single isolated free-headed pile with an individual fixed-headed pile from a group. Attributed $G_e$ 's greater than 1 to double curvature bending caused by the restraint of the pile cap. They found that as the load increased to the yield load, $G_e$ decreased and approached unity. Determined that cap soil contact can have a significant effect on the resistance to lateral loads. Determined that when more than half of the piles are battered the cap soil contact has very little effect.
Hughes, J.M. Fendall, H.D. Goldsmith, P.R. (1980)	Conducted <b>1 g model tests</b> on two in-line 0.8 by 0.8 in square steel piles with pinned-head connections.	dry sand placed by pluviation and vibra-compaction	Used photogrammetric and radiographic techniques to observe sand movements around driven piles. Observed movement in sand grains up to 6D from pile centerline during driving. Determined that the method of sand placement has a substantial effect on stiffness, ... <i>continued</i> .

Table A.1. Continued.

Reference	Lateral Load Test Description	Foundation Soil	Principal Findings
Hughes, J.M. (1980) <i>continued</i>	<i>continued from previous page</i>		...even if densities are the same. The front pile took more load than the rear, up to a spacing of 13D. Observed that elastic continuum methods were less than adequate in predicting the soil interaction effects that were measured during the experiments.
Matlock, H. Ingram, W.B. Kelley, A.E. Bogard, D. (1980)	Conducted <b>full-scale field tests</b> on 5- and 10-pile circular groups of 6-inch-diameter free-headed pipe piles, spaced at 3.4D and 1.8D, respectively.	soft to very soft clay	Measured static deflections of the 5-pile group (3.4D spacing) were twice the single-pile values, and those for the 10-pile group (1.8D spacing) were 3 times as great. However, variations in measured bending moments were generally less than 10 % and rarely exceeded 20 %. Group effects measured during cyclic loading were substantially reduced from static values.
Holloway, D.M. Moriwaki, Y. Perez, J.Y. (1981)	Conducted <b>full-scale field tests</b> on a 2 by 4 group of 14-inch-diameter fixed-headed timber piles spaced at 2.6D c/c. Piles driven 35 feet into a very dense alluvial outwash deposit.	alluvial soils overlying limestone bedrock	Observed a failure mechanism described as the leading piles “punching” into the soil, while the trailing pile response was altered as the soil mass within the group “tracked” the leading piles. Strain gage data indicated that a significantly larger portion of the shear force was transferred to the leading row of piles compared to the trailing row of piles.



Table A.1. Continued.

Reference	Lateral Load Test Description	Foundation Soil	Principal Findings
Schmidt, H.G. (1981) and Schmidt, H.G. (1985)	Conducted <b>full-scale field tests</b> on bored piles (concrete drilled shafts). Measured the lateral resistance of in-line (pile files) 47-in-diameter bored piles at spacings of 2D, 2.2D and 3D. Shafts were tested free-headed with bore lengths of 28 feet.	uniform medium-dense sand above the water table	Concluded that group action (for pile files) was negligible at spacing of 3D or greater. At spacing less than 3D the leading pile behaves as an isolated pile and the middle and trailing pile behaviors coincide. Minimum $G_c$ 's of 0.75 to 0.8 were measured at a spacing of 2D. Determined that bending moments were generally the same regardless of pile location or pile spacing.
Barton, Y. O. (1984)	Conducted <b>centrifuge tests</b> on groups of 2, 3, and 6 piles at accelerations ranging from 30g to 120g. Measured interaction factors between pairs of piles at various spacings and orientations to direction of loading.	fine sand prepared under water at $D_r=79\%$ and $\phi=43^\circ$	One of the earliest studies of group interaction effects using the centrifuge. Demonstrated that nonlinear pile group response is evident even at small strains. Determined that elastic methods do not accurately model soil non-linearity effects caused by group action, even at small strain strains. Developed interaction factors for pairs of piles in groups of different sizes with different pile spacings.
Cox, W.R. Dixon, D.A. Murphy, B.S. (1984)	Conducted <b>1g model tests</b> on groups of 1-inch-diameter steel tubing inserted to depths ranging from 2 to 8 diameters. Performed tests on single piles and on 3 and 5 pile groups with clear spacings of 0.5, 1, 2, 3, and 5 diameters.	very soft processed clay placed in a 25 in by 25 in by 16 – inch-deep test box $S_u = 0.42$ ksf	Evaluated group efficiencies by examining the response of piles in side-by-side and in-line arrangements. Determined that group effects were negligible when side-by-side spacing exceeds 3D and in-line spacing exceeds 8D.

Table A.1. Continued.

Reference	Lateral Load Test Description	Foundation Soil	Principal Findings
Selby, A.G. Poulos, H.G. (1984)	Conducted <b>1g model tests</b> on pile groups ranging in size from 2 to 9 piles at spacings ranging from 3D to 5D. Model piles were 0.35-in-diameter, 11.4-in-long aluminum tubes. Pile heads were constrained by a stiff steel segmental cap. Test tank size was 23.6 by 17.7 by 27.6 in deep.	uniform sand, rained into the tank around pre-assembled pile groups	Measured significantly higher moments and shears in leading piles compared to central and trailing piles. They called this effect “shielding”. Elastic and continuum analytical methods were unsuccessful in predicting the uneven spread of moments and shears among the piles because these methods did not account for the “shielding” effects.
Baguelin, F. Jezequel, J.F. Meimon, Y. (1985) and Meimon, Y. Baguelin, F. Jezequel, J.F. (1986)	Conducted <b>full-scale field tests</b> on a 3 x 2 pile group spaced at 3D in the direction of load and 2D normal to load direction. Piles consisted of boxed I-beams, 11.2 by 10.6 in, driven 24.6 ft. Pin-headed connections were used.	1 m of CH over 13 ft of CL over 13 ft of SM	Measured increased group effect with load, characterized by differences in behavior between rows. Determined that shear and moments were nearly constant between piles in a given row. However, measured higher shear forces and moments in the leading row compared to the trailing row. Determined that cyclic loading tended to equalize the interaction factors between rows.

Table A.1. Continued.

Reference	Lateral Load Test Description	Foundation Soil	Principal Findings
Brown, D.A. Reese, L.R. (1985) and Brown, D.A. Reese, L.R. O'Neill, M.W. (1987)	Conducted <b>full-scale field tests</b> on a 3 x 3 group of steel pipe piles spaced at 3D c/c. A loading frame was used that provided moment-free connections at each pile head.	stiff overconsolidated clay, $S_u = 1.2$ to 1.7 ksf, piles were driven close-ended to a depth of 43 feet	Measurements indicated that load transferred to the piles was predominately a function of the row-to-row position of the pile rather than the position of the pile normal to the direction of load. Large proportions of shear were measured in the leading row, with successively less shear distributed to the middle and back rows. Observed that elasticity based approaches do not adequately address the reduction of soil resistance caused by soil interaction effects.
Clark, J.I. Mckeown, S. Lester, W.B. Eibner L.J. (1985)	Conducted <b>full-scale field tests</b> on small free –headed groups (2 to 3 piles) of 3-ft to 5-ft-dia. drilled shafts. Testing conducted during construction of the Olympic Oval Facility in Calgary.	23 ft of compact sand overlying firm ablation till	Determined that measured results did not agree with calculated results for single piles. Attributed the discrepancy to group effects and consequently reduced the single pile soil stiffness by 24 %.
Sarsby, R.W. (1985)	Conducted <b>1g model tests</b> on groups containing 2 to 4 0.24-in-dia mild steel bars spaced at 2D to 17D. The groups were oriented in a single line of piles and were tested in a free-headed condition. Piles were driven through sand placed in a steel tank of size 31.5 by 35.5 by 35.5 in deep.	poorly graded, dry, medium-fine sand, $\phi = 38^\circ$ , placed and compacted in layers	Determined that group efficiency does not markedly change with deformation. Observed that pile efficiency factors determined using Poulos's interaction factors agreed with measured results for small pile groups, but was conservative for large groups. ...continued

Table A.1. Continued.

Reference	Lateral Load Test Description	Foundation Soil	Principal Findings
Sarsby, R.W. (1985) <i>continued</i>	<i>continued from previous page</i>		...Concluded that the load–deflection curve could accurately be described by a simple power law.
Morrison, C. Reese, L.C. (1986) and Brown, D.A. Morrison, C. Reese, L.R. (1988)	Conducted <b>full-scale field tests</b> on a 3 x 3 group of steel pipe piles spaced at 3D c/c. A loading frame was used that provided moment-free connections at each pile head. (This test setup was previously used in the Brown et al., 1987 study.)	In situ soils were removed and med. dense sand was placed and compacted around the piles at a $D_r$ of 50 %, $\phi=38.5^\circ$ .	Defined the term “shadowing”, in which the soil resistance of a pile in a trailing row is reduced because of the presence of the pile ahead of it. Developed the concept of using a p-multiplier to modify the single pile p-y curve to obtain a group pile p-y curve. Suggested using p-multipliers of 0.8, 0.4, and 0.3 for the leading, middle, and back rows, respectively of pile groups spaced at 3D c/c.
Franke, E. (1988)	Conducted <b>1g model tests</b> on 1 x 3 and 3 x 1 groups with moveable heads. Test piles were 1.6-in-diameter and were grouped in spacings ranging from 2D to 8D.	fine sand rained around the pre-installed piles at different relative densities	Determined that group interaction effects occur when pile spacing in the direction of load is less than 6D and/or the spacing perpendicular to load direction is less than 3D. Developed normalized interaction factors as a function of pile spacing and sand density for rigid and flexible piles.
Blaney, G.W. O’Neill, M.W. (1989)	Conducted full-scale field tests on a 3 x 3 group of 10.75-in-dia steel piles constrained by a rigid concrete cap. Dynamic loading tests were performed using a linear inertia mass vibrator attached to the top of the pile cap, which was constructed approximately 2.6 feet above the ground surface.	stiff overconsolidated clay, $S_u = 1.2$ to 1.7 ksf, piles were driven close-ended to a depth of 43 feet	Concluded that the response of the system was largely controlled by the superstructure response (applied dynamic loading). Determined that the stiffness of individual group piles were approximately 70% of the stiffness of a comparable single pile.

Table A.1. Continued.

Reference	Lateral Load Test Description	Foundation Soil	Principal Findings
Lieng, J.T. (1989)	Conducted <b>1g model tests</b> on 2 vertical piles at various spacings. Piles were 5.9-in-dia., 102-in-long, and 0.2-in-thick aluminum pipes.	dry loose sand was rained into a 13 by 13 by 10 ft tank	Determined that group efficiency is inversely related to magnitude of applied load. Observed that rear piles develop resistance in deeper layers than the front piles because the shear resistance in the upper layers of soil around the rear piles is reduced due to shadowing effects. Did not detect any pile-soil-pile interaction between piles in a given row for spacings greater than 3D.
Ochoa, M. O'Neill, M.W. (1989)	Conducted <b>full-scale field tests</b> on the same 3 x 3 group of 10.75-inch diameter piles that were used in Brown's 1988 study.	In situ soils were removed and med. dense sand was placed and compacted around the piles at a $D_r$ of 50 %.	Developed lateral interaction $\alpha$ -factors, which relate to the stretching of the deflection portion of the pile resistance curve. The $\alpha$ factors cannot be used directly to analyze individual piles because they are not explicitly applied to p-y curves. The factors were found to increase with increasing load magnitude and decrease with increasing number of load cycles.
Shibata, T. Yashima, A. Kimura, M. (1989)	Conducted <b>1g model tests</b> on 31.5-in-long, 0.87-in-diameter aluminum and chloridized-vinyl pipes. Universal joints were attached to pile heads to provide free rotation of pile tops. Piles were installed in the test tank during soil preparation by the "boiling technique". Pile groups ranged in size from 2 to 16 piles at spacings ranging from 1.8D to 9.1D.	Uniform sand was "boiled" into test tank by pumping water with an upward gradient through the bottom of the tank. $D_r=20\%$ .	Compared measured test results to theoretical predictions using the method developed by Randolph (1981) for flexible free-headed piles. Good agreement was obtained between predicted and measured values of group efficiency, with a maximum discrepancy of 30 %.

Table A.1. Continued.

Reference	Lateral Load Test Description	Foundation Soil	Principal Findings
Liu, J.L. (1991)	Conducted <b>1g model tests</b> on 28 sets of bored pile groups with different pile spacings, diameters, geometric arrangements, and lengths.	silt – (no additional information provided on soil characteristics or test details)	Concluded: 1) front row piles take the largest share of applied lateral load, 2) pile group interaction varies with pile spacing and number of piles in the direction of load, 3) partial restraint of pile head results in redistribution and decrease of bending moments in pile head and shaft, and 4) cap side resistance and bottom friction increase the overall lateral bearing capacity.
Zhang, L. Hu, T. (1991)	Conducted <b>centrifuge tests</b> on piles and pile groups. Placed soil and installed piles at 1g, loaded piles at 50g.	soil 1: uniform silty clay, soil 2: stratified deposit of silty clay over fine sand	Studied the effects of residual stresses in piles and the variation of stresses between piles during static and cyclic loading. Negligible residual stresses were measured in the clay, while substantial residual stresses were measured in the sand and stratified soil layers.
Adachi, T. Kimura, M. Kobayashi, H. Morimoto, A. (1994)	Conducted <b>centrifuge tests</b> on two aluminum pipe piles with pinned heads at 40g acceleration. The pile spacing and skew angle were varied to investigate group effects.	dry sand at a relative density of about 90 %	Concluded that for a 2-pile in-line group, the front pile takes a larger portion of shear than the rear pile. Developed interaction factors for various pile spacings and skew angles.

Table A.1. Continued.

Reference	Lateral Load Test Description	Foundation Soil	Principal Findings
Kotthaus, M. Grundhoff, T. Jessberger, H.L. (1994)	Performed <b>centrifuge tests</b> on three aluminum tubes with fixed-heads at 50g acceleration. Pile row spacings of 3D and 4D were used. Soil was placed after installing the piles, at 1g. Tank size was 2.8 by 1.4 by 2.6 ft deep.	fine-grained sand placed by pluvial deposition at $D_r = 98\%$	Determined that group efficiency effects varied as a function of pile displacement, up to a limiting displacement of approximately 10 % of the pile diameter, for 3D and 4D row spacings.
McVay, M. Bloomquist, D. Vanderlinde, D. Clausen, J. (1994) and McVay, M. Casper, R. Shang, T.I. (1995)	Conducted <b>centrifuge tests</b> on 3 x 3 groups of free-headed piles at 3D and 5D center to center spacing. Piles were driven and laterally loaded in flight at 45g acceleration.	medium loose ( $D_r=33\%$ , $\phi=34^\circ$ ) and medium dense ( $D_r=55\%$ , $\phi=30^\circ$ ) sand, classified as SP	COM624P was used to back-calculate p-multipliers for each pile row. The group efficiency ( $G_e$ ) was independent of soil density and was only a function of pile group geometry. $G_e$ at 3D spacing was 0.74 and $G_e$ at 5D was 0.94.
Chen, L.T. Poulos, H.G. (1996)	Conducted <b>1g model tests</b> on pile groups using 1-in-dia. aluminum tubes, 3.28-ft-long. Three types of groups geometries were tested: in-line rows, side-by-side rows, and in square (box) arrangements. Tests were conducted on free-headed and fixed-headed groups at spacings ranging from 2.5D to 7.5D.	calcareous sand rained into an aluminum tank of dimensions 19.5 by 16.0 by 27.6 in deep	Evaluated group effects based on the position of a pile in a group, pile spacing, the number of piles, and the head fixity. Determined that a rigid pile cap reduces the positive bending moment and causes a relatively large negative bending moment in the upper portion of the pile. Evaluated group efficiencies based on maximum positive bending moments and compared experimental results to those calculated using the boundary element computer program PALLAS.

Table A.1. Continued.

Reference	Lateral Load Test Description	Foundation Soil	Principal Findings
Rao, S.N. Ramakrishna, V.G. Raju, G.B. (1996)	Conducted <b>1g model tests</b> using 21.5-mm-diameter, 1,000-mm-long, mild steel pipe piles. Two and three pile groups were tested at spacings ranging from 3D to 6D.	marine clay, LL=82 % and PL=32 %	Experimentally determined that pile group capacity depends on the spacing and arrangement of piles. Determined that for spacings greater than 6D in the direction of load, or 3D normal to load direction, $G_e$ approached 1. Performed a simplified plane strain 3D finite element analysis and tabulated comparisons between measured and calculated group efficiencies.
Gandhi, S.R. Selvam, S. (1997)	Conducted <b>1g model tests</b> on groups with 2 to 9 piles in 21 different configurations. The piles consisted of 0.72-in-O.D. aluminum pipes installed at c/c spacings varying from 4D to 12D.	Clean fine to medium sand placed at 60 % relative density in a 2.3 by 2.3 by 2.0 ft deep test tank.	Developed relationships for nondimensional interaction load factors in terms of pile spacing and relative stiffness, T. Where, $T = (EI/n_p)^{1/5}$ . Determined the optimum pile spacing (in the direction of load) was two times T, for maximum group efficiency.
Rollins, K.M. Weaver, T.J. (1997)	Conducted <b>full-scale field tests</b> on a 3 x 3 pile group at 3D spacing. The piles were 12-in-I.D. closed-end steel pipes driven to a depth of 30 ft. Pinned-headed connections were used to apply the test loads.	cohesive soils classified as ML, CL-ML, or CL with an avg. $S_u$ of 0.5 to 1.0 ksf	Measured group efficiency factors for individual pile rows. Presented design curves for p-multipliers as a function of pile spacing for leading row and trailing row piles. Did not observe any consistent trends in the load distribution among piles in the same row.



Table A.1. Concluded.

Reference	Lateral Load Test Description	Foundation Soil	Principal Findings
Ruesta, P.F. Townsend, F.C. (1997)	Conducted <b>full-scale field tests</b> (Roosevelt Bridge Project) on 2 groups (one fixed- and one free-headed) of 16 prestressed concrete piles spaced at 3D. Piles were jetted 25 ft and driven 29 ft.	loose fine sand to 15 ft depth, $D_r=30\%$ and $\phi=32^\circ$ , underlain by v. dense cemented sand	Measured p-multipliers of 0.8, 0.7, 0.3, and 0.3 from leading to trailing rows for the free-headed test pile group. Fixed-head tests gave approximately the same results. The pile group load-deflection efficiency was 80 %. The variation of bending moments between different rows was less than 15 %.
McVay, M. Zhang, L. Molnit, T. Lai, P. (1998)	Conducted <b>centrifuge tests</b> on 3 x 3 through 7 x 3 groups of fixed-headed piles at 3D c/c spacings. Piles were pushed and laterally loaded in flight at 45g acceleration.	medium loose ( $D_r=36\%$ , $\phi=34^\circ$ ) and medium dense ( $D_r=55\%$ , $\phi=37^\circ$ ) sand Classified as SP	Concluded that an individual pile row's contribution to the group's lateral resistance did not change with size of group, only with its row position. Observed that position of pile within a row had no significant effect on its lateral resistance. Provided p-multipliers for laterally loaded pile groups with 3 to seven rows of piles spaced at 3D. Concluded that Brown et al.'s (1988) p-multiplier approach is accurate for matching the total group load and individual row distributions.

Table A.2. Summary of pile group analytical studies.

Reference	Method of Analysis	Principal Findings
Kim, J.B. (1969)	analytical approach	Developed a procedure and computer program that incorporate group effects for closely spaced piles with the equivalent cantilever method of analyzing single piles. Group effects are accounted for by modifying the coefficient of subgrade reaction based on pile spacing and pile location within the group.
Poulos, H.G. (1971a) and Poulos, H.G. (1971b)	elasticity theory	Modeled pile-soil interactions using elastic continuum methods that consider the soil to act as a 3-D, linearly elastic, homogeneous, isotropic, semi-infinite medium. Used Mindlin's equations to develop factors that account for additional displacements ( $\alpha_p$ ) and rotations ( $\alpha_\theta$ ) caused by interactions from adjacent piles. Developed, in chart form, interaction factors for free-head and fixed-head piles subjected to horizontal loads and moments applied at the ground surface.
Focht, J.A. Koch, K.J. (1973)	hybrid method	Developed a hybrid procedure that uses p-y curves to model pile-soil interaction and Mindlin's equations with elasticity based $\alpha$ -factors to approximate the group effects of pile-soil-pile-interaction. (The original hybrid method for analyzing pile groups.) Presents a procedure for including interaction effects of closely spaced piles by applying y-multipliers to single pile p-y curves. Recommend using a soil modulus, $E_s$ , that corresponds to low stress levels in the soil. They recommend a value between the initial tangent modulus and 25 % of the ultimate stress.
O'Neill, M.W. Ghazzaly, O.I. Ha, H.B. (1977)	hybrid method	Presented a method for analyzing pile groups using a hybrid-type of analysis. Deviated from the Focht-Koch procedure by modifying unit-load-transfer curves individually to account for stresses induced by adjacent piles. The method is based on a discrete element formulation for pile-soil load transfer behavior coupled with an elastic half-space representation of the pile-soil-pile interaction effects.

Table A.2. Continued.

Reference	Method of Analysis	Principal Findings
Banerjee, P.K. Davies, T.G. (1980)	elastic continuum with boundary element methods	Extended general boundary element methods (using reciprocal work theory) to incorporate elasto-plasticity models through an initial stress, an initial strain, and a modified body force algorithm. Demonstrated that group response is dependent on pile spacing and geometric arrangement.
Desai, C.S. Kuppusamy, T. Alameddine, A.R. (1980)	2-D finite element study	Determined parametrically that the relative stiffness of cap, pile, and soil medium have a considerable influence on the distribution of load in piles within a group. Determined that for stresses in the linear range, this method yields results similar to other numerical procedures such as Hrennikoff's approach.
Randolph, M.F. (1981)	finite element parametric study with elasticity approach	Performed parametric studies using finite element methods and Poulos's elasticity approach to develop algebraic equations for estimating the lateral response of single piles. Treated the soil as an elastic continuum with either a constant or linearly varying modulus. Extended the analysis to consider pile groups by developing expressions for interaction factors for closely spaced piles. The solutions are simpler than previous continuum methods because they are independent of the embedment length of the pile. Randolph reports that only in rare cases will the length of the pile be a factor.
Hariharan, M. Kumarasamy, K. (1982)	analytical approach	The authors address group effects by applying two multipliers to the p-y curve for a single pile, one for the load and the other for the displacement. The multipliers are determined by normalizing the stresses and deformations in a horizontal layer due to movement of the piles (equations determined using elastic continuum methods). Average multipliers are used for all the piles in a group, rather than different multipliers for different piles. The authors suggest this assumption is sufficiently accurate for design purposes.

Table A.2. Continued.

Reference	Method of Analysis	Principal Findings
Tamura, A. Ozawa, Y. Sunami, S. Murakami, S. (1982)	3-D finite element study	Performed 3-D finite element analyses using the hyperbolic model to represent the stress-strain characteristics of the soil. Performed parametric studies to evaluate group effects related to pile spacing and quantity of piles. Determined that pile group effects increase as the number of piles in the direction of load application increases and as pile spacing decreases. Observed that the inner piles took a greater portion of load and had larger group effects than the outer piles.
O'Neill, M.W. (1983) Brown, D.A. Reese, L.C. (1985) and Reese, L.C. Wang, S.T. (1996)	empirical analytical approach	Developed the p-multiplier approach to account for pile group shadowing effects. The p-y curve is softened or weakened by multiplying the soil resistance, p, by a reduction factor, $f_m$ . This method is combined with a structural matrix analysis package in the computer program GROUP.
Bogard, D. Matlock, H. (1983)	analytical approach - modified unit load transfer procedure	Developed a method for constructing nonlinear resistance curves for use with a Winkler-type soil model. Pile group behavior was modeled by replacing the group with an imaginary or equivalent pile and the soil behavior was softened by applying a group efficiency factor. They concluded that the deflection of piles in a group is related to both the deflection of the piles acting individually and the deflection of the large equivalent pile. Deflections are determined by combining the nonlinear component from group-pile interaction with the nonlinear component from individual-pile deflection within the field of global soil deformation.
Reese, L.C. Wright, S.G. Aurora, R.P. (1984)	hybrid method	Evaluated the use of hybrid approaches for analyzing the lateral response of pile groups. Presented a modification to the Focht and Koch (1973) hybrid approach in which the elastic deflections used in the group deflection equations are estimated from the results of p-y analyses performed at load levels where load-deflection behavior is linear.

Table A.2. Continued.

Reference	Method of Analysis	Principal Findings
Sogge, R.L. (1984)	2-D finite element study	Presented the results of 2-D finite element analyses using a straightforward beam-element program that unified the soil model with the structural model. Demonstrated the suitability of using the coefficient of subgrade reaction to represent the soil strength.
Dunnivant, T.W. O'Neill, M.W. (1986) and O'Neill, M.W. Reese, L.C. Cox, W.R. (1990)	empirical analytical approach	Used experimental studies to develop a stiffness distribution model, which is sometimes referred to as the $\beta$ method. Presented p-y reduction factors (p-multipliers) for side-by-side, in-line, and skewed arrangements of piles at various spacings. The method provides a means to account for shadowing effects in which the leading piles carry more load than the trailing piles.
Leung, C.F. Chow, Y.K. (1987)	semi-theoretical hybrid approach	Developed a hybrid method in which the individual pile response is modeled by the conventional p-y approach while group interaction is based on flexibility coefficients obtained from Mindlin's solution.
Najjar, Y.M. Zaman, M.M. (1988)	3-D finite element study	Performed nonlinear 3-D finite element analyses to investigate the effects of loading sequence and soil nonlinearity on the deformation behavior of a pile group. The behavior of the pile and cap was assumed linear. A nonlinear constitutive model was used for the soil. Observed that loading sequence and soil nonlinearity can significantly affect the lateral and axial response of pile groups. Developed a compute code for post-processing results and for plotting contours of the stress and displacement components of the pile-cap-soil system.
Lieng, J.T. (1989)	analytical approach	Developed a plasticity approach based on the concepts of effective stress analysis. The approach is similar to Janbu's tangent modulus method for calculating the settlement of a strip footing. Developed an expression for calculating the minimum pile spacing at which shadow effects approach zero.

Table A.2. Continued.

Reference	Method of Analysis	Principal Findings
Novak, M. Janes, M. (1989)	analytical approach	Developed closed-form expressions for evaluating group stiffness and damping. These expressions can be applied to estimate group response under small displacements, as a result of static and dynamic lateral loads.
Ochoa, M. O'Neill, M.W. (1989)	elasticity theory	Presented a method for analyzing pile groups using elasticity theory with experimentally determined interaction factors.
Brown, D.A. Shie, C.F. (1991)	3-D finite element study	Performed a detailed parametric study using a 3-D finite element model to evaluate the combined effects of superposition of elastic strains and shadowing. Two constitutive models for soil were used; an elastic-plastic constant yield strength (Von Mises envelope) for undrained loading of saturated clay, and an extended Drucker-Prager model with a nonassociated flow rule was used for sand. Developed recommendations for modifying p-y curves (as a function of pile spacing) using p- and y-multipliers. Observed that these multipliers vary as a function of depth and soil type, but the variations are small and do not warrant consideration in design.
Clemente, J.L. Sayed, S.M. (1991)	semi-empirical analytical approach	Developed a semi-empirical expression for estimating group response using elasticity theory. Presented expressions and charts for estimating the radial and circumferential hoop strain components around a pile. Developed a procedure to estimate pile group efficiencies using these radial strain components.

Table A.2. Continued.

Reference	Method of Analysis	Principal Findings
Iyer, P. Sam, C. (1991)	elasticity theory	Developed a method for estimating the stresses in a 3-pile cap using 3-D elasticity solutions expressed in terms of the Galerkin vector and double-Fourier series. The cap was modeled as a thick rectangular block with patch loadings on the top and bottom faces. Concluded that this method of structural analysis was more accurate than the truss analogy and beam methods.
Garassino, A.L. (1994)	hybrid method	The author presents an iterative elasticity approach for representing group behavior in which a p-multiplier is used to scale down the ultimate resistance and a y-multiplier is used to modify the deflection using Poulos's elastic theory. The author presented a general review of various other methods including finite element and subgrade reaction approaches.
Ooi, P.S. Duncan, J.M. (1994)	hybrid method - group amplification procedure	Performed a parametric study of pile group response using the Focht-Koch procedure. Developed a method for estimating the increased deflections and bending moments in laterally loaded piles and drilled shafts caused by group interaction effects. Developed design charts and equations for determining deflections and bending moments of closely spaced piles.
Narasimha, Rao Ramakrishna, V.G. (1995)	2-D finite element study	Analyzed 2-pile and 3-pile groups with pile spacing varying from 3D to 8D and with cap thickness varying from 0.12 in to 0.60 in. (The pile caps were not in contact with the soil.) Determined that the lateral resistance of a pile group depends not only on the spacing between piles but also on the thickness of the pile cap. The pile cap deforms as a flexible body when its thickness is small and it deforms as a rigid body at larger thickness.

Table A.2. Concluded.

Reference	Method of Analysis	Principal Findings
Ashour, M. Pilling, P. Norris, G. Perez, H. (1996)	analytical approach	Developed an analytical approach (incorporated into the computer program SWSG) known as the strain wedge model to evaluate the response of piles and pile groups. The model relates 1-D beam on elastic foundation analysis to 3-D soil pile interaction response, which is based on the deformation of soil within a plastic wedge in front of the pile. Plane stress conditions are assumed within the wedge and group effects are quantified by considering the overlap of passive wedges and accompanying strains.
Rao, S.N. Ramakrishna, V.G. Raju, G.B. (1996)	2-D finite element study	Performed simplified plain strain finite element analyses to evaluate group efficiencies for various pile spacings and geometric arrangements. Compared calculated results with those obtained from 1g model tests.
Gandhi, S.R. Selvam, S. (1997)	analytical approach	Present a nondimensional method for predicting pile response based on a power function relationship. Multiplication factors, determined from 1g model tests, were used to model group behavior.



**APPENDIX B**

**DETAILS OF LOAD TEST FACILITY AND COST OF  
CONSTRUCTION**

Table B.1. Pile driving system specifications.

<b>Pile hammer: ICE model 30S double-acting diesel hammer</b>	
rated energy	22,500 ft-lb
minimum energy	9,000 ft-lb
stroke at rated energy	7.5 ft
maximum attainable stroke	7.67 ft
speed	44 to 67 blows per minute
hammer weight	6,250 lb
ram weight	3,000 lb
anvil weight	560 lb
typical operating weight with cap	7,340 lb
<b>Nylon pile driving cushion</b>	
thickness	1.5 in
stiffness	$85 \times 10^6$ lb/in
elastic modulus	$35 \times 10^4$ psi
<b>Aluminum pile driving cushion</b>	
thickness	0.5 in
stiffness	$69 \times 10^6$ lb/in
elastic modulus	$10 \times 10^6$ psi

Data furnished by Drive-Con, Inc., Jessup, Maryland.

Table B.2. Summary of pile driving data.

Pile number	Initial pile length <sup>1</sup> (ft)	Pile head elevation <sup>2</sup> (ft)	Pile tip elevation (ft)	Pile head cutoff elev. <sup>3</sup> (ft)
P1	20.0	100.77	80.77	97.20
P2	20.0	98.49	78.49	97.20
P3	20.0	98.52	78.52	97.20
P4	20.0	99.96	79.96	97.20
P5	20.0	98.35	78.35	96.45
P6	20.0	98.45	78.45	96.45
P7	20.0	98.45	78.45	96.45
P8	20.0	98.47	78.47	96.45
P9	20.0	99.05	79.05	99.05
P10	20.0	98.79	78.79	98.79
P11	11.3	98.22	86.92	97.20
P12	11.3	98.12	86.87	97.20
P13	11.3	98.20	86.89	97.20
P14	11.3	98.09	86.87	97.20

## Notes:

1. As-delivered length of HP 10x42, ASTM A-36 carbon steel pile sections.
2. Elevation measurements are based on a project datum of 100.00. Average ground surface elevation = 97.80.
3. Excess pile stickup was cut off after driving to provide 0.3 feet of clearance between the pile and the top surface of the pile cap. The final surface elevation was 97.50 for the two 36-inch-deep caps and 96.75 for the 18-inch-deep cap.

Table B.3. Potentiometer standard specifications.

<b>Deflection instrument</b>	<b>Longfellow linear transducer</b>	<b>Celesco cable-extension transducer</b>
Model Number	SLF-S-150-D-1	PT101-0010-111-1110
Sensor resistance	9000 $\Omega$	500
Linearity	0.10 % full scale	0.15 % full scale
Excitation voltage	10 V	10 V
Full scale rating	6 in	10 in

Table B.4. Instrument calibration data.

Instrument number	Model	Serial number or type	Block number	Channel number	Board number <sup>1</sup>	Calibration slope (in/volt)	Module AIM3A serial No.
1 – SLF	150-D-1	H84, 8341	16	0	5	-0.5948	0582607
2 - SLF	150-D-1	H84, 8341	--	--	--	-0.5956	--
3 – SLF	150-D-1	H84, 8341	--	--	--	-0.5948	--
4 – SLF	150-D-1	H84, 8341	17	1	5	-0.5953	0582607
5 – SLF	150-D-1	H84, 8341	18	2	5	-0.6003	0582607
6 – SLF	150-D-1	H84, 8341	19	3	5	-0.5954	0582607
7 – SLF	150-D-1	H84, 8341	--	--	--	-0.5950	--
8 – SLF	150-D-1	H84, 8341	--	--	--	-0.5952	--
9 – SLF	150-D-1	H84, 8341	--	--	--	-0.5947	--
10 - Celesco	PT 101	A40564	5	0	3	1.0571	0568533
11- Celesco	PT 101	A55963	6	1	3	1.0597	0568533
12 - Celesco	PT 101	A40574	11	2	3	2.1253	0568533
13 - Celesco	PT 101	A40571	12	3	3	2.1208	0568533
14 - Celesco	PT 101	A55964	10	7	2	1.06142	0568531
15 - Celesco	PT 101	A55966	15	8	2	1.05767	0568531
16 - Celesco	PT 101	F0857898	1	0	2	1.0958	0568531
17- Celesco	PT 101	F0857894	2	1	2	1.0829	0568531
18 - Celesco	PT 101	F0857897	3	2	2	1.0865	0568531
19 - Celesco	PT 101	F0857893	4	3	2	1.0870	0568531
20 - Celesco	PT 101	F085796	7	4	2	1.0830	0568531
21 - Celesco	PT 101	F085795	8	5	2	1.0946	0568531
Load cell	200 kip	VPI – 02	13	0	4	11,124.9 b = 0.00232	0582608
Time block	sec	--	14	--	--	--	--

- Notes:
1. Interface channel number = board number – 1.
  2. System module AMM2 in slot No. 1 of Keithley 500A system.
  3. Calibrated with Keithley 10 V power supply and 2 kHz low-pass filter.
  4. Some instruments listed in the table were not used in the first series of tests.

Table B.5. Cost of equipment and materials.

244 ft of HP 10x42 piles	\$8,300
Pile driving and transporting services – donated, Coalfield Services, Inc.	5,000
VDOT # 57 stone (64 tons)	460
Limestone sand (6 tons)	90
Crusher run gravel (32 tons)	200
4,000 psi ready mix concrete (13 cy)	1,000
Wood	400
Rebar	400
Structural nuts, bolts, and washers	300
Steel bars, plates, etc	350
Miscellaneous fittings, angles, nuts, bolts, paint, tarps, etc.	1,250
Hand tools	350
1987 Dodge Caravan – donated, anonymous donor	2,500
Tent shelter	1,700
Enerpac 200 ton double acting ram	4,000
Enerpac PEM3405 hydraulic pump – borrowed, VPI	0
Honda generator (1600 watt) – borrowed, VPI	0
Northstar generator (5000 watt)	1,000
Gateway 2000 personal computer – donated, VPI	500
Keithley 500A data collection system – borrowed, VPI	0
Celsco transducers (6)	2,200
Celesco and Longfellow transducers (6 each) – borrowed, VPI	0
Strain gauges for 200 kip load cell (8), terminal strips, elect. cable	200
Wacker BS60Y compactor and Troxler nuclear gage – borrowed, VPI	0
Bobcat front-end loader	0
Miscellaneous backhoe services (approx. 25 hours donated by VPI)	0
Machine shop labor (welding, milling, and lathe work)	2,700
Wheel barrow	60
Concrete epoxy	120
Miscellaneous supplies	1,000
Total:	\$34,080

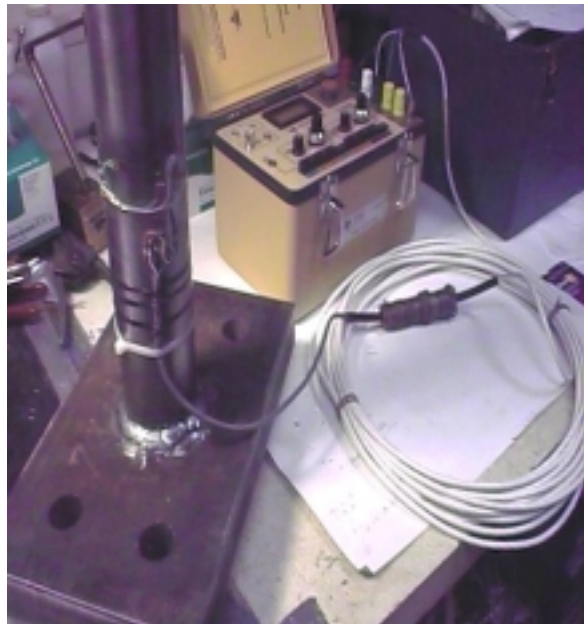
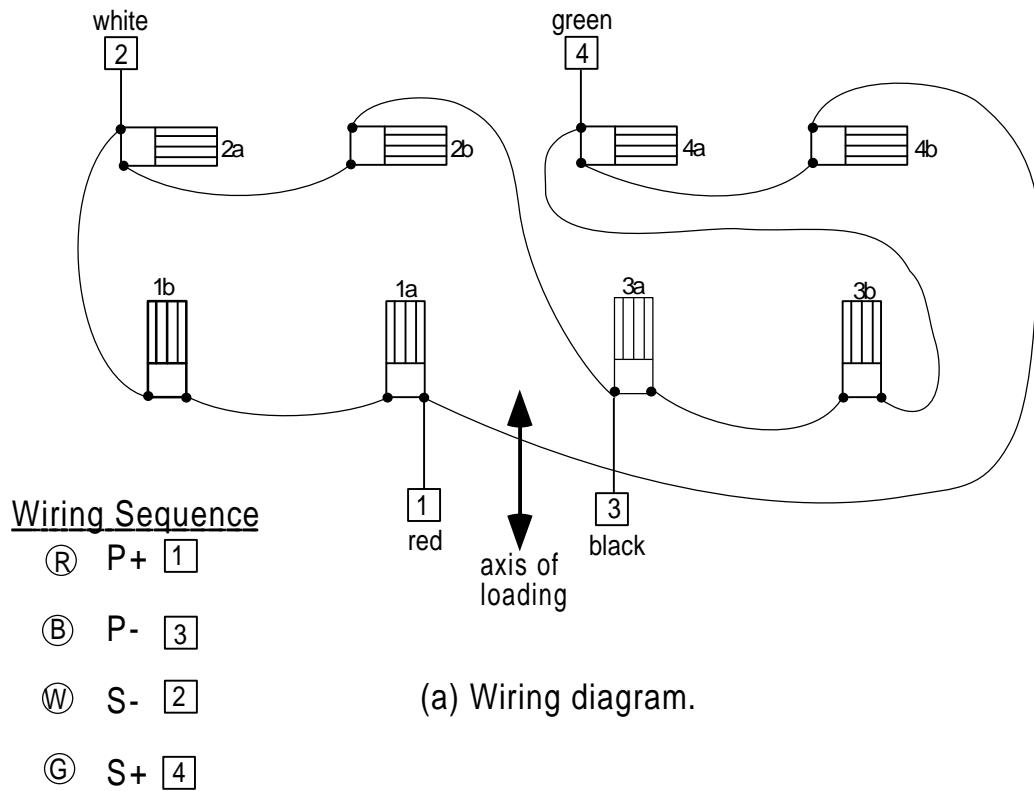
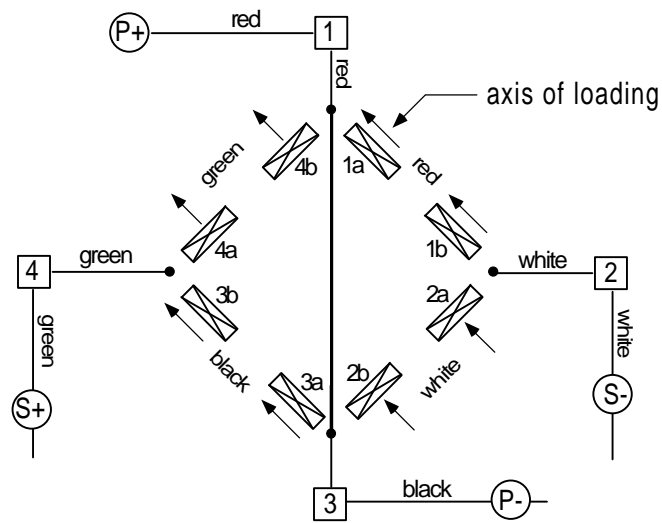


Figure B.1. Building a 200 kip load cell using  $\frac{1}{4}$ -inch strain gauges connected in a Wheatstone full-bridge circuit.



(a) Wiring diagram.



(b) Wheatstone bridge diagram.

Figure B.2. Load cell strain gauge circuit for measuring load.



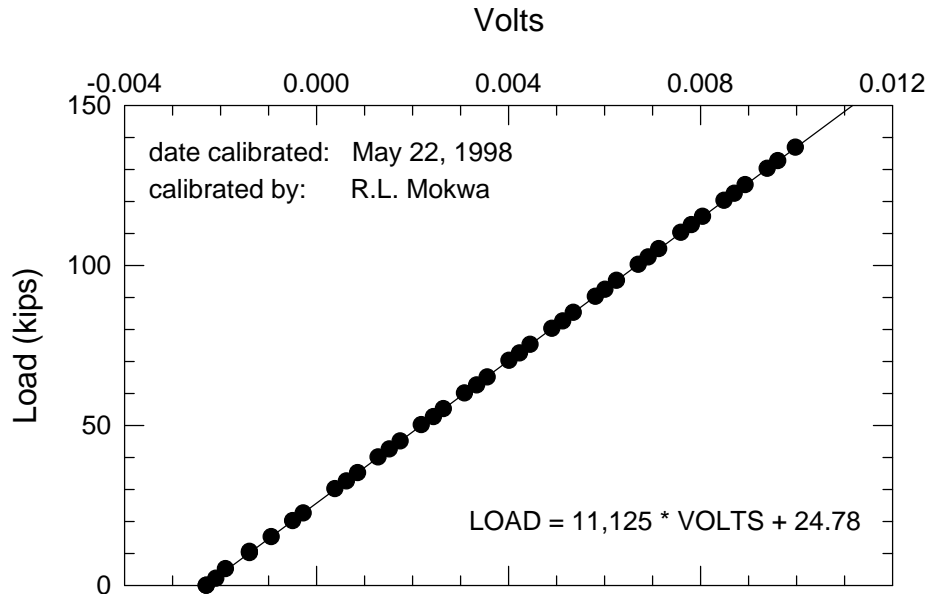


(a) 150 kip load cell.

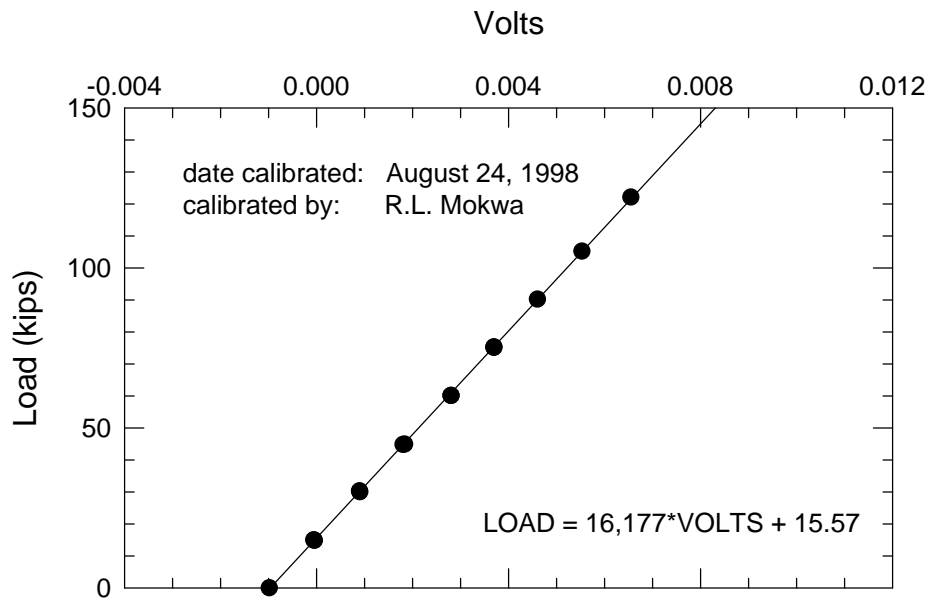


(b) Load test in progress at north pile.

Figure B.3. Single pile test setup.



(a) 200 kip load cell.



(b) 150 kip load cell.

Figure B.4. Calibration curves for load cells.

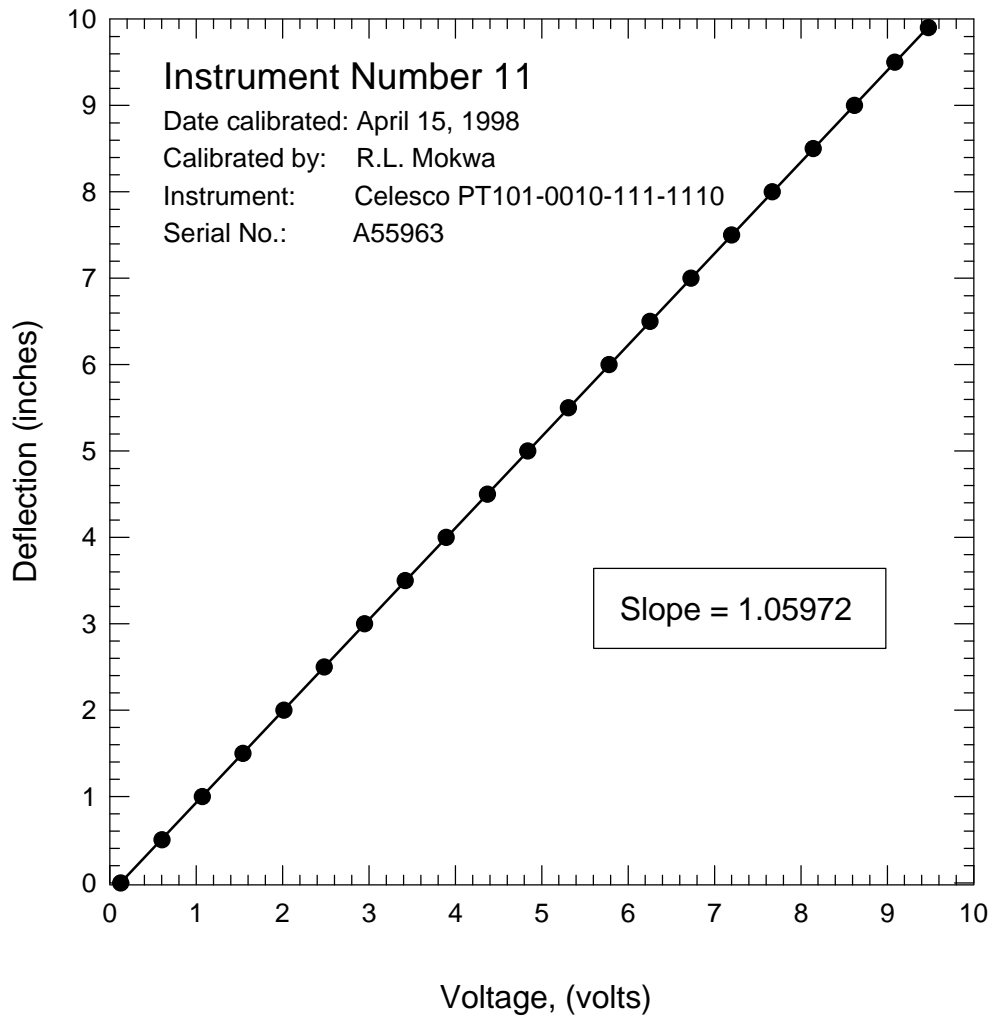


Figure B.5. Calibration curve for deflection transducer No. 11.

**APPENDIX C**  
**SOIL BORING LOGS**



The Charles Edward Via, Jr. Department of Civil Engineering	<b>BORING NUMBER</b> <b>BH-1</b>	<b>SHEET 1 OF 1</b>
<b>SOIL BORING LOG</b>		

PROJECT: Laterally Loaded Pile Cap Research LOCATION: Kentland Farms Site  
 ELEVATION: 98.92 ft DRILLING CONTRACTOR: Va Tech Geotechnical Department, Blacksburg, VA  
 DRILLING METHOD AND EQUIPMENT: Mobile B80 with 4-in solid stem augers (SPT tests were not conducted)  
 WATER LEVELS AND DATE: 18.0 ft 8/15/97 START: 8/14/97, 1300 FINISH: 8/14/97, 1400 LOGGER: R. Mokwa

DEPTH BELOW SURFACE (FT)	SAMPLE			STANDARD PENETRATION TEST RESULTS  6'-6'-6' (N)	SOIL DESCRIPTION  SOIL NAME, USCS GROUP SYMBOL, COLOR, MOISTURE CONTENT, RELATIVE DENSITY OR CONSISTENCY, SOIL STRUCTURE MINERALOGY	COMMENTS  DEPTH OF CASING, DRILLING RATE, DRILLING FLUID LOSS, TESTS AND INSTRUMENTATION
	INTERVAL	NUMBER AND TYPE	RECOVERY (FT)			
0						This boring was conducted to probe for rock depth. SPT tests and sampling were not conducted. The soil descriptions given are based on the auger cutting returns as observed at the hole collar.
5					<u>SILTY SAND</u> , (SM), It brown, silt moist, fine-grained sand, silt plastic, some gravel to 1-in in size, mica particles evident.	
10					<u>SANDY SILT</u> , (ML), brown, moist, silt. plastic, some mica particles in cuttings.	
15					<u>SANDY SILT</u> , (ML), brown, moist, silt. plastic, clay balls in cuttings.	Driller reports formation becoming stiffer with depth.
20					<u>SANDY SILT</u> , (ML), brown, moist, silt. plastic.	Driller reports a gravel or cobble layer at 16.5 ft.
25					<u>SILT</u> , (ML), blue-gray, moist, plastic.	Smooth augering.
30					Auger refusal at 30.3 ft.	Driller reports gravel or cobble layer at 28 ft. Smooth augering from 28.5 to 30 ft. Auger refusal at 30.3 ft. Driller suspects very stiff layer, but reports drilling action does not indicate rock. Bottom of hole at 30.3 ft.

Figure C.1. Soil Boring Log BH-1.



The Charles Edward Via, Jr. Department of Civil Engineering	<b>BORING NUMBER</b> <b>BH-2</b>	<b>SHEET 1 OF 1</b>
<b>SOIL BORING LOG</b>		

PROJECT: Laterally Loaded Pile Cap Research LOCATION: Kentland Farms Site  
 ELEVATION: 98.80 ft DRILLING CONTRACTOR: Va Tech Geotechnical Department, Blacksburg, VA  
 DRILLING METHOD AND EQUIPMENT: Mobile B80 with 4-in solid stem augers and 140 lb drop hammer  
 WATER LEVELS AND DATE: none encountered START: 8/14/97, 1500 FINISH: 8/14/97, 1730 LOGGER: R. Mokwa

DEPTH BELOW SURFACE (FT)	SAMPLE			STANDARD PENETRATION TEST RESULTS	SOIL DESCRIPTION	COMMENTS
	INTERVAL	NUMBER AND TYPE	RECOVERY (FT)			
0						Topsoil 1.4 ft thick
2.5	2.5 - 4.0	SS-1	0.7	6-15-19 (34)	<u>SANDY LEAN CLAY, CL</u> , dk. brown, dry, hard, fine-grained, silt. organic, plastic.	Driller reports stiff layer at 4.0-4.3 ft 2-in broken rounded gravel piece in cuttings at 5 ft.
5.0	4.0 - 6.5	SS-2	1.5	6-10-14 (24)	<u>SANDY LEAN CLAY, CL</u> , brown, dry, very stiff, silt. plastic clay, fine-grained sand, mica particles evident.	
7.5	6.5 - 9.0	SS-3	1.5	5-6-10 (16)	<u>SANDY SILT, ML</u> , brown, silt. moist, very stiff, med. plastic silt, fine sand, some mica particles.	Smooth augering, little resistance to downthrust.
11.0	9.0 - 12.5	SS-4	1.5	3-5-6 (11)	<u>SANDY SILT, ML</u> , brown, silt. moist, stiff, med. plastic silt, fine sand, mica particles evident. (higher moisture content and more plastic than SS-3)	
15.5	12.5 - 17.0	SS-5	1.1	2-1-5 (6)	<u>CLAYEY SAND, SC</u> , gray, moist, loose, low plastic clay, fine sand, gravel pieces in end of spoon, 3-in layer of red-brown plastic clayey sand in center of sample.	Spoon bouncing on gravel piece during last 2 blows for SS-5. Driller reports gravelly layer at 17.5 - 18 ft.
20.5	17.0 - 20.9	SS-6	0.4	(50/4")	<u>SILT, (ML)</u> , blue-gray, dry, hard, cemented, low plasticity, (pulverized weathered shale).	Bottom of hole @ 20.9 ft. Dry, stiff blue-gray silt on end of auger flights at 19 to bottom of hole.

Figure C.2. Soil Boring Log BH-2.



The Charles Edward Via, Jr. Department of Civil Engineering	BORING NUMBER <b>BH-3</b>	SHEET 1 OF 1
<b>SOIL BORING LOG</b>		

PROJECT: Laterally Loaded Pile Cap Research LOCATION: Kentland Farms Site  
 ELEVATION: 99.01 ft DRILLING CONTRACTOR: Va Tech Geotechnical Department, Blacksburg, VA  
 DRILLING METHOD AND EQUIPMENT: Mobile B80 with 4-in solid stem augers and 140 lb drop hammer  
 WATER LEVELS AND DATE: 18.2 ft 8/15/97 START: 8/15/97, 1000 FINISH: 8/15/97, 1300 LOGGER: R. Mokwa

DEPTH BELOW SURFACE (FT)	SAMPLE			STANDARD PENETRATION TEST RESULTS  6'-6'-6' (N)	SOIL DESCRIPTION  SOIL NAME, USCS GROUP SYMBOL, COLOR, MOISTURE CONTENT, RELATIVE DENSITY OR CONSISTENCY, SOIL STRUCTURE MINERALOGY	COMMENTS  DEPTH OF CASING, DRILLING RATE, DRILLING FLUID LOSS, TESTS AND INSTRUMENTATION
	INTERVAL	NUMBER AND TYPE	RECOVERY (FT)			
0						Topsoil 1.2 ft thick
2.5	2.5 - 4.0	SS-1	1.0	9-13-16 (29)	SANDY LEAN CLAY, CL, lt. brown, moist, very stiff, fine-grained sand, low plast. clay, mica particles evident.	
5	5.5 - 7.5	SS-2	1.4	7-10-15 (25)	SANDY SILT, ML, lt. brown, moist, very stiff, low plastic silt, fine sand, occnl. small 1/4" gravel, mica particles evident.	Driller reports augering thru a gravelly/cobbley layer from 5 to 5.5 ft. Smooth augering below 5.5 ft.
7.5	7.5 - 9.0	SS-3	1.5	5-8-10 (18)	SANDY SILT, ML, brown, moist, very stiff, low plastic silt, fine sand, occnl. small 3/4" gravel, some mica particles evident.	Smooth augering, little resistance to downthrust.
10	10.5 - 12.0	SS-4	1.5	5-4-6 (10)	SANDY SILT, ML, brown, moist, stiff, low plastic silt, fine sand, occnl. small 3/4" gravel, some mica particles evident.	
15	15.5 - 17.0	SS-5	1.4	2-4-6 (10)	SANDY LEAN CLAY, CL, brown, moist, stiff, low plastic clay, fine sand, gravel pieces in end of spoon.	Driller reports augering thru occnl. thin gravel layers from 15 to 20 ft. No difficulty in penetrating with the augers. Blue-gray silt appears in cuttings at 17 ft.
20	20.5 - 20.8	SS-6	0.4	38-50/3" (50/3")	SILTY CLAY WITH SAND, CL-ML, blue-gray, moist, hard, low plasticity, (pulverized weathered shale).	Bottom of hole @ 20.75 ft.

Figure C.3. Soil Boring Log BH-3.



The Charles Edward Via, Jr. Department of Civil Engineering	BORING NUMBER <b>BH-4</b>	SHEET 1 OF 1
<b>SOIL BORING LOG</b>		

PROJECT: Laterally Loaded Pile Cap Research

LOCATION: Kentland Farms Site

ELEVATION: 97.44 ft

DRILLING CONTRACTOR: Va Tech Geotechnical Department, Blacksburg, VA

DRILLING METHOD AND EQUIPMENT: Mobile B80 with 4-in solid stem augers and 140 lb drop hammer

WATER LEVELS AND DATE: 16.0, 1/26/98

START: 1/26/98, 13:30 FINISH: 1/26/98, 1640

LOGGER: R. Mokwa

DEPTH BELOW SURFACE (FT)	SAMPLE			STANDARD PENETRATION TEST RESULTS  6'-6'-6' (N)	SOIL DESCRIPTION  SOIL NAME, USCS GROUP SYMBOL, COLOR, MOISTURE CONTENT, RELATIVE DENSITY OR CONSISTENCY, SOIL STRUCTURE MINERALOGY	COMMENTS  DEPTH OF CASING, DRILLING RATE, DRILLING FLUID LOSS, TESTS AND INSTRUMENTATION
	INTERVAL	NUMBER AND TYPE	RECOVERY (FT)			
0						
2.0	2.0 - 3.5	SS-1	1.2	5/9/17 (26)	<u>SANDY LEAN CLAY</u> , CL, dk. brown, moist, v. stiff, fine-grained, silt. organic, low plastic.	Driller reports gravelly layer from 2.5 to 3.5 ft. Encounter cobbles at 3.5'. Unable to penetrate with augers. Move rig 2' east and resume augering.  Smooth augering 3.5-5.0 ft.
5	5.5 - 6.4	ST-2	1.8	pushed 0.9'	<u>SANDY SILT</u> , (ML), brown, moist, low plast. silt, fine-grained sand.	Shelby tube ST-2 contains 0.9 ft of slough. Unable to advance ST-2 beyond 6.4' depth because of cobble or boulder. Driller reports gravel layer from 6.4-7.0 ft. Smooth augering from 7-7.5 ft.
10	6.4 - 7.5	ST-3	2.3	pushed 2.3' med. resistance	<u>SANDY LEAN CLAY</u> , CL, dk. brown, moist, fine-grained sand, low plastic silt.	Smooth augering, little resistance to downthrust. Obtain bag sample of auger cuttings at 10-11.0 ft.
	7.5 - 9.8	SS-4	1.5	7-11-14 (25)	<u>SANDY LEAN CLAY</u> , CL, dk. brown, moist, v. stiff, fine-grained sand, low plastic silt.	
	9.8 - 11.3	ST-5	2.3	pushed 2.3' (easy push)		
15	11.3 - 12.0	SS-6	0.1	4-1-1 (2) cuttings	<u>POORLY GRADED SILTY SAND</u> (SP), brown, wet, v. loose, low plasticity.	Smooth augering.  Measured GWT at 16.0 ft after SS-6. Obtain bag sample of auger cuttings at 16-16.5 ft. Driller reports difficult advancement at 16 ft.
	12.0 - 14.3	SS-7	0.1	10-50/1" (50/1")	<u>SANDY LEAN CLAY</u> , CL, dk. brown, moist, v. stiff, fine-grained sand, low plastic silt. <u>SILT</u> , ML, brown-gray, wet, low plasticity, v. hard.	
	14.3 - 15.8					
	15.8 - 16.5					
	16.5 - 17.1					Bottom of hole @ 17.1 ft.

Figure C.4. Soil Boring Log BH-4.





The Charles Edward Via, Jr. Department of Civil Engineering	<b>BORING NUMBER</b> <b>BH-5</b>	<b>SHEET 1 OF 1</b>
<b>SOIL BORING LOG</b>		

PROJECT: Laterally Loaded Pile Cap Research      LOCATION: Kentland Farms Site  
 ELEVATION: 97.72 ft      DRILLING CONTRACTOR: Va Tech Geotechnical Department, Blacksburg, VA  
 DRILLING METHOD AND EQUIPMENT: Mobile B80 with 4-in solid stem augers and 140 lb drop hammer  
 WATER LEVELS AND DATE: 15.4, 1/25/98      START: 2/2/98, 12:15      FINISH: 2/2/98, 15:15      LOGGER: R. Mokwa

DEPTH BELOW SURFACE (FT)	SAMPLE			STANDARD PENETRATION TEST RESULTS  6'-6" (N)	SOIL DESCRIPTION	COMMENTS
	INTERVAL	NUMBER AND TYPE	RECOVERY (FT)			
	0	0.0	ST-1			
5	2.1 3.6	ST-2	2.3	pushed 2.3'		Left ST-2 in hole, retrieved using fish-tailed auger, some sample disturbance likely in top of Shelby tube.
10	5.9 8.2	ST-3	2.3	pushed 2.3'		Driller reports soft soil, easy to push ST-3, ST-4, and ST-5. Pushed ST-3, ST-4, and ST-5 consecutively, then augered-out hole to 12.8', prior to pushing ST-6.
15	10.5 12.8	ST-4	2.3	pushed 2.3'		
20	15.1	ST-5	2.3	pushed 2.3'		Continue augering after ST-6 at 15.1 ft. Driller reports gravel layer at 16 ft. Driller reports smooth augering from 17-19 ft.
25		ST-6	2.3	pushed 2.3'	<u>SILTY CLAY - CLAYEY SILT, CL-ML</u> , brown, moist, low plasticity.	Back into gravels at 19' to bottom of hole.  Obtained bag sample from auger flights at 19-21 ft. Very slow advancement at 21 ft. Bottom of hole @ 21.6 ft.
				auger cuttings		

Figure C.5. Soil Boring Log BH-5.



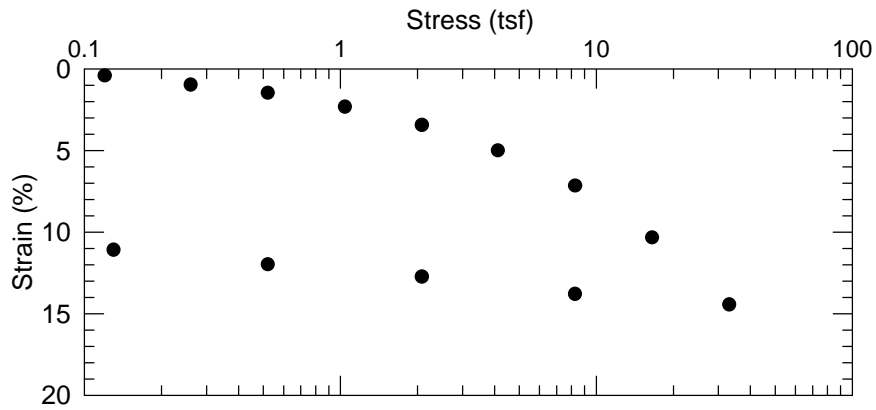
The Charles Edward Via, Jr. Department of Civil Engineering	BORING NUMBER <b>BH-6</b>	SHEET 1 OF 1
<b>SOIL BORING LOG</b>		

PROJECT: Laterally Loaded Pile Cap Research LOCATION: Kentland Farms Site  
 ELEVATION: 98.04 ft DRILLING CONTRACTOR: Va Tech Geotechnical Department, Blacksburg, VA  
 DRILLING METHOD AND EQUIPMENT: Mobile B50 with 4-in solid stem augers and 140 lb drop hammer  
 WATER LEVELS AND DATE: None Encountered START: 1/26/98, 15:00 FINISH: 1/26/98, 15:40 LOGGER: R. Mokwa

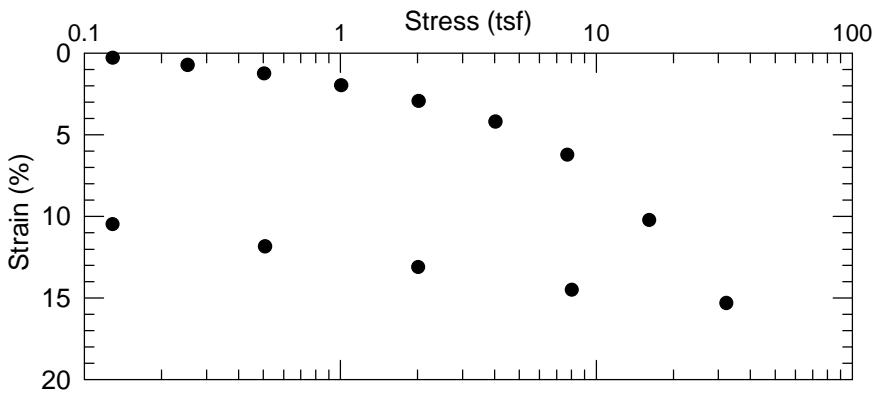
DEPTH BELOW SURFACE (FT)	SAMPLE			STANDARD PENETRATION TEST RESULTS	SOIL DESCRIPTION	COMMENTS
	INTERVAL	NUMBER AND TYPE	RECOVERY (FT)			
0	0.5	SS-1	1.5	3-4-7 (11)	SANDY LEAN CLAY, CL, dk. brown, moist, stiff, fine-grained, silt. organic, low plastic.	Very difficult to push ST-2. Shelby tube bent during push and the bottom was partially crushed. Considerable sample disturbance likely.  Bottom of hole @ 5.8 ft.
	2.0					
5	3.5	ST-2	1	pushed 2.3	SANDY LEAN CLAY, CL, dk. brown, moist, soft, fine-grained, silt. organic, low plastic.	
	5.8					

Figure C.6. Soil Boring Log BH-6.

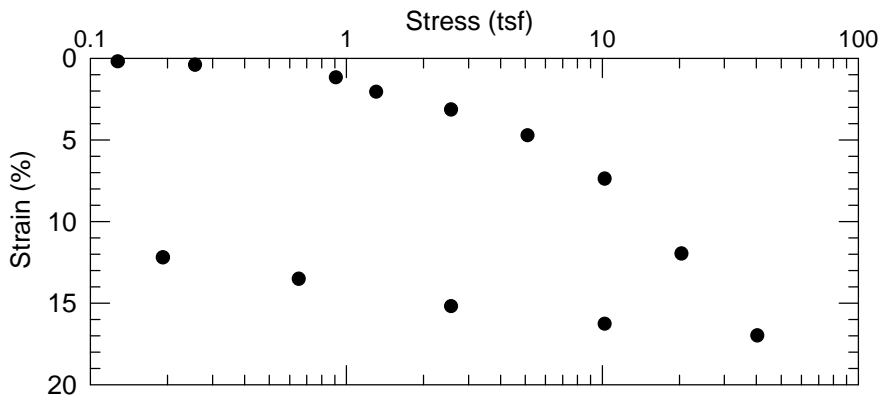
**APPENDIX D**  
**LABORATORY TEST RESULTS**



(a) Sample BH5-ST-3



(b) Sample BH5-ST-4



(c) Sample BH4-ST-5

Figure D.1. Consolidation curves for natural soil, strain vs. log p.

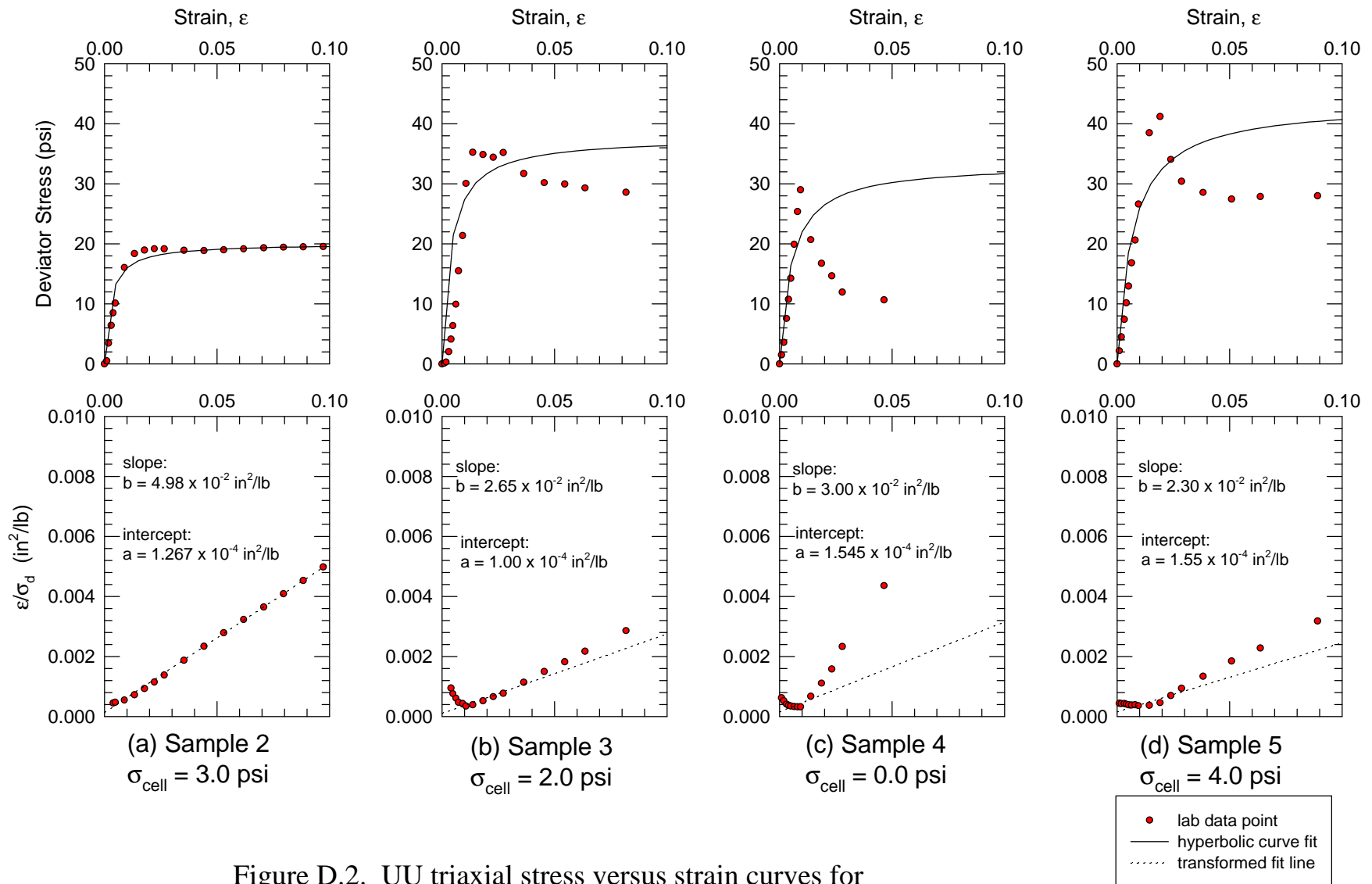


Figure D.2. UU triaxial stress versus strain curves for natural soil (1 of 3).

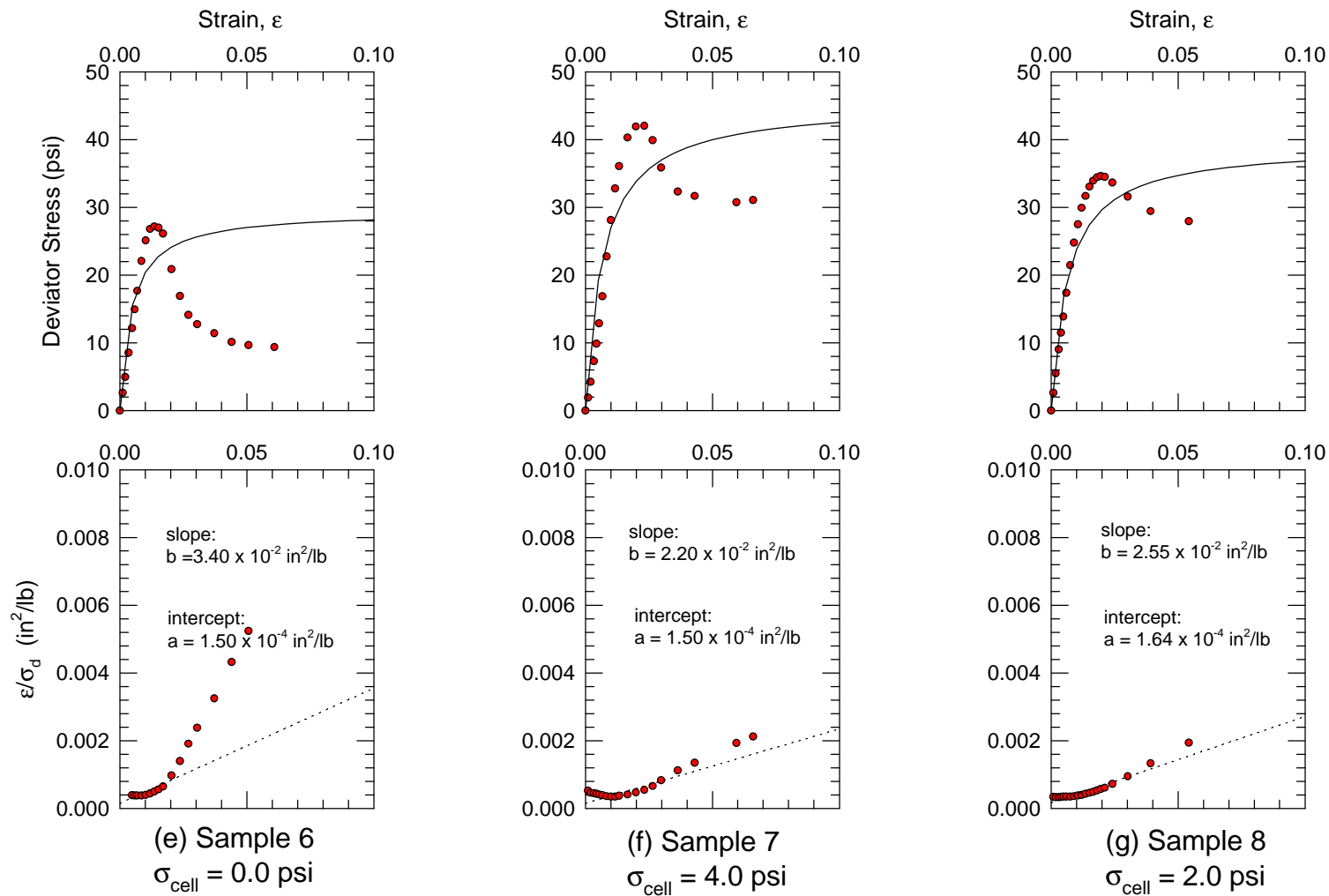


Figure D.3. UU triaxial stress versus strain curves for natural soil (2 of 3).

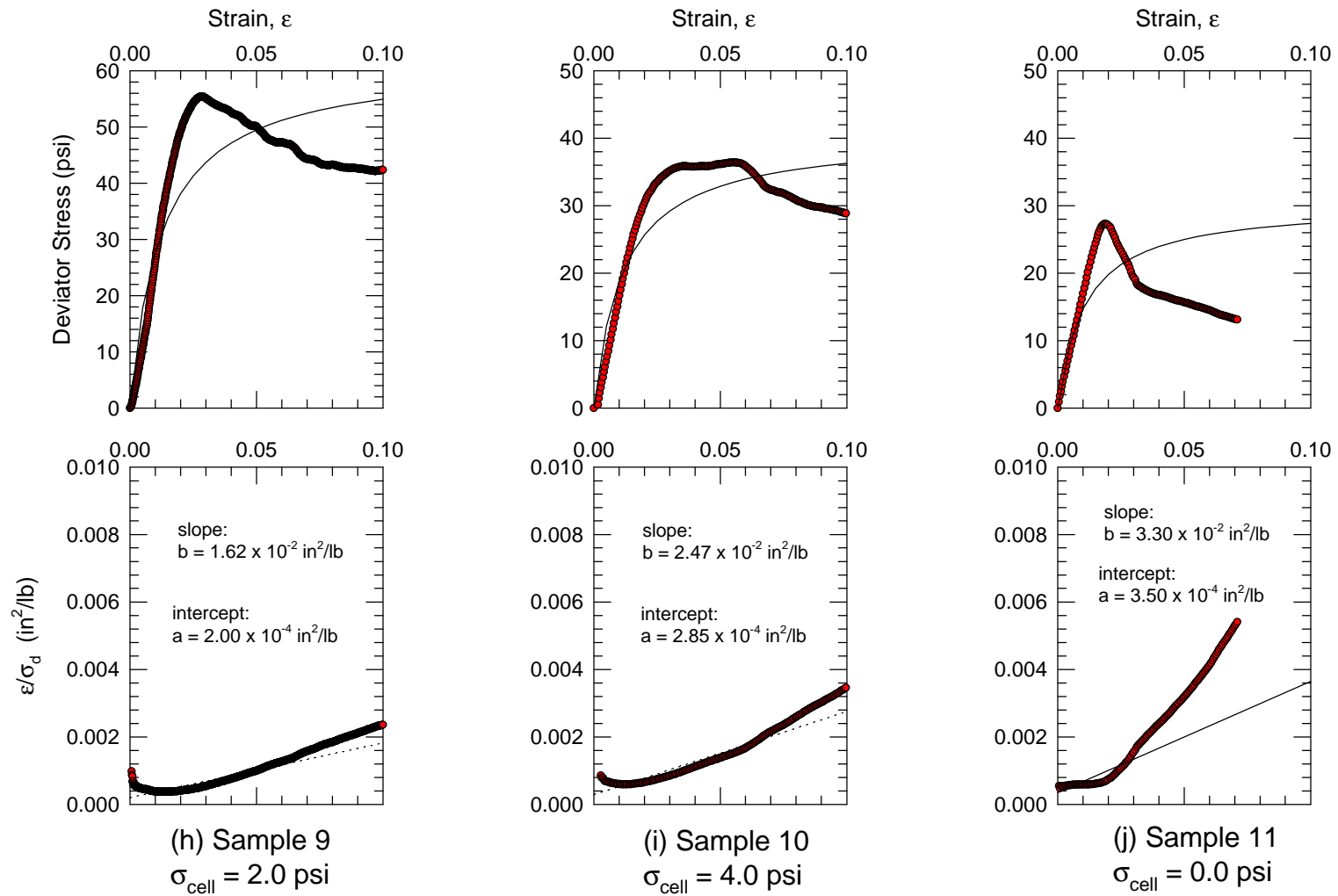


Figure D.4. UU triaxial stress versus strain curves for natural soil (3 of 3).

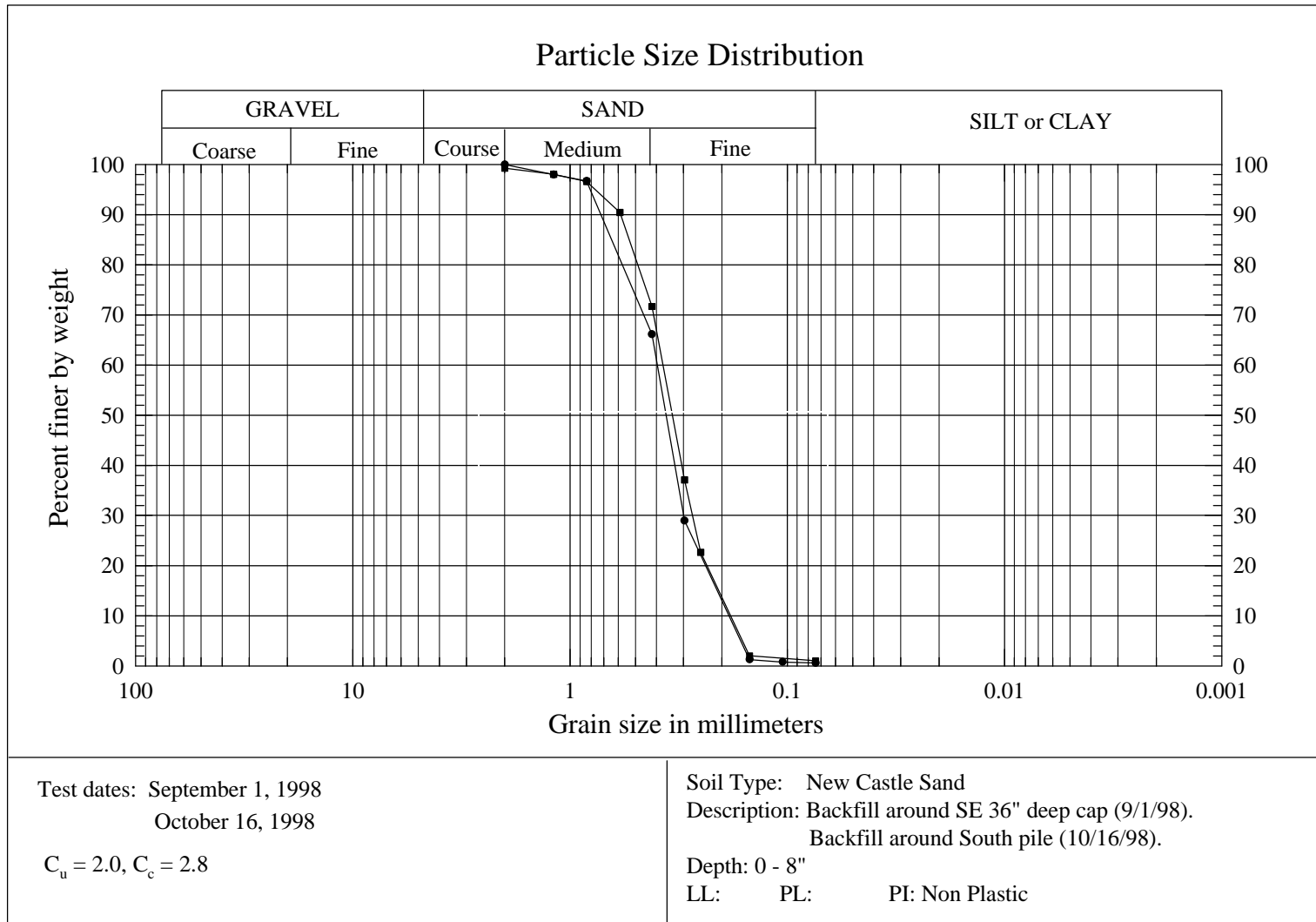


Figure D.5. Grain size distribution curves for New Castle Sand.



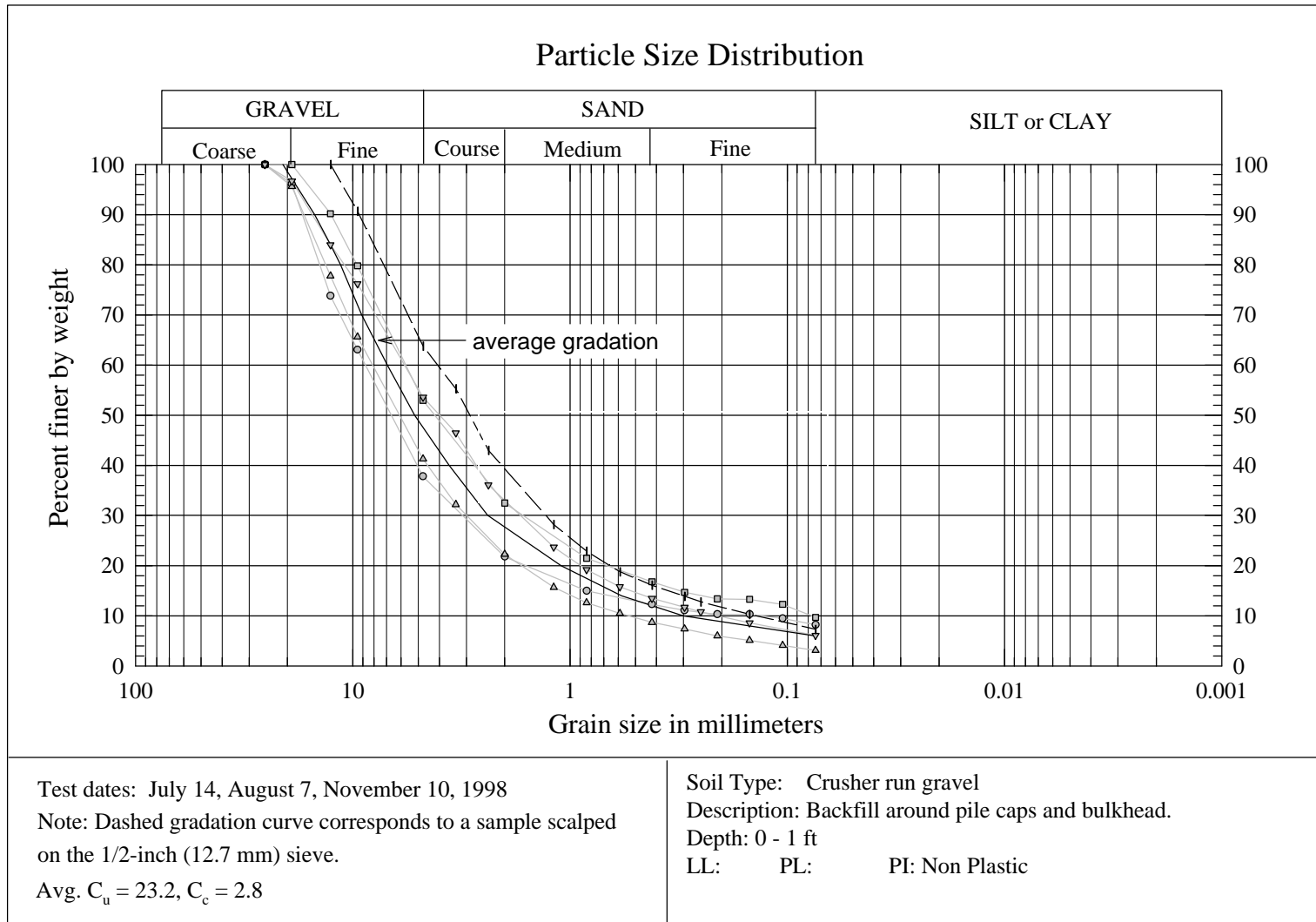
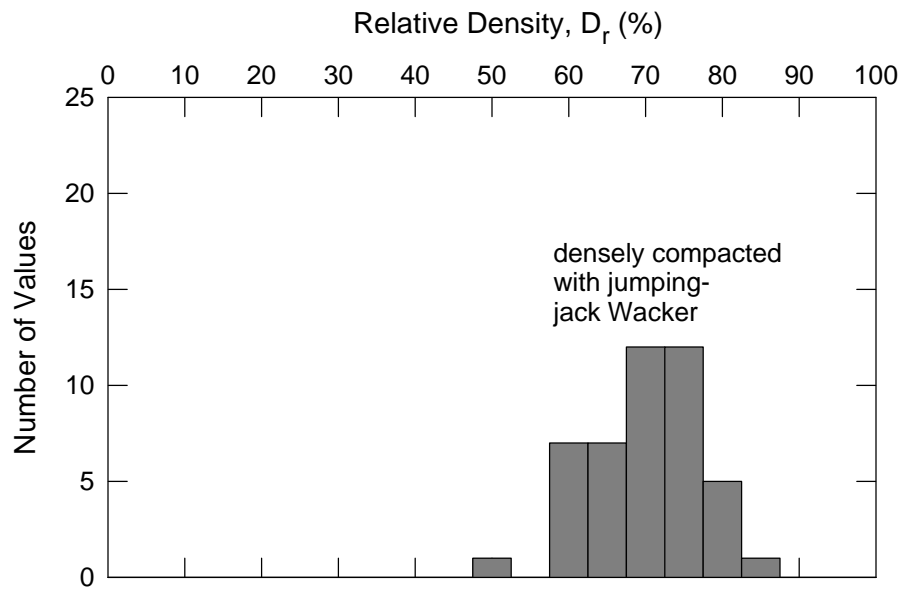
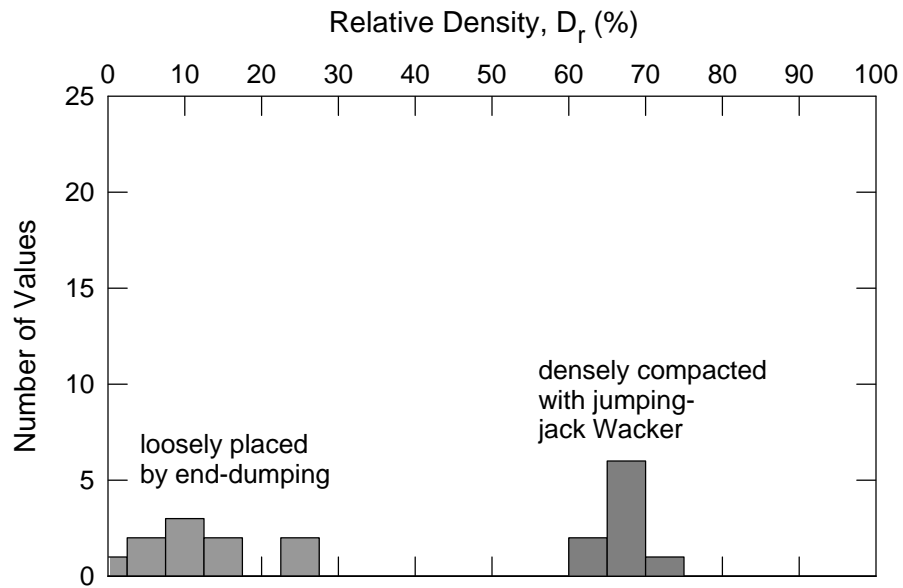


Figure D.6. Grain size distribution curves for crusher run gravel.



(a) Crusher run gravel.



(b) New Castle sand.

Figure D.7. Distribution of relative density values based on nuclear gage field test results.

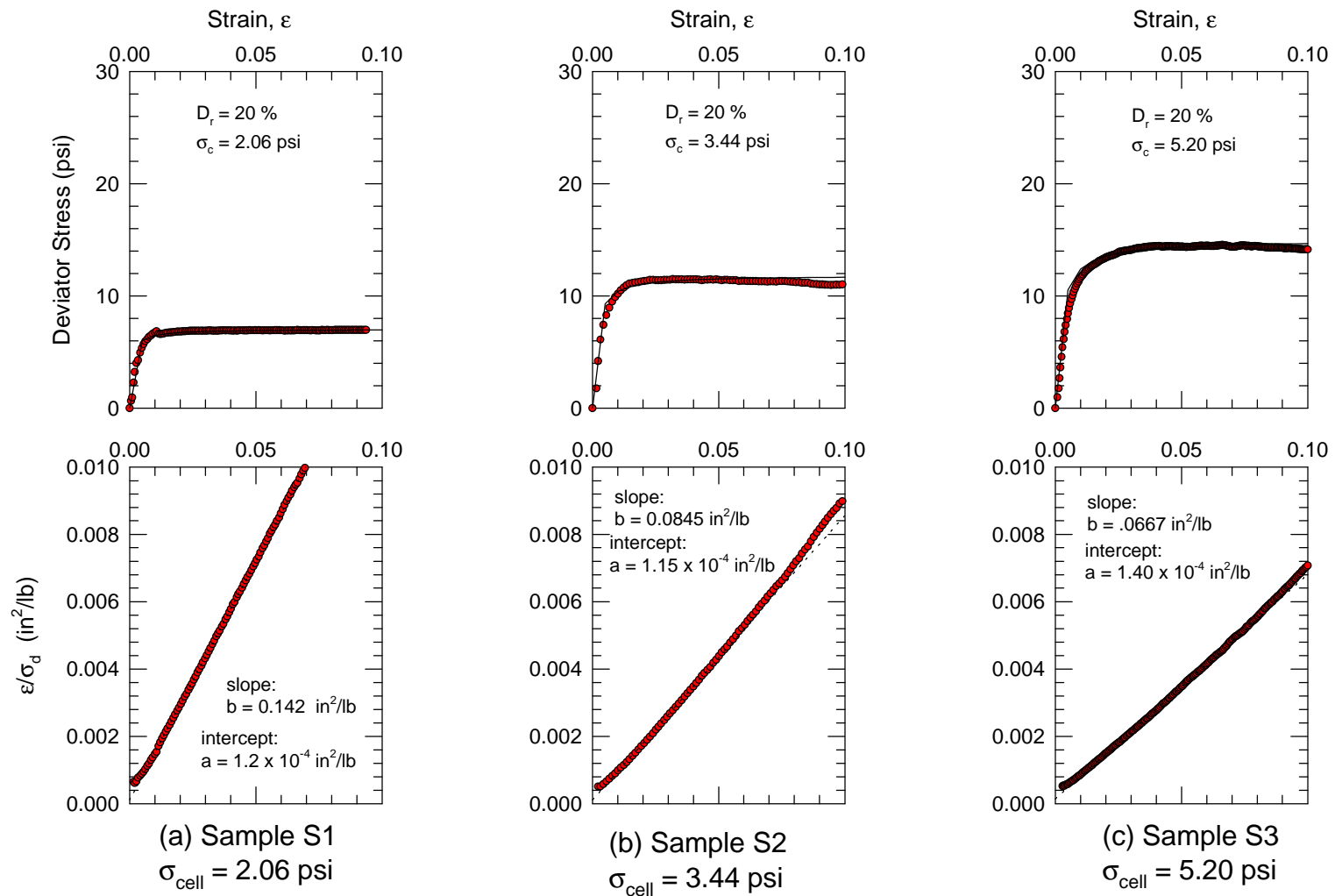


Figure D.8. CD triaxial stress versus strain curves for New Castle sand,  $D_r = 20\%$ , (1 of 3).

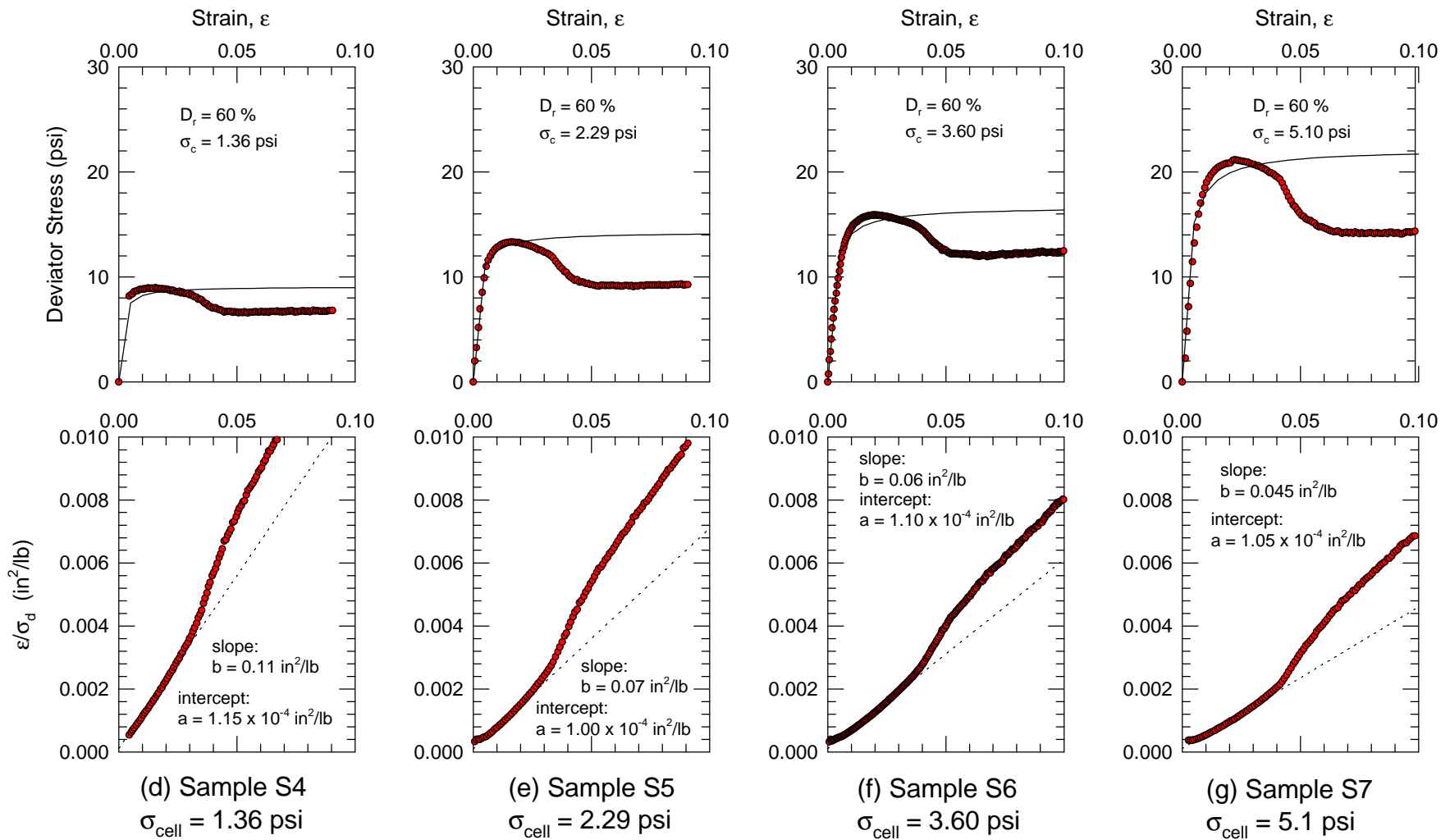


Figure D.9. CD triaxial stress versus strain curves for New Castle sand,  $D_r = 60\%$ , (2 of 3).

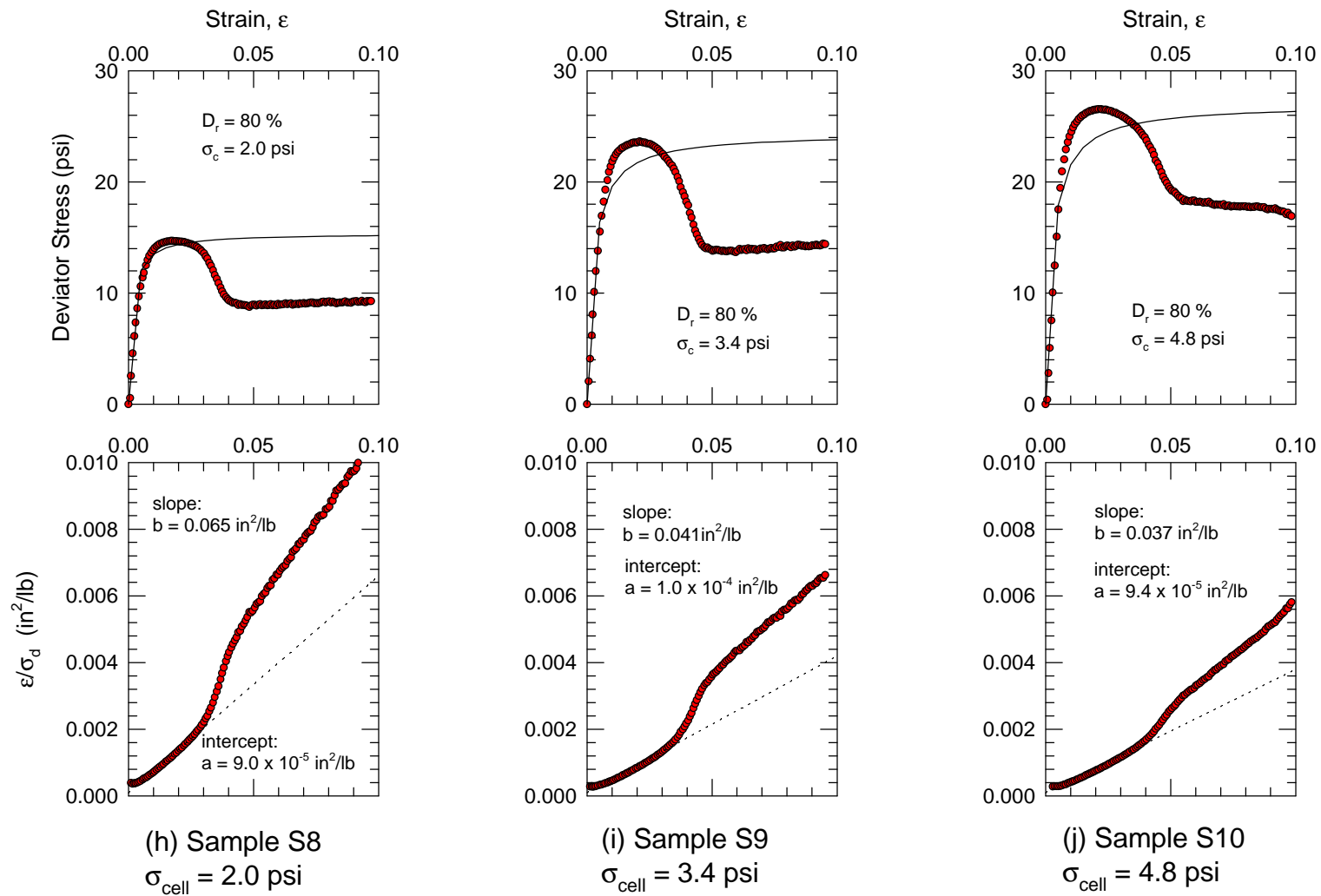


Figure D.10. CD triaxial stress versus strain curves for New Castle sand,  $D_r = 80\%$ , (3 of 3).

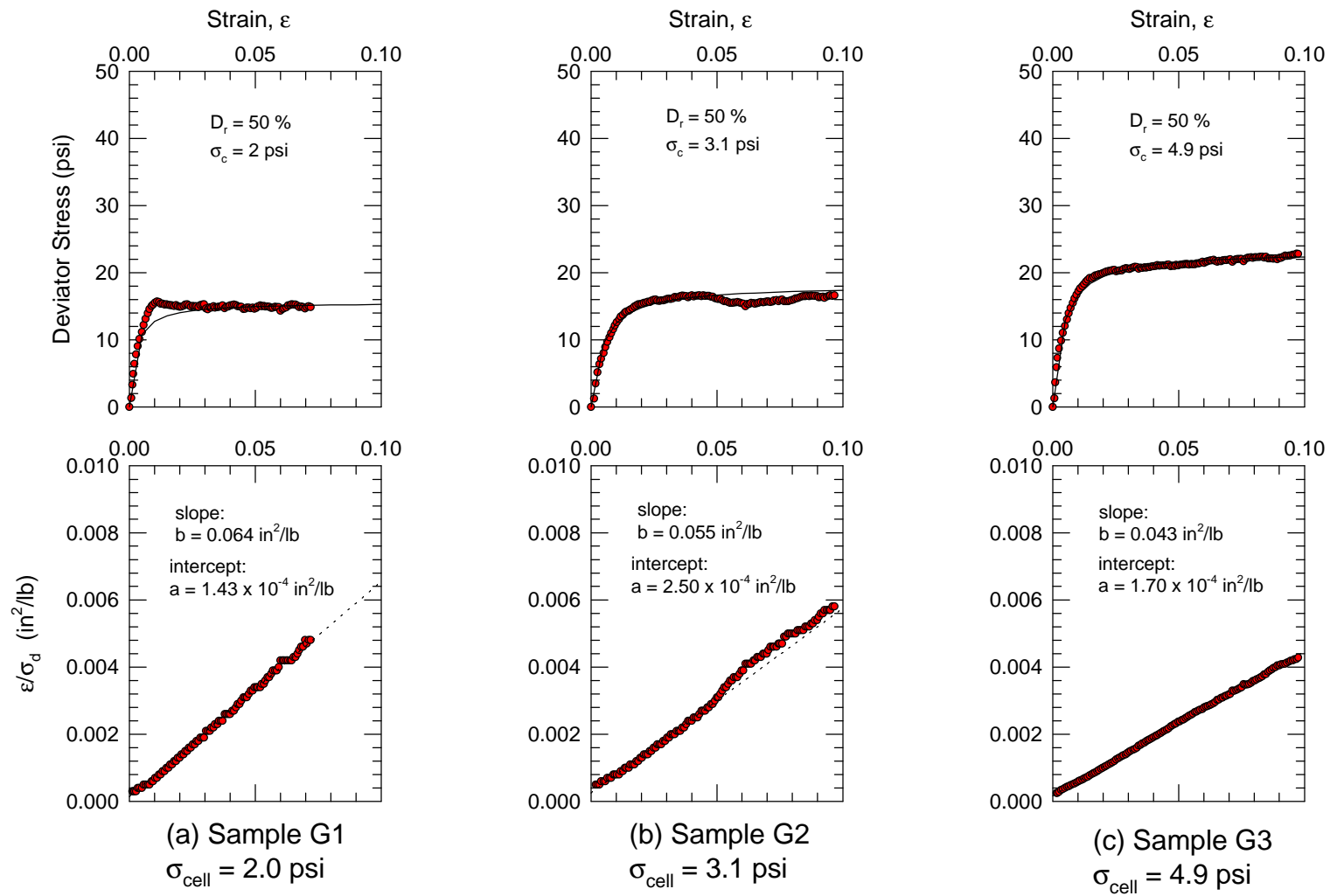


Figure D.11. CD triaxial stress versus strain curves for crusher run gravel,  $D_r = 50\%$ , (1 of 3).

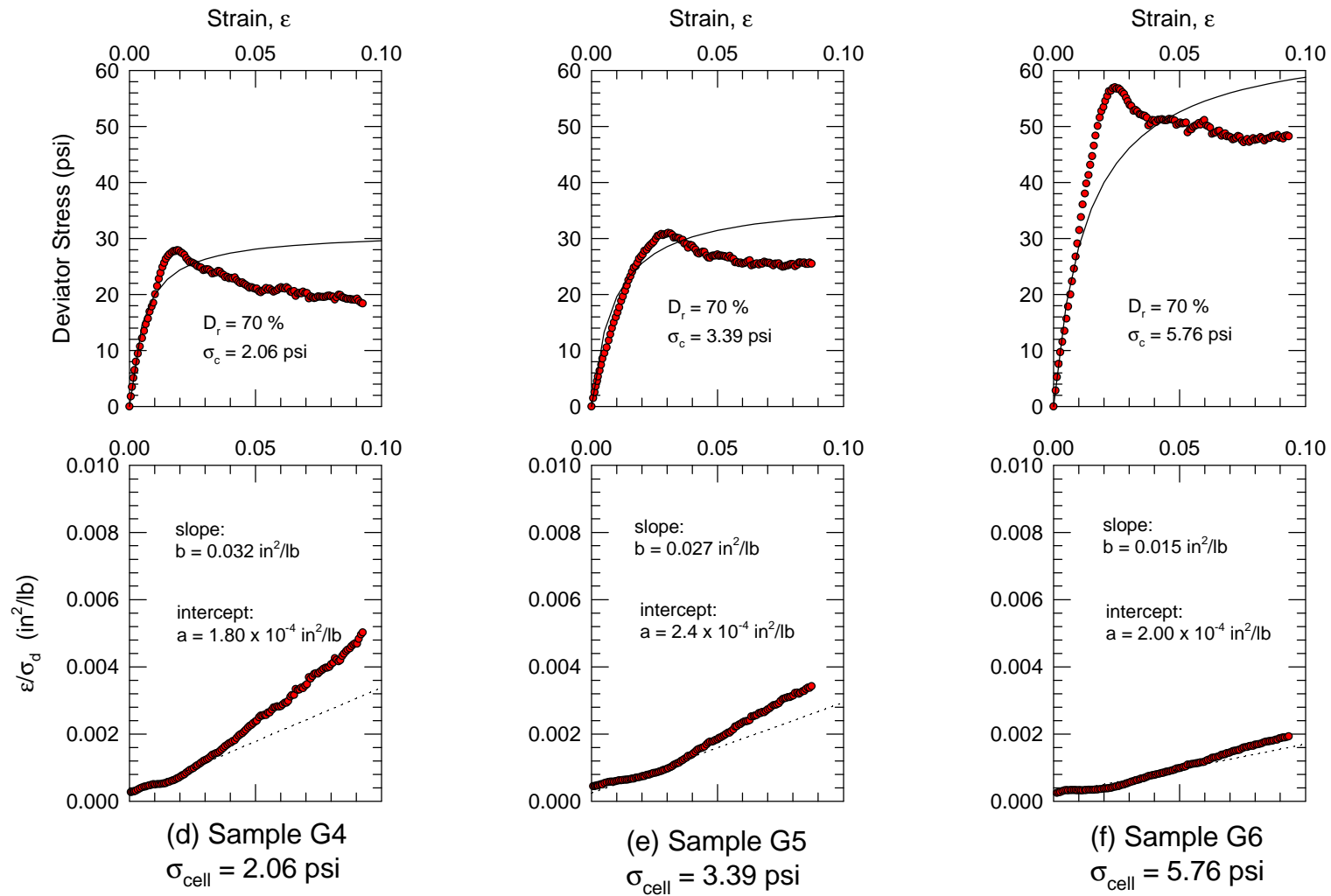


Figure D.12. CD triaxial stress vs. strain curves for recompacted samples of crusher run gravel,  $D_r = 70\%$ , (2 of 3).

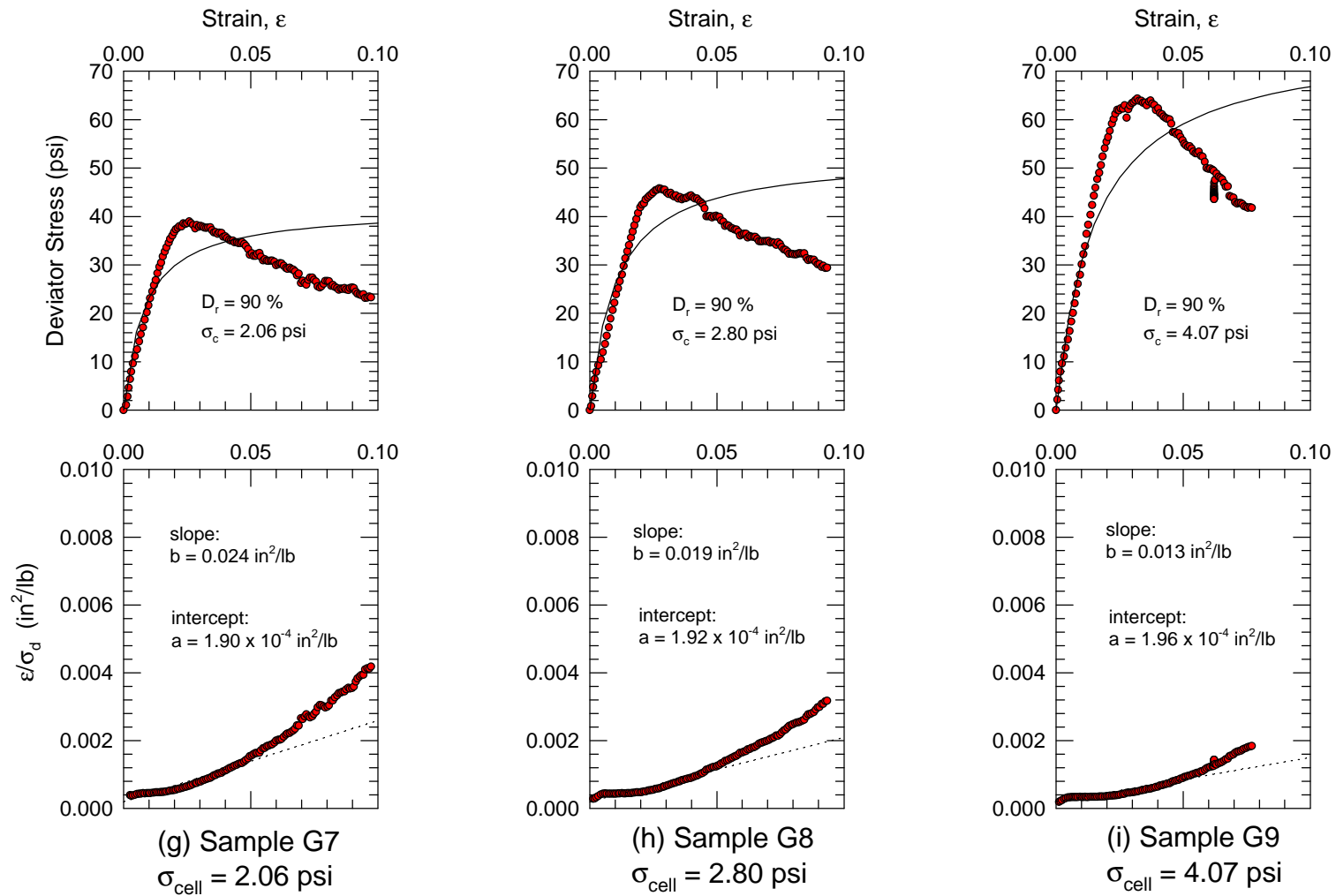


Figure D.13. CD triaxial stress vs. strain curves for recomacted samples of crusher run gravel,  $D_r = 90\%$ , (3 of 3).



## APPENDIX E - EQUATIONS FOR $K_q$ AND $K_c$ FACTORS FOR THE BRINCH-HANSEN (1961) THEORY

### E.1 Introduction

Included in this Appendix are the equations used to calculate the earth pressure coefficients for Brinch-Hansen's (1961) theory. These coefficients account for three-dimensional loading effects of soils that possess both cohesion and friction.

### E.2 Equations for $K_q$ and $K_c$

$$K_q = \frac{K_q^o + K_q^\infty a_q \frac{x}{D}}{1 + a_q \frac{x}{D}} \quad \text{Equation E.1}$$

where:

$K_q$  = passive earth pressure coefficient due to weight of soil at intermediate depth,

$K_q^o$  = passive earth pressure coefficient due to weight of soil at ground surface,

$$K_q^o = \left( e^{\left(\frac{1}{2}\pi + \phi\right)\tan\phi} \cos\phi \tan\left(45^\circ + \frac{1}{2}\phi\right) - \left( e^{-\left(\frac{1}{2}\pi - \phi\right)\tan\phi} \cos\phi \tan\left(45^\circ - \frac{1}{2}\phi\right) \right) \right)$$

$K_q^\infty$  = passive earth pressure coefficient due to weight of soil at great depth,

$$K_q^\infty = N_c d_c^\infty K_o \tan\phi,$$

$$\alpha_q = \frac{K_q^o K_o \sin\phi}{(K_q^\infty - K_q^o) \sin\left(45^\circ + \frac{1}{2}\phi\right)}$$

$x$  = depth below ground (units of length),

$D$  = shaft diameter (units of length),

$K_o$  = at-rest earth pressure,

$K_o = 1 - \sin\phi$ , and

$\phi$  = friction angle of foundation soil.

$$K_c = \frac{K_c^o + K_c^\infty a_c \frac{x}{D}}{1 + a_c \frac{x}{D}} \quad \text{Equation E.2}$$

where:

$K_c$  = passive earth pressure coefficient due to cohesion at intermediate depth,

$K_c^o$  = passive earth pressure coefficient due to cohesion at ground surface,

$$K_c^o = [e^{(\frac{1}{2}\pi + \phi)\tan\phi} \cos\phi \tan(45^\circ + \frac{1}{2}\phi) - 1] \cot\phi,$$

$K_c^\infty$  = passive earth pressure coefficient due to cohesion at great depth,

$$K_c^\infty = N_c d_c^\infty$$

$$\alpha_c = \frac{K_c^o}{K_c^\infty - K_c^o} 2 \sin(45^\circ + \frac{1}{2}\phi),$$

$\phi$  = friction angle of foundation soil,

$N_c$  = bearing capacity factor,

$$N_c = [e^{\pi \tan\phi} \tan^2(45^\circ + \frac{1}{2}\phi) - 1] \cot\phi,$$

$d_c^\infty$  = depth coefficient at great depth, and

$$d_c^\infty = 1.58 + 4.09 \tan^4 \phi.$$

## APPENDIX F – LOG SPIRAL EARTH PRESSURE THEORY

### F.1 Introduction

This Appendix describes the approach used to calculate passive earth pressures using the log spiral theory. Dr. J. M. Duncan developed an early version of this numerical analysis procedure. The equations presented in this appendix were coded in an *EXCEL* macro using the Visual Basic Applications programming language. The macro program is embedded in an *EXCEL* workbook named *PYCAP*, which was developed by the author for calculating p-y curves for embedded pile caps. The workbook *PYCAP* contains a number of different worksheets. Log spiral earth pressure calculations are performed in the worksheet named *Log Spiral*. Although the procedure described in this appendix was initially developed for pile caps, it applies equally as well to retaining walls, bulkheads, and other backfilled or embedded structures.

In the passive zone, the theoretical failure surface consists of two zones: 1) the Prandtl zone, which is bounded by a logarithmic spiral, and 2) the Rankine zone, which is bounded by a plane, as shown in Figure F.1(a). The shape of the log spiral failure surface, is shown in Figure F.1(b). The theory is based on the principle that force vectors acting on the log spiral failure surface make angles of  $\phi$  with the tangent to the spiral, and the lines of action of the force vectors pass through the center of the spiral.

The procedure described in this appendix was used to determine the ultimate passive earth pressure,  $E_p$ , and the individual components of  $E_p$ , which can be described as:

$$E_p = (P_{p\phi} + P_{pc} + P_{pq}) \quad \text{Equation F.1}$$

where  $E_p$  is the ultimate passive earth pressure force per unit length (force/length),  $P_{p\phi}$  is the component due to soil weight and friction (force/length),  $P_{pc}$  is the component due to soil cohesion (force/length),  $P_{pq}$  is the component due to surcharge (force/length), and  $b$  is the cap width or the length of the wall. Performing the calculations in this manner provides a means of isolating the three primary components of passive earth pressure. The contribution from

each component is computed using the log spiral earth pressure theory, as described in the following sections.

## F.2 Log Spiral Numerical Approximation

The procedure used to determine the components of  $E_p$  is described in this section. The procedure uses the trigonometric properties of the log spiral, as shown in Figure F.1(b). The equation defining the log spiral surface is:

$$r = r_o e^{(q \tan \phi \theta)} \quad \text{Equation F.2}$$

where  $r$  is the radius of the log spiral at an angle  $\theta$  from  $r_o$ ,  $r_o$  is the starting radius that positions the spiral onto the wall-soil geometry,  $\theta$  is the angle between  $r$  and  $r_o$ , and  $\phi$  is the soil friction angle. This equation forms the kernel of the iterative technique, which is based on equations of equilibrium and geometry. The primary variables and dimensions used in the procedure are shown in Figure F.2.

The minimum value of passive earth pressure is determined by iteration. An initial value of the dimension  $w$  is assumed, and the corresponding value of the passive earth pressure force ( $E_p$ ) is computed as described in the following pages. The value of  $E_p$  includes all three components:  $P_{p\phi}$ ,  $P_{pc}$ , and  $P_{pq}$ . The iteration loop is repeated by assuming a smaller or larger value of  $w$  and another value of the passive earth pressure force is computed. If this value of  $E_p$  is smaller than the first computed value of  $E_p$ , the value of  $w$  is adjusted again. By adjusting the assumed value of  $w$  (larger or smaller), the minimum value of  $E_p$  is computed with an accuracy of 0.005 %.

The program determines the location of the center of the log spiral by iterating on the values of  $r$  and  $x_o$  until the dimensions of the failure surface are consistent. After determining the geometry and sizes of the failure zones, the earth pressure forces are determined from equilibrium, assuming the shear strength of the soil is fully mobilized along the slip surface.

The procedure is started by determining the shape of the failure surface, using the following equations:

$$\mathbf{a} = 45 - \frac{\mathbf{f}}{2} \quad \text{Equation F.3.a}$$

$$w = \overline{af} \quad \text{Equation F.3.b}$$

$$H_d = \overline{df} = w \tan \mathbf{a} \quad \text{Equation F.3.c}$$

$$y_o = x_o \tan \mathbf{a} \quad \text{Equation F.3.d}$$

$$r_o = \sqrt{(H + y_o)^2 + x_o^2} \quad \text{Equation F.3.e}$$

$$\mathbf{q}_{\max} = 90 - \tan^{-1} \left( \frac{x_o}{H + y_o} \right) - \mathbf{a} \quad \text{Equation F.3.f}$$

$$r = \sqrt{w^2 + H_d^2} + \frac{x_o}{\sqrt{x_o^2 + y_o^2}} \sqrt{x_o^2 + y_o^2} \quad \text{Equation F.3.g}$$

The log spiral surface is fitted to the wall geometry and soil shear strength using the following steps:

1. Compute  $H_d$  using Equation F.3.c
2. Assume an initial value of  $x_o$
3. Compute  $y_o$  using Equation F.3.d
4. Compute  $r_o$  using Equation F.3.e
5. Compute  $\theta$  using Equation F.3.f
6. Compute  $r$  using the log spiral Equation, F.2
7. Compute  $r$  using Equation F.3.g
8. Compare the computed  $r$  values from steps 6 and 7

9. If the  $r$  values are in agreement with the tolerances established, continue with the procedure, otherwise, return to step 2 and modify  $x_o$

The following steps are used to estimate the weight of soil within the log spiral failure zone (defined by points abdf), and the location of the weight resultant,  $W$ , as shown in Figure F.3(a).

Compute the dimensions and centroid of area abdf, shown in Figure F.3.

$$H_d = r \sin \mathbf{a} - y_o \quad \text{Equation F.4.a}$$

$$l_1 = \frac{2}{3} H + y_o \quad \text{Equation F.4.b}$$

$$k = w \frac{H + 2H_d}{3(H + H_d)} \quad \text{Equation F.4.c}$$

$$l_2 = x_o + k \quad \text{Equation F.4.d}$$

$$l_3 = \frac{2}{3} H_d + y_o \quad \text{Equation F.4.e}$$

Calculate the soil weight,  $W$ , by estimating the area enclosed by points abdf:

$$W = \gamma [\text{Area within the log spiral from b to d } (A_{1s}) - \text{Area of triangle oab } (A_{t1}) + \text{Area of triangle adf } (A_{t2})]$$

$$W = \gamma [A_{1s} - A_{t1} + A_{t2}]$$

$$W = \mathbf{g} \left( \frac{r_1^2 - r_o^2}{4 \tan \mathbf{f}} - \frac{1}{2} x_o H + \frac{1}{2} w H_d \right) \quad \text{Equation F.5}$$

Break  $E_p$  into its horizontal and vertical components:

$$\text{horizontal component} = E_p \cos \delta$$

$$\text{vertical component} = E_p \sin \delta$$

Using equilibrium, determine  $P_{p\phi}$ ,  $P_{pc}$ , and  $P_{pq}$ , as described below.

**Compute  $P_{pf}$  - the earth pressure due to weight of soil.** (Refer to Figure F.3a.)

The soil above the top of the wall is treated as a surcharge, and its strength is ignored in the calculations. Calculate the Rankine earth pressure due to soil weight,  $E_{PRF}$ , acting on the vertical face defined by points  $df$ :

$$E_{PRF} = \frac{1}{2} g H_d^2 \tan^2 \left( 45 + \frac{f}{2} \right) \quad \text{Equation F.6}$$

Calculate  $P_{p\phi}$  by summing moments about the spiral origin, point O:

$$P_{pf} = \frac{l_2 W + l_3 E_{PRF}}{(l_1 \cos d - x_o \sin d)} \quad \text{Equation F.7}$$

**Compute  $P_{pc}$  - earth pressure due to cohesion.** (Refer to Figure F.3b.)

$$l_4 = x_o + \frac{w}{2} \quad \text{Equation F.8}$$

$$l_5 = y_o + \frac{H_d}{2} \quad \text{Equation F.9}$$

Calculate the Rankine earth pressure due to cohesion,  $E_{PRC}$ , acting on the vertical face defined by points  $df$ :

$$E_{PRC} = 2c \tan \left( 45 + \frac{f}{2} \right) H_d \quad \text{Equation F.10}$$

Calculate the moment due to cohesion,  $M_c$ , about point O:

$$M_c = \frac{c}{2 \tan \mathbf{f}} (r_1^2 - r_o^2) \quad \text{Equation F.11}$$

Calculate  $P_{pc}$  by summing moments about point O:

$$P_{pc} = \frac{M_c + l_5 E_{PRc} + \alpha c H x_o}{(l_1 \cos \mathbf{d} - x_o \sin \mathbf{d})} \quad \text{Equation F.12}$$

where  $\alpha$  is the adhesion between the cohesive soil and wall, the factor  $\alpha$  can range from 0 to 1.

**Compute  $P_{pq}$  - earth pressure due to surcharge.** (Refer to Figure F.3c.)

Calculate the Rankine earth pressure due to surcharge,  $E_{PRq}$ , acting on the vertical face defined by points df:

$$E_{PRq} = q_s \tan^2 \left( 45 + \frac{\mathbf{f}}{2} \right) H_d \quad \text{Equation F.13}$$

Calculate  $P_{pq}$  by summing moments about point O:

$$P_{pq} = \frac{l_4 w q_s + l_5 E_{PRq}}{(l_1 \cos \mathbf{d} - x_o \sin \mathbf{d})} \quad \text{Equation F.14}$$

### F.3 Log Spiral Solution

The individual components can be combined to compute the ultimate passive earth pressure,  $E_p$ , in units of force per unit length, as follows:

$$E_p = (P_{p\phi} + P_{pc} + P_{pq}) \quad \text{Equation F.15}$$

where  $P_{p\phi}$  is the component due to soil weight and friction,  $P_{pc}$  is the component due to soil cohesion,  $P_{pq}$  is the component due to surcharge, and  $b$  is the width of the cap or wall.

The earth pressure coefficient for friction and soil weight is defined as:



$$K_{pf} = \frac{2P_{pf}}{gH^2} \quad \text{Equation F.16a}$$

the earth pressure coefficient for cohesion is defined as:

$$K_{pc} = \frac{P_{pc}}{2cH} \quad \text{Equation F.16b}$$

and the earth pressure coefficient for surcharge is defined as:

$$K_{pq} = \frac{P_{pq}}{qH} \quad \text{Equation F.16c}$$

Combining these three equations, the ultimate passive pressure force per unit length,  $E_p$ , can be expressed in a more traditional form as:

$$E_p = \frac{1}{2}gH^2K_{pf} + 2cHK_{pc} + qHK_{pq} \quad \text{Equation F.17}$$

The value of  $E_p$  is modified in *PYCAP* for three-dimensional effects using factors developed by Ovesens (1964) from experiments on embedded anchor blocks.

The value of  $E_p$  is incorporated into a hyperbolic formulation, which is used to develop pile cap p-y values for lateral analyses. The complete process, including the generation of pile cap p-y values, is performed in the program *PYCAP*.

The  $K_{p\phi}$  value determined using the log spiral method approaches the Rankine value of  $K_p$  as  $\delta$  approaches zero. For this reason, and because numerical difficulties occasionally occur when  $\delta$  is less than 2 degrees, *PYCAP* automatically defaults to the Rankine value of  $K_p$  when  $\delta$  is less than 2 degrees. In this case, the ultimate passive force,  $E_p$ , is expressed as:

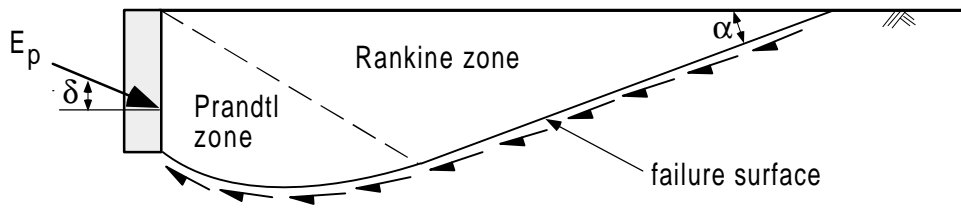
$$E_p = \frac{1}{2}gH^2K_p + 2cH\sqrt{K_p} + qHK_p \quad \text{Equation F.18}$$

where  $K_p$  is determined from Rankine theory as:

$$K_p = \tan^2\left(45 + \frac{f}{2}\right) \quad \text{Equation F.19}$$

When  $\phi = 0$ , *PYCAP* defaults to a different method for calculating  $E_p$ , which is called the  $\phi = 0$  sliding wedge method. This method is described in Appendix G.

Figure F.4 contains an example of the worksheet named *Log Spiral*, which performs the calculations described in this appendix. Values for pile cap p-y curves, created using  $P_{ult}$ , are presented in the *Summary* worksheet of *PYCAP*. An example of the *Summary* worksheet is shown in Figure F.5.

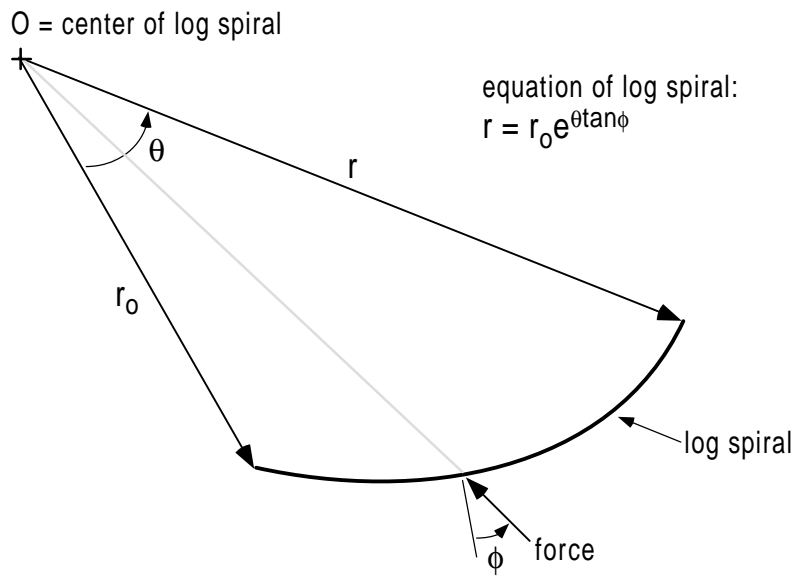


$E_p$  = passive earth pressure

$\delta$  = wall friction angle

$\alpha = 45 - \phi/2$

(a) Theoretical shape of passive failure zone.



(b) Log spiral.

Figure F.1. Log spiral approximation.

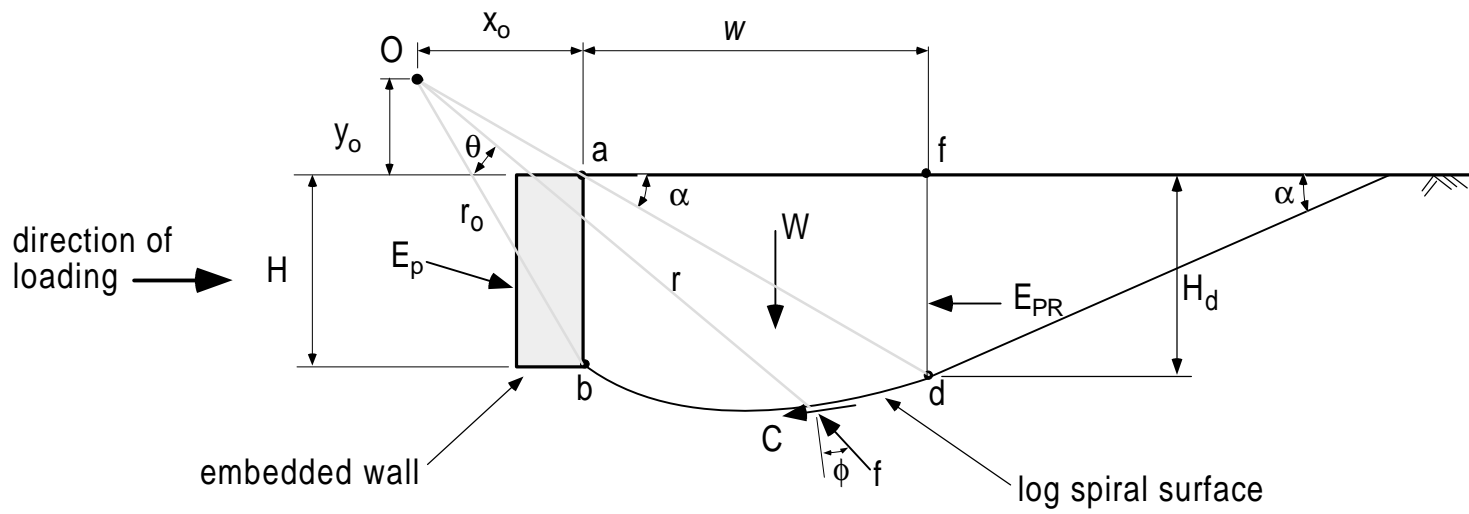
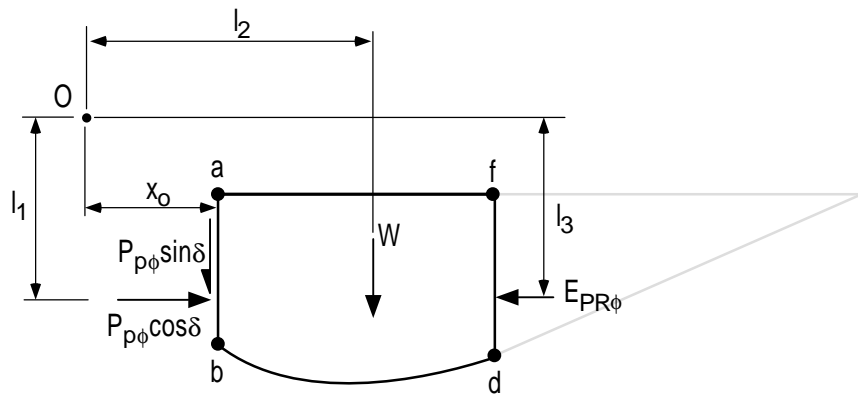
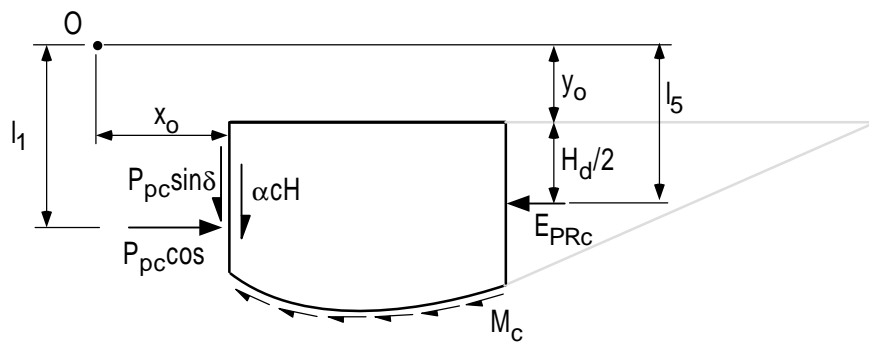


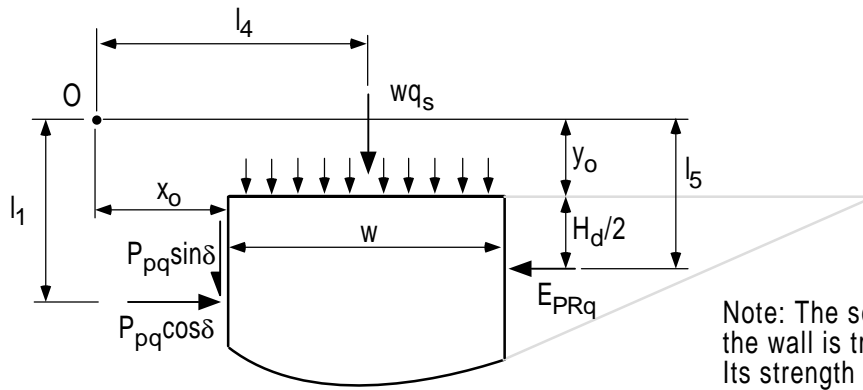
Figure F.2. Dimensions for log spiral method.



(a) Free body diagram for determining  $P_{p\phi}$ .



(b) Free body diagram for determining  $P_{pc}$ .



(c) Free body diagram for determining  $P_{pq}$ .

Note: The soil above the top of the wall is treated as a surcharge. Its strength is ignored.

Figure F.3. Free body diagrams of the log spiral failure zone.

## Log Spiral Passive Earth Pressure Calculation Worksheet

Created by R.L. Mokwa and J.M. Duncan - August 1999

Project: Bulkhead in natural soil  
 Date: 9/1/99  
 Calculated by: RLM

Enter data in column C of input table and press  
 Ctrl+a to calculate  $K_p$  and earth pressures.

**Input values - Use "summary" worksheet for data entry.**

Cap height, H (ft) =	3.50
Friction angle, $\phi$ (degrees) =	37.0
Cohesion, c (psf) =	970
Wall friction angle, $\delta$ (degrees) =	4
Unit weight, $\gamma$ (pcf) =	122
Surcharge, $q_s$ (psf) =	0.0
Adhesion factor, $\alpha$ =	0.00
Cap width, b (ft) =	6.30

**Rankine Earth Pressure Theory ( $\delta = 0$ )** **Results**

Coefficient of active earth pressure, $K_a$ =	0.25
Coefficient of passive earth pressure, $K_p$ =	4.02
Passive force due to $\gamma$ (lb/ft) =	2,820
Passive force due to $q_s$ (lb/ft) =	0
Passive force due to c (lb/ft) =	13,619
Total passive pressure force, $E_p$ (lb/ft) =	16,439

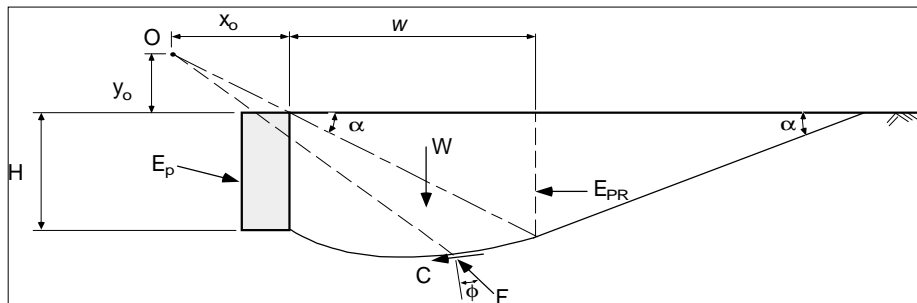
**Log Spiral Earth Pressure Theory** **Results**

Zone width, w (ft) =	4.06
$K_{p\phi}$ =	4.65
Passive force due to $\phi$ (lb/ft) =	3,471
Passive force due to $q_s$ (lb/ft) =	-
Passive force due to c (lb/ft) =	14,343
Total passive pressure force, $E_p$ (lb/ft) =	17,814
friction, $\phi$ component $K_{p\phi}$ =	4.65
surcharge, $q_s$ component $K_{p q}$ =	0.00
cohesion, c component $K_{p c}$ =	2.11

**Coulomb Earth Pressure Theory** **Results**

Coefficient of passive earth pressure, $K_p$ =	4.56
Passive force due to $\gamma$ (lb/ft) =	3,224
Passive force due to $q_s$ (lb/ft) =	0
Passive force due to c (lb/ft) =	14,504
Total passive pressure force, $E_p$ (lb/ft) =	17,727

Log spiral geometric configuration used in spreadsheet calculations



continued on next page

Figure F.4 (1 of 3). Example of *Log Spiral* worksheet.

**Block capacity using Ovesen's (1964) theory for cohesionless soil (Log Spiral).**

cap width (ft) =	6.3	$K_a = 0.25$
cap height (ft) =	3.5	$K_{p\phi} = 4.65$
overburden (ft) =	0.0	$E = 0.00$
spacing factor =	1.0	
$\gamma_{avg}$ (pcf) =	122.0	
$\phi_{avg}$ (deg) =	37.0	
B =	1.0	
Ovesen's shape factor, R =	<b>1.43</b>	
$R_{max}$ =	2	

**Capacity calculations using Log Spiral theory.**

Ult. force due to $\phi$ , $F_\phi$ , (lb) =	21867
Ult. force due to c, $F_c$ , (lb) =	90360
Ult. force due to $q_s$ , $F_q$ , (lb) =	0

**Capacity calculations applying Ovesen's (1964) 3-D shape factor to  $\phi$  and c terms.**

- Apply Ovesen's 3-D shape factor to the  $\phi$ , c, and  $q_s$  forces.
- Limit the maximum value of R to 2.0.

$$P_{ult} = R(F_\phi + F_c + F_q)$$

$P_{ult}$ (lb) =	160416
$P_{ult}$ (kips) =	<b>160</b>

**Capacity calculations for  $\phi = 0$  conditions.**

Use  $\phi = 0$  sliding wedge formulation, after Reese (1997).

$$P_{ult} = 0.5(4 + 2\alpha + \gamma H/c + 0.25H/b)cbH$$

$P_{ult}$ (lb) =	48970
$P_{ult}$ (kips) =	<b>48.97</b>

Figure F.4 (2 of 3). Example of *Log Spiral* worksheet.

**Log spiral calculations - programmed in macro.**

Intermediate value of $E_p$ =	17,814
$\alpha$ =	26.5
$H_d$ =	2.02
$x_o$ =	10.32
$y_o$ =	5.15
$r_o$ =	13.46
theta =	0.235
$r_1$ =	16.0684
$r_2$ =	16.0680
Difference between $r_1$ and $r_2$ =	0.00
$l_1$ =	7.48
a =	1.85
$l_2$ =	12.17
$l_3$ =	6.49
$l_4$ =	12.35
$l_5$ =	6.16
$\tan \phi$ =	0.754
Weight of soil, W (lb per ft) =	1,413
$\tan (45+\phi/2)$ =	2.01
Rankine $E_{PR\phi}$ (lb per ft) =	1,005
Rankine $E_{PRq}$ (lb per ft) =	-
Rankine $E_{PRc}$ (lb per ft) =	7,876
Moment due to cohesion $M_c$ (ft lb per ft) =	49,530
$\cos \delta$ =	0.998
$\sin \delta$ =	0.061
(soil weight, $\phi$ component) $P_{P\phi}$ =	3,471
(surcharge component) $P_{Pq}$ =	-
(cohesion component) $P_{Pc}$ =	14,343
$\tan (45-\phi/2)$ =	0.50

Figure F.4 (3 of 3). Example of *Log Spiral* worksheet.



## Ultimate Capacity Calculation Sheet

Created by R.L. Mokwa and J.M. Duncan - August 1999

Date: 9/1/99  
 Description: Bulkhead in natural soil  
 Engineer: RLM

### Input Values (red)

cap width,	b (ft) =	6.30
cap height,	H (ft) =	3.50
embedment depth,	z (ft) =	0.00
surcharge,	$q_s$ (psf) =	0.0
cohesion,	c (psf) =	970.0
soil friction angle,	$\phi$ (deg.) =	37.0
wall friction,	$\delta$ (deg.) =	3.5
initial soil modulus,	$E_i$ (kip/ft <sup>2</sup> ) =	890
poisson's ratio,	$\nu$ =	0.33
soil unit weight,	$\gamma_m$ (pcf) =	122.0
adhesion factor,	$\alpha$ =	0.00
$\Delta_{max}/H$ , (0.04 suggested, see notes) =		0.04
<b>Calculated Values (blue)</b>		
$K_s$ (Rankine) =		0.25
$K_p$ (Rankine) =		4.02
$K_p$ (Coulomb) =		4.56
$K_{p\phi}$ (Log Spiral, soil weight) =		4.65
$K_{pq}$ (Log Spiral, surcharge) =		0.00
$K_{pc}$ (Log Spiral, cohesion) =		2.11
$E_p$ (kip/ft) =		17.81
Ovesen's 3-D factor, R =		1.43
$k_{max}$ , elastic stiffness (kip/in) =		890.5
<b><math>P_{ult}</math> (kips) =</b>		<b>160.4</b>

### Notes:

$E_p$  = passive earth pressure per foot of wall

$$E_p = (P_{p\phi} + P_{pq} + P_{pc}) = 0.5\gamma H^2 K_{p\phi} + qHK_{pq} + 2cHK_{pc}$$

$K_{p\phi}$ ,  $K_{pq}$ ,  $K_{pc}$  = Log spiral earth pressure coefficients

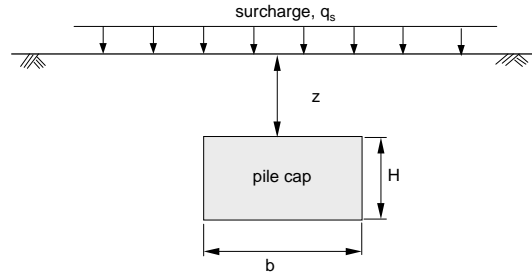
$$\text{for } \delta = 0, E_p = 0.5\gamma H^2 K_p + qHK_p + 2cH(K)^{0.5}$$

$$P_{ult} = E_p R b \quad (\text{passive force on wall})$$

$$\text{for } \phi = 0, P_{ult} = 0.5cbH(4 + \gamma H/c + 0.25H/b + 2\alpha)$$

$\Delta_{max}/H$  = movement required to fully mobilize passive pressures

Suggested value:  $\Delta_{max}/H = 0.04$  (Clough and Duncan, 1991)



### LPILE

#### p-y values for pile cap

Depth (in) ==>	y (in)	p (lb/in)	
0	10		<=== No. of data points
0.00	0.0		definig p-y curves
0.01	202.0		
0.03	553.8		
0.05	849.6		
0.10	1417.7		
0.20	2129.6		
0.50	3048.1		
1.00	3559.9		
2.00	3819.4		
10.00	3819.4		
Depth (in) ==>	42	10	<=== No. of data points
0.00	0.0		definig p-y curves
0.01	202.0		
0.03	553.8		
0.05	849.6		
0.10	1417.7		
0.20	2129.6		
0.50	3048.1		
1.00	3559.9		
2.00	3819.4		
10.00	3819.4		

Figure F.5. PYCAP Summary worksheet for bulkhead in natural soil.

## APPENDIX G –PASSIVE WEDGE MODEL FOR $\mathbf{f} = 0$

This appendix describes the formulation for estimating the ultimate passive resistance,  $P_{ult}$ , that is developed in  $\phi = 0$ , cohesive soils. The method follows closely the approach developed by Reese (1997) for modeling the failure zone in front of a laterally loaded pile. This approach assumes that the ground surface rises and translates in the direction of load. The failure wedge is assumed to be a plane surface, as shown in Figure G.1.

The equations developed in this appendix are used in the spreadsheet *PYCAP* for calculating the ultimate passive force developed in front of a pile cap for  $\phi = 0$  soils. For  $\phi > 0$  or  $c-\phi$  soils, the log spiral method described in Appendix F was used.

$P_{ult}$  is determined from equilibrium of the forces shown in Figure G.1. These forces are defined below.

Body force, or weight of soil in the failure wedge =  $W$ .

$$W = \frac{1}{2} \mathbf{g}bH^2 \tan \mathbf{q} \quad \text{Equation G.1}$$

Shear force between cap and wedge =  $F_f$ .

$$F_f = \mathbf{a}cbH \quad \text{Equation G.2}$$

where  $\alpha c$  is the adhesion between the cohesive soil and wall.

Shear force on bottom of sliding wedge =  $F_s$ .

$$F_s = \frac{cbH}{\cos \mathbf{q}} \quad \text{Equation G.3}$$

Shear force on side of sliding wedge =  $F_t$ .

$$F_t = \frac{1}{2} cH^2 \tan \mathbf{q} \quad \text{Equation G.4}$$

Normal force acting on bottom of sliding wedge,  $F_n$ , is determined by summing forces in the vertical direction:

$$F_n = \frac{1}{2}gbH^2 \frac{1}{\cos q} + acbH \frac{1}{\sin q} + cH^2 + \frac{cbH}{\sin q} \quad \text{Equation G.5}$$

Ultimate passive force,  $P_{ult}$ , is determined by summing forces in the horizontal direction:

$$P_{ult} = cbH \frac{\sin q}{\cos q} + cH^2 \frac{\sin^2 q}{\cos q} + \frac{1}{2}gbH^2 + acbH \frac{\cos q}{\sin q} + cH^2 \cos q + cbH \frac{\cos q}{\sin q} \quad \text{Equation G.6}$$

Angle of failure wedge =  $\alpha$ .

$$a \approx 45 + \frac{f}{2} \quad \text{Equation G.7}$$

For the case of  $\phi = 0$ ,  $\alpha \approx 45$  degrees. Making this substitution into Equation G.7 results in:

$$P_{ult} = \frac{cbH}{2} \left( 4 + 2a + \frac{gh}{c} + \frac{2.8H}{b} \right) \quad \text{Equation G.8}$$

Reese (1997) modified Equation G.8 based on results of fullscale tests performed by Matlock (1970). Reese's semi-empirical equation for the soil resistance per unit length, assuming a linear increase with depth, is given as:

$$p_{ult} = \frac{2P_{ult}}{H} = cb \left( 3 + \frac{gx}{c} + \frac{Jx}{b} \right) \quad \text{Equation G.9}$$

where  $x$  is the depth below ground surface. Matlock determined the value of  $J$  to be 0.5 for soft clay and about 0.25 for medium stiff clay. Reese assumed that because of cyclic loading,  $\alpha = 0$ . Integrating Equation G.9 with respect to  $x$ , between the limits of  $x = 0$  and  $x = H$ , results in the following expression for  $P_{ult}$ :

$$P_{ult} = \frac{cbH}{2} \left( 6 + \frac{gH}{c} + \frac{JH}{b} \right) \quad \text{Equation G.10}$$

Reese's (1997) semi-empirical equation for  $P_{ult}$ , Equation G.10, is similar in form to Equation G.8, except that Reese's equation (G.10) does not contain a term for adhesion,  $\alpha c$ , and some of the constant values have been adjusted, presumably to match the results of Matlock's (1970) pile load tests. The effects of soil adhesion are implicitly included in Equation G.10 for the piles that were used in Matlock's (1970) study. However, this expression may not accurately reflect the influence that adhesion has on pile caps, which are typically much wider than Matlock's test piles (which were 13 inches in diameter). For this reason, a modified version of the theoretical expression was used by Reese and Matlock with the term  $2.8H/b$  replaced by  $JH/b$ . Because soft clays are seldom used as backfill around pile caps,  $J$  was assumed to equal 0.25 (Matlock's recommendation for medium stiff clays.)

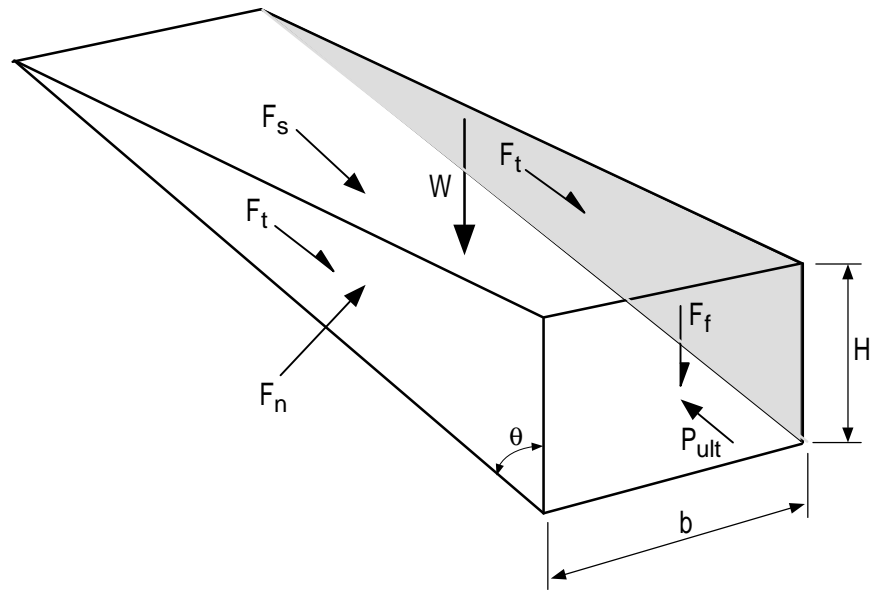
Changing the coefficient of the last term in equation G.8 from 2.8 to 0.25, based on Matlock's recommendation, results in the following expression for calculating  $P_{ult}$  for undrained,  $\phi = 0$ , conditions:

$$P_{ult} = \frac{cbH}{2} \left( 4 + 2a + \frac{gH}{c} + \frac{0.25H}{b} \right) \quad \text{Equation G.11}$$

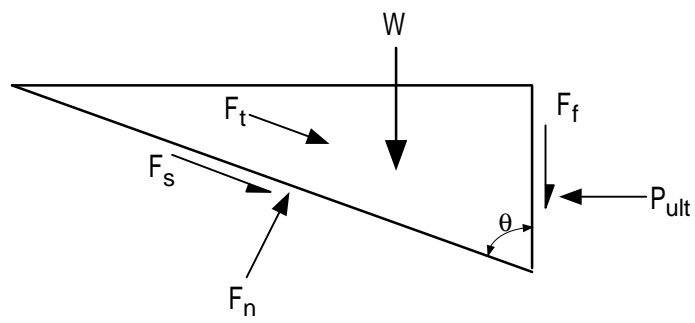
This expression provides results that are consistent with the log spiral/Ovesen approach (described in appendix F) for small values of  $\phi$  and  $\delta$ . For example, for a 5-foot-wide, 3-foot-deep cap with  $c = 1000$  psf,  $\gamma = 120$  pcf,  $\alpha = 0$ , and  $\phi = 0$ ,  $P_{ult}$  determined from Equation G.11 is 33.8 kips. In comparison, using the modified log spiral approach with  $\phi = \delta = 2^\circ$  resulted in  $P_{ult}$  equal to 34.0 kips. Calculations for  $\phi = 0$  conditions are performed in the worksheet named *Log Spiral*, which is part of the *PYCAP* workbook.

In summary, Equation G.11 was used in this study to calculate the ultimate resistance of pile caps for  $\phi = 0$  soil conditions. The program *PYCAP* automatically defaults to this expression whenever  $\phi = 0$ . The calculated  $P_{ult}$  value is incorporated into a hyperbolic

formulation, which is used for developing p-y curve values for pile cap analyses. The entire process, including the generation of pile cap p-y values, is automated in the program *PYCAP*.



Orthogonal view of failure wedge



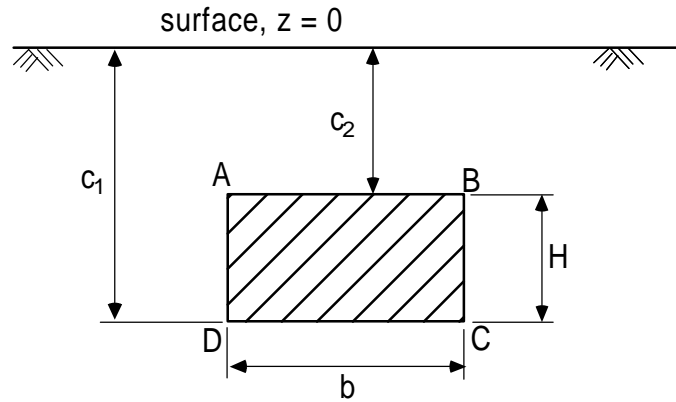
Side view of failure wedge

Figure G.1.  $\phi = 0$  passive wedge model,

## APPENDIX H – EQUATIONS FOR COMPUTING THE INITIAL ELASTIC STIFFNESS, $k_{max}$

### H.1 Introduction

This Appendix presents the equations that were used to compute the initial elastic stiffness for the pile caps,  $k_{max}$ . The method is based on elasticity equations developed by Douglas and Davis (1964) for calculating the horizontal displacement,  $y$ , at the upper and lower corners of a rectangular area in a semi-infinite, isotropic, homogeneous, elastic half-space. The dimensions that are used in the equations are shown in the sketch below.



### H.2 Equations for Calculating Deflection

For a uniform horizontal pressure,  $p$ , the deflection,  $y_1$  at upper corners A and B is given by equation H.1. The deflection,  $y_2$ , at lower corners C and D is given by Equation H.2.

$$y_1 = \frac{pb(1-n)}{16pE_i(1-n)} \{(3-4n)F_1 + F_4 + 4(1-2n)(1-n)F_5\} \quad \text{Equation H.1}$$

$$y_2 = \frac{pb(1-n)}{16pE_i(1-n)} \{(3-4n)F_1 + F_2 + 4(1-2n)(1-n)F_3\} \quad \text{Equation H.2}$$

where:

$p$  = uniform horizontal pressure applied to the rectangular area ABCD,

$\nu$  = Poisson's ratio,

$E_i$  = initial soil tangent modulus,

$b$  = cap width, and

$F_1$  through  $F_5$  = influence factors defined in Section H.3.

### H.3 Equations for Calculating Influence Factors $F_1$ Through $F_5$

$$F_1 = -(K_1 - K_2) \ln \left( \frac{K_1 - K_2}{2 + \sqrt{4 + (K_1 - K_2)^2}} \right) - 2 \ln \left( \frac{2}{(K_1 - K_2) + \sqrt{4 + (K_1 - K_2)^2}} \right) \quad \text{Equation H.3}$$

$$F_2 = 2 \ln \left( \frac{2(K_1 + \sqrt{1 + K_1^2})}{(K_1 + K_2) + \sqrt{4 + (K_1 + K_2)^2}} \right) + (K_1 + K_2) \ln \left( \frac{2 + \sqrt{4 + (K_1 + K_2)^2}}{(K_1 + K_2)} \right) - K_1^2 \left( \frac{\sqrt{4 + (K_1 + K_2)^2}}{(K_1 - K_2)} - \frac{\sqrt{1 + K_1^2}}{K_1} \right) \quad \text{Equation H.4}$$

$$F_3 = -2K_1 \ln \left( \frac{K_1}{1 + \sqrt{1 + K_1^2}} \right) + (K_1 + K_2) \ln \left( \frac{(K_1 + K_2)}{2 + \sqrt{4 + (K_1 + K_2)^2}} \right) - \ln \left( \frac{(K_1 + K_2) + \sqrt{4 + (K_1 + K_2)^2}}{2(K_1 + \sqrt{1 + K_1^2})} \right) + \frac{(K_1 + K_2)}{4} \left[ \sqrt{4 + (K_1 + K_2)^2} - (K_1 + K_2) \right] - K_1 \left( \sqrt{1 + K_1^2} - K_1 \right) \quad \text{Equation H.5}$$

$$F_4 = -2 \ln \left( \frac{2(K_2 + \sqrt{1 + K_2^2})}{(K_1 + K_2) + \sqrt{4 + (K_1 + K_2)^2}} \right) + (K_1 - K_2) \ln \left( \frac{2 + \sqrt{4 + (K_1 + K_2)^2}}{(K_1 + K_2)} \right)$$



$$+ K_2^2 \left( \frac{\sqrt{4 + (K_1 + K_2)^2}}{(K_1 + K_2)} - \frac{\sqrt{1 + K_2^2}}{K_2} \right) \quad \text{Equation H.6}$$

$$F_5 = 2K_2 \ln \left( \frac{K_2}{1 + \sqrt{1 + K_2^2}} \right) - (K_1 + K_2) \ln \left( \frac{K_1 + K_2}{2 + \sqrt{4 + (K_1 + K_2)^2}} \right) \\ + \ln \left( \frac{(K_1 + K_2) + \sqrt{4 + (K_1 + K_2)^2}}{2(K_2 + \sqrt{1 + K_2^2})} \right) - \left( \frac{K_1 + K_2}{4} \right) \\ \times \left( \sqrt{4 + (K_1 + K_2)^2} - (K_1 + K_2) \right) - K_2 \left( K_2 - \sqrt{1 + K_2^2} \right) \quad \text{Equation H.7}$$

where:

$$K_1 = \frac{2c_1}{b},$$

$$K_2 = \frac{2c_2}{b},$$

$c_1$  = depth to bottom of rectangular area, and

$c_2$  = depth to top of rectangular area.

The displacement at other points within plane ABCD can be determined using interpolation, assuming deflections vary linearly over the loaded area..

#### H.4 Equations for $k_{\max}$

$k_{\max}$  is the slope of the load-deflection curve. The load versus deflection relationship computed using Douglas and Davis's (1964) elasticity equations is linear. Thus,  $k_{\max}$  is the applied load divided by the corresponding deflection of the cap. The applied load, P, or horizontal force on the cap is given by Equation H.8 as:

$$P = p(b)(h) \quad \text{Equation H.8}$$

where  $p$  is the applied horizontal pressure,  $b$  is the cap width, and  $h$  is the cap depth.

The average deflection at the top corner and the bottom corner of the cap,  $y_c$ , is:

$$y_c = \frac{y_1 + y_2}{2} \quad \text{Equation H.9}$$

The initial elastic stiffness,  $k_{\max}$ , is the slope of the load-deflection curve, given by Equation H.10, as:

$$k_{\max} = \frac{P}{y_c} \quad \text{Equation H.10}$$

The units of  $k_{\max}$  are force per length, [F/L].

## VITA

Robert Leonard Mokwa was born in Pittsburgh, Pennsylvania on December 3, 1961. After graduating from Woodrow Wilson High School in Beckley, West Virginia, Bob attended Virginia Tech where he received a Bachelor of Science Degree in Civil Engineering in 1984. He attended Purdue University from 1984 to 1986, and received a Master of Science Degree in Civil Engineering. He worked as a geotechnical engineer and project manager for CH2M HILL in Boise, Idaho from 1986 to 1996, and is a licensed Professional Engineer in the states of Idaho, Utah, and Montana.

In the fall of 1996, Bob began his doctoral studies in geotechnical engineering at Virginia Tech, serving as a part-time instructor during 1998 and 1999. His dissertation research project was awarded the 1999 Paul E. Torgerson Graduate Student Research Excellence Award at Virginia Tech.

